



UNIVERSITY OF
LIVERPOOL

Implantable Antennas for Biomedical Applications

by

Rula Alrawashdeh

Submitted in accordance with the requirements for the award of the degree of Doctor of
Philosophy of the University of Liverpool

February 2015

Copyright

Copyright © 2015 Rula S. Alrawashdeh. All rights reserved.

The copyright of this thesis rests with the author. Copies (by any means) either in full, or of extracts, may not be made without prior written consent from the author.

To my parents, husband and family: Thank you for all your efforts and for your support.

To my daughter: Your smile has always inspired me.

Table of Contents

Copyright	i
Table of Contents	iii
Acronyms	vii
Acknowledgments	ix
List of Publications	x
Abstract	xii
Chapter 1.Introduction	1
1.1 Background	1
1.2 Research Motivations and Objectives.....	5
1.3 Organization of Thesis	9
Chapter 2.Implantable Antennas: Basics and Literature Review	12
2.1 Introduction.....	12
2.2 The Effect of the Human Body on the Antenna Performance	13
2.2.1 The Effect of the of the Human Body on the Antenna Radiation Efficiency and Rdaiated Power	18
2.2.2 The Effect of the Human Body on the Antenna Bandwidth.....	22
2.2.3 The Effect of the Human Body on the Antenna Radiation Pattern.....	24
2.3 Literature Review.....	27
2.3.1 Implantable Antenna Design	27
2.3.1.1 Rigid Embedded Implantable Antennas	27
2.3.1.2 Flexible Implantable Antennas	46
2.3.2 Evaluations in the Anatomical Body Model	53
2.3.3 Metamaterials for Implantable Antennas	59
2.3.4 Estimation of Body Path Losses.....	60

2.3.4.1	In-In Body Communications	61
2.3.4.2	In-On Body Communications	62
2.3.4.3	In-Off Body Communications.....	63
2.3.5	Models and Methods of Measurements.....	64
2.3.5.1	In Vitro Test	64
2.3.5.2	In Vivo Test.....	67
2.4	Summary	69
Chapter 3.Design of Flexible Implantable Antennas.....		71
3.1	Introduction.....	71
3.2	A Methodology to Design Implantable Antennas.....	73
3.2.1	The Methodology Parameters.....	75
3.3	Flexible Antennas for Muscle/Beneath Skin and Bone implants.....	77
3.3.1	U-Shaped Loop Antenna	77
3.3.2	A Small Meandered Loop Antenna.....	82
3.3.3	Antennas for Bone Implants	84
3.3.4	A comparison between the Design Considerations of Bone and Muscle Implantable Antennas	90
3.4	The Effect of the Insulation Layer on the Performance of Loop Antennas	91
3.5	The Effect of the Internal Components of the Implant on the Antenna Performance	92
3.6	The Specific Absorption Rate (SAR) Results	94
3.7	In Vitro Measurements	96
3.7.1	Measurements of the Reflection Coefficient	98
3.7.1.1	The Effect of the Insulation Layer on Measurements.....	101
3.7.2	Measurements of the Antenna Radiation Pattern and Gain.....	103
3.7.3	Measurements of the Antenna Performance Robustness	105
3.8	Summary	109

Chapter 4.Evaluation in the Anatomical Body Model	111
4.1 Introduction	111
4.2 The Effect of the Shape, Dimensions and Aspect Ratios of the Simplified Body Models on the Antenna Performance	113
4.2.1 The Effect of the simplified Body Shape on the Antenna Performance.....	114
4.2.2 The Effect of the Body Dimensions and Aspect Ratio on the Antenna Performance	116
4.3 Performance of the Conformal U-shaped Loop Antenna in the Anatomical Body Model of an Adult	118
4.3.1 Performance for Different Body Parts of Simulation	118
4.3.2 Performance Evaluation at Different Positions and Orientations.....	127
4.3 Performance of the 10 mm Meandered Loop Antenna in the Child Voxel Body Model.....	137
4.5 Summary	141
Chapter 5.Metamaterials for Implantable Applications.....	143
5.1 Introduction	143
5.2 A Broadband Implantable Loop Antenna Based on Complementary split Ring resonators (CSRRs)	145
5.2.1 Design and Performance.....	149
5.2.2 Realization and Measurements.....	159
5.3 Layers Based on Multiple Split Ring Resonators (MSRRs) around the Implantable Antenna.....	162
5.3.1 Performance around the 15 mm U-shaped Loop Antenna	163
5.3.1.1 Performance with Different Layer Thicknesses	169
5.3.1.2 Performance in the Anatomical Body Model	170

5.3.1.3	Investigations about Biocompatibility	174
5.3.1.4	Realization and Measurements	175
5.3.1.4.1	The Reflection Coefficient.....	175
5.3.1.4.2	The Percent of Power Improvement	176
5.3.1.4.3	Gain Measurements	177
5.3.2	Performance around an Implantable Patch Antenna	178
5.4	Summary	179
Chapter 6.Path Loss Estimation for Implantable Applications		181
6.1	Introduction.....	181
6.2	Communication between Implantable Antennas	184
6.3	The Effect of the Body Model Orientation on the Overall Path Loss.....	190
6.4.	Path Loss Estimation of a Wireless Power Transfer Channel.....	194
6.5	Investigations about the Optimum Antenna Type for Near Field Communications with Implantable Antennas	196
5.4	Summary	200
Chapter 7.Conclusions & Future Work		203
7.1	Conclusions.....	203
7.2	Future Work.....	207
References.....		209
Appendix A		224
Appendix B		229

Acronyms

AT	Ambient Temperature
AUT	Antenna Under Test
AVG	Average
BER	Bit Error Rate
BSN	Body Sensor Network
CSRR	Complementary Split Ring Resonator
CST	Computer Simulation Technology
DNG	Double Negative
EIRP	Effective Isotropic Radiated Power
ESAs	Electrically small antennas
GPS	Global Positioning System
IBSN	Implantable Body Sensor Network
Im	Imaginary
ISM	Industrial Scientific & Medical
LHM	Left Handed Metamaterial
LOS	Line Of Sight
MedRadio	Medical Device Radiocommunications Service
MSRR	Multiple Split Ring Resonators
NLOS	None Line Of Sight
NRI	Negative Refractive Index
PIFA	Planar Inverted F Antenna
PSK	Phase Shift Keying
PTFE	PolyteTraFluoroEthylene
PVC	Polyvinyl Chloride

Re	Real
RMS	Root Mean Square
RX	Receiver
SAR	Specific Absorption Rate
TX	Transmitter
WBAN	Wireless Body Area Network
WMTS	Wireless Medical Telemetry Service

Acknowledgements

Foremost, I would like to express my sincere gratitude to my supervisor Prof. Yi Huang for the continuous support of my Ph. D study and research, for his patience, motivation, enthusiasm, and immense knowledge. His guidance has helped me throughout the research and writing up this thesis. Beside my supervisor, I would like to thank Dr. Jiafeng Zhou for his motivation and insightful comments during our group meetings. My sincere thanks also go to Dr. Waleed Al-Nuaamy and Dr. Ali Al-Ataby for their beneficial feedback and stimulating questions during the annual review at our department.

I should also thank my home sponsor for the financial fund to pursue my study. It was a great support to improve my occupation and get introduced to new cultures abroad.

Thanks must also be paid to my colleagues at the Wireless Engineering Research Group; in particular to Neda Khiabani, Muayad Kod and Cao Ping for the stimulating discussions in a work related context. I would also like to thank Qian Xu for his help as a software expert in our group.

Last but not the least, I would like to offer my special thanks to my parents and family for their support and help. I am eternally grateful for everything they have done. I would also like to express my gratitude to my husband Badi, who has endured the inevitable long-distance life due to my studies. I am very thankful for his patience, motivation and love.

List of Publications

1. **R. Alrawashdeh**, Y. Huang, M. Kod, and A. Abu Bakar Sajak, "A broadband flexible implantable loop antenna with complementary split ring resonators," *Antennas and Wireless Propagat. Lett.*, vol. PP, no. 99, DOI: 10.1109/LAWP.2015.2403952, Feb. 2015.
2. P. Cao, Y. Huang, J. W. Zhang, **R. Alrawashdeh** and X. Zhu, "A compact planar UWB antenna with quintuple band-notched characteristics," *IET Microwaves, antennas and propagation*, vol. 9, no. 3, pp. 206-216, Feb. 2015.
3. L. Xing, Y. Huang, S. Al Ja'afreh, Q. Xu and **R. Alrawashdeh**, "A further investigation on water antenna," *IET Microwaves, antennas and propagation*, DOI: 10.1049/iet-map.2014.0298, Jan. 2015.
4. M. Kod, J. Zhou, **R. Alrawashdeh** and Y. Huang, "Wireless charging of implantable battery using Rectanna", in Proc. *LAPC*, Loughborough, UK, 2014.
5. **R. Alrawashdeh**, Y. Huang, A. Abu Bakar Sajak, L. Xing and M. Kod, "Orientation effect of implantable antennas on performance" in *Proc. APS/URSI*, Memphis, TN, USA, 2014, pp.973-974.
6. L. Xing, Y. Huang, Y. Shen, S. Al Ja'afreh, Q. Xu and **R. Alrawashdeh**, "Broadband U-shaped water antenna for DVB-H applications" in *Proc. IEEE APS/URSI*, Memphis, TN, USA, 2014, pp.1930-1931.
7. **R. Alrawashdeh**, Y. Huang, and A. Abu Bakar Sajak, "A flexible loop antenna for biomedical bone implants" in *Proc. EuCAP*, the Hague, Netherlands, 2014, pp. 861-864.
8. A. Abu Bakar Sajak, Y-C. Shen, Y. Huang, N. Khiabani and **R. Alrawashdeh**, "An investigation on THz antennas using Graphene as a substrate" in *Proc. EuCAP*, the Hague, Netherlands, 2014, pp. 1017- 1020.

9. A. Abu Bakar Sajak, Y-C. Shen, Y. Huang, N. Khiabani and **R. Alrawashdeh**, “The effect of substrate on the performance of THz Antenna” presented in *IET Colloquium on Millimetre-wave and Terahertz Engineering & Technology*, Liverpool, 2014.
10. **R. Alrawashdeh**, Y. Huang, and Q. Xu, “Evaluation of implantable antennas in anatomical body models” *CST-article* 2014.
11. **R. Alrawashdeh**, Y. Huang, and P. Cao, “Flexible meandered loop antenna for implants in the MedRadio and ISM bands,” *Electronics Letters*, vol. 49, no. 24, pp. 1515-1517, Nov. 2013.
12. **R. Alrawashdeh**, Y. Huang, and P. Cao, “A flexible loop antenna for total knee replacement implants in the MedRadio band,” in *Proc. LAPC*, Loughborough, UK, 2013, pp. 225-228.
13. **R. Alrawashdeh**, Y. Huang, and P. Cao, “A conformal U-shaped loop antenna for biomedical applications,” in *Proc. EuCAP*, Gothenburg, Sweden, 2013, pp. 157-160.
14. **R. Alrawashdeh**, Y. Huang, P. Cao and E. Lim, “A new small conformal antenna for capsule endoscopy,” in *Proc. EuCAP*, Gothenburg, Sweden, 2013, pp. 220-223.
15. J. Wang, E. Lim, Z. Wang, Y. Huang, T. Tillo, M. Zhang and **R. Alrawashdeh**, “UWB Planar antennas for wireless capsule endoscopy,” in *Proc. iWAT*, Karlsruhe, Germany, 2013, pp. 240-243.

Abstract

Recently, the interest in implantable devices for biomedical telemetry has significantly increased. Amongst the different components of the implantable device, the antenna plays the most significant role in the wireless data transmission. However, the human body around the antenna alters its overall characteristics and absorbs most of its radiation. Therefore, this thesis is mainly focused on improving the antenna characteristics (bandwidth and radiation efficiency) to overcome the human body effect and investigating new structures that reduce the power absorption by the human body tissues.

A novel antenna design methodology is developed and used to design new flexible implantable antennas of much lighter weight, larger radiation efficiency, and wider bandwidth than existing embedded antennas. These antennas work for multiple ((401-406 MHz) MedRadio, 433 MHz and 2.45 GHz ISM) bands which satisfy the requirements of low power consumption and wireless power transfer. This has been combined with thorough investigations of the antenna performance in the anatomical human body. New effective evaluation parameters such as the antenna orientation are investigated for the first time.

New structures inspired by complementary and multiple split ring resonators (CSRRs and MSRRs) are designed. The structures are found to reduce the electric near field and hence the absorbed power which increases the radiated power accordingly. This new promising function of metamaterial based structures for implantable applications is investigated for the first time.

The path loss (between pacemaker and glucose monitoring implantable antennas inside the anatomical body model) and (between an implantable and external antennas for a wireless power channel at 433 MHz) are estimated. Moreover, the optimum antenna type for on-in body communication is investigated. Loop antennas are found to outperform patch antennas in close proximity to the human body.

Chapter 1

Introduction

1.1 Background

Recently, the interest in implantable devices for biomedical applications such as cancer treatment by hyperthermia, drug delivery and healthcare monitoring [1, 2, and 3] has significantly increased. Implantable devices can sense bio-signals such as the temperature, blood pressure, etc. from inside the human body and transmit them to an external device (the reverse communication is also possible). The external device is either placed in the close proximity to the human body (in the near field region of the antenna) or at a distance of a few metres (in the far field region of the antenna). Two examples on these applications are shown in Figs. 1.1 and 1.2, respectively. The application in the far field region is the focus of this thesis. The information received by the external device is post-processed by monitoring units and medical experts who treat the patient accordingly as shown in Fig. 1.2. This allows some diseases, such as cancer or diabetes, to be diagnosed in their very early stages, while critical medical conditions, such as heart attacks or strokes, can be prevented [3]. This is also very helpful for healthcare systems by monitoring several bio-physical parameters such as glucose and blood sugar level. Indeed, many devices such as pacemakers, implantable glucose sensors and wireless capsule pills have demonstrated the importance of implants in treatment and health monitoring [3].

The implantable device is composed of several components such as a battery, sensors and an antenna. An example of an implantable device is illustrated in Fig. 1.3. Among all of these components, the antenna plays the most significant role in building up the communication link from inside the human body to an external receiver. It can be seen from the figure that the antenna exploits a considerable space inside the implant. Thus, the antenna may play an important role in the overall size and weight reduction of the implantable device.

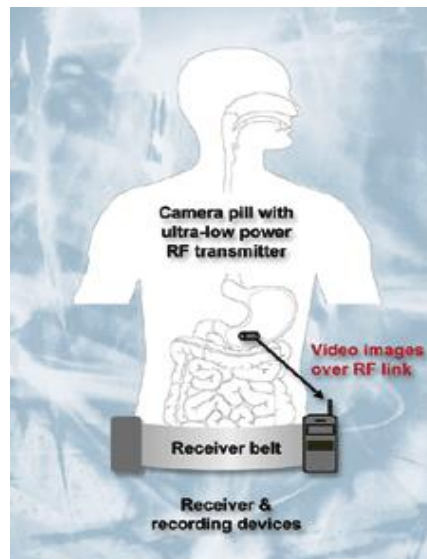


Fig. 1.1: Wearable receiver of wireless capsule endoscopy [4].

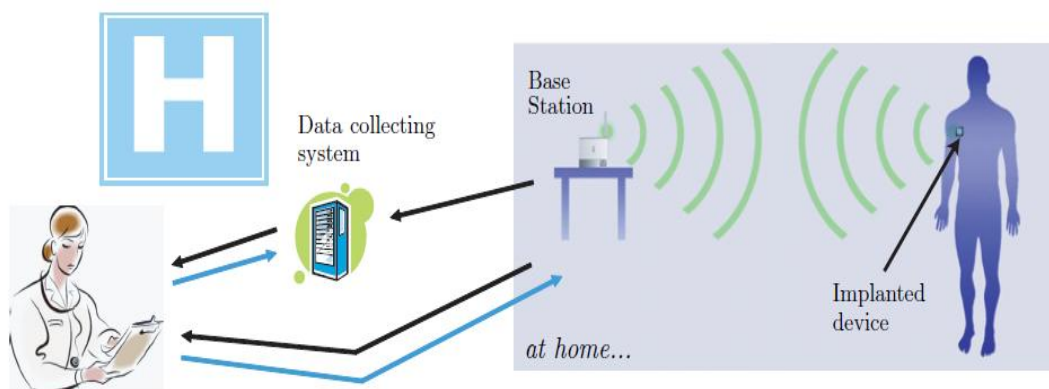


Fig. 1.2: Illustration of a health monitoring system [3].

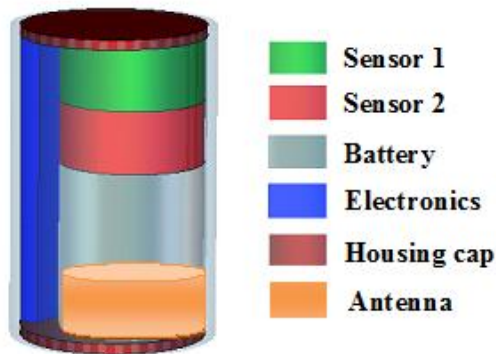


Fig. 1.3: Illustration of an implantable device.

To achieve the intended functions of the implantable device successfully, the implantable antennas should be carefully designed. However, implantable antenna design is very challenging which is mainly due to the following reasons:

1. Physical limitations and frequency band allocations: The Medical Device Radio Communications (MedRadio) band is mainly allocated for implantable applications. This band covers the 401 – 406, 413 – 419, 426 – 432, 438 – 444, and 451 – 457 MHz [5] and is well suited for this service, due to the signal propagation characteristics in the human body, compatibility with the incumbent users of the band (meteorological aids such as weather balloons), and its international availability. The range of frequencies within this band represents a good choice as higher frequencies suffer from larger human body attenuation [6]. However, this band selection presents challenges to the design due to its relatively low frequency range. For antennas to resonate in a relatively low frequency band, they have to be of a large size, this cannot be the case for implantable antennas which have to be in a small implantable device. Therefore, miniaturization is needed. This may result in electrically small antennas which suffer from small radiation efficiency. On the other hand, the small physical size of these antennas causes small gain values. Unlike the normal physically small antennas in free space, implantable antennas obtain a

relatively wide bandwidth because of the human body loss. However, this wide bandwidth is obtained at the cost of smaller radiation efficiency. This will be further explained later. Other frequency bands such as the 433 MHz and 2.45 GHz ISM bands are also used for biomedical applications. The 433 MHz is mainly used for wireless power transfer from an external antenna to the implantable device. This has the advantage of avoiding surgeries to replace the implant battery. It also reduces the size of the implantable device by saving the internal space that is exploited by the battery. This frequency band supports higher data rate transmissions in comparison with lower frequencies that are normally used for inductive coupling. However, this requires dual- ((401-406) and 433 MHz ISM bands) or broad-band antennas. The 2.45 GHz is mainly used for wakeup applications to save power by transmitting data only when is needed [7]. This also introduces the requirements of multi or broad-band implantable antennas. It is worth mentioning that using the 2.45 GHz for data transmission leads to larger attenuations of the signal in the human body tissues in comparison with the MedRadio band.

2. The complicated medium of propagation: The main challenges of implantable antenna design are due to the human body environment in which these antennas radiate. Unlike free space, human bodies are composed of different tissues of large relative permittivity and conductivity which are distributed asymmetrically. This causes attenuation in the tissue layer and reflection at the boundaries between the tissues. It is worth mentioning that further losses (i.e. free space losses) are added when the wave travels in free space from the human body to an external receiver (more details about this communication path loss and link budget will be provided in Chapters 2 and 6). This shows the main difference between the case of the near and far field implantable communications; much smaller losses are obtained for the case of near field communication as the receiver is directly attached to the human

body or placed at a shorter distance (the free space loss is directly proportional to the distance from the human body to the external device).

The human body modifies the antenna behaviour; the relatively large permittivity of the body tissues helps in miniaturizing the antenna size. Moreover, the losses widen the antenna bandwidth (more details will be provided in the following chapter). However, a trade-off between the bandwidth and radiation efficiency has to be carefully applied to satisfy both of following:

- Ensure a robust performance in the human body where detuning happens.
 - Satisfy the required budget of the intended communication.
3. The specific absorption rate (SAR) and power limitations: In order to prevent hazardous heating of the biological tissues, implantable antennas have to comply with the SAR specifications. The IEEE C95.1-1999 standard restricts the SAR averaged over any 1 g of tissue in the shape of a cube (1 g-AVG SAR) to less than 1.6 W/kg [8]. The IEEE C95.1-2005 standard restricts the SAR averaged over any 10 g of tissue in the shape of a cube (10-g AVG SAR) to less than 2 W/kg [9]. The maximum input power that is provided to the antenna should satisfy these limitations. Moreover, the maximum equivalent isotropic radiated power (EIRP) has to be less than -16 dBm in the MedRadio band [10].

1.2 Research Motivations and Objectives

Biomedical telemetry has a significant role in improving people's life and health. Therefore, many designs of implantable and ingestible antennas were proposed. However, none of them has completely satisfied the overall requirements (small size, light weight, wide bandwidth, relatively large radiation efficiency and gain) for actual implants of robust

performance. While some designs were of a good radiation characteristics, the overall implant dimensions were large [3, 11, 12, and 13]. Moreover, most of these designs are of a very narrow bandwidth which causes a frequency detuning out of the MedRadio band after actual implantation in the real human body and after a short period of implantation [3]. On the other hand, the small designs in [14, 15] obtained very small gain values in the anatomical body model. Most of these antennas were heavy in weight and non-conformal to the implant structure. Although, the flexible designs in [16, 17] were light in weight and conformal to the structure, they were used for implants of large sizes and attenuations. Therefore, the primary motivation of this research is the development of a new set of implantable antennas that satisfy all the requirements that are mentioned above for an efficient design and can be used actually for real implantable devices. The added values of flexible antennas and considerable limitations and shortcomings of their previous designs motivate a particular focus on the development of efficient flexible antennas.

Because of the difficulty of the experimental validation in the actual human body, evaluation in the anatomical human body is very important. However, few designs [3] were evaluated in the full anatomical human body. Generally, that evaluation was brief and at one position and orientation only. The anatomical human body model mimics the multilayer human body accurately and sometimes is the only tool of an accurate evaluation. Therefore, it is very important to understand its actual effect on the antenna performance. For example, unlike the radiation pattern in simplified and homogeneous body models [18], the radiation pattern is more directional in these anatomical models. A Lot of ambiguities still exist about the effective design parameters such as the implant orientation on the antenna performance in the full anatomical body model. Although the orientation effect was briefly indicated in [19], its effect on the overall antenna characteristics was not thoroughly investigated. For all these cases, it is very important to understand the effect of the size of the simulated anatomical body part on the antenna performance and overall characteristics. Although this

parameter is expected to have a considerable effect on the antenna performance, it has been neglected by most of previous studies such as in [20]. All of these points were interesting propositions which supplied the motivation to:

- Investigate the effect of different implantation areas and tissues of the anatomical body model on performance. This is to evaluate the robustness of the antenna performance and select the optimum position of implantation for health monitoring implants.
- Discuss the conditions and requirements for an accurate and a quick evaluation of the implantable antenna performance.
- Elaborate and quantify the orientation effect on performance which was ignored previously despite of its importance.

The requirements of low power consumption and emergence of small passive implants motivate the design of a broadband antenna that works for the (401-406 MHz) MedRadio, 433 MHz and 2.45 GHz ISM bands. These bands support the functionalities of wireless data transmission, power transfer and wakeup receiver, respectively [21].

Metamaterials are structures of many interesting features. They have been used to miniaturize antennas and improve their impedance matching which is reflected on a larger overall radiation [18, 22]. They have also been used to reduce the SAR in the human head [23]. Moreover, they are used to control the electric and magnetic field around the antenna [24, 25]. This is very beneficial for implantable antennas which become more efficient if their electric near field is reduced. These special features motivate investigating the effect of complementary split ring resonators (CSRRs) and multiple split ring resonators (MSRRs) based top loading layer on the performance of implantable antennas in the human body. The CSRRs are integrated to a broadband loop antenna to:

- Improve the antenna matching for $S_{11} < -10$ dB.
- Improve the overall antenna radiation. This is obtained by reducing the electric near field. When it is reduced, the absorbed power is decreased hence the radiated power is increased accordingly. This will be explained in details in Chapter 5.

MSRRs are used to design a top loading layer around the implantable device and antenna to improve the overall radiation from the antenna regardless of the antenna structure. The main reason of the small radiated power from the implantable antenna is the power loss due to absorption of the antenna radiation by the surrounding human body tissues. The use of insulation layers to reduce the absorbed power has already been investigated in [26]. However, the resultant improvement was very limited and small especially for a thin layer and small implant. Therefore, the use of a new type of more efficient layers based on MSRRs has been proposed. Up to the author's best knowledge, metamaterials are used to improve the radiation of implantable antennas for the first time in this thesis. Although some metamaterials based designs were proposed for implantable antennas such as in [18, 27], they were only used to miniaturize the antenna and obtain resonance at another frequency by coupling to another radiator (SRR coupled to a spiral).

The human body forms an important part of in-in, in-on and in-off body communication paths. In-in (in to in) body communication comprises communication between implantable antennas inside the human body, in-on (in to on) body communication comprises communication between an implantable antenna and another antenna worn by the human body or placed on it, and in-off (in to off) body communication comprises communication between an implantable antenna and another external antenna outside the human body in the free space. The path loss between implantable antennas in an anatomical body model was estimated in [28]. However, it was for communication channels at 2.45 GHz

where attenuations are larger than that at 403 MHz. Implantable antennas of a relatively large size were considered in that study and thus the path loss was almost under-estimated. Moreover, the effect of the implant orientation especially at the same position which is found to be very effective on overall path loss variations was not considered. Off-body channels and path losses were characterized in [29, 30]. However, the effect of the body orientation on the overall path loss variations was not considered in those studies. This effect has to be evaluated for long term health monitoring implants as the human body moves and rotates around the receiver over the long health monitoring process. Although some antennas were designed for the applications of wireless power transfer, the path loss at 433 MHz was rarely estimated. Such estimation is very important to quantify the required link budget for the entire power transfer system. While the optimum implantable antenna type was investigated, the optimum wearable or on body antennas for an efficient on-in or in- on body communication was not investigated. It should be pointed out that an accurate estimation of the body path loss provides a valuable and reliable data source for doctors and designers. It also helps to boost many related applications. All of these aspects have provided another motivation to estimate these path losses accurately.

1.3 Organisation of Thesis

This thesis includes 7 chapters and is outlined as the following:

Chapter 2 is to review and discuss the foundations of radio communications in a lossy matter and study the general effect of the human body on antenna performance. It also reviews the work related to implantable antenna design and communication paths. This chapter is important as it establishes a background for all concepts and investigations in the following chapters.

Chapter 3 presents a general design methodology for flexible implantable antennas. This methodology is used to design many broadband antennas that cover the MedRadio (401-406) and 433 MHz ISM bands for different applications and types of implants. This chapter also presents the related measurements in a liquid body phantom and pork. This chapter is very important as it provides a general methodology for flexible implantable antenna designs that suit different applications and guarantee performance in the real human bodies. New flexible antennas that are more efficient than previous antennas are proposed in this chapter. In addition, this chapter presents a simple tool to measure the performance robustness of implantable antennas over a long period of implantation and material variations.

Chapter 4 concerns evaluating the antenna performance in the anatomical body models. To emphasize the importance of such an evaluation, the reliability of using the simplified body models is firstly investigated. Then, the performance of some of the proposed antennas at this thesis is evaluated at different positions and orientations in the anatomical body model. The following three parameters are investigated in depth for the first time in this chapter:

- The radiation pattern in the anatomical body model in comparison with that in the simplified body model.
- The implant orientation even at the same position of implantation.
- The body part which should be considered in simulations for an accurate and a quick evaluation.

The analysis in this chapter provides important guidelines for an accurate evaluation of the antenna performance. It also elaborates for the first time some effective parameters that have to be considered seriously during the design and surgery processes.

Chapter 5 is divided into two parts, the first part deals with the utilization of metamaterial inspired structure based on (CSRRs) for a more efficient implantable antenna. The second part of this chapter investigates the use of metamaterial based layers around the implantable antenna to improve the overall radiation from the human body. The results show an optimistic potential for using metamaterials for more efficient transmission from the implantable antenna to an external receiver. They also show a new function of metamaterials based structures in the lossy human body which is the reduction of the absorbed power.

Chapter 6 estimates and quantifies the loss of a communication path between a pacemaker and a glucose monitoring device. The benefit of this type of communication is indicated in [28]. Both of the glucose monitoring and pacemaker devices need to communicate with a device outside the human body to control some bio-parameters. The glucose monitoring implant can communicate with the pacemaker/central hub which then can communicate with a receiver placed outside the body. The data transfer from the in-body implants to the receiver placed outside the body thus only needs to take place from one of the in-body implant. This reduces the need for various sensors to communicate with receivers outside the body. For efficient communication, the communication path losses should be carefully estimated. Therefore, the losses of this communication path is estimated and quantified. The results of this estimation represent a good source of data for doctors and other designers in the field. It also provides the link margins for different orientations and positions of the implantable antenna. This chapter also estimates the path loss between an implantable and external loop antenna for a power transfer communication. This chapter also evaluates the body orientation effect on the path loss for in-off body communications. Further investigations on the optimum wearable antenna type to communicate with implantable antennas are also conducted in this chapter.

Chapter 7 summarizes conclusions and discusses future work.

Chapter 2

Implantable Antennas: Basics and Literature Review

2.1 Introduction

The performance of the implantable device and antenna is mainly influenced by the lossy and asymmetric human body. Unlike free space, human body tissues are lossy and of large relative permittivity. Therefore, the antenna performance in the human body is different from that in free space. The radiation in such a sensitive environment requires the compliance with many conditions such as the specific absorption rate and power regulations. This also imposes difficulties in the measurements which have to be conducted in human body mimicking phantoms. A good understanding of the antenna behaviour in the human body is necessary for a successful antenna design. This chapter provides a summary of the relevant theoretical basics for antenna designs in lossy media and compare it generally with the case in free space. It also provides a revision of the research areas of this work and aims particularly to:

- Summarize all the basic required knowledge for the design of implantable antennas.
- Review the subject areas of this thesis. This is very important to understand the current challenges and contributions of this work.

- Build a solid base for the analyses in the following chapters.

To achieve these purposes, this chapter is arranged into two parts: the effect of the lossy human body on the overall antenna characteristics is summarized in the first part. Then, the research on the following topics is reviewed in the second part of this chapter:

- Implantable antenna design (rigid and flexible antennas for near and far field applications).
- Evaluations in simplified and anatomical body models.
- The use of metamaterials for implantable antennas.
- Estimation of in-in, in-on and in-off body path losses.
- Models and methods of measurements.

The main contributions of this chapter to the thesis content are:

- Summary of the required knowledge to understand implantable antennas behaviour in the human body.
- Provision of a solid background for the investigations in the following chapters.
- Summary of the previous designs and investigations that are related to the subject areas of the thesis.

2.2 The Effect of the Human Body on the Antenna Performance

Unlike free space, the human body is lossy and frequency dependent. The conductivity of muscle and skin which are common tissues of implantation is 0.79 and 0.69 S/m, respectively at 403 MHz while the conductivity of the stomach, colon and small intestine are 1, 0.86 and 1.9 S/m, respectively at this frequency. The relative permittivity of the human body tissues are also of large values (57.1, 0.69, 67.5, 62.5 and 66) for these tissues, respectively at 403 MHz [31]. The effect of the large conductivity and permittivity is mainly reflected on a larger attenuation loss (L_α (dB)) inside human tissues which can be calculated using [32]:

$$L_\alpha = 20 \log_{10}(e^{-\alpha l}) \quad (2.1)$$

where l (m) is the distance that the signal travels in the tissue and α (Np/m) is the attenuation constant which can be calculated using Eq. 2.2 [32].

$$\alpha = \omega \sqrt{\mu \varepsilon} \left[\frac{1}{2} \sqrt{1 + \left(\frac{\sigma}{\omega \varepsilon} \right)^2} - 1 \right]^{1/2} \quad (2.2)$$

where ω (rad/m) is the angular frequency, μ is the tissue permeability (H/m) and equals to free space permeability (μ_0) for all the nonmagnetic human body tissues, ε (F/m) is the permittivity of the tissue which equals to ($\varepsilon_0 \varepsilon_r$) where ε_0 is the free space permittivity and ε_r is the relative permittivity, and σ is the tissue conductivity (S/m).

It should be mentioned that these electromagnetic properties (permeability, and permittivity) are complex quantities as defined in Eqs. (2.3-2.4) [3, 33].

$$\begin{aligned} \varepsilon &= \varepsilon_0 (\varepsilon'_r - j \varepsilon''_r) \\ &= \varepsilon_0 \left(\varepsilon'_r - j \frac{\sigma'}{\omega \varepsilon_0} \right) \end{aligned} \quad (2.3)$$

$$\mu = \mu_0(\mu'_{r} - j\mu''_{r}) \quad (2.4)$$

The human bodies are non-magnetic and thus do not present magnetic losses (the imaginary part of effective permeability is zero). For simplicity, ϵ_r and μ_r are used in this thesis to represent ϵ'_{r} and μ'_{r} , respectively.

In addition to attenuation losses, extra losses due to reflections (L_r (dB)) at the boundary between the tissues occur which can be calculated using Eqs. (2.5 - 2.7) [32]. Normal incidence is assumed in Eq. (2.6).

$$L_r = -20\log_{10}(\Gamma) \quad (2.5)$$

$$\Gamma = \frac{\eta_2 - \eta_1}{\eta_2 + \eta_1} \quad (2.6)$$

$$\eta = \sqrt{\frac{j\omega\mu}{\sigma + j\omega\epsilon}} \quad (2.7)$$

where η (Ω) is the intrinsic impedance and Γ is the reflection coefficient at the boundary between tissues.

It is also obvious from these equations that the losses increase at higher frequencies. This explains the benefits of allocating the (401-406 MHz) MedRadio band mainly for data transmission rather than the 2.45 GHz ISM band which is also used sometimes for medical applications [34]. It should be pointed out that larger conductivity and smaller permittivity are always obtained at higher frequencies. For example, the conductivities of muscle, skin, stomach, colon and small intestine at 2.45 GHz are 1.74, 1.46, 2.2, 2 and 3.17 S/m, respectively whereas the relative permittivity for these tissues at this frequency is 52.7, 38, 62.1, 53.8 and 54.4, respectively. However, it is obvious from these values that the increase

rate of the conductivity is much larger than the reduction of the permittivity. In addition to the reflection at the boundary between tissues, a part of the signal will be reflected back at the boundary between the skin layer and free space. This is due to the large difference in their electromagnetic properties and intrinsic impedances.

The received signal power by the off-body receiver can be calculated using Eq. (2.8) [14, 35].

$$P_{RX} = P_{TX} + G_{TX} + G_{RX} - L_p - e_p - ML_{TX} - ML_{RX} \quad (2.8)$$

where P_{RX} and P_{TX} (dBm) are the received and transmitted power, respectively, G_{TX} (dB) is the transmitter antenna gain. This gain value is normally negative for implantable antennas as it includes in-body (attenuations and reflections) losses, G_{RX} (dB) is the receiver antenna gain, e_p (dB) is the polarization mismatch factor, ML_{TX} (dB) is the transmitter impedance mismatch loss, ML_{RX} (dB) is the receiver impedance mismatch loss. L_p (dB) is the path loss which can be obtained using Eq. (2.9) [29]:

$$L_p = 10n \log\left(\frac{d}{d_0}\right) + 10 \log\left(\frac{4\pi d_0}{\lambda_0}\right)^2 + S \quad (2.9)$$

where n is the path loss component which is environment-dependent. $n = 1.5$ for line-of-sight (LOS) indoor propagation, while $n = 3$ for none-line-of-sight (NLOS) indoor propagation, $d_0 \leq d$ is a reference distance which is assumed to be 1 m in this thesis, λ_0 (m) is the wavelength which is inversely proportional to the frequency. and S is the random scatter around the mean [14, 29]. In the case of free space loss $n = 2$ and hence Eq. (2.9) simplifies to [36]:

$$L_f = 20 \log_{10}\left(\frac{20 \times \pi \times d}{\lambda_0}\right) \quad (2.10)$$

where L_f (dB) is the free space loss.

Gain in free space (receiver antenna gain for this case) is defined as the ratio of the radiation intensity in a given direction from the antenna to the total input power accepted by the antenna divided by 4π . If the direction is not specified, the direction of the maximum radiation is implied. Mathematically, the gain (dimensionless), can be written as [37]:

$$G = \frac{4\pi U}{P_{in}} \quad (2.11)$$

Where U (W/unit solid angle) is the radiation intensity and P_{in} (W) is the total input power accepted by the antenna. The radiation intensity is linked to the average radiated power intensity (S_{avg} (W/m²)) by distance (r (m)) squared, that is [37]:

$$U = r^2 S_{avg} \quad (2.12)$$

The gain in a conducting medium (G_{con}) is obtained in [38] as:

$$G_{con} = \frac{4\pi R g^2}{R_r} \quad (2.13)$$

where R_{rad} (Ω) is the radiation resistance, $R_{intrinsic}$ (Ω) is the intrinsic resistance which is given by:

$$R_{intrinsic} = \sqrt{\frac{\omega\mu}{2\sigma}} \quad (2.14)$$

g is a function involving the parameters of the medium and is given as:

$$g = \frac{|H|de^{d/\delta}}{I_i} \quad (2.15)$$

$|H|$ (A/m) is the magnitude of the magnetic field taken in the maximum field direction of the antenna under consideration at distance d (m). δ is the skin depth and I_i (A) is the input current [38]. This shows that the gain of the antenna in a conducting medium such as the case of the implantable antenna inside the human body increases if the magnetic field of the antenna increases.

In a free space environment, the near field is mainly reactive, thus neither affecting the radiated nor the absorbed power. In the case of implantable antennas, on the contrary, the near field strongly couples with the closest surrounding material, thus increasing the lost power [3]. This is reflected on smaller radiation efficiency as explained in the following subsection.

2.2.1 The Effect of the Human Body on the Antenna Radiation Efficiency and Radiated Power

The effect of the lossy medium on the antenna radiation efficiency and resistance has already been investigated [3, 38]. The conventional techniques for determining the antenna radiation efficiency and resistance are found to be incorrect inside the lossy medium [38]. However, this applies to an infinite lossy medium. For the case of implantable antennas, the receiver will be placed somewhere in free space outside the human body. Therefore, the classical definition of radiation efficiency (η) in Eq. (2.16) will be used at this thesis in accordance with [3].

$$\eta = \frac{P_{rad}}{P_{source}} \quad (2.16)$$

where P_{rad} (W) is the radiated power which is evaluated in free space at far field, P_{source} (W) is the source power. For the case of antennas in the human body, the source power is divided

into the radiated, absorbed and reflected power ($P_{rad} + P_{abs} + P_{reflected}$). For the same source power, the larger absorbed power reduces the antenna radiated power and radiation efficiency, correspondingly. The absorbed power is normally large and much larger than the reflected power for the case of implantable antennas. As explained above, this is due to the near field coupling with the human body tissues which causes larger power absorption. Therefore, the radiation efficiency for implantable antennas is usually small. The effect of the electric near field on the antenna radiated power and specific absorption rate (SAR) can be explained using Eqs. (2.17-2.18). The larger electric near field increases the absorbed power which reduces the overall radiated power. Moreover, it increases the SAR [3, 39].

$$P_{abs} = \frac{\omega}{2} \int_V \epsilon_0 \epsilon''_r |E|^2 dV \quad (2.17)$$

$$SAR = \frac{P_L}{\rho} = \frac{\sigma |E|^2}{2\rho} \quad (2.18)$$

where E (V/m) is the electric field and ρ (kg/m³) is the mass density.

The radiation efficiency of an antenna is defined in terms of its radiated and loss resistances [37]:

$$\eta = \frac{R_{rad}}{R_{rad} + R_L} \quad (2.19)$$

where R_{rad} (Ω) is the radiation resistance and R_L (Ω) is the loss resistance.

The radiation efficiency links the antenna gain to directivity (D) as:

$$G = \eta D \quad (2.20)$$

Directivity is a measure of the concentration of the radiated power in a particular direction. It is defined as the ratio of the radiation intensity in a given direction from the antenna to the radiation intensity averaged over all directions. The average radiation intensity is equal to the total radiated power divided by 4π . If the direction is not specified, the direction of the maximum radiation is implied. Mathematically, the directivity (dimensionless) can be written as:

$$D = \frac{U(\theta, \phi)}{U(\theta, \phi)_{avg}} = \frac{4\pi U(\theta, \phi)}{P_t} \quad (2.21)$$

The antenna radiation efficiency increases as the radiation resistance increases. The R_{rad} can be calculated using Eq. (2.22) [40]:

$$R_{rad} = \frac{P_{rad}}{I_i^2} \quad (2.22)$$

This shows that the radiation resistance directly depends on the radiated power. However, unlike the radiated power in free space, the radiated power of a small loop antenna in a non-magnetic lossy medium depends on the radial distance in close proximity (the radius of the sphere) around the antenna [41].

$$P_{rad} \approx \frac{\sigma \mu^2 \omega^2 (IdA)^2}{12\pi R} \quad (2.23)$$

where $I dA$ (A. m²) is the current area element, R (m) is the radius of the enclosing sphere around the loop antenna. This radial dependency implies that the near field contributes to the antenna loss and radiation [3]. This dependency becomes stronger for the case of a short dipole antenna which is of an electrical type as shown in Eq. (2.24) [41].

$$P_{rad} \approx \frac{1}{6\pi\mu\omega} \left(\frac{Idl}{\sigma} \right)^2 \frac{1}{R^3 \delta^2} \quad (2.24)$$

where l (A. m) is the current length element and δ is the skin depth. The detailed derivation of Eqs. (2.23-2.24) is provided in Appendix A.

It is shown from the equation that the radiation resistance and radiated power of the short dipole antenna decay with $(1/R^3)$ rather than $(1/R)$. Therefore, it is less efficient than the magnetic loop antenna in the human body. That is why loop antennas are selected for the designs in this thesis.

For the cases when the receiver is placed in close proximity to the human body such as the case of wearable receivers (e.g. capsule receivers), other definitions of the radiation efficiency could be more appropriate [3, 42]. However, this is beyond the main scope of this thesis. The free space or propagation losses do not contribute to the overall path losses for this case. On the other hand, reflections at the boundary between skin or clothes and free space still exist and count for the overall loss.

It is clear now that the antenna radiation efficiency of implantable antennas is mainly degraded because of the strong near field coupling between the radiator and surrounding body tissues. Therefore, insulation layers help in reducing this coupling by confining most of the losses in an area of low losses [3]. They also minimize the lossy area around the antenna and thus increasing the radiation efficiency. This effect has thoroughly studied in [3]. However, these layers are not very effective on magnetic type antennas which are selected for the designs and investigations in this thesis. This is due to the following:

- In agreement with [3], the effect of dielectric properties of real insulation layers on magnetic sources such as loop is negligible.
- In order to keep the overall implant size small, insulation layers are normally thin. Therefore, their beneficial effect on increasing the radiation efficiency is small in accordance with the findings in [3].

2.2.2 The Effect of the Human Body on the Antenna Bandwidth

Although, implantable antennas are ideally small in size and thus are expected to be of a narrow bandwidth, the losses which are introduced by the surrounding tissues widen the antenna bandwidth. This is because small portion of the radiated power is reflected back to the source (most of the radiated power from the source is absorbed by the human body tissues) [3]. The analysis in this thesis focuses on the design of wide bandwidth antennas to obtain the following:

- Overcome the frequency detuning which happens at different body tissues.
- Overcome the frequency detuning which happens at different positions in the same organ.
- Overcome the frequency detuning which happens at different orientations (around the same axis and different axes).

However, this wide bandwidth has to be obtained with good radiation efficiency. Therefore, this thesis suggests using flexible antennas which are wide in bandwidth and at the same time of relatively large radiation efficiency. The methodology of obtaining these contradicting conditions will be explained in the following chapter.

The effect of the antenna implantation inside the human body on its bandwidth is compared in a lossy and lossless human body model in Fig. 2.1. For an accurate comparison, both body models are of the same characteristics except for conductivity. The lossy body model mimics muscle at 403 MHz. Therefore, its conductivity is 0.79 S/m. On the other hand, conductivity of the lossless body model is zero. The antenna of investigations is a flexible U-shaped loop antenna. More details about it will be provided in the following chapter.

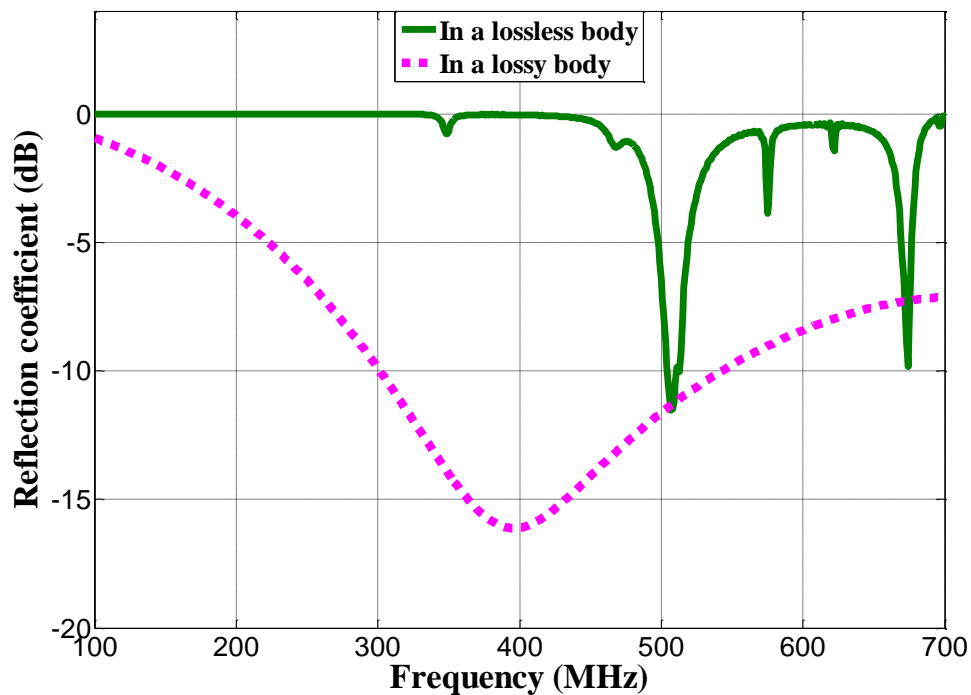


Fig. 2.1: The reflection coefficient of an implantable antenna in a lossless and lossy human body models.

The figure shows that the lossy human body tissues around the antenna widen the 10 dB bandwidth to be around 20 times the corresponding bandwidth in the lossless body model. At the same time, the resonant frequency in the lossy body model is lower by 110 MHz than in the lossless body model. It can also be seen from the figure that the flexible antenna bandwidth is around 240 MHz which is wide enough to overcome the frequency detuning in the real human body (more details will be provided in Chapter 4).

To investigate the source of its wide bandwidth, a comparison with other antennas is conducted. The comparison comprises both of rigid and embedded antennas. The flexible implantable antennas in [17, 42] are of wider bandwidth than the antennas in [3, 12, 14, and 27] although they are used for implants of the same size. It is worth mentioning that for more accurate comparison the antennas should be of almost the same size. However, general characteristics can be formulated for both types of antennas which can be used for the same

implantable device. This is attributed to the conformity of the flexible antennas; because the antenna is flexible, it exploits the entire wall of the implant. Therefore, much larger dimensions can be exploited for the antenna over the same implant size. The direct relationship between the antenna physical size and its bandwidth is well known to antenna designers. For example, a conformal rigid antenna which was embedded in an implant of 5 mm in radius and 30 mm in [3] was of a very narrow bandwidth (< 20 MHz). This is around 13 times narrower than the bandwidth of the conformal antenna that is presented in this thesis despite of the smaller implant size (half in length) and the same radiation efficiency for the proposed antenna in this thesis.

2.2.3 The Effect of the Human Body on the Antenna Radiation Pattern

The antenna radiation of an antenna is a plot of the radiated field as a function of the angle at a fixed distance, which should be considered large enough to be considered farfield [37]. The effect of the lossy medium on the antenna radiation pattern is investigated in [38]; it was found that the lossy medium broaden the radiation pattern in comparison with air as shown in Fig. 2.2.

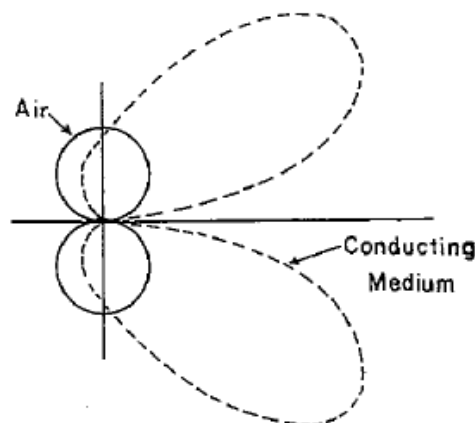


Fig. 2.2: Effect of the lossy medium on the polar radiation pattern [38].

This effect was studied in an unlimited lossy medium. Another important effect that is investigated in this work is the antenna position effect. While the radiation pattern is expected to change for different positions in the asymmetric anatomical body model, our investigations show that the radiation pattern differs even in the symmetric body model. To show this effect in the simplified body models, the position of the implantable antenna and device is changed inside the same simplified body model. It is worth mentioning that an elliptic cylindrical simplified body model of a muscle equivalent dielectric material and the dimensions of (180, 100 and 50 mm) are used in all of the previous investigations. However, to emphasize this effect even in a more symmetrical body structure, a body model of a cylindrical shape which is 100 mm in diameter and height is used as shown in Fig. 2.3.

The polar radiation patterns when the antenna is placed at the origin, 40 mm from the origin on the x and y axes are shown in Fig. 2.4. It can be seen from the figure that the main lobe direction differs totally when the antenna is simulated at the origin from the cases when the antenna is simulated at x and y = 40 mm. Around 149 and 159 degrees difference from the case at origin is obtained at x and y = 40 mm, respectively).

The main lobe magnitude for the cases at x= 40 mm and origin is almost the same (-16.3 dBv/m) while 5 dBv/m smaller main lobe magnitude is obtained for the case at y = 40 mm. The 3 dB angular widths are 149, 234.9 and 213.1 degrees at origin, x= 40 mm and y = 40 mm, respectively. The difference in the maximum field intensities is due to the following reason; the most effective antenna part is around the feeding point. When the antenna parts around it are surrounded by thicker lossy tissues, more absorption occurs and this reduces the overall far field strength (smaller radiation). The antenna parts around the feeding point are surrounded by the same thickness of the body tissue at x= 0 and x= 40 mm. Therefore, almost the same magnitude of the main lobe is obtained for both of them. On the other hand, much thicker tissue layer surrounds them when the antenna is at y= 40 mm. Therefore, a

smaller main lobe magnitude is obtained at this case. The antenna orientation in the body model and its parts are shown in Fig. 2.3. This shows the importance of evaluating the radiation pattern for implantable antennas at a position that exactly represents the actual case in the real human body. Moreover, additional effects such as the orientation are expected in the actual human body which is investigated in a following chapter.

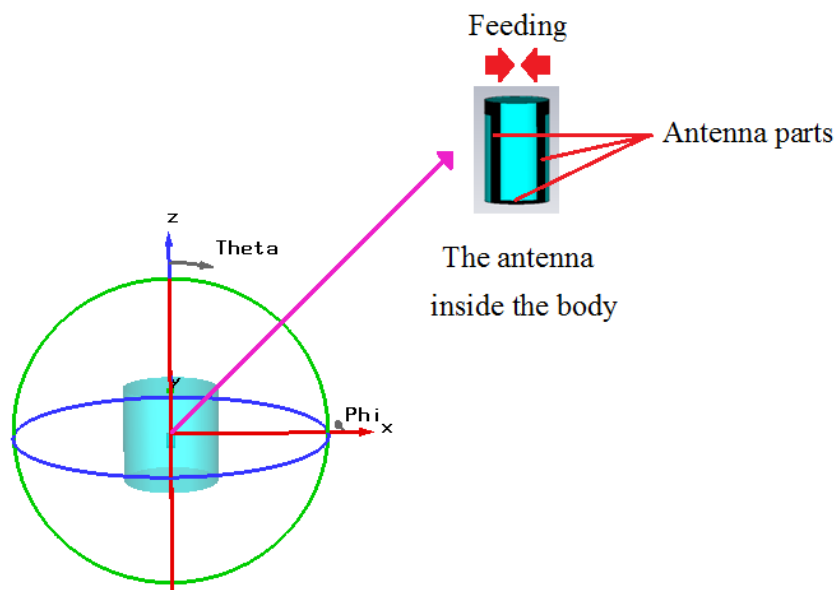


Fig. 2.3: The simplified cylindrical body model to study the effect of the implantable antenna position on the radiation pattern; dimensions are not to scale.

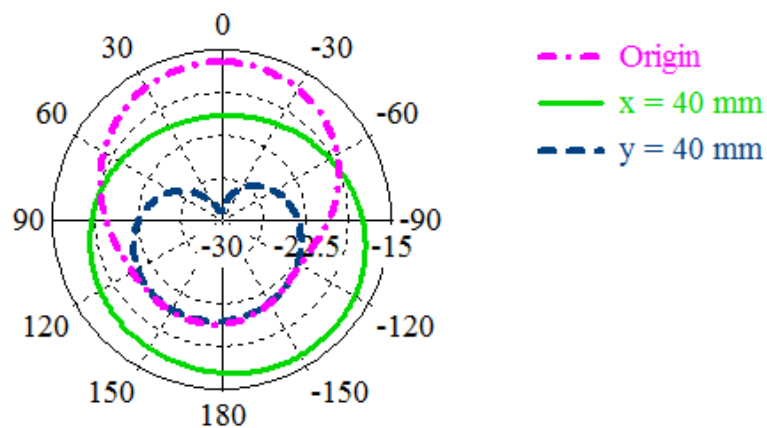


Fig. 2.4: The polar radiation pattern in the azimuth plane (around the body) when the antenna is placed at different positions: (a) origin ($x= 0, y= 0$ mm) (b) $x = 40$ mm (c) $y = 40$ mm.

2.3 Literature Review

The most significant work that was conducted in the subject areas of the thesis is reviewed in the following sections:

2.3.1 Implantable Antenna Design

Existing implantable antennas can be categorized into flexible and rigid antennas. Each of these groups is reviewed as the following:

2.3.1.1 Rigid Embedded Implantable Antennas

These antennas are made of rigid copper and can be only placed inside the implantable device (cannot be bent around it because of its non-flexibility). Many antennas under this category were proposed; a spiral meandered Planar Inverted-F Antenna (PIFA) was proposed in [12]. That antenna is shown in Fig. 2.5. It is of a large size ($24 \times 32 \times 8$) mm³ for real implants. Moreover, its shape is not conformal to cylindrical implants; the edges leaves an unexploited space around them which waists a considerable internal space. Furthermore, despite of the antenna relatively large size, it obtained a narrow bandwidth of around 50 MHz as shown in Fig. 2.6. A much wider bandwidth is desirable in order to guarantee coverage of the bands of interest at different implantations locations and orientations. This will be further discussed in a following chapter.

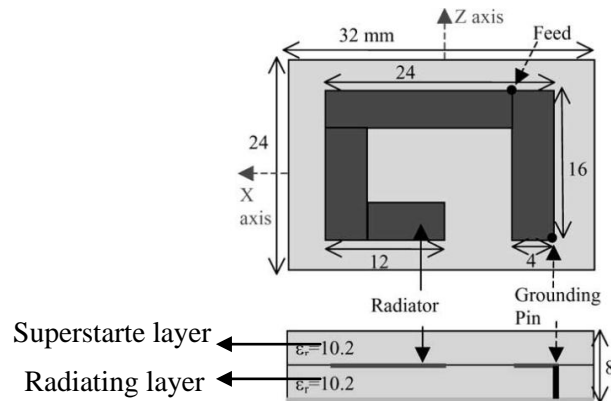


Fig. 2.5: A spiral PIFA antenna proposed in [12]; top and side views.

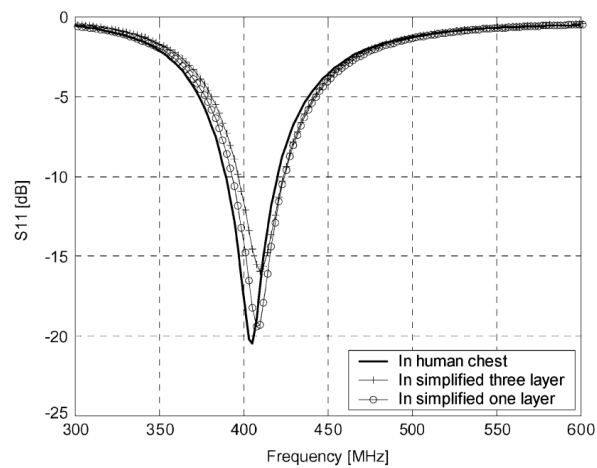


Fig. 2.6: The reflection coefficient of the spiral PIFA in [12].

The PIFA designs in [43] had also the same problem of the large size and non-conformity as shown in Fig. 2.7. They also had a bandwidth narrower than 50 MHz around the MedRadio band. A $(19.5 \times 10.8 \times 2.5)$ mm³ PIFA was also proposed in [44] for implantable applications at 868 MHz. The attenuation in the human body tissues and free space loss at this frequency are larger than that at the MedRadio band.

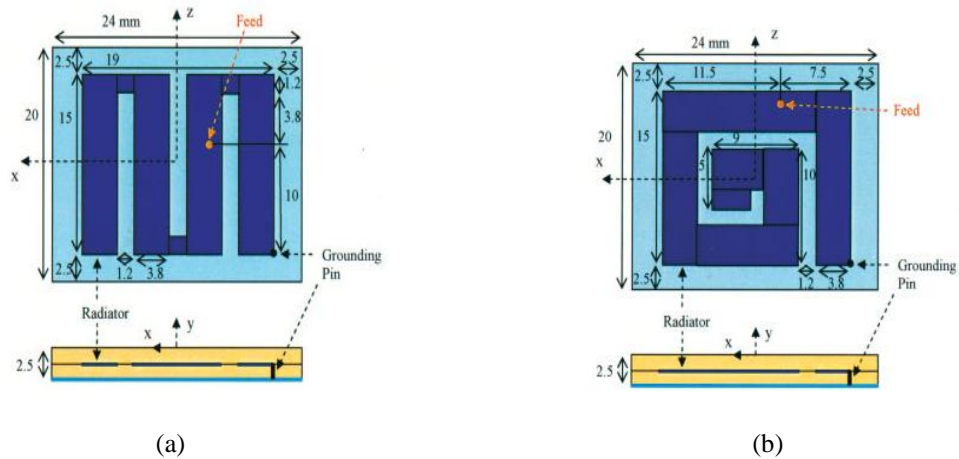
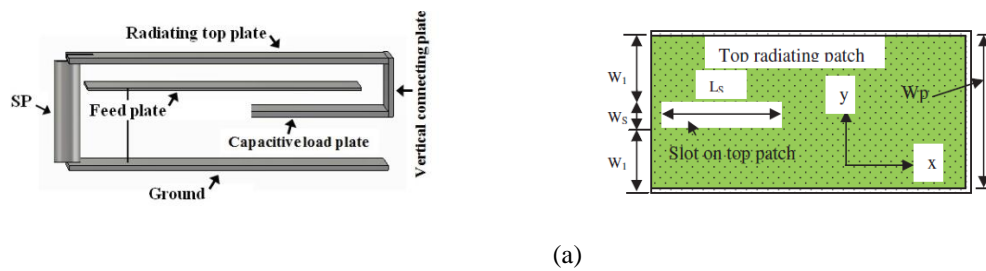
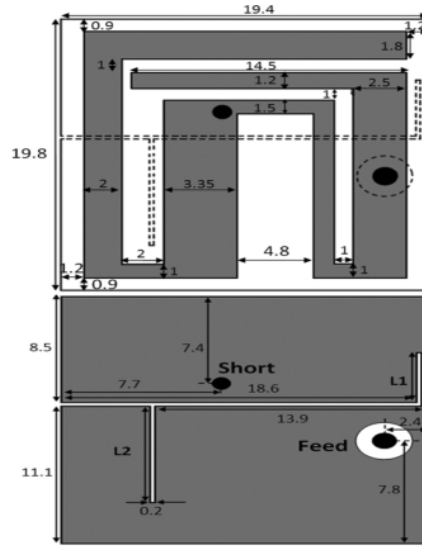


Fig. 2.7: The antennas in [43]: (a) Meandered PIFA, (b) Spiral PIFA.

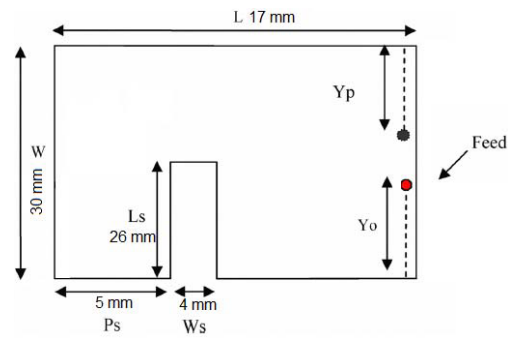
The PIFA is selected for those designs due to several reasons; it can resonate at a frequency around 400 MHz over small physical dimensions and low profile. It also has a smaller electric near field in comparison with other electrical type antennas. A single (915-928 MHz), dual (356- 610 MHz and 2.45 GHz ISM) and triple (433 MHz ISM, WTMS a 1430 MHz, and 2.45 GHz ISM) band slot PIFA antennas were also proposed in [45, 46, and 47]. Those antennas were of $(12 \times 12 \times 4)$, $(19.4 \times 19.8 \times 1.27)$ and $(19 \times 30 \times 1.6)$ mm³ in sizes, respectively which are relatively large for rigid structures for implantable applications. Those antenna structures and reflection coefficient are shown in Figs. 2.8 and 2.9, respectively. The slot was exploited in those designs to control the matching level, miniaturize the antenna and improve the antenna magnetic properties. This is reflected on larger radiation as explained in Chapter 2.



(a)

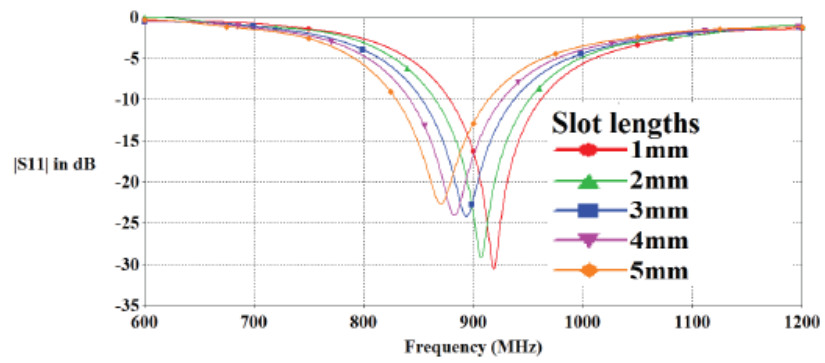


(b)

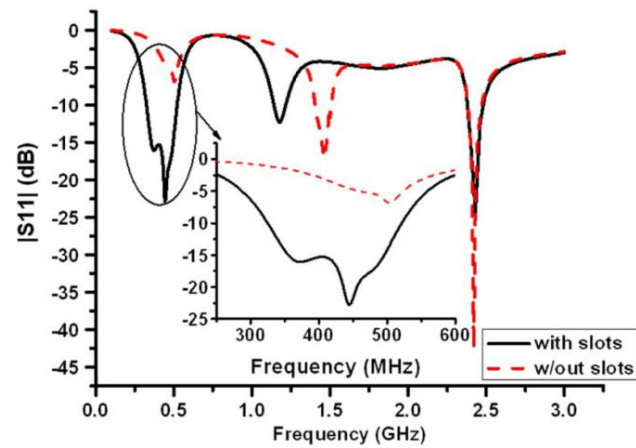


(c)

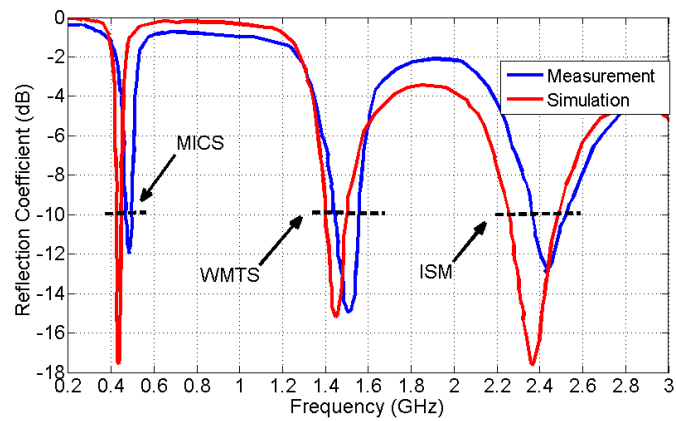
Fig. 2.8: Slot PIFA antennas in: (a) [45], (b) [46], and (c) [47].



(a)



(b)



(c)

Fig. 2.9: The reflection coefficient of the slot PIFA antennas in: (a) [45], (b) [46], and (c) [47].

Slot antennas were also proposed in [32, 48] for bone and arm implantation at frequencies of 20 and 2.45 GHz, respectively which were of much larger attenuation and free space loss than at MedRadio band. A stripline-fed slot antenna was also designed for muscle implants in [49]. That design was composed of two Rogers RT 6010 substrates as shown in Fig. 2.10 which probably made the implant heavy. Although the antenna worked for the 2.45 GHz ISM band as shown in Fig. 2.11, it obtained a relatively large size of $(12.5 \times 14.7 \times 2.54)$ mm³.

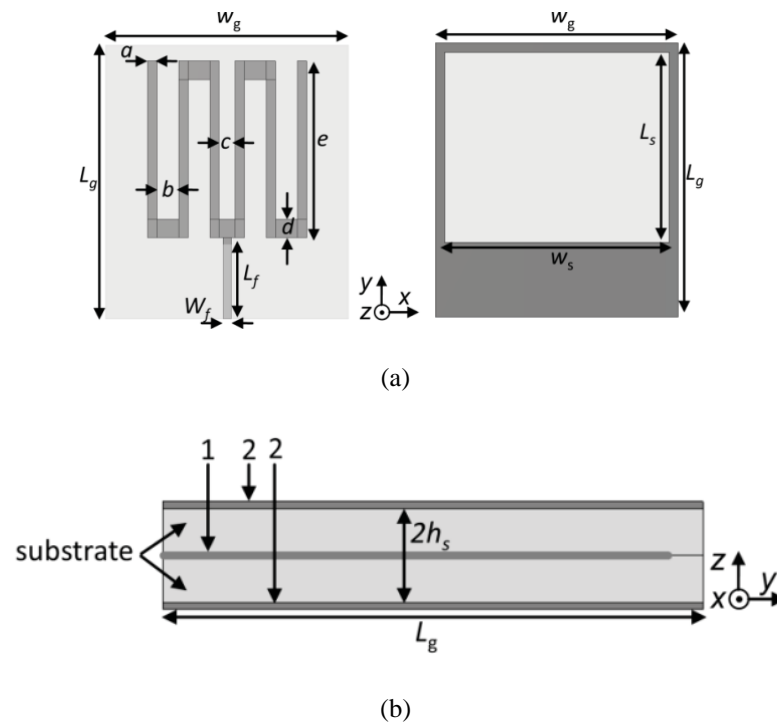


Fig. 2.10: The stripline-fed slot antenna in [49]: (a) Top view, (b) Side view

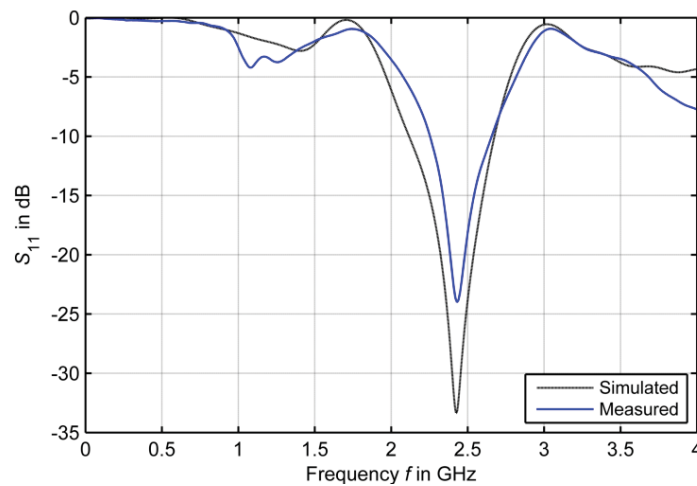


Fig. 2.11: The reflection coefficient of the stripline-fed slot antenna in [49].

A slot line between a low-dielectric medium and a high-dielectric medium-like skin was used in [15] to work for the MedRadio and 433 MHz ISM bands and obtained a small size of $(10 \times 12 \times 1.5 \text{ mm}^3)$. The antenna structure and reflection coefficient are shown in Figs. 2.12 and 2.13, respectively.

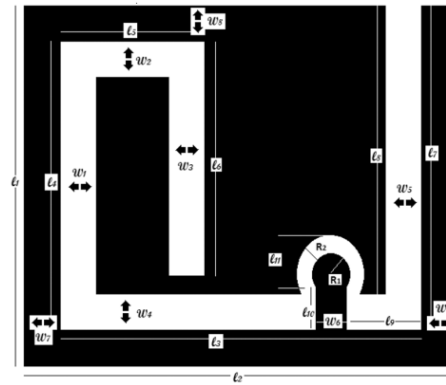


Fig. 2.12: The antenna in [15].

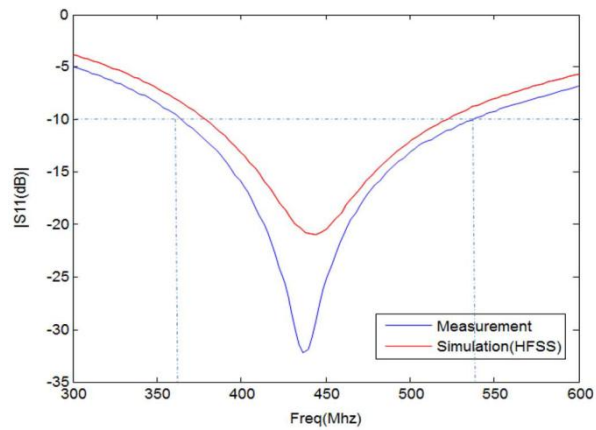


Fig. 2.13: The reflection coefficient of the antenna in [15].

A slot antenna was proposed in [50] as shown in Fig. 2.14 to work for the MedRadio (401-406 MHz) and 433 MHz ISM bands with a size of $(10 \times 11 \times 1.27 \text{ mm}^3)$. A good matching between the simulation in skin and measurement in skin gel was obtained. However, a much narrower bandwidth was obtained when that antenna was simulated in the human model as shown in Fig. 2.15.

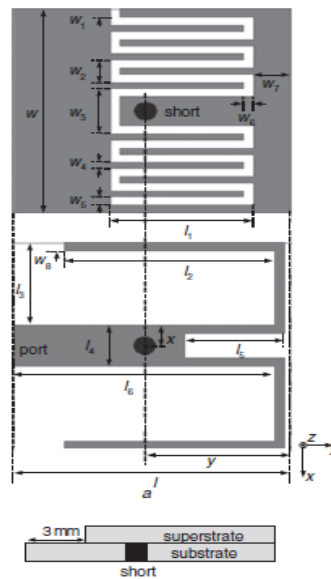


Fig. 2.14: The slot antenna in [50].

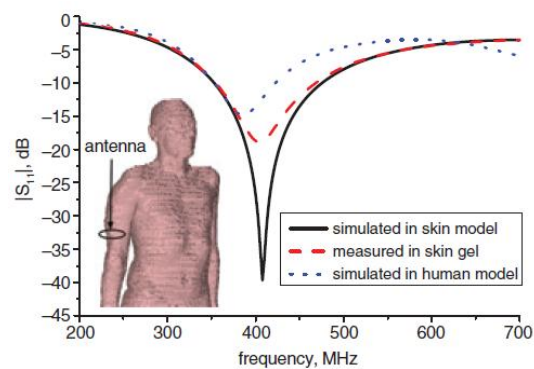


Fig. 2.15: The reflection coefficient of the slot antenna in [50].

Loop antennas were also popular for implantable designs as they are magnetic and of many attractive characteristics in general [39]. A meandered loop antenna was designed in [51] as shown in Fig. 2.16. It was designed on a circular Rogers 3010 substrate of 5.5 mm in radius and 0.635 mm in height to cover the (401-406) MedRadio and 902-928 MHz bands as shown in Fig. 2.17. That antenna had been coated both on the top and bottom with a biocompatible material called SU8 with the thickness of 50 μm . The maximum gain values of the proposed antenna in the arm of the CST Gustav body model were -35.6 and -26.3 dBi at 402 MHz and 902 MHz, respectively. Those gain values were much smaller than most of

the previous mentioned designs such as in [3]. This shows that the relatively wide bandwidth of that antenna was obtained due to the large coupling with the human body tissues rather than the antenna structure itself. Another rigid loop antenna was proposed in [52] for implantation in the head. The details of its radiation characteristics were not provided.

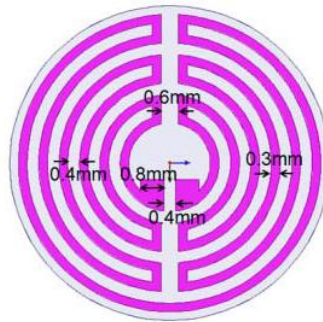


Fig. 2.16: The loop antenna in [51].

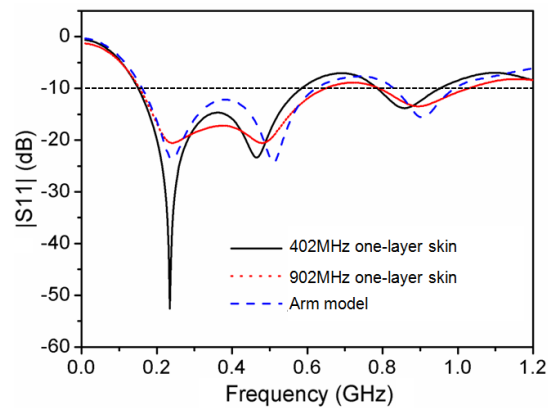


Fig. 2.17: The reflection coefficient of the antenna in [51].

Monopole antennas were also proposed in [53, 54] as shown in Fig. 2.18.

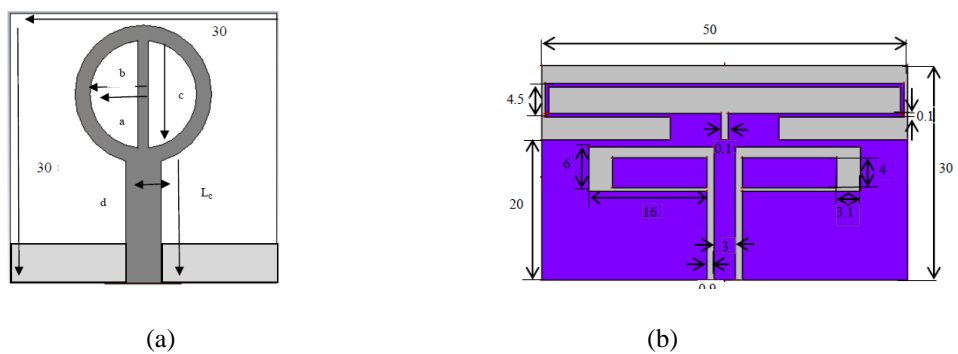


Fig. 2.18: The monopole antenna in: (a) [53], (b) [54]; units: mm.

Those antennas worked for the 2.45 GHz ISM band and at 686 MHz. However, these antennas were large in size.

A dual band (MedRadio and 2.45 GHz ISM) antenna was proposed in [11] as shown in Fig. 2.19. That design obtained 20.4 and 35.3% simulated and measured 10-dB bandwidth around the MedRadio band as shown in Fig. 2.20. However, it had narrower simulated and measured bandwidth of only 4.2 and 7.1%, respectively around the 2.45 GHz ISM band. More accurate evaluation should be conducted to validate performance and matching for the 2.45 GHz ISM band in the more realistic multilayer body model.

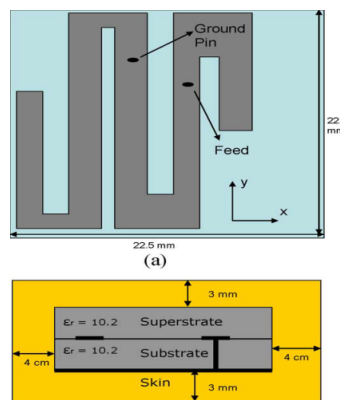


Fig. 2.19: The antenna in [11].

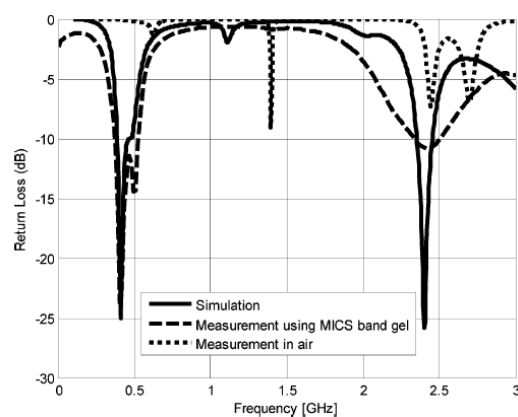


Fig. 2.20: The reflection coefficient of the antenna in [11].

Another dual band (MedRadio and 2.45 GHz ISM) antenna was proposed in [27] which is shown in Fig. 2.21. The design utilized a split ring resonator that was coupled to a

spiral to obtain dual band coverage and miniaturize the design to a size of $(13.5 \times 13.5 \times 5.1)$ mm³. However, both bands were very narrow as shown in Fig. 2.22.

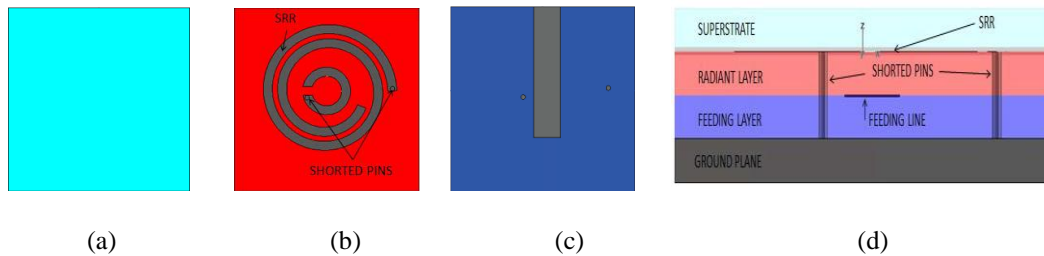


Fig. 2.21: The antenna in [27]: (a) Superstrate (b) SRR radiant layer (c) Feeding layer (d) Side view.

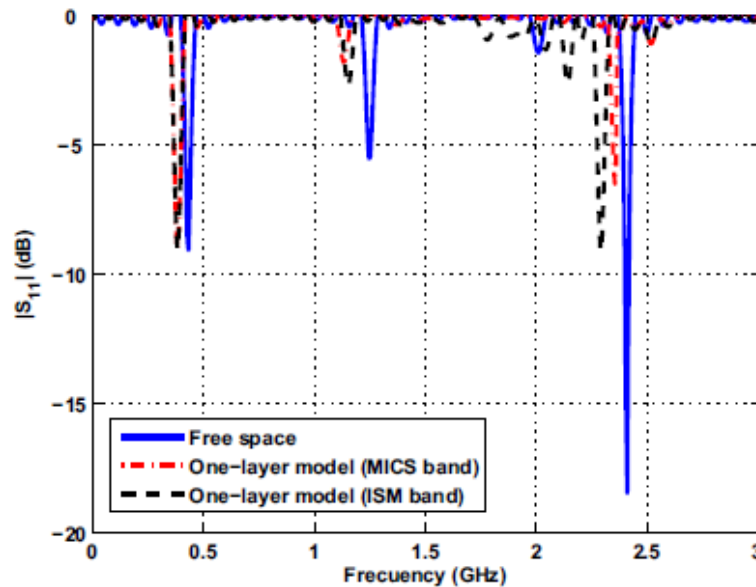


Fig. 2.22: The reflection coefficient of the antenna in [27].

All of the previous designs used the 2.45 GHz ISM band to save power consumption by exploiting a wake up receiver as the device transmits data only when is needed.

Multilayer stacked designs also obtained small sizes of $(10 \times 10 \times 1.9)$ and $(8 \times 8 \times 1.9)$ mm³ for the antennas in [55, 56], respectively as shown in Fig. 2.23. Those designs obtained wider than 50 MHz bandwidth around 400 MHz as shown in Fig. 2.24. However, that design utilized more than one rigid layer which probably increased the overall weight of the antenna

and implantable device. Moreover, the rectangular shape was not conformal to cylindrical implants.

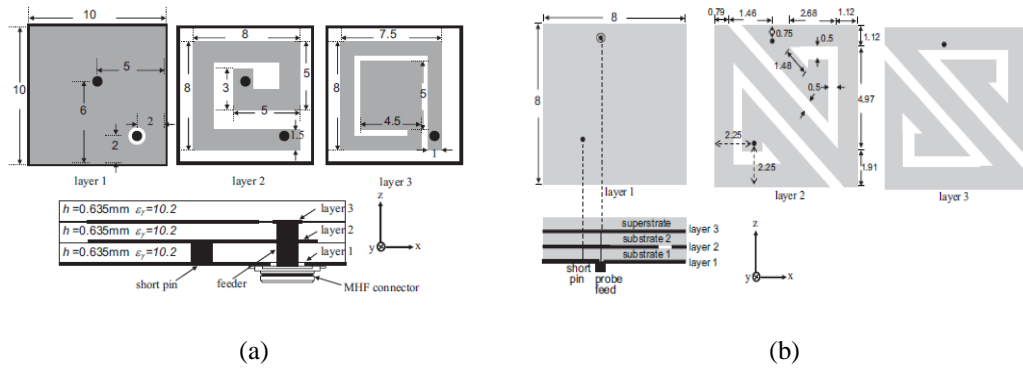


Fig. 2.23: The proposed antenna in: (a) [55], (b) [56].

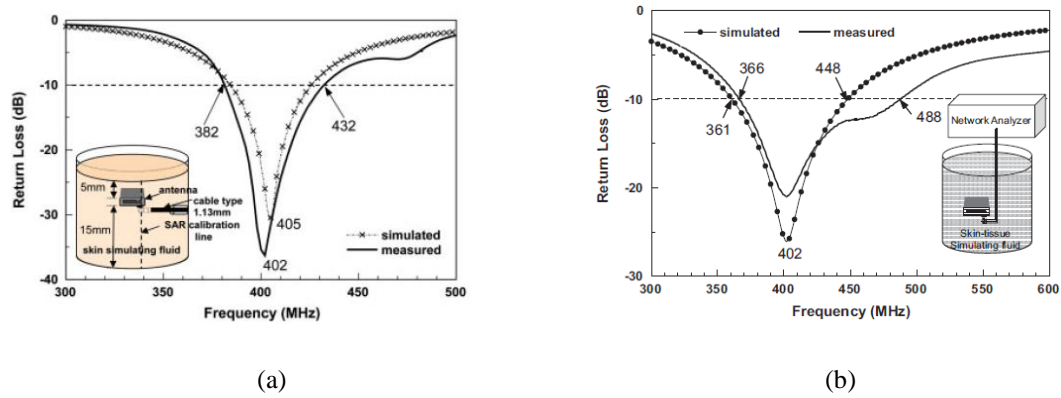


Fig. 2.24: The reflection coefficient of the antenna in: (a) [55], (b) [56].

Another multilayer antenna of circular patch was proposed in [57] for intra-cranial pressure (ICP) monitoring. The antenna is shown in Fig. 2.25.

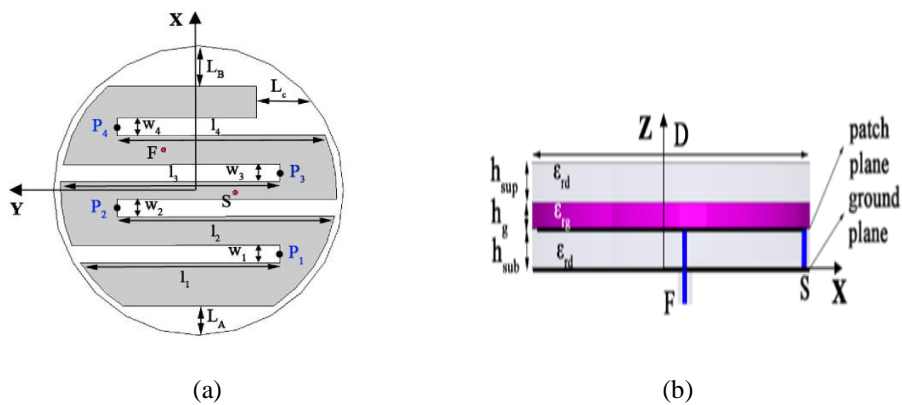


Fig. 2.25: The proposed antenna in [57]: (a) Top view, (b) Side view.

Although the antenna had a diameter of 24 mm, it had a very narrow bandwidth as shown in Fig. 2.26.

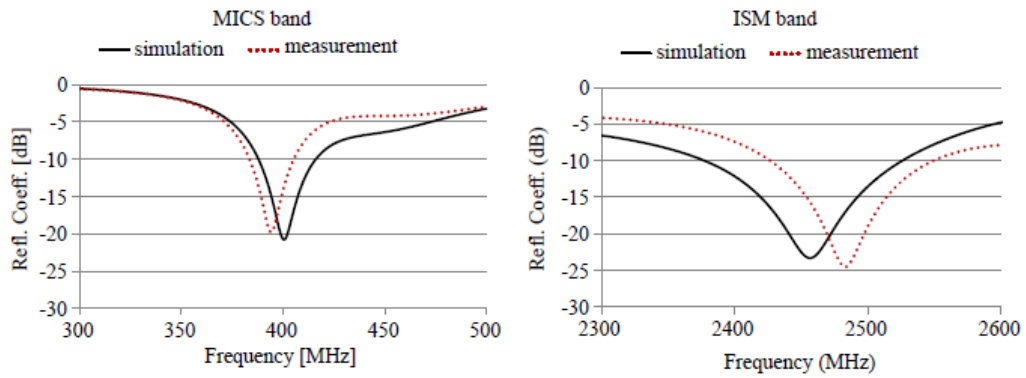


Fig. 2.26: The reflection coefficient of the antenna in [57]

Multilayer design that works for triple bands (MedRadio, 433 MHz and 2.45 GHz ISM) was proposed in [21] as shown in Fig. 2.27.

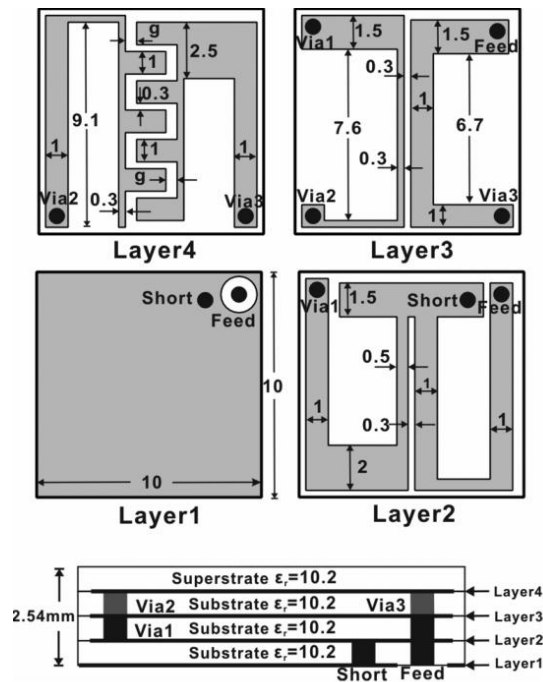


Fig. 2.27: The triple band antenna in [21].

Despite of the wide band coverage of almost 200 MHz around the MedRadio band as shown in Fig. 2.28, the frequency band around 2.45 GHz was very narrow.

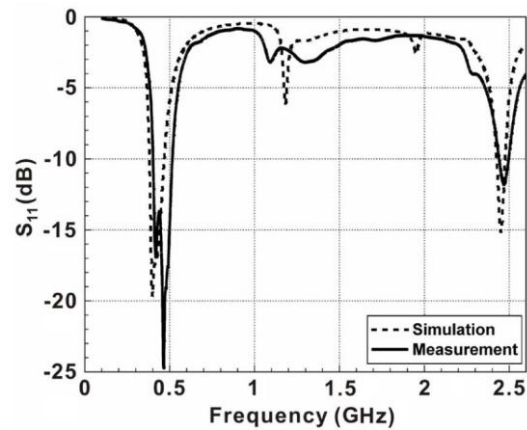


Fig. 2.28: The reflection coefficient of the triple band design in [21].

A multilayer S-shaped quad-band antenna for (401–406 MHz) MedRadio, (1427–1432 MHz) WMTS, and (433-434MHz and 2.4–2.4835 GHz) ISM bands was proposed in [58]. That antenna revealed a compact size of (10×10×2.45 mm³) as shown in Fig. 2.29. However, that antenna was composed of three substrates and one superstrate of Rogers 3210 which made the implant relatively heavy. Moreover, although the bandwidth of 200 MHz was obtained around the MedRadio band as shown in Fig. 2.30, narrow bandwidths were obtained around the other bands.

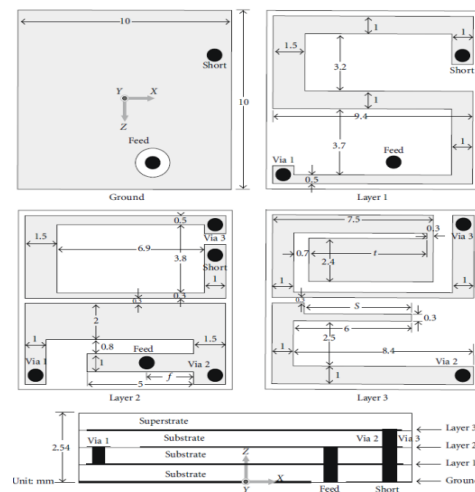


Fig. 2.29: The quad band antenna in [58].

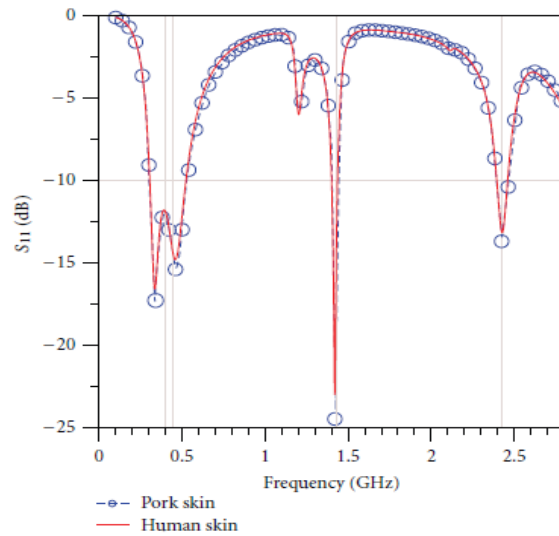


Fig. 2.30: The reflection coefficient of the quad band antenna in [58].

Antennas were also proposed for other frequencies; a three dimensional dipole antenna was proposed in [59] for retinal applications at 1.41 GHz. Another antenna was proposed in [60] for implantable applications at 1.575 GHz Global Positioning System (GPS) frequency band. The dimensions of both of these designs were $(1.6 \times 4 \times 2.8)$ and $(20 \times 10 \times 4.7)$ mm³, respectively. Antennas at much higher frequencies of 6.7, and 31.5 GHz were reported in [61, 62] for muscle/beneath skin and bone implants. However, it is obvious that much larger attenuations in the human body tissues are obtained at these frequencies in comparison with the MedRadio band.

Designs that are conformal to the implant structure were rarely proposed. A dual band antenna (the MedRadio and 2.45 GHz ISM) of a conformal ground was discussed in [7]. The design provided a good exploitation of the structure. However, the implant size was still large (5 mm in radius and 30 mm in length) and the antenna exploited a considerable internal space. Moreover, the antenna bandwidth was very narrow (< 20 MHz) around the MedRadio band and disagreement between simulations and measurements was obtained around the 2.45 GHz ISM band. That design and its reflection coefficient are shown in Figs. 2.31 and 2.32, respectively.

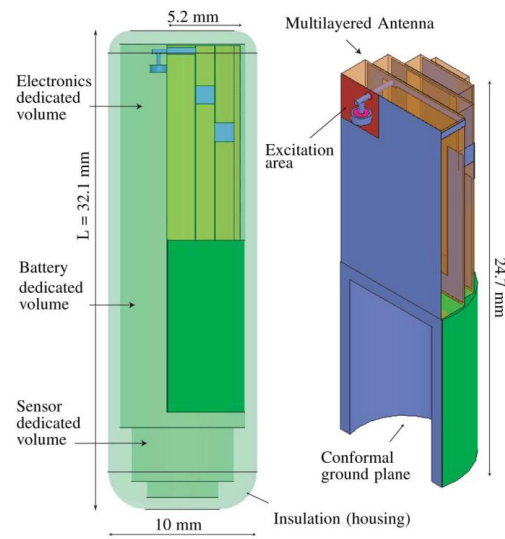


Fig. 2.31: The dual band conformal antenna in [7].

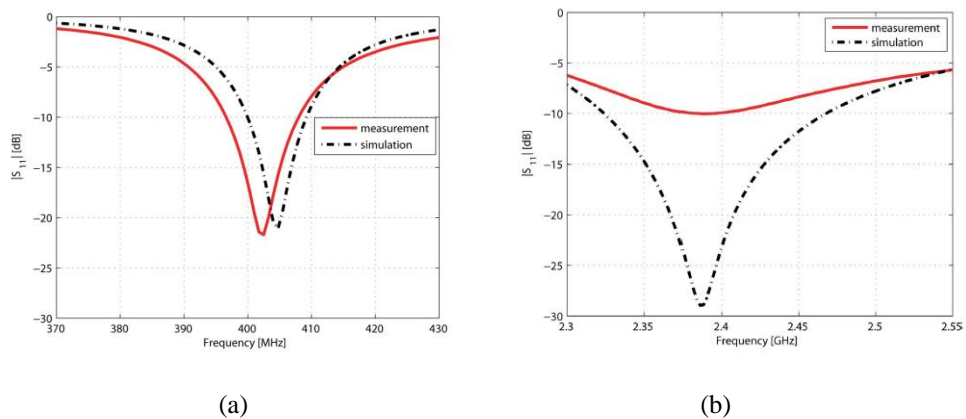
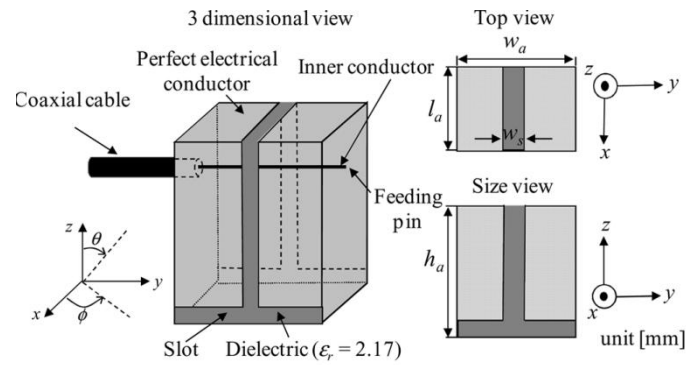


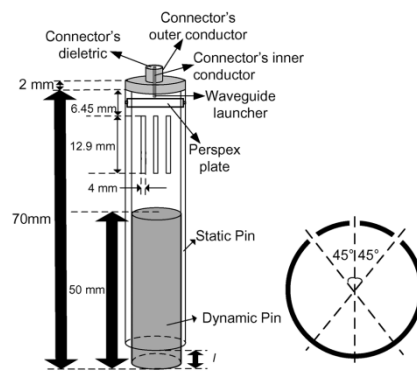
Fig. 2.32: The reflection coefficient of the conformal antenna in [7] for the: (a) MedRadio band, (b) 2.45 GHz ISM band.

Other conformal designs obtained conformity using a slot such as the antennas in [32, 48]. These antennas are shown in Fig. 2.33.

Some conformal designs for pacemaker applications were proposed in [63, 64] as shown in Fig. 2.34. A 3D ground is considered to allocate the necessary electronics.



(a)



(b)

Fig. 2.33: The conformal slot antenna in: (a) [48], (b) [32].

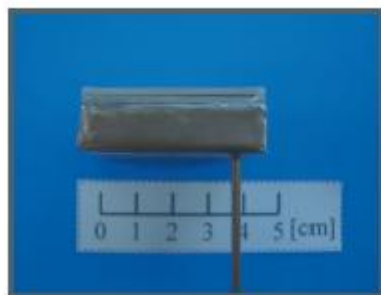


Fig. 2.34: The conformal slot antenna in: (a) [63], (b) [64].

It should be mentioned that the above mentioned designs were proposed for far field bio-telemetric applications where the receiver was placed in free space at a distance of over two meters. Other embedded antennas were also proposed for near field applications where the external receiver is worn by the human or placed somewhere on the body. A popular

example of those applications is the wireless capsule endoscopy. The capsule has a cylindrical shape as shown in Fig. 2.35 [65] of (5-5.5) mm in radius and (14-17) mm in length. It also has two hemispheres on its top and bottom. The camera which takes photos or videos from the human body is placed in one of them. Several designs were proposed for wireless capsule endoscopy and most of them were conformal to its structure. Examples were provided in [65-67] as shown in Fig. 2.36. The reflection coefficients for these designs are shown in Fig. 2.37.

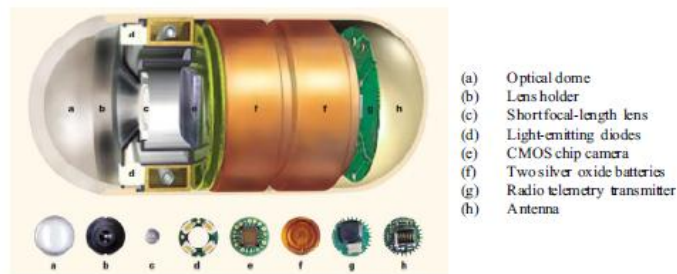


Fig. 2.35: A layout structure of a wireless capsule and its components [65].

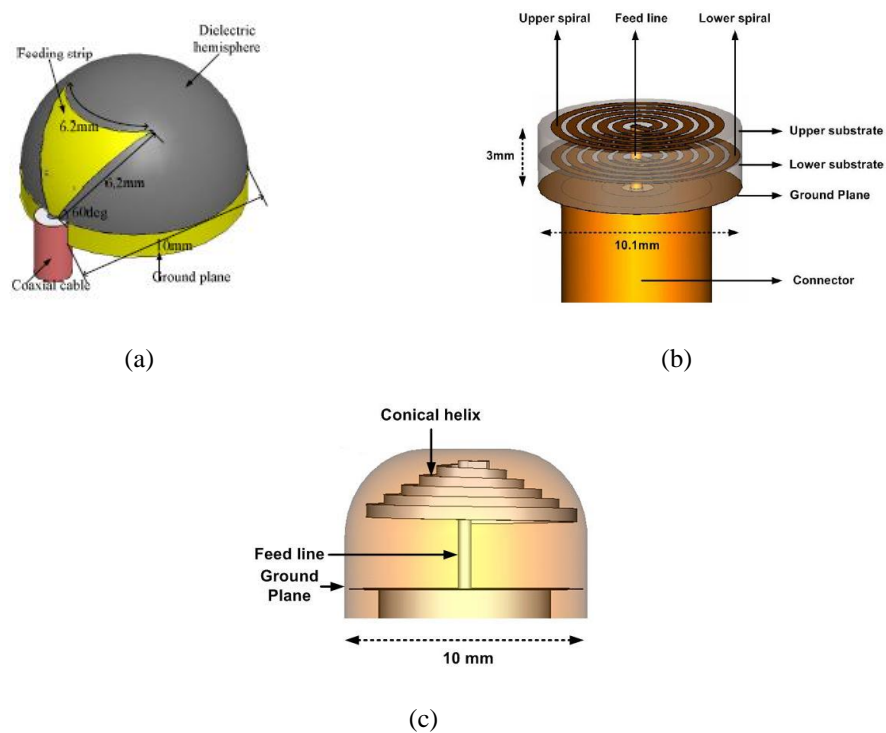


Fig. 2.36: The capsule antennas in: (a) [65], (b) [66], and (c) [67]

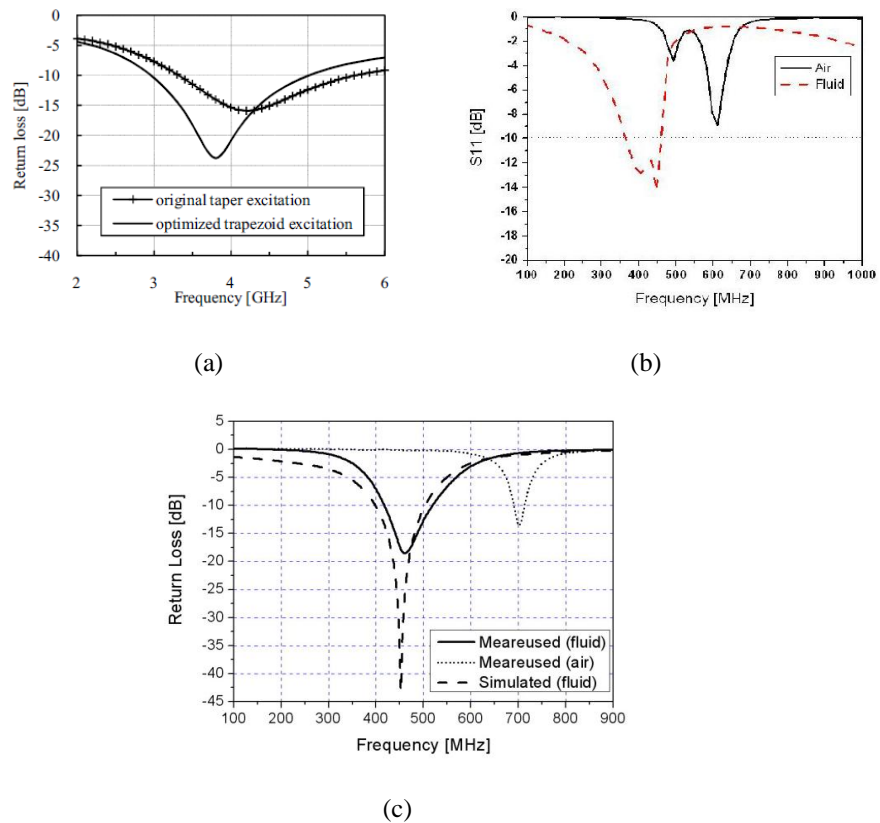


Fig. 2.37: The reflection coefficient of the capsule antennas in: (a) [65], (b) [66], and (c) [67].

Although the antennas in [66, 67] were conformal to the capsule structure, they were of a relatively narrow bandwidth that is around 100 MHz. This bandwidth is not enough to overcome the detuning which happens when the capsule passes through different organs of the digestive tract (the stomach, small intestine and colon). On the other hand, the dielectric resonator in [65] was of a heavy weight. Moreover, its ultra wide bandwidth was obtained over a band of high frequencies which are susceptible to larger attenuations in the human body tissues. Many other designs of similar radiator shapes were also proposed which were of the same main shortcomings. For example, a printed spiral antenna was proposed in [68] for gastrointestinal applications over short ranges (receiver in close proximity to the body) at low frequencies. Another capsule shaped printed antenna for short range communication was designed in [69] for relatively high frequencies (3.5-4.5 GHz).

As explained above, most of the proposed designs were heavy in weight and narrow in bandwidth. They also exploited a considerable space inside the implant. This restricts the battery size and implant life accordingly. Moreover, it restricts the number of sensors inside the implant and the variety of the implant applications accordingly (more sensors provide more functions). These problems also exist for the conformal embedded designs. However, they can be mitigated with the use of flexible designs which are thin and can be bent around the implant wall leaving extra space of internal components or reduce the implant size for the same components. Obviously, they can also reduce the implant weight significantly. Most of the existing flexible designs in literature are summarized in the following section.

2.3.1.2 Flexible Implantable Antennas

In order to facilitate bending, implantable antennas need to be thin which strict the techniques of miniaturizing them. While PIFA was a good option for rigid embedded designs as explained above, it cannot be easily obtained for flexible designs of a very thin substrate and radiator. This makes meandered and spiral radiators suitable for such flexible designs. However, spiral radiator is difficult to design over a loop structure that is preferred for magnetic applications as this requires a thick third dimension (the substrate thickness).

Few flexible designs were proposed for bio-telemetric applications. A folded slot dipole was proposed in [16] to work for the 2.4 GHz ISM band. Although that design was surrounded fully by a biocompatible layer, it was large for real implants. That design and its reflection coefficient are shown in Figs. 2. 38 and 2. 39, respectively.

Another folded dipole antenna was proposed in [70]. The proposed antenna in that design was fabricated from a narrow strip with a width of 0.1 mm and bent into a folded structure; the whole size was of $(20.3 \times 0.8 \times 0.8)$ mm³ in size and the gap was 0.5 mm as shown in Fig. 2.40.

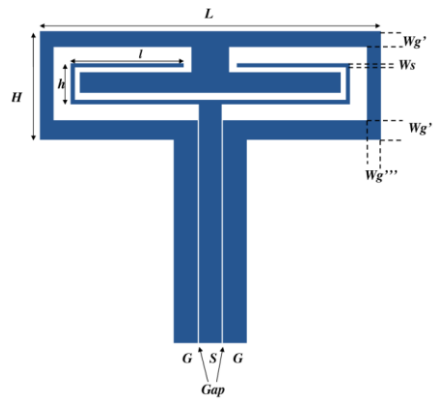


Fig. 2.38: The folded slot dipole antenna in [16].

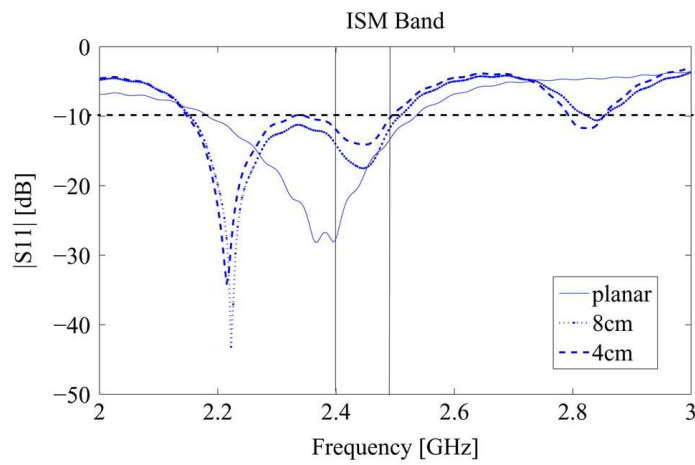


Fig. 2.39: The reflection coefficient of the folded slot dipole in [16] for planar and bent structures around cylinders of 4 and 8 cm.

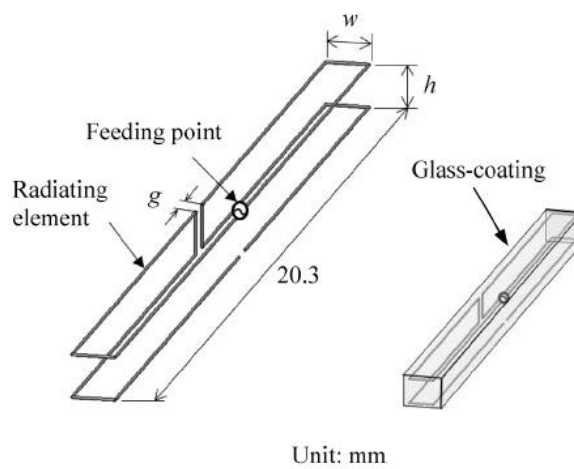


Fig. 2.40: The folded dipole antenna in [70].

The antenna worked for the UHF (0.951-0.956 GHz) as shown in Fig. 2.41. Therefore, it obtained a maximum gain of -23.5 in a human arm. It should be pointed out here that although the attenuation is larger at around 0.95 GHz, a larger gain value is obtained due to the larger antenna electrical size at this frequency [3]. However, the free space loss is much larger at this frequency than at around 400 MHz. The antenna matching was much better without a glass coating. Therefore, a more accurate evaluation at different tissues of implantation in the multilayer anatomical body models was supposed to be conducted to evaluate matching robustness with the glass coating.

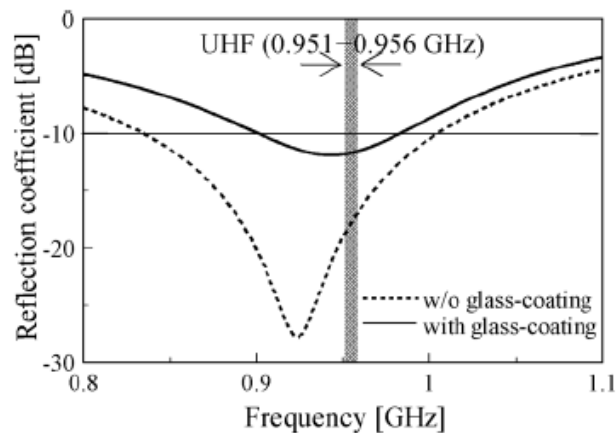


Fig. 2.41: The reflection coefficient of the folded dipole in [70] with and without coating.

A broadband UHF implanted 3D conformal antenna for implanted central venous catheters (CVC) was designed in [17]. The antenna was used for a truncated cone of 16 and 10 mm base and upper radii, respectively and 10 mm in height. The antenna around the cone implant is shown in Fig. 2.42. The antenna worked for a broadband range from below the (401-406 MHz) MedRadio to above the 2.45 GHz ISM band as shown in Fig. 2.43. It is obvious that the broad bandwidth is obtained due to the larger physical dimensions of the antenna in comparison with other implantable antennas. The measured gain is -28.95 dBi and -36.9 dBi in vertical and horizontal polarization, respectively in the MedRadio band and -25.5 dBi and -19.9 dBi, respectively at 2.45 GHz in a simplified body model of rectangular shape and the following size (355×255×160) mm³. The antenna broad bandwidth was

attributed to its large dimensions. Although that antenna had obtained good characteristics in general, the antenna was not evaluated in the anatomical body model.

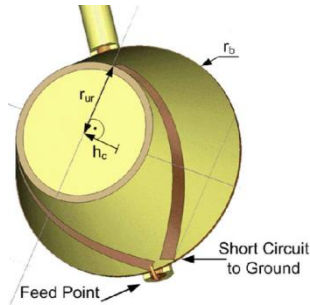


Fig. 2.42: The broadband 3D conformal design in [17] around a cone implant.

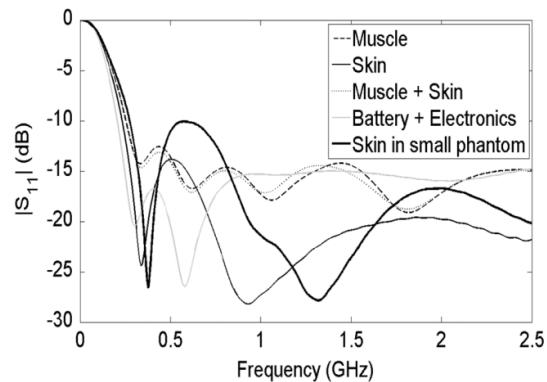


Fig. 2.43: The reflection coefficient of the broadband 3D conformal design in [17].

A hybrid of Archimedean spiral and Hilbert based curve 3D-folded antenna was designed in [71] and fabricated on ceramic denture (ZrO₂) to work for the MedRadio band for the purposes of health monitoring. That design structure and reflection coefficient is shown in Figs. 2.44 and 2.45, respectively.

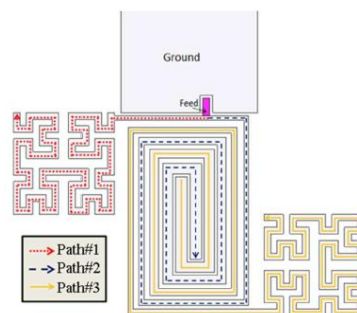


Fig. 2.44: The conformal antenna in [71].

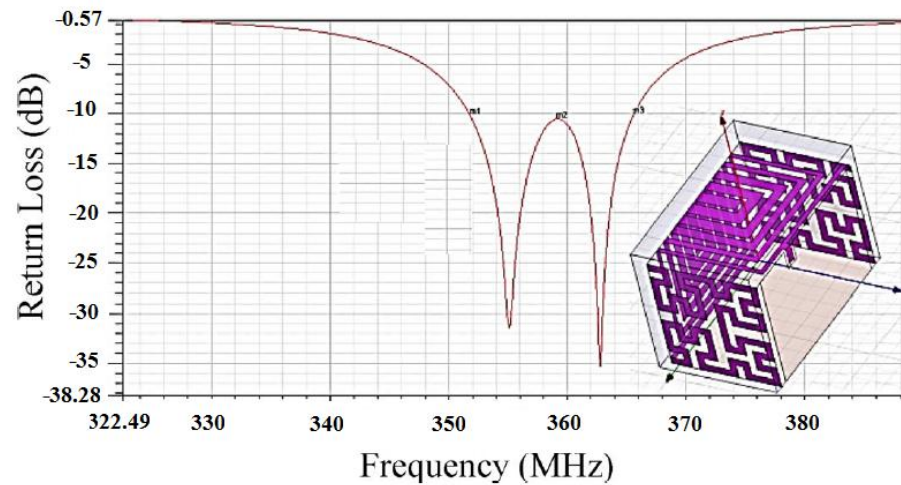


Fig.2.45: The reflection coefficient of the antenna in [71].

The antenna exploited the structure efficiently to maximize the antenna bandwidth and obtain a maximum gain of -6.78 dBi at around 400 MHz. However, the small size of the human body part of implantation which is the mouth helped in obtaining this gain value as the losses of the smaller human body tissue are smaller. Therefore, the antenna radiation efficiency and gain were larger in this case.

Flexible designs were also proposed for capsule endoscopy. An outer wall loop antenna was proposed in [42] for a capsule of 5.5 mm in radius and 28 mm in length as shown in Fig. 2.46. The antenna had an ultra-wide bandwidth (370-630 MHz) for $S_{11} < -10$ dB as shown in Fig. 2.47. That antenna obtained a robust performance at different organs of the digestive tract due to its ultra-wide bandwidth. Despite of the good characteristics and robust performance of that antenna, the communication link between that antenna and an external antenna was only evaluated over a short distance of 15 cm. Moreover, it cannot be used for children capsules which should be much smaller in size.

Fig. 2.48 shows another flexible antenna which was proposed in [72]. The antenna was a meandered dipole with an offset feed as shown in Fig. 2.47. The offset feed worked to

improve that antenna matching to cover the 1935-1400 MHz WMTS band as shown in Fig. 2.49.

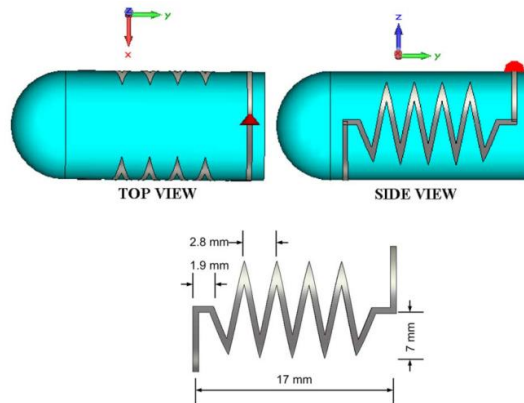


Fig. 2.46: The outer wall loop capsule antenna in [42].

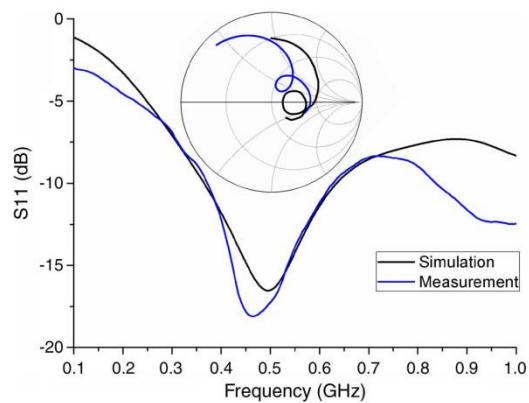


Fig. 2.47: The reflection coefficient of the outer wall loop capsule antenna in [42].

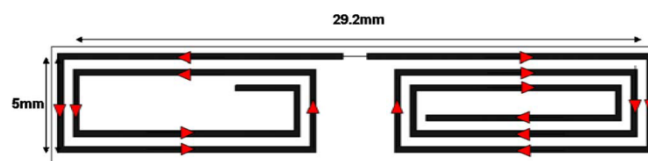


Fig. 2.48: The conformal meandered capsule antenna in [72].

A conformal design with a CSRR top loading layer was proposed in [18]. However, it was of a single and narrow band (2.45 GHz).

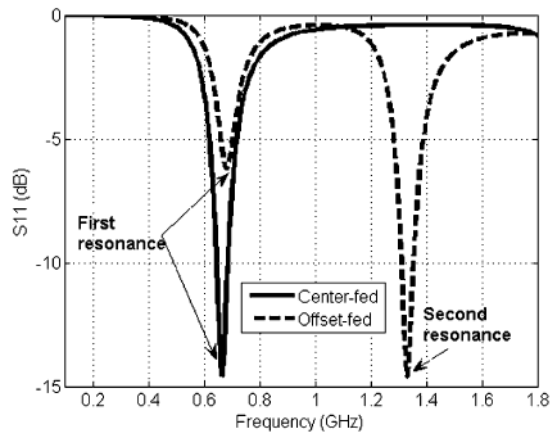


Fig. 2.49: The reflection coefficient of the conformal meandered capsule antenna in [72].

A zigzag dipole capsule antenna for medication compliance monitoring was realized by inkjet printing in [73]. That antenna worked for a large frequency at around 6 GHz. The design structure and its reflection coefficient are shown in Figs. 2.50 and 2.51, respectively.



Fig. 2.50: The Zigzag antenna in [73] printed directly onto surface of 00 size gelatin capsule.

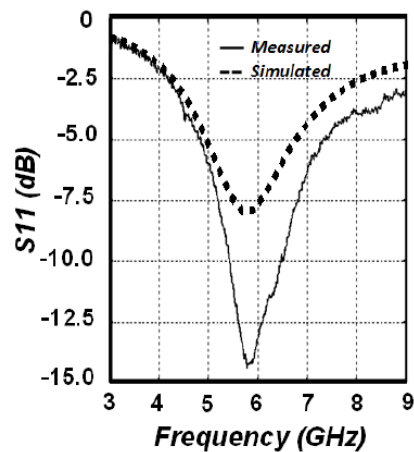


Fig. 2.51: The reflection coefficient of the Zigzag capsule antenna in [73].

The summary shows that although some conformal and flexible designs were proposed, they did not satisfy all the conditions for a successful implantable antenna design. The wide and broad bandwidth has been obtained at the cost of a small radiation efficiency and large size. Moreover, a study of the structure optimization for maximizing radiation over a broad bandwidth was not investigated for all of these designs. Therefore, new designs that can overcome the shortcomings of the previous flexible designs are needed.

2.3.2 Evaluations in the Anatomical Body Model

The antenna design usually begins in a simplified body model of a small size. This is to save the simulation time and accelerate the overall design process. However, these body models do not represent the asymmetric and multilayer structure of the real body. The reliability and validity of using simplified body models to evaluate overall antenna characteristics are studied in Chapter 4. However, it is important at this stage to review the simplified body models which were used for the design and evaluation of implantable antennas. Different simplified body models of different shapes, structures and dimensions were used in literature. Cylindrical and rectangular body models of a single layer were used to evaluate muscle, beneath skin and bone implantable devices [7, 16, 17, and 42]. These body models were homogeneous and mainly of skin and muscle equivalent materials. These body models showed a good tool of evaluating the reflection coefficient of antennas in the arm and chest where a slight frequency detuning was obtained after the actual implantation in the real human body [3]. This is because antennas were placed in muscle or beneath skin in both cases. However, it is important to point out that these body models are not reliable for evaluating the radiation characteristics of implantable antennas (this will be further explained in Chapter 4). Multilayer (skin, fat, muscle and bone) simplified body models were also used in [12, 16]. However, they were still far from the actual multilayer structure of the body model which is of random distributions of tissues. Moreover, small thicknesses

of skin and fat layers were used for these body models [16] representing the external layers around the muscle. A single layer, elliptic body model was also used in [74] to evaluate capsule antennas due to its better resemblance of the trunk structure. On the other hand, spherical body models were used to evaluate antennas in the head [12, 75]. Some of those body models are shown in Fig. 2.52. An elliptic cylindrical body model is used in this thesis. This model is specifically selected for this work because of its intermediate performance between the cylindrical and rectangular body models. While the reflection coefficient is found to be almost the same for different body models, the radiation efficiency can be overestimated in the rectangular body models (more details will be provided in Chapter 4). Although, the reflection coefficient is unaffected by the body shape, it is influenced by its equivalent material. The large relative permittivity of the human body tissues shifts the resonant frequency down in comparison with the case of free space according to equation (2.25):

$$f_r = \frac{f_0}{\sqrt{\epsilon_r}} \quad (2.25)$$

where f_0 is the resonant frequency in free space (Hz). This equation shows that the resonant frequency will differ in the different body tissues based on their relative permittivity. While a large variation between the muscle, bone and fats are expected because of the large difference in their dielectric properties [31], less difference is expected between muscle and skin. Although, the relative permittivity in the simplified body model mainly refers to the tissue in which the antenna is directly implanted, the value of the effective relative permittivity is difficult to be exactly determined in the anatomical body model which has different asymmetric layers.

It should be pointed out that the comparison between the antenna performance in different body models is inaccurate. This is mainly due to the different radiation characteristics in different simplified body model. The simplicity, uniformity and

homogeneity of simplified body models result in inaccurate evaluation. Therefore, an accurate evaluation in the more realistic anatomical body models should be conducted.

Anatomical body models provide the optimum vehicle to study and explain the internal and external structures of the human body. Different simulation tools (CST [76], HFSS [77], etc) provide these anatomical body models. The CST Voxel family will be used in this thesis. It is a group of seven human model voxel data sets created from seven persons of different gender, age and stature [78] as shown in Fig. 2.53 and their characteristics are summarized in Table 2.1

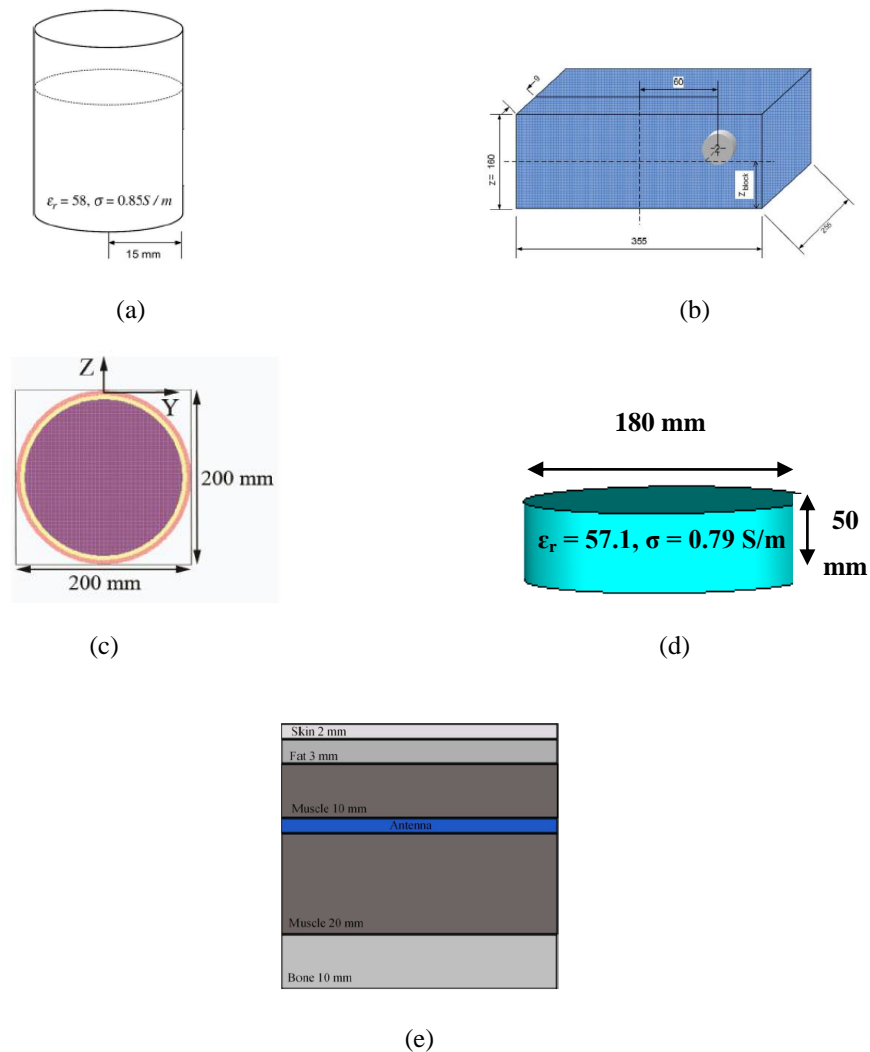


Fig. 2.52: Examples of simplified body models: (a) Cylindrical in [42], (b) Rectangular in [17], (c) Spherical in [75], (d) Elliptical cylindrical in this work, and (e) Multilayer in [16].

Human body tissues are age and gender dependent. In addition, the structure of the human bodies and their tissues differ from one person to another. For example, Laura has a smaller fat layer thickness in comparison with Emma. This affects the overall effective permittivity around the antenna and thus different resonance and radiation characteristics of the antenna are expected in these body models.

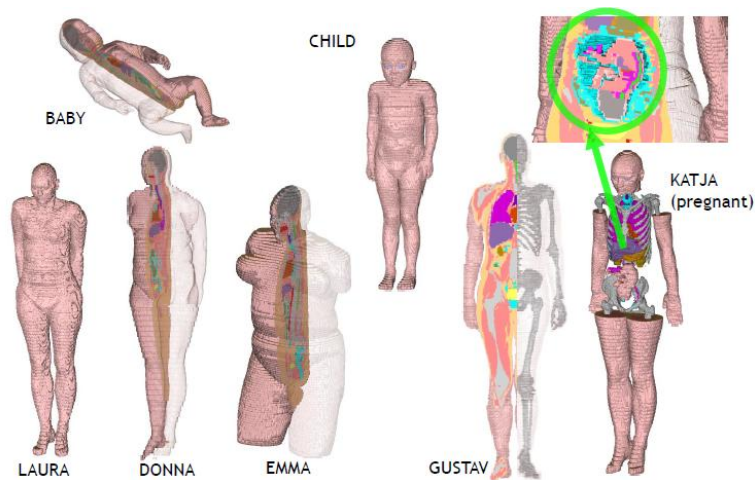


Fig. 2.53: The CST Voxel body models [78].

These body models need a license to be imported for use. The appropriate frequency which defines the material properties of the voxel data model tissues can also be selected. Special simulation specifications are required to guarantee a good performance inside them. For example, point ports have to be used instead of the face ports. In addition, to overwrite voxel material which replaces all other (even PEC) material of any priority, its mesh priority should be set to -1 and the priority for all other material to greater or equal zero [79].

A cross section of the internal structure of two positions inside these body models is provided in Fig. 2.54. The figure shows the complicated structure of the human body model and the difficulty of determining an exact equivalent relative permittivity around the implantable antenna. Therefore, the exact positioning of the antenna in a logical practical position (beneath skin directly) is not an easy task. This multilayer structure makes the

antenna performance affected by its position and the surrounding material. Further investigations will be provided in Chapter 4.

Table 2.1: Main characteristics of the CST Voxel family members [78]

Model	Age/Sex	Heigh (cm)	Mass (Kg³)	Resolution (mm³)
Baby	8-week female	57	4.2	0.85×0.85×4.0
Child	7y female	115	21.7	1.54×1.54×8.0
Donna	40y female	176	79	1.875×1.875×10
Emma	26y female	170	81	0.98×0.98×10
Gustav	38y male	176	69	2.08×2.08×8.0
Laura	43y female	163	57	1.875×1.875×5.0
Katja	43y pregnant, 24w	163	62	1.775×1.775×4.84

Most of the previous studies aimed at validating the implantable antenna design in a more realistic body model. The implantable antennas in [3, 70] were evaluated in the area above the left and hip and arm, respectively of an anatomical body of an adult. On the other hand, the design in [72] was evaluated in the area above the hip and in the digestive tract, respectively. Another antenna was also evaluated in an anatomical head model [14]. However, in all those studies simulations and evaluations were only conducted at a single position. The performance of two different antennas (dipole and spiral PIFA) was evaluated in [12] at two positions (the head and beneath chest, respectively). However, the performance of each antenna performance was not compared at the two positions. Therefore, the effect of the different tissues on each antenna performance was not studied and

generalized. The characteristics of the dipole antenna in that reference were also compared in spherical and real head models at a single position. The shoulders effect on the radiation pattern was also studied in that reference. The study only compared the near and far electric field intensities and the radiation pattern between the two cases.



Fig. 2.54: A cross sectional top view of a cylindrical implantable device (encircled in blue) in the: (a) Area above the left hip, (b) Arm of an anatomical CST adult model.

The general effect of implantation in the anatomical body model on the radiation pattern was highlighted in [80]. However, that effect was only indicated and not investigated for a specific antenna type.

The frequency detuning and impedance mismatch of implantable antennas were studied and quantified inside the human body in [81]. Four anatomical models of two adults and children were used. The resonant frequency and reflection coefficient were compared at different organs and tissues of implantation. They were also compared between the adult and child body models. The maximum frequency shifts in the different body tissues and models were derived. However, that study was only conducted on the reflection coefficient. Further evaluation of the overall antenna radiation characteristics should be conducted.

As the human body tissues are asymmetric, the implantable device is surrounded by different body tissues. The thickness of each tissue also differs around them even for the same tissue material. Therefore, the antenna performance and characteristics are expected to differ for different orientations. This was briefly indicated in [19] for a rotating capsule

antenna. However, investigations about the SAR only were conducted in that reference. The influence of antenna rotation on the in-out body path loss was also studied in [30]. However, the rotation around two perpendicular axes on the capsule cylinder was investigated in that reference. The orientation effect around the same axis should be investigated to select the optimum orientation of implantable device during the surgery process.

2.3.3 Metamaterials for Implantable Antennas

Metamaterials are of many attractive characteristics. They can be used to miniaturize antennas and improve the overall radiation from some of them [54, 82]. They were used for different biomedical applications such as medical imaging and microwave hyperthermia. Due to a higher focusing resolution, the left-handed metamaterial (LHM) lens had the potential to acquire higher imaging resolution and easy in-depth scanning, which will simplify the detection system design [83]. The most prominent property of metamaterial lens is the ability of negative-refractive index (NRI) to focus the electromagnetic field of a source. Hence it can generate appropriate focusing spot in biological tissue as required in microwave hyperthermia treatment [84]. However, these applications were in the near field of the antenna. Metamaterials were rarely used for biomedical telemetry (in the far field antenna region). The design in [27] used a split ring resonator (SRR) to miniaturize the antenna. It also obtained resonance at another frequency band by coupling the SRR to a spiral. However, that design was rigid and of very narrow bandwidths. A conformal design with a CSRR top loading layer was proposed in [18]. However, it was of a single and narrow band (2.45 GHz) design. A series of fully implantable and resorbable metamaterial devices resonant at terahertz frequencies was fabricated in [85] by patterning SRRs made of electrically conductive biocompatible and biodegradable magnesium onto a silk substrate composed solely of protein and water with controllable degradation rate. It should be pointed

out here that biodegradable implants and exploiting terahertz frequencies for implantable applications are beyond the focus of this work.

Performance of an insulated electric dipole antenna that was coated with a layer of a double negative (DNG) metamaterial operating in a lossy medium was considered in [86]. That antenna bandwidth was significantly improved with that coating. However, that was obtained for the cost of reducing the radiation resistance. Moreover, the effect of the coating with DNG on the overall antenna characteristics was not thoroughly investigated.

A study of using metamaterials to reduce the SAR in the human head was performed in [32]. It was found that the specific absorption rate (SAR) in the head can be reduced by placing the metamaterials between the antenna and head. The SRR was designed to display a stop band at the frequencies of interest for SAR reduction. 27.57 and 37.62% SAR reduction was obtained at 900 and 1800 MHz bands, respectively for the cellular phone. That was obtained at the cost of reducing the radiated power from the antenna by 13.5 and 4.87% at these bands, respectively.

An interesting feature of metamaterials or metamaterials modified structures is their ability to control the electromagnetic near fields of the antenna [24, 82]. This could be very useful for implantable applications as the radiated power is increased by reducing the electric near field of the implantable antenna. All these features of metamaterials or metamaterials modified structures have motivated the investigations in Chapter 5 about using them for implantable applications.

2.3.4 Estimation of Body Path Losses

The implantable antenna plays a major role in different wireless communication channels. The previous investigations in this area are reviewed in the following sub-sections:

2.3.4.1 In-In Body Communications

A wireless body area network (WBAN) is a network, consisting of nodes that communicate wirelessly and are located on or in the body of a person. There are various applications for such a network in the areas of medicine, sports and multimedia [28]. Considering a multi-implant case, the implants can communicate with the pacemaker/central hub present in the body which then can communicate with a receiver placed outside the body. Because of the human body complexity, not too many studies were conducted to estimate the in-body channel and path losses. An experimental investigation into the in-body channel in 400 MHz MICS Band was conducted in [87] by taking into account the joint effect of human movement and multipath effects, the measurements have been conducted in a populated office at very short distances. The channel path loss in homogeneous body models was characterized in [88-90] at 2.45 GHz. Those investigations were conducted in a homogeneous body phantom of a large (equivalent to an adult) size and muscle equivalent properties. However, the homogeneous body model does not provide an accurate resemblance of the real human body which is heterogeneous. Moreover, the homogeneous muscle equivalent body model overestimates the overall loss in comparison with the heterogeneous body model [3]. This is because it is mainly composed of muscle. Muscle has much larger losses than other tissues such as fat. The performance of an implantable antenna in a homogeneous and heterogeneous human body shaped model is compared in Appendix B. Although paths and channels were characterized in [28] in a heterogeneous body model at 2.45 GHz, the orientation effect of the implantable antenna and device on its performance was not evaluated and quantified. Moreover, up to the author's best knowledge no losses were estimated at 403 MHz inside a heterogeneous body model.

2.3.4.2 In-On Body Communications

For the case of in-on body communications such for the wireless capsule endoscopy, the implantable antenna communicates with a wearable or on-body receiver. The path loss and its variation in terms of system frequency and location of the capsule were presented in [20] along with guidelines about the optimum system frequency for WCE. The difference between the maximum and minimum path loss at different anatomical regions was also quantified in that reference. However, (10×10×D (up to 17 cm (varying))-shaped, sliced tissues from the selected locations were only used rather than using the whole body. This is expected to underestimate the path losses. Our investigations show that losses may be underestimated by more than 1 dB when only some parts of the body model are used in simulations.

The communication between an implantable dipole and a receiving loop antenna was evaluated and compared with and without a buffer layer in [91]. The buffer layer has a dielectric constant between air and human body model. Therefore, it reduces the reflections at the boundary between them. The benefit of using a loop antenna is highlighted in that reference. However, the performance between a loop and a more directive antenna was not compared to generalize a conclusion about the optimum antenna type for such investigations.

An investigation about the advantages, disadvantages and tradeoffs of applying directive antennas to implant-on boy ultra wideband (UWB) communications was conducted in [92]. It was concluded that directive antennas can reduce unnecessary exposure of human body tissues to electromagnetic radiation, reduce exposure to near band interference and save energy. However, when directive antennas are used, receive/transmit beam direction needs to be guaranteed. It is important to point out that directive antennas such as log periodic or horn are non-conformal to the body surface. On the other hand, planar antennas such as a patch which can be designed to have relatively large gain values than loop antennas are electrical

in type. This means that they are much susceptible to losses than magnetic type antennas. This will be further investigated in Chapter 6.

A communication link between a capsule meandered loop antenna and an on-body receiver over 15 cm was experimentally evaluated in [42] at 500 MHz. However, a simplified body model of an equivalent homogeneous muscle material was used.

2.3.4.3 In-Off Body Communications

The implantable antenna works with an external device that is normally controlled by a physician. Most of the proposed implantable antennas were designed and evaluated to obtain this function at a distance of over 2 meters [3, 17]. Numerical and experimental investigations of biotelemetry radio channels and wave attenuation in human subjects with ingested wireless implants were introduced in [29]. The study covers commonly used frequencies in telemedicine applications: ultrahigh frequencies at 402 MHz, 868 MHz and the industrial, scientific and medical (ISM) band frequency at 2.45 GHz. A numerical electromagnetic analysis is applied to model in/off-body radio propagation channels and the resulted parameters demonstrated the importance of digital phantom accuracy in the characterization of wave absorption and attenuation with regards to organ contents, specifically for the digestion system. Path gain variations of biotelemetry radio channels, in the close vicinity of the subject, with wireless implants were measured using a near field scanner. Simulation results were verified with measurement in good agreement.

The signal propagation characteristics for mm-size neural implants were modeled in [93]. Animal tests were carried out, proving the validity of the simulation model of the neural radio link over a wide range of frequency from 100 MHz to 6 GHz. This is due to the much more symmetry around the implant for this case in comparison with other channels such as from the arm. Both of these studies in [29, 93] were conducted with a receiving

antenna which is placed in the near field region of the implantable antenna. Further work is required to quantify and highlight the effect of changing orientation and polarization of the wireless implant and body on the overall telemetry system performance.

Wireless power transfer between the implantable antenna and an external receiving one represents an important example on the in-off body communications in the near field. The 433 MHz ISM band is normally used for these applications [21]. A distance of up to 50 cm is preferred to guarantee an efficient power transfer. Many antennas were proposed for wireless power transfer [21, 94]. In all these designs, overall estimation of the path losses between both antennas was not provided, although such estimation is very important to quantify the required input power that should be provided to the antenna to satisfy the link budget at a specific distance.

2.3.5 Models and Methods of Measurements

Measurements of implantable antennas are very challenging. A body mimicking phantom is required to conduct the measurements. Moreover, the cable contributes to the antenna radiation. Two types of measurements are normally conducted:

- In Vitro test; using simplified body phantoms and pork.
- In Vivo test, using living animals such as rats and pigs.

2.3.5.1 In Vitro Test

It is very risky to implant the antenna directly into the human and animal body without an accurate and full evaluation of the implantable antenna and device. Therefore, the implantable antenna is normally measured firstly in simplified body phantoms. These phantoms can be realized from liquid, gel and pork. Liquid body phantoms are of the following characteristics:

- Homogeneous.
- Easy to prepare from distilled water, sugar and NaCl (commonly available as dishwasher salt [3]). The percent of each component is controlled to obtain the dielectric properties of a specific body tissue. For example the following percentages of 51.3, 47.3 and 1.4% for water, sugar and salt, respectively obtain the dielectric properties of muscle at 403 MHz ($\epsilon_r = 57.1$, $\sigma = 0.79$ S/m). However, the resultant dielectric properties should be measured using some equipments such as Agilent 87050E dielectric probe [95]. This is to check the resultant value and add more percentages of these ingredients if needed. An example is illustrated in Fig. 2.55.
- Conformal to any container shape.

Most of the previous designs [3, 42] used these body models due to their easy and quick realization.



Fig. 2.55: An example illustrates the measurement of liquid body phantom dielectric properties [3]

Gel phantoms can be prepared by adding toxic HydroxylEthylCelulose (HEC) (1% of it to the above percents mimics muscle at the MedRadio band [3]) to provide rigidity for a tissue mimicking structure. The following characteristics are common for gel body phantoms:

- Of a longer preparation time than liquid body phantoms.
- Homogeneous.
- Rigid, easy to move and fix.

An example of a skin mimicking gel was presented in [11] and shown in Fig. 2.56. Water, sugar and NaCl salt were used for its preparation. The recipe was provided for the MedRadio and 2.45 GHz ISM bands in that reference.

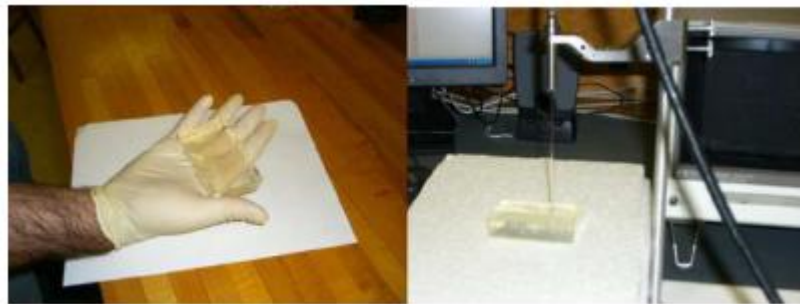


Fig. 2.56: A skin mimicking gel [11].

Pork was also used in some references [21]. Pork has the following features:

- Heterogeneous. This saves the required time to prepare different phantoms for different frequencies.
- Of asymmetric tissues distribution which is of better resemblance of the real human body.
- Can be used directly without a preparation. This saves the time and effort which are needed to prepare liquid and gel phantoms.

An example that illustrates using pork for measurements is shown in Fig. 2.57.

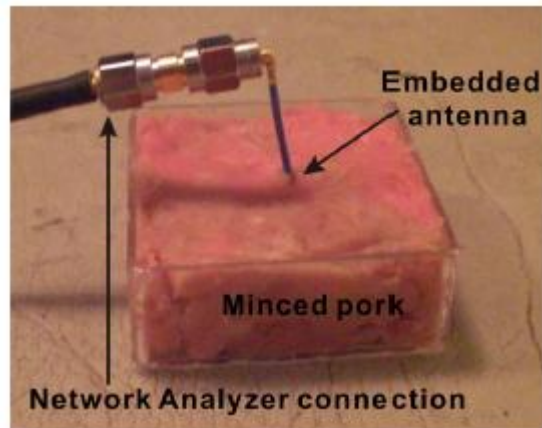


Fig. 2.57: Pork for implantable antennas measurement [21]

Pork can be used as slices or mince. Both of liquid body phantom and pork are used in this thesis.

For accurate overall measurements, the implantable antenna should be isolated from the surrounding body phantom. This is to reduce the cable effect. In fact, the currents present on the external surface of the outer conductor are dissipated in the high loss materials (constituting the simulating body tissues) [96]. This contributes to further radiation and variations of the reflection coefficient. This effect will be further discussed and evaluated in Chapter 3.

2.3.5.2 In Vivo Test

Another test that is usually performed before actual long term implantation in the human body is the In Vivo test. This test provides a facility to evaluate the effect of in body temperature. Rats were used in [93, 97]. Examples are illustrated in Fig. 2.58. Two antennas of two different sizes were evaluated in [97] in different rats of different ages. It was found that the antenna of the smaller size was more sensitive to frequency detuning.

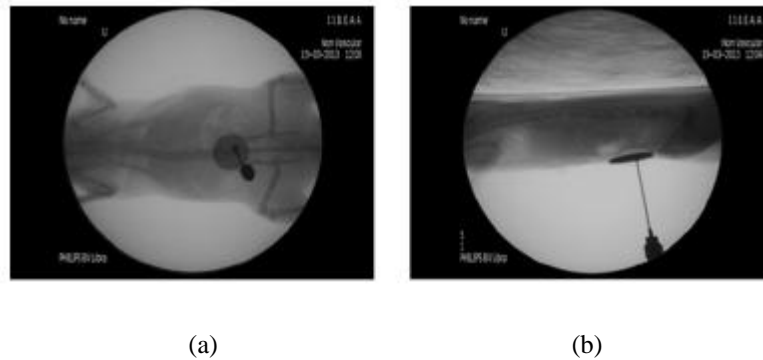


Fig. 2.58: X-ray fluoroscopy images indicating the implantable antenna site inside the rats: (a) Face view (b) Profile view [97].

Pigs were also used in [3, 93]. An entire implantable device was developed in [3] and implanted at different depths in the pig as shown in Fig. 2.59.



Fig. 2.59: An implantable device implanted at two different depths inside a pig [3].

Some physical parameters of that pig such as temperature were monitored by establishing communication with an external BSN unit at 2.5 meters above the cage over 15 days as shown in Fig. 2.60. It is worth mentioning that less detuning inside pig was obtained in comparison with the case inside rats.



Fig. 2.60: Monitoring of pork in-body temperature [3].

2.4 Summary

In this chapter, the general effect of the lossy human body on the implantable antenna performance has been reviewed and summarized. The lossy and multilayer structure of the human body:

- Absorbs most of the antenna radiation.
- Widens the antenna bandwidth.
- Changes the antenna radiation pattern shape and main lobe direction and magnitude at different positions.

The subject areas of the thesis were also reviewed in this chapter. The following points can be summarized:

- To guarantee a robust performance in the human body, the implantable antenna should be of a small size, light in weight, of a wide bandwidth, of good matching

and conformal to the implant structure. However, most of the previous implantable antennas satisfied some of these conditions only. Therefore, new antennas that satisfy all the requirements for a successful design and robust performance in the human body are required.

- Most of the previous antennas were either evaluated in simplified body models or at only one position or orientation in the anatomical body model. This not enough for an accurate validation of the implantable antenna performance. Therefore, thorough investigations in the anatomical body model should be conducted.
- New structures that may reduce the power absorption by the human body tissues around the antenna should be investigated. Therefore, metamaterials based structure which can reduce the electric near field and power absorption correspondingly is suggested and reviewed.
- The implantable antenna plays an important role in different body communication paths. Some previous studies investigated the overall losses of such communication paths. However, the loss of some application specific paths should be estimated and studied. The optimum on-body antenna type that improves the overall near field communication with the implantable antenna should also be investigated.

Chapter 3

Design of Flexible Implantable Antennas

3.1 Introduction

One of the most effective ways to minimize the weight and size of the implantable device is to use flexible antennas. The flexible antenna can be bent around the implant wall leaving most space for the internal components. This allows the use of bigger batteries for a longer implant life or more sensors for multiple applications. Flexible designs are of larger physical dimensions which enable a better structure utilization. For example, an antenna of wider parts is of a larger radiation efficiency (this will be further explained in this chapter). Moreover, larger antenna is of a wider bandwidth and gain [96]. Although, some flexible implantable antennas were proposed, they were of a large size and/or for the 2.45 GHz ISM bands where in-body attenuations and free space loss are larger than at the MedRadio (401-406 MHz) band [16, 17]. Because of the added values of flexible antennas in general and the shortcomings of the few existing designs (up to the author best knowledge, only one design at 2.45 GHz [16] for bio-telemetric applications in the far-field before this work was started), this thesis focuses on the design of efficient flexible antennas for bio-telemetric (far field) applications that satisfy all the requirements for a successful design (small size, light weight, large radiation efficiency and gain, wide bandwidth, performance robustness against material variations and long term implantation in the real human body). This chapter is mainly focused on the following objectives:

- Developing a general methodology to design flexible implantable antennas. The methodology considers the aspects of optimizing the antenna structure to maximize the antenna radiation. It also considers optimizing the antenna structure for a robust performance in the anatomical body model.
- Developing and designing several flexible antennas for implantation in different body tissues and sites (muscle, beneath skin and bone) which have the following desired characteristics:
 - Small size.
 - Cover the 401-406 MHz MedRadio band for data transmission and the 433-434 MHz ISM for wireless power transfer.
 - Have a wide bandwidth with good radiation characteristics. This wide bandwidth guarantees coverage of both bands of interest in the actual human bodies of different ages, gender and structures.
- Presenting the In vitro test results and a simple method in the lab to measure the robustness of the antenna performance against material and temperature variations.

To achieve these purposes, this chapter is arranged as the following: Firstly, the two-step design methodology is presented. This methodology is used to design several antennas for muscle/ beneath skin and bone implantation. In a following section of this chapter, different in vitro measurements are presented to evaluate and validate the performance of the proposed antennas in a human body mimicking liquid and pork.

The main achievements in this chapter are:

- A general methodology to design implantable antennas is developed. In comparison with the few proposed methodologies such as in [97], it is the only one that provides details about optimizing the antenna structure to achieve the maximum radiation and guarantees a robust performance in the anatomical human body.
- The smallest flexible implantable antenna that works for the MedRadio and 433-434.8 MHz ISM bands for $S_{11} < -10$ dB with a bandwidth of over 200 MHz are designed.
- A total knee replacement implantable antenna that works for the MedRadio band for $S_{11} < -10$ dB is designed for the first time.
- A bone implantable antenna that works for the MedRadio and 433 MHz ISM bands for $S_{11} < -10$ dB is designed for the first time.
- A simple procedure in the lab is used to measure the antenna performance robustness against material and temperature variations after an actual and long-term implantation in the human body.

3.2 A Methodology to Design Implantable Antennas

An efficient implantable antenna design requires the satisfaction of many requirements which combine conformity, light weight, wide bandwidth and robust performance. The antenna is also preferred to be of a magnetic type such as a loop which is of many attractive characteristics and more efficient in the nonmagnetic human body as explained before. To achieve these purposes, a general design methodology is formulated at this section. The

proposed methodology comprises two steps, the first step is the optimization in the simplified body model; this allows the selection of the optimum design structure and parameters within a relatively short time. The second step is the evaluation of the antenna in an anatomical body model for different orientations which allows refinement if needed and an accurate evaluation in the non-uniform human body. The optimization in the simplified body model takes the effect of the internal components and insulation layers into considerations. A schematic diagram of the methodology is shown in Fig. 3.1 and its parameters are discussed in the following sections.

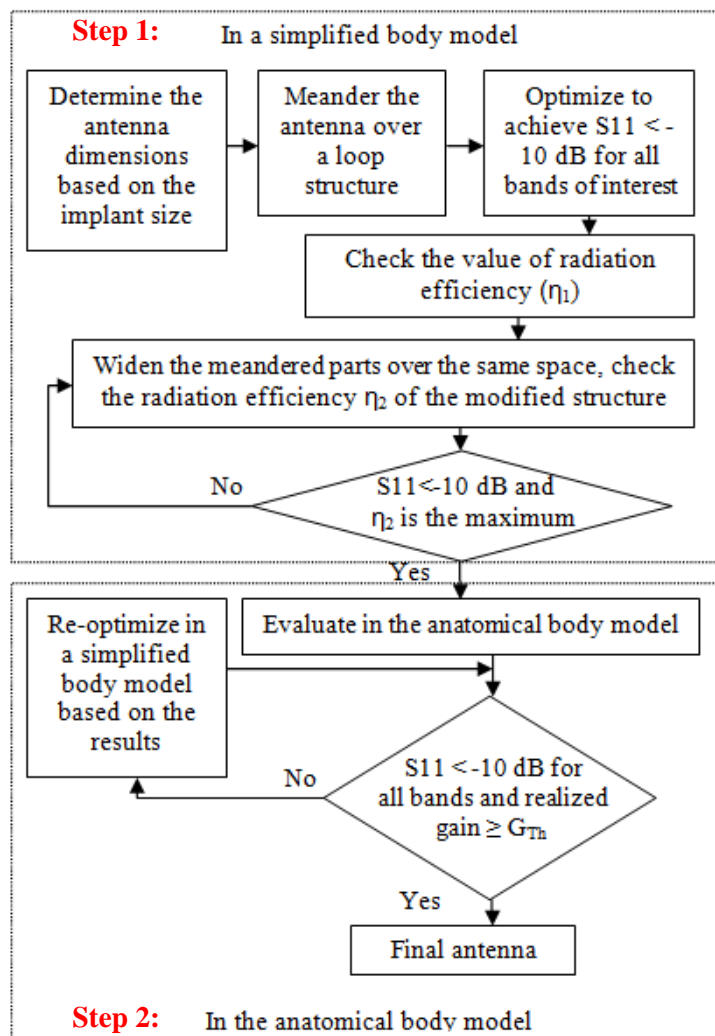


Fig. 3.1: The proposed design methodology.

3.2.1 The Methodology Parameters

The optimum parameters are defined and specified based on the pre-mentioned requirements and as the following:

- Antenna bandwidth of wider than 200 MHz for $S_{11} < -10$ dB around each band of interest in the simplified body model: this wide bandwidth is preferred to guarantee coverage of the targeted bands (MedRadio and 433 MHz ISM bands) for different positions and orientations in the more realistic human bodies. $S_{11} < -10$ dB is preferred as the antenna reflection coefficient is expected to be altered inside the anatomical body model and in different human body models. Hence, a good antenna matching will be always guaranteed. For example, if the antenna is optimized for $S_{11} < -6$ dB inside the simplified body model at this step, it might be disturbed to be $S_{11} < -2$ dB inside the anatomical body model which results in a large power reflection. On the other hand, if the antenna is optimized for $S_{11} < -10$ dB in the simplified body model, a good matching will be obtained for most cases even if the reflection coefficient is altered in the anatomical body model or in different body models.
- Antenna radiation efficiency and gain: it is found that wider parts of loop and meandered antennas lead to larger radiation efficiency. However, this is found to be accompanied with an up-shift of the resonant frequency. When the width of the vertical parts increases (W), the spacing (S) between them decreases (look at Fig. 3.2). This reduces the effective capacitance at the feed point and the resonant frequency is therefore increased [98]. Therefore, the optimum radiation efficiency is defined as the maximum one that can be

obtained for wider parts that allows the coverage of all bands of interest for $S_{11} < -10$ dB over the available physical space.

The first step is finished when the following conditions are all satisfied:

1. The maximum possible radiation efficiency is obtained.
2. $S_{11} < -10$ dB for the bands of interest (MedRadio band mainly).
3. A bandwidth of wider than 200 MHz around the resonant frequency (around 403 MHz mainly).

Although the simplified body model provides a reliable tool to evaluate the antenna general characteristics (the reflection coefficient and largest radiation efficiency and gain for a specific structure), it cannot be relied upon to provide an accurate and exact values of the antenna radiation characteristics as explained in Chapter 2. Therefore, the targeted gain values which are directly proportional to the antenna radiation efficiency are specified in the anatomical body model which is of much larger size and asymmetric. A realized gain (the implantable antenna gain and the body losses) of larger than or equal to -37 and -20 dBi are aimed at 403 MHz and 2.45 GHz, respectively in the arm of an adult anatomical body model which is enough to build a communication link of 20, and 2 meters at 403 MHz and 2.45 GHz, respectively considering the link budget in Eqs. (2.8-2.10).

It is worth mentioning that only step one is provided and discussed in this chapter while the evaluation step in the anatomical body model is presented and discussed in Chapter 4. The methodology parameters can be specified based on requirements and objectives of each system. Therefore, this methodology can be generalized for different systems. It has been used in the following sections to propose antennas for different implantable applications.

3.3 Flexible Antennas for Muscle/Beneath Skin and Bone Implants

3.3.1 U-Shaped Loop Antenna

As explained above, a loop antenna has been selected for the designs in this thesis. To make an antenna resonate at a relatively low frequency such as the case of implantable antennas, miniaturization is needed. To achieve this objective, the radiator of the proposed antenna is designed as a meandered structure so a longer current path is realized for the same available physical space. Meandered structure represents a good choice for loop and flexible antennas where only a very thin substrate layer can be exploited. In addition to meandering, the large dielectric permittivity of the human body tissues which surround the antenna will further reduce the resonant frequency of the antenna. The designs in this chapter consider the use of cylindrical structure of implantable devices which is a popular structure for many reasons (more conformal to the tissues and facilitate the surgery process). The first structure aims for implants of 5 mm in radius and 30 mm in length which are the dimensions of the implant in [7]. The benefit of using flexible substrate and radiator is very obvious at this stage where a total width of 30 ($\approx 2 \times \pi \times 5$) mm is exploited for this antenna. This is much larger than the dimensions of rigid antennas that need to be embedded inside an implant of 5 mm in radius. Following the proposed strategy, the antenna is firstly optimized in a simplified body model of an elliptic cylindrical shape which is shown in Fig. 2.52 of the following size ($180 \times 100 \times 50$ mm³) and of a muscle equivalent material to achieve the maximum radiation efficiency (0.21%) for this case and at the same time to work for the MedRadio and 433 MHz ISM bands for $S_{11} < -10$ dB. The antenna forms a loop when bent around the implant. The flat and bent structure views of the proposed antenna are shown in Fig. 3.2 and its dimensions are summarized in Table 3.1. The reflection coefficient is shown

in Fig. 3.3. The antenna has a broad band of around 250 MHz which is wider than the targeted 200 MHz bandwidth.

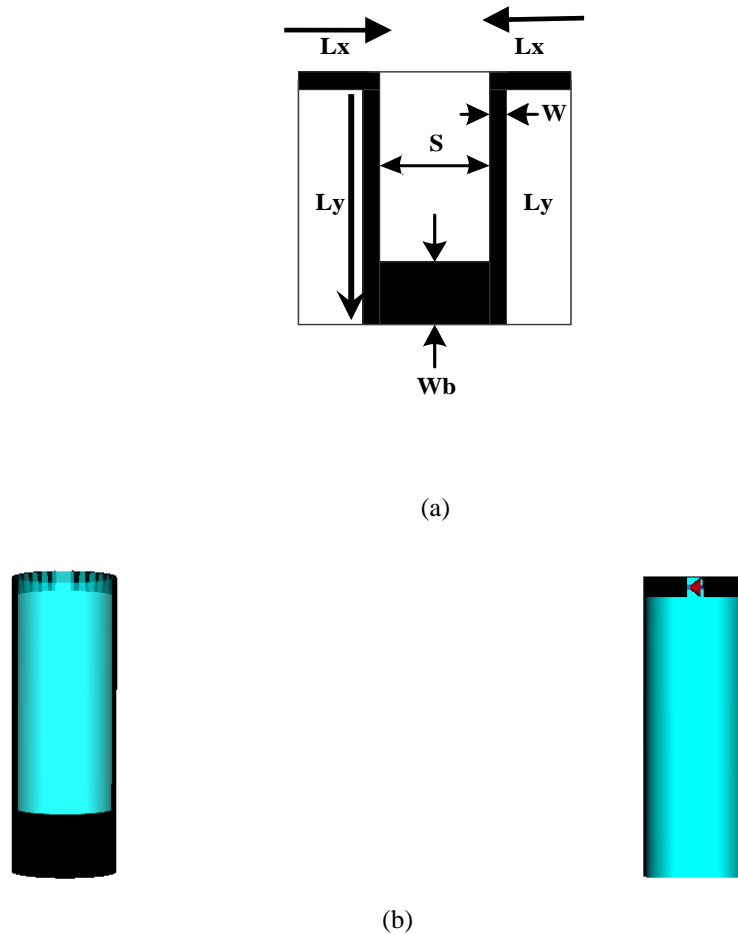


Fig. 3.2: 30 mm in length U-shaped loop antenna: (a) Flat structure (b) Bent structure.

Table 3.1: Dimensions of the proposed 30 mm length U-shaped loop antenna

Parameter	Symbol	Dimension (mm)
Length of the horizontal top arm	L_x	9
Length of the vertical arm	L_y	28
Spacing between the two parallel vertical arms	S	12
Width of the bottom part	W_b	7.5
Width of the horizontal top and vertical arms	W	2

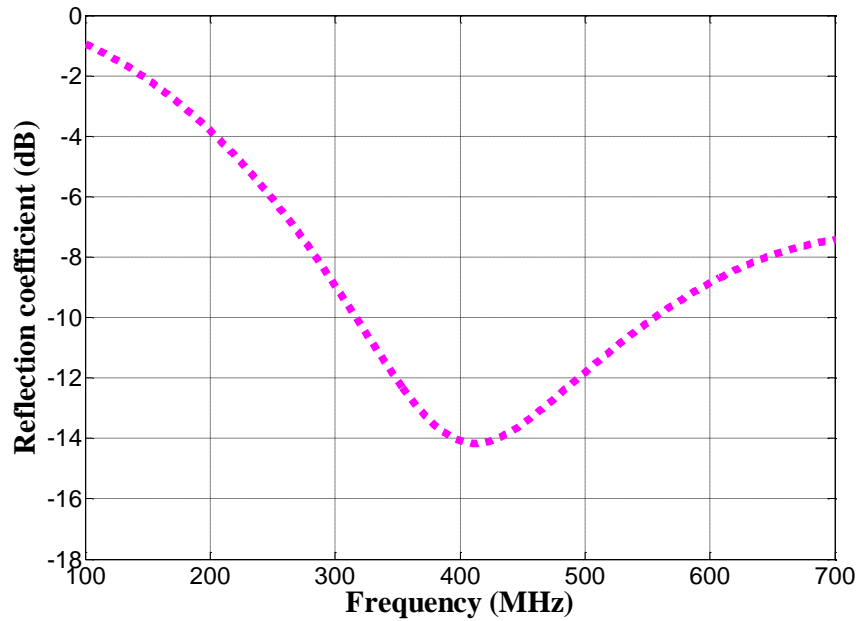


Fig. 3.3: The reflection coefficient S_{11} of the proposed 30 mm in length U-shaped loop antenna.

Following the same methodology and exploiting the effect of the width of the meandered parts on the resonant frequency and radiation efficiency, the same structure is optimized for a smaller implant of half the length (15 mm only). The new antenna structure is shown in Fig. 3.4. The width of the bottom part is minimized to 0.5 mm to compensate for the shorter distance between the horizontal meanders. For further down-shift of the resonant frequency, the spacing distance between the two parallel vertical arms is increased by 2 mm which is reflected on shorter horizontal top arms (1 mm less of each). The width of the other parts (excluding the bottom part) is kept the same.

The effect of this spacing distance on the antenna resonant frequency is further illustrated in Fig. 3.5 where simulations have been conducted with two different values of (S) (2 and 8 mm). It can be seen from the figure that the resonant frequency is shifted downwards from 490 to 423 and then 402 MHz but the bandwidth is increased with the spacing S from 2 to 8 and then 14 mm, respectively.

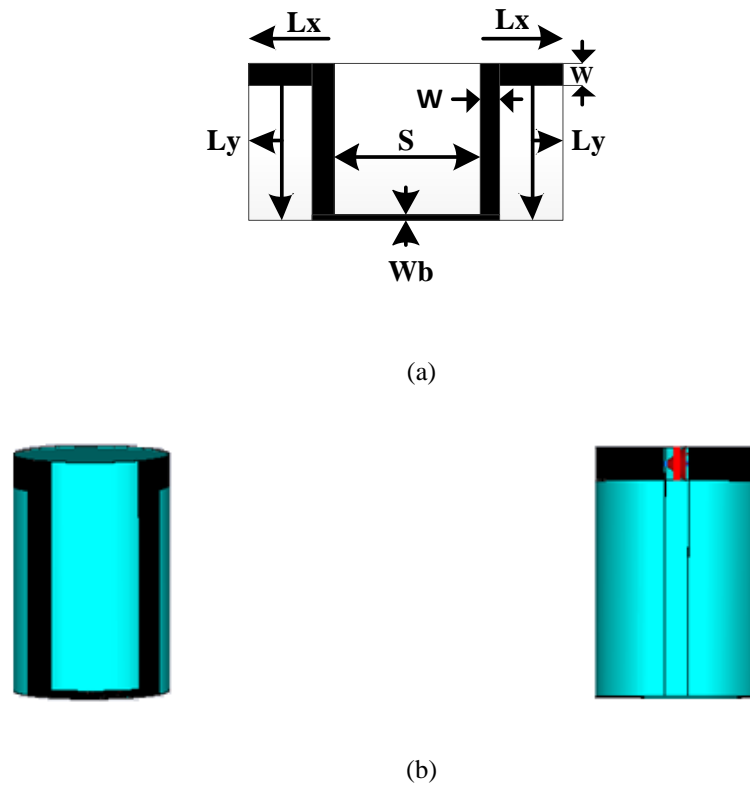


Fig. 3.4: 15 mm in length U-shaped loop antenna : (a) Planar view, (b) Bent view.

The structure has other important parameters, such as the spacing ($L_y - W_b$) between the horizontal meanders. The effect of this spacing on the resonant frequency of meandered antennas has been also discussed in [98]. It is found that increasing this spacing increases the self-inductance, and therefore, decreases the resonant frequency significantly. This effect is shown in Fig. 3.6 where the resonant frequency has been shifted down from 504 MHz to 402 MHz by increasing this spacing from 12 mm to 12.5 mm. It is also shown that the bandwidth is increased by around 50 MHz when ($L_y - W_b$) is increased by only 0.5 mm.

Based on the results, the final dimensions of the antenna are selected and summarized in Table 3.1 to provide resonance at 402 MHz and at same time to cover the 433 MHz ISM band with good frequency margins about both bands (the solid line in Figs. 3.5 and 3.6, respectively). The wide bandwidth (300-600 MHz) behaviour of this antenna is desired in order to cover both bands regardless of any frequency shift which may happen in reality due

to changes of the human body environment. The maximum obtained radiation efficiency and gain in the simplified body model (the elliptic cylindrical that is mentioned above) which achieves the design targets are 0.136% and -26 dB, respectively.

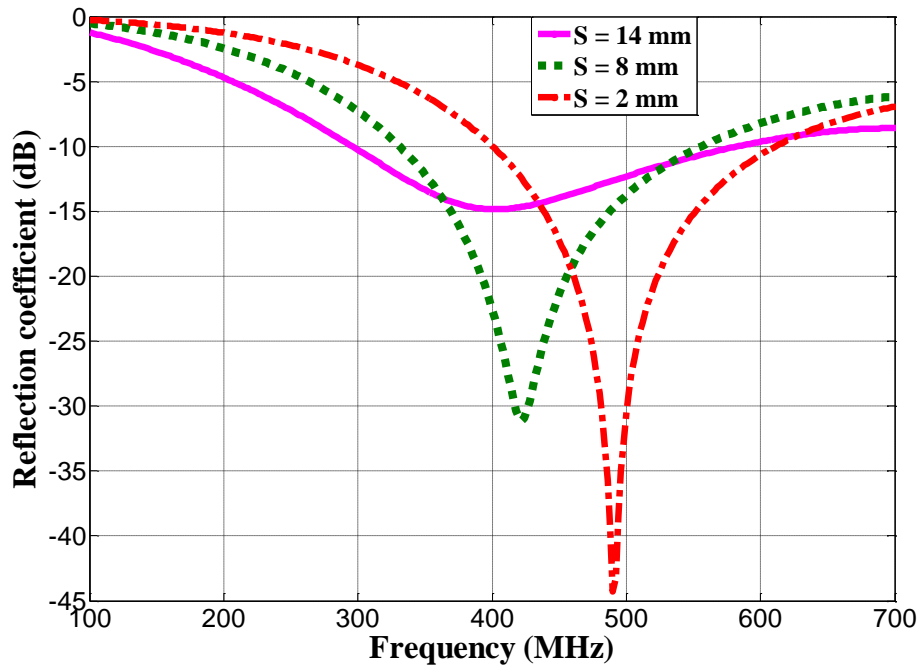


Fig. 3.5: The effect of spacing distance between antenna symmetrical halves (S) on the resonant frequency of the proposed 15 mm U-shaped loop antenna.

It is shown that almost the same matching and resonant frequency of both of these U-shaped loop antennas are obtained. However, a wider bandwidth is obtained for the 15 mm in length U-shaped loop antenna. This is wider bandwidth is obtained because S is larger for the 15 mm in length antenna as explained above. The exact (S) values are selected for each antenna to obtain the design targets as explained above.

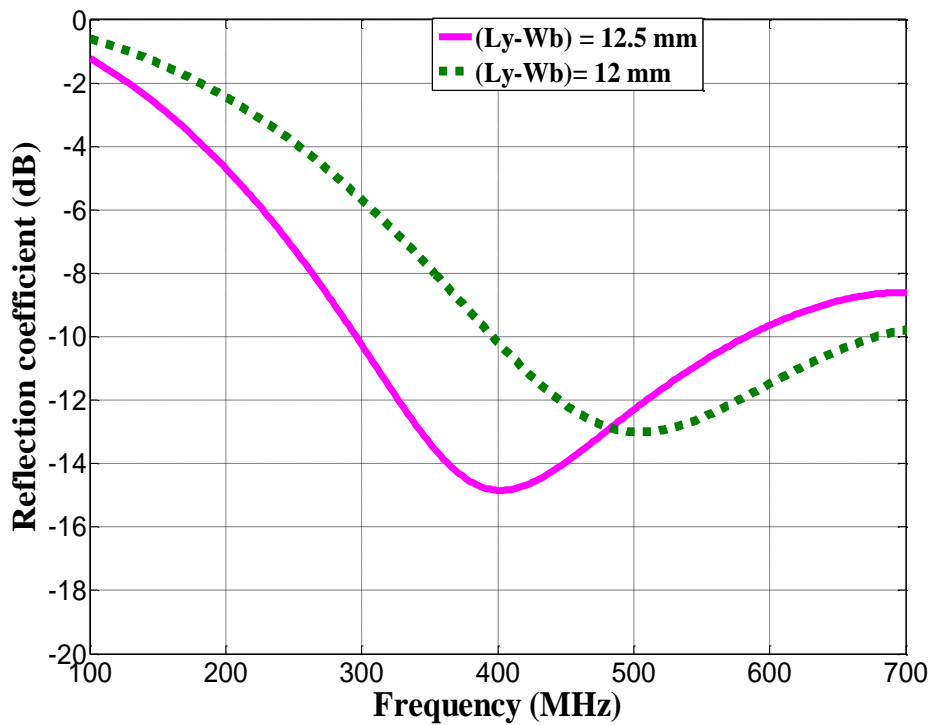


Fig. 3.6: The effect of the spacing ($L_y - W_b$) on the resonant frequency of the proposed 15 mm in length U-shaped loop antenna.

3.3.2 A Small Meandered Loop Antenna

Another antenna is proposed following the same strategy for a smaller implant that can be used for capsules for children [99]. Because the antenna and implant size is small, a smaller radiation efficiency and gain are expected. However, children bodies and organs present smaller losses because of their smaller sizes. The antenna size is minimized by adding more meanders and thus introducing a longer current path which results in a new structure. This antenna can be bent around implants of 3.2 mm in radius and 10 mm in length. This represents 56 and 50% smaller than the radius and length of the 15 mm U-shaped loop antenna. The antenna has also a wide bandwidth which covers both bands of interest.

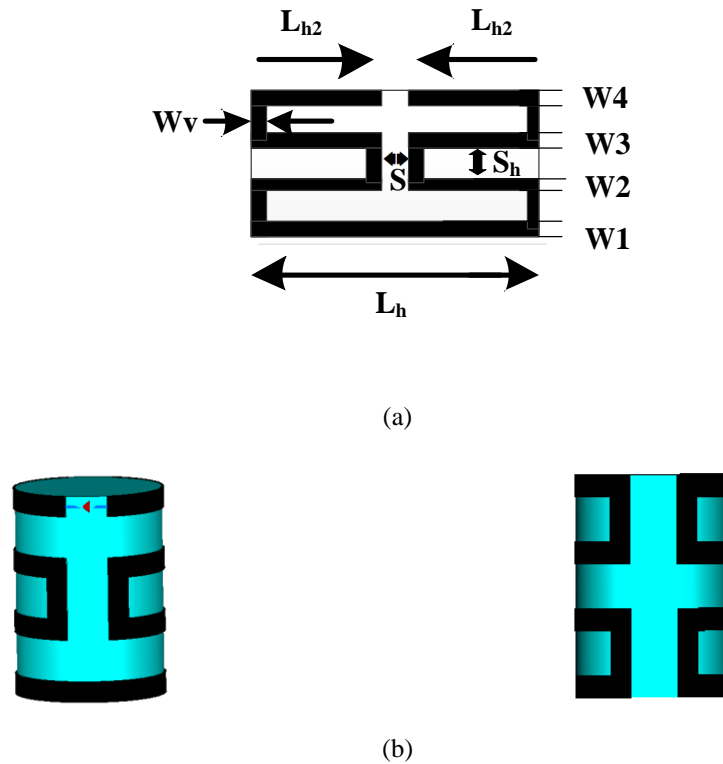


Fig. 3.7: 10 mm meandered loop antenna: (a) Planar view, (b) Bent view.

The antenna parameters have a similar effect to the proposed U-shaped loop antenna parameters and this is exploited very well to optimize the antenna design to cover both of the MedRadio (401-406 MHz) and 433 MHz ISM bands for $S_{11} < -10$ dB as shown in Fig. 3.8.

The final dimensions are summarized in Table 3.2 to obtain resonance at around 403 MHz and cover both bands of interest with a radiation efficiency of 0.074%. The maximum 3D gain is -28.4 dBi.

S controls the feed capacitance in a direct relationship for this antenna (the feed points and S are at the same plane unlike the case of the U-shaped loop antenna). This means that a narrower S will increase the feed capacitance and shifts the resonant frequency down (to obtain resonance at 402 MHz). Furthermore, it increases the antenna bandwidth in comparison with the case of smaller S values. As S is very small for this structure, the antenna has obtained almost the same bandwidth of the larger U-shaped loop antennas.

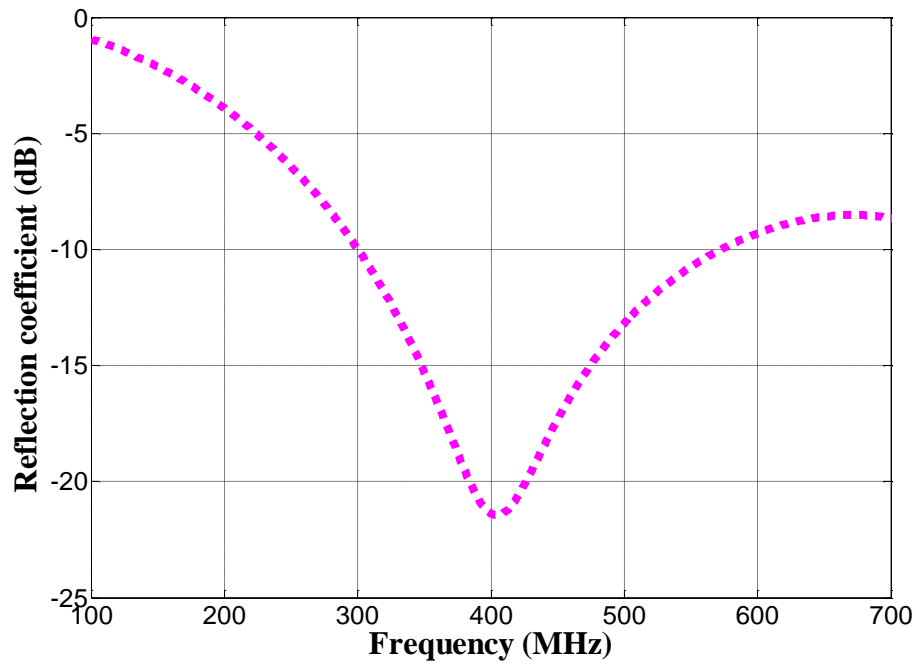


Fig. 3.8: The reflection coefficient S11 of the proposed 10 mm meandered loop antenna

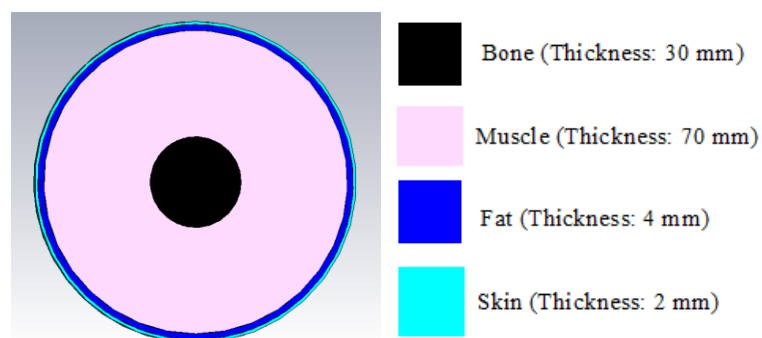
Table 3.2: Dimensions of the proposed 10 mm meandered loop antenna

Parameter	Symbol	Dimension (mm)
Length of the horizontal top meander	L_{h2}	9
Length of the horizontal bottom meander	L_h	20
Spacing between the two parallel vertical meanders	S_m	2
Width of the horizontal meanders	W_1, W_2, W_3, W_4	1
Width of the vertical meanders	W_v	1
Spacing between horizontal meanders	S_h	2

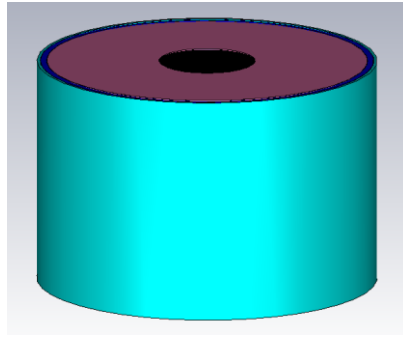
3.3.3 Antennas for Bone Implants

The position of implantation is based on the application of the implantable antenna. Muscle or beneath skin implants can be proposed for many applications such as cardiac

pacemakers, glucose and health monitoring [14, 11, and 100]. Implants in bone have also many important functions such as bone healing, growth and checkups of artificial joints [32, 101]. The dielectric properties of bones differ from muscle; ($\epsilon_r = 13.1, \sigma = 0.09$ S/m) and ($\epsilon_r = 22.43, \sigma = 0.24$ S/m) for bone cortical and cancellors at 403 MHz, respectively. Because these values are smaller than the corresponding values for muscles, further miniaturization is needed to allow resonance at the MedRadio band. However, bone implants are normally used to replace actual parts of bones and thus have normally large dimensions in order to achieve their functions [32]. Based on these characteristics and following the same strategy of designing flexible implantable antennas, a flexible loop antenna for bone implants is designed [102] at the centre of a multilayer cylindrical body model of bone ($\epsilon_r = 13.1, \sigma = 0.09$ S/m), muscle ($\epsilon_r = 57.1, \sigma = 0.79$ S/m), fat ($\epsilon_r = 5.6, \sigma = 0.04$ S/m) and skin ($\epsilon_r = 46.7, \sigma = 0.69$ S/m) at the MedRadio (401-406 MHz) band as shown in Fig. 3.9. The antenna is placed at the centre of the bone layer (the inner cylinder colored in black in Fig. 3.9). A multilayer structure is considered this time because muscle layers around bone are normally thick which affects the value of equivalent dielectric permittivity and conductivity around the implants.



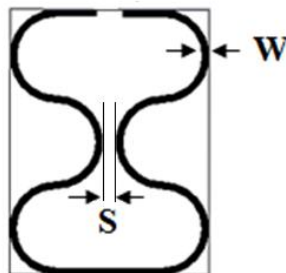
(a)



(b)

Fig. 3.9: The multilayer body model: (a) Top view, (b) Side view.

The antenna aims for implants of 5 mm in radius and 40 mm in length which is 30 mm shorter than the implant in [32]. Circular meander shapes are used for the design. The spacing distance between the vertical symmetric parts S is 2 mm, the width of each part (W) is 1 mm and the total radiator length is 137 mm. The antenna flat and bent structures are shown in Fig. 3.10.



(a)



(b)

Fig. 3.10: Circular meandered loop antenna for bone implants: (a) Flat structure (b) Bent structure.

The structure and length of the radiator are selected to work for the (401-406) MHz MedRadio and 433 MHz ISM bands for $S_{11} < -10$ dB as shown in Fig. 3.11. The antenna radiation efficiency and gain are 0.08% and -27.6 dBi, respectively at 403 MHz. This antenna is the first proposed flexible bone antenna that covers these bands.

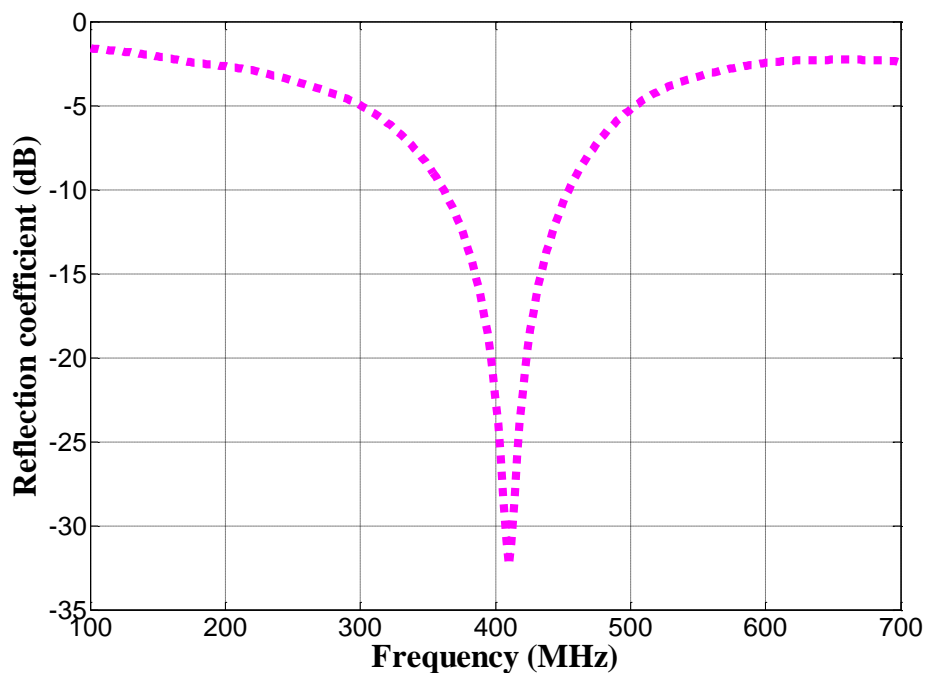


Fig. 3.11: The reflection coefficient S_{11} of the proposed bone implantable antenna.

One of the popular implants which work in bone is the total knee replacement implant which is usually composed of two parts, one part replaces the knee itself and another part which is used to fix the implant in the thigh bone [103]. A simplified structure of such an implant is shown in Fig. 3.12. In order to check up the functionality of the implanted knee after surgery an implanted sensor is placed in the cylindrical fixation part (coloured in green). The antenna exploits the entire external wall of the sensor that is surrounded by a biocompatible (Polyethylene ($\epsilon_r = 2.26$, $\tan\delta = 0.0002$) layer of 2 mm in thickness which represents the outer shell of the part of fixation, this is a popular material for knee

replacement implants [104]. This thickness is selected in order to support the main function of this part that is fixation. Because of this thick insulation layer, the effective permittivity around the antenna is reduced and thus a longer radiator is needed to achieve almost the same resonance. Therefore, a new structure is exploited as shown in Fig. 3.13 with a total radiator length of 217 mm this time. A longer meandered parts are obtained by exploiting a circular shape. A longer radiator is needed because of the smaller effective relative permittivity around the antenna this time as a thicker insulation layer is used [105] and is placed at the same position of the circular meandered loop antenna that is proposed for bone implants in the previous section. The antenna bandwidth is narrowed because of the smaller effect of losses this time as explained in Chapter two. The reflection coefficient is shown in Fig. 3.14.

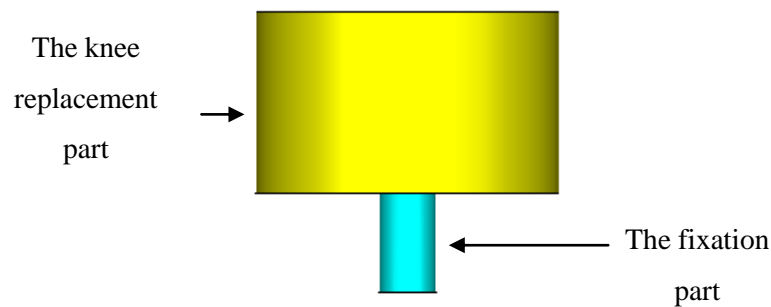
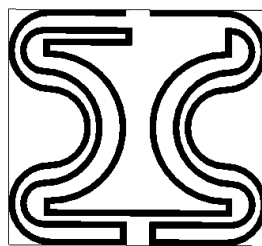


Fig. 3. 12: A simplified structure of a total knee replacement implant



(a)



(b)

Fig. 3.13: Circular meandered loop antenna for total knee replacement implants: (a) Flat structure, (b) Bent structure.

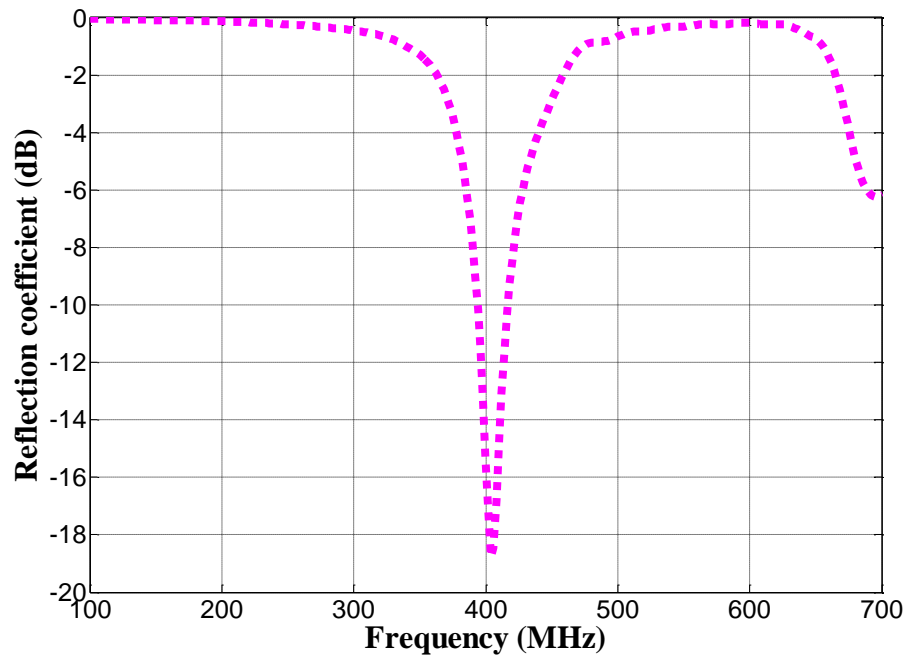


Fig. 3.14: The reflection coefficient S_{11} of the proposed antenna for total knee replacement implant.

The antenna has now got a narrower bandwidth (not covering the 433 MHz ISM for $S_{11} < -10$ dB) because of the smaller coupling with the human body tissues due to the use of a thick insulation layer (the losses effect on widening the antenna bandwidth is smaller). This is also reflected on larger radiation efficiency and gain which are 0.4% and -21 dBi, respectively at 403 MHz for this structure.

3.3.4 A Comparison between the Design Considerations of Bone and Muscle Implantable Antennas

As the design of implantable antennas is strongly influenced by the dielectric properties of body tissues, different design considerations and parameters have to be taken into account when designing implantable antennas in different tissues. The following main points have to be considered for bone implantable antennas in comparison with muscle or beneath-skin implantable antennas.

- The dielectric permittivity of the muscle and skin in the MedRadio band is much larger than that of bone as shown previously. This requires more miniaturization for bone implantable antennas of small sizes which results in a narrower bandwidth and thus mistuning difficulties in the actual time-variant human bodies.
- Bone implants have generally larger dimensions than muscle implants in order to achieve their functionalities of replacing some supportive parts of bones. This helps in obtaining a resonance at around 400 MHz despite of the small value of bone permittivity in comparison muscle and skin permittivity.
- More losses are added for the case of propagation from bone to the external receiver outside the body because of the attenuation in an extra layer which is bone and reflections at the boundary between the muscle and bones. This means that for the same transmitter and receiver and under the same link conditions for the case of muscle implants, bone implantable devices can communicate over a shorter distance.
- The specific absorption rate for the case of bone implants is much smaller than the corresponding rate for muscle or beneath skin implants. This is because of the larger mass density of bone in comparison with the mass densities of muscle and skin. An

- investigation about the SAR values for all of the proposed antennas will be provided in a following section.

3.4 The Effect of the Insulation Layer on the Performance of Loop Antennas

It is important to use an insulation layer in order to prevent the direct contact between the antenna and body tissues [16]. However, the presence of insulation layers affects the performance of implantable antennas in the human body. These layers reduce the power dissipation due to absorption in the biological tissue which increases the radiated power. On the other hand, their presence decreases the effective permittivity around the antenna which shifts the resonant frequency up. Therefore, these layers have to be carefully considered in the design process.

The increase of the insulation thickness improves the benefit of its presence. However, most of implants are of a small size and this thesis focuses on using thin insulation layers which are placed around loop antennas. On the other hand, the thicker insulation layer shifts the resonant frequency up. The effect of the insulation layer thickness on the performance of the 15 mm U-shaped loop antenna is shown in Fig. 3.15.

It can be seen from the figure that the resonant frequency is shifted up from 403 to 425 MHz by increasing the thickness from 0.25 to 0.4 mm, respectively. The same antenna bandwidth is almost obtained for both cases. A good antenna matching ($S_{11} < -10$ dB) is obtained for both cases.

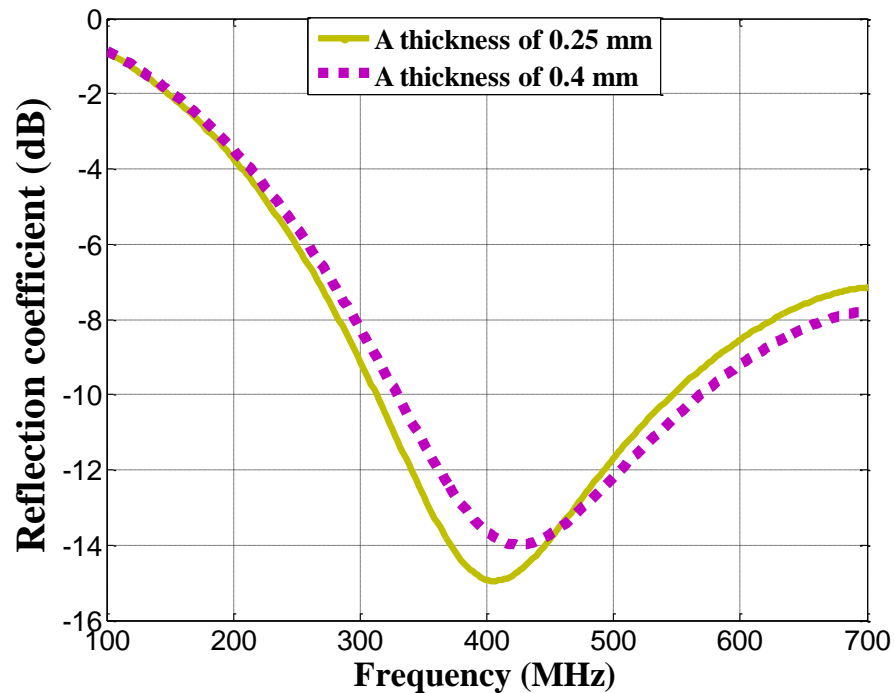


Fig. 3.15: Simulated S11 when the antenna is surrounded by insulation layers of 0.25 and 0.5 mm in thickness, respectively.

3.5 The Effect of the Internal Components of the Implant on the Antenna Performance

The antenna has to do an integral role with other components inside the implantable device to transmit the signal from inside the human body to the external receiver. These components are the battery, sensors which sense the bio- signals such as the temperature and pressure and electronics, etc. These components are expected to affect the antenna performance and therefore, their effect should be evaluated. To enable this evaluation, the internal components are classified into two groups; conducting and dielectric components.

For example, the battery is a conducting component while the sensor is a dielectric. In this work, a copper cylinder is used to mimic battery while FR-4 substrate is used to mimic sensors and other dielectrics [3]. A suggested layout structure of the internal components can be shown in Fig. 1.3.

Simulations with different copper cylinders of 4 mm and 8 mm in length inside the implant around which the 15 mm U-shaped loop antenna is wrapped are shown in Fig. 3.16.

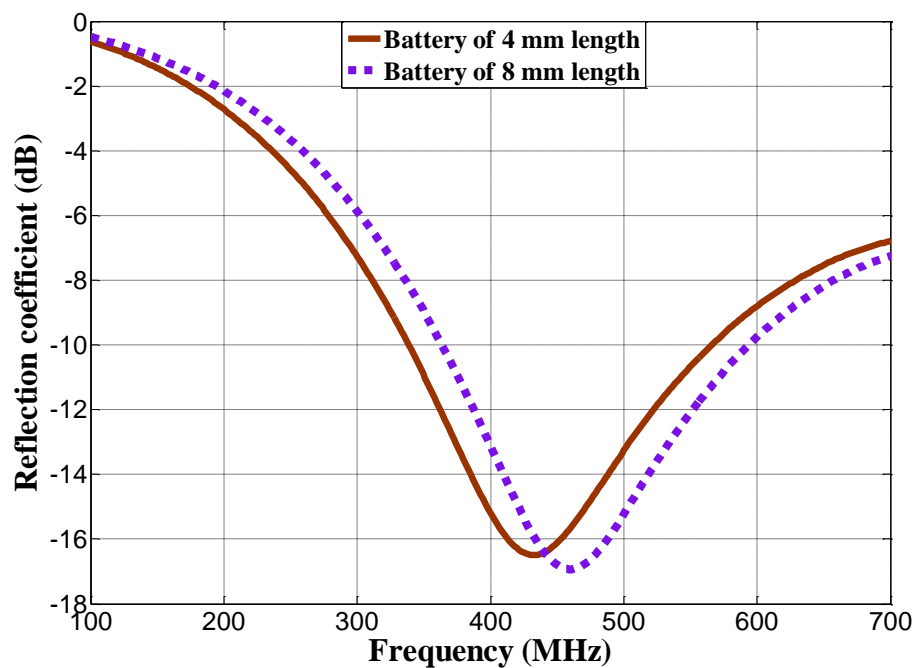


Fig. 3.16: Simulated S11 of the 15 mm U-shaped loop antenna with batteries of 4 and 8 mm in length, respectively.

The figure shows that the batteries tend to shift the resonant frequency up from 400 MHz to 444 and 460 MHz, respectively. However, both bands of interest are still covered with frequency margins of more than 30 MHz, maximum gain variations are only about 0.4 dB with these batteries. This shows another benefit of the broad bandwidth of implantable antennas which is the robustness against the frequency shift that may happen with internal components.

3.6 The Specific Absorption Rate (SAR) Results

The 1-g SAR is computed for all of the proposed antennas in this chapter because its regulation is much stricter than the corresponding 10-g SAR regulations. Computations are conducted using CST at 403 MHz in the simplified homogeneous elliptic body model which is used in this chapter. Although, homogeneous body models tend to overestimate the SAR, it is better for worst case considerations [3]. For more reasonable results, SAR is evaluated in the anatomical body model in Chapter 4. For further worst case considerations, computations are also conducted without insulation layers around the antenna. The results of the maximum RMS 1-g AVG SAR and the maximum allowed input power to the antenna are summarized in Table 3.3.

The maximum input power to the antenna is determined based on the 1-g SAR specifications. All of the maximum input power values are larger than 0 dBm which is normally provided to implantable antennas [2, 15]. It is important to ensure that the maximum input power does not exceed these values in order not to harm the human body tissues.

The results in the table show that the larger antennas are of smaller SAR values. This is actually due to the smaller lossy area around them. The larger implantable device replaces more lossy tissues. Therefore, the lossy area around it becomes smaller. When the losses are smaller (this is indicated by a smaller conductivity value in Eq. (3.4) [38]), a smaller power absorption and thus SAR (W/kg) are obtained.

$$SAR = \frac{P}{\rho} = \frac{\sigma |E|^2}{2\rho} \quad (3.4)$$

where P (W/m^3) is the power loss density, ρ (kg/m^3) is the mass density, σ (S/m) is the conductivity and $|E|$ (V/m) is the electric field intensity.

Table 3.3: SAR results for the proposed antennas in this chapter at 403 MHz

The antenna	Max RMS 1-g SAR (W/kg) for an input power of 1 W	Max input power (mW)/dBm
30 mm U-shaped loop	242	3.3/5.19
15 mm U-shaped loop	301	2.66/4.25
10 mm meandered loop	343	2.33/3.67
Circular meandered loop antenna for bone implant	39.77	20.12/13.04
Circular meandered loop antenna for total knee replacement implant	30	26.67/14.26

Much smaller SAR values are obtained for bone implantable antennas as shown in the table. This is due to the larger mass density of bone ($1810 \text{ kg}/\text{m}^3$) in comparison with muscle ($1041 \text{ kg}/\text{m}^3$), skin ($1010 \text{ kg}/\text{m}^3$) and fat ($950 \text{ kg}/\text{m}^3$) at 403 MHz [31]. Moreover, bone has much smaller conductivity than muscle and skin as explained in Section 3.3.3. The larger mass density (ρ) and smaller conductivity (σ) of bone in comparison with muscle reduce

the SAR values for antennas implanted in bone in comparison for antennas implanted in muscle.

3.7 In Vitro Measurements

As mentioned in Chapter 2, liquid body models and pork are used in this work to evaluate the proposed antenna performance. The recipe in [3] was used to prepare the liquid body model, gradual quantities of salt and sugar were added to water while heating it up to guarantee good melting of the overall ingredients (more details about the percents of these ingredients are provided in Chapter 2). The resultant mixture is cooled down and its dielectric properties are measured using Agilent dielectric probe. More rough quantities of salt and sugar are added to optimize the properties. The preparation procedure is shown in Fig. 3.17 and the resultant relative permittivity and conductivity are summarized in Table 3.4.

Different pieces of pork of different structures are used (both of them are shown in a following figure). One of them contains more muscle than fat while the another one contains more fat than muscle. This is to measure the performance robustness against variations in the dielectric properties and structures of the body phantoms. While minced pork can be used, multilayer pork is used to reflect the actual non-uniform body structure. The dielectric properties of pork is measured using the same probe. The probe is placed at muscle layer and fat layer each time. The conductivity and relative permittivity for these pieces are summarized in Table 3.5.

Each antenna is bent around a cylinder of the biocompatible material Propylene and surrounded by an insulation layer. It is then connected by a coaxial cable to the network analyzer and placed in the liquid body or pork phantoms. The results are presented in the following sub-sections:

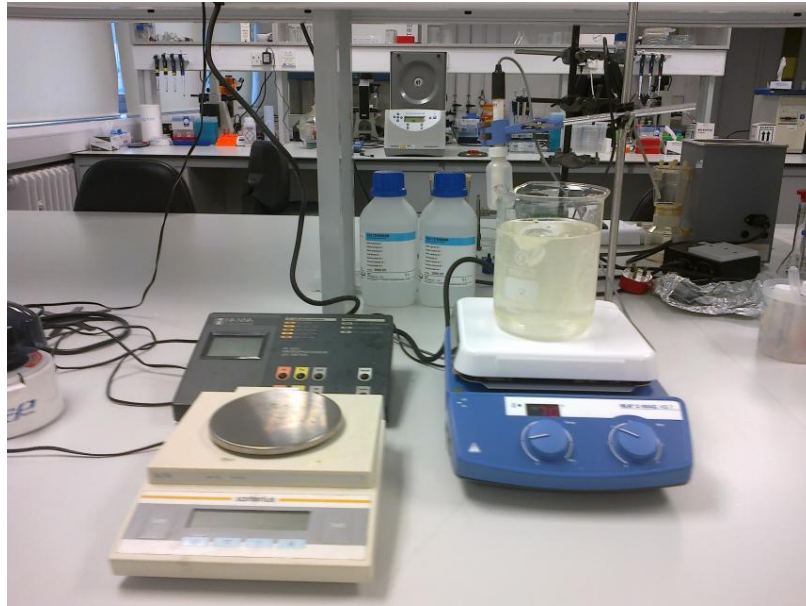


Fig. 3.17: The liquid body phantom during the preparation process. Material weight scale and a lab liquid boiler are used.

Table 3.4: The measured electromagnetic properties of the liquid body phantom

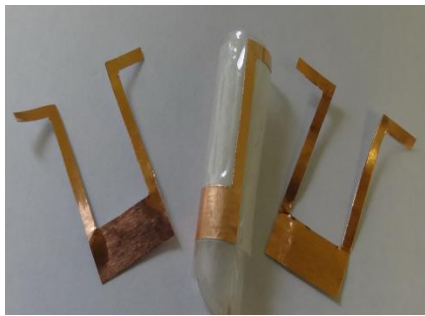
Frequency (MHz)	Relative permittivity	Conductivity (S/m)
403	57	0.79
433	56.86	0.812

Table 3.5: The measured electromagnetic properties of pork

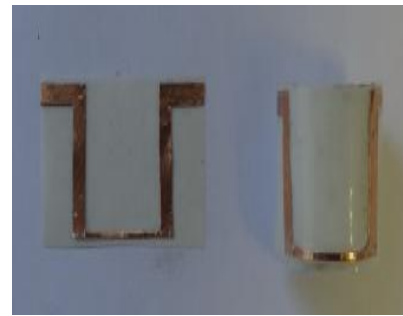
Freq (MHz)	Relative permittivity				Conductivity (S/m)			
	Piece 1		Piece 2		Piece 1		Piece 2	
	Muscle	Fat	Muscle	Fat	Muscle	Fat	Muscle	Fat
403	59	6	59.2	6.4	0.82	0.04	0.77	0.061
433	58.7	5.8	59	6.1	0.85	0.042	0.84	0.062
2450	53.5	5.5	52.7	5	1.7	0.11	1.74	0.012

3.7.1 Measurements of the Reflection Coefficient

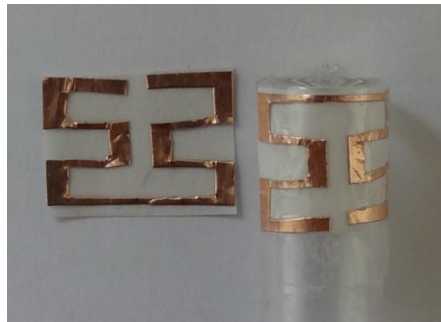
Some of the proposed antennas were realized by cutting a piece of a copper sheet as shown in Fig. 3.18 (dimensions are not for the same scale at each photo).



(a)



(b)



(c)

Fig. 3.18: Realized prototypes of the proposed antennas: (a) The 30 mm U-shaped loop antenna, (b) The 15 mm U-shaped loop antenna, and (c) The 10 mm meandered antenna.

The realized antennas have a very light weight and can be bent around different implants of different shapes. Measurements are conducted while the antenna is bent around cylindrical tubes. The measurements of the reflection coefficient are conducted by placing the antenna under test at the centre of the body model which has the same shape and dimensions ($180 \times 100 \times 50 \text{ mm}^3$) of the elliptic cylindrical body model and filled once with the liquid body phantom and once with pork. The body phantoms that are used in measurements are shown in Fig. 3.19. Results inside Piece 1 of pork of the more muscle is firstly attempted. The results for the U-shaped loop antennas are shown in Fig. 3.20. The

figures show that both measurements and simulations match very well. The antenna covers both bands of interest and maintaining the same broad bandwidth. The results of the reflection coefficient for the small meandered antenna in these body phantoms are shown in Fig. 3.21. Matching is also obtained for this case. The variations in the reflection coefficient from one position to another are found to be negligible in the homogeneous body model and phantom.

Therefore, the centre position is selected for all the measurements in the liquid body phantom.

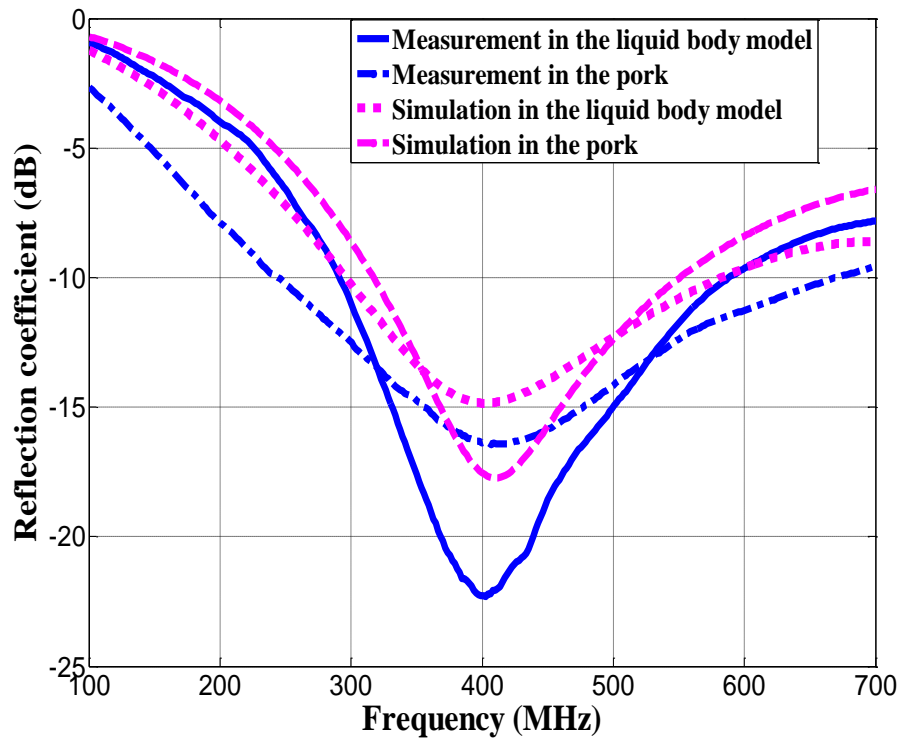


(a)

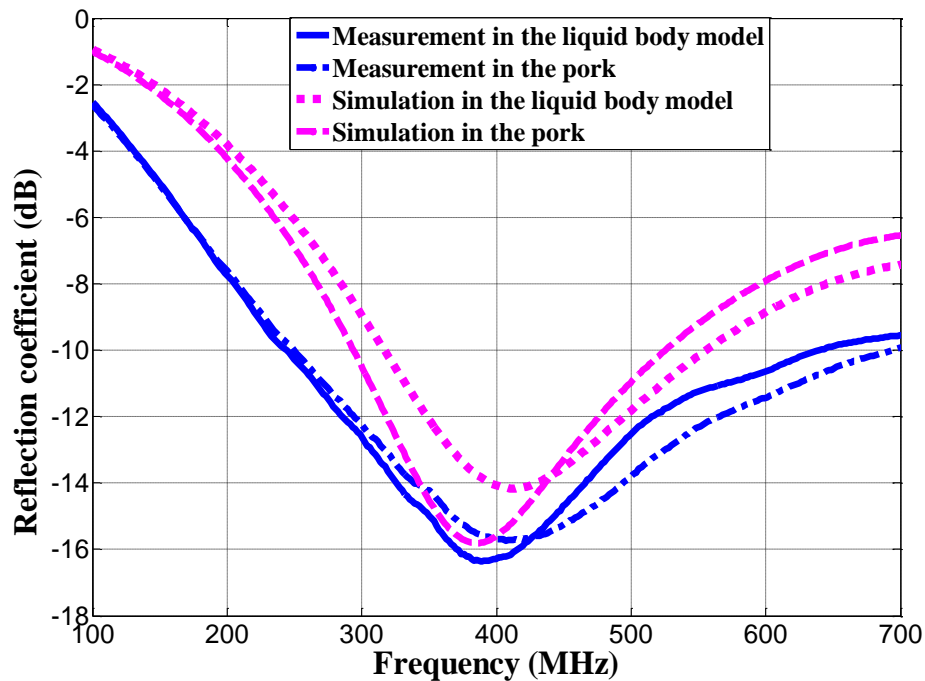


(b)

Fig. 3.19: Body phantoms of measurements: (a) The liquid body model (b) Pork Piece 1 and Piece 2, respectively.



(a)



(b)

Fig. 3.20: The simulated and measured reflection coefficient in liquid body phantom and pork of the:

(a) 15 mm U-shaped loop (b) 30 mm U-shaped loop antenna.

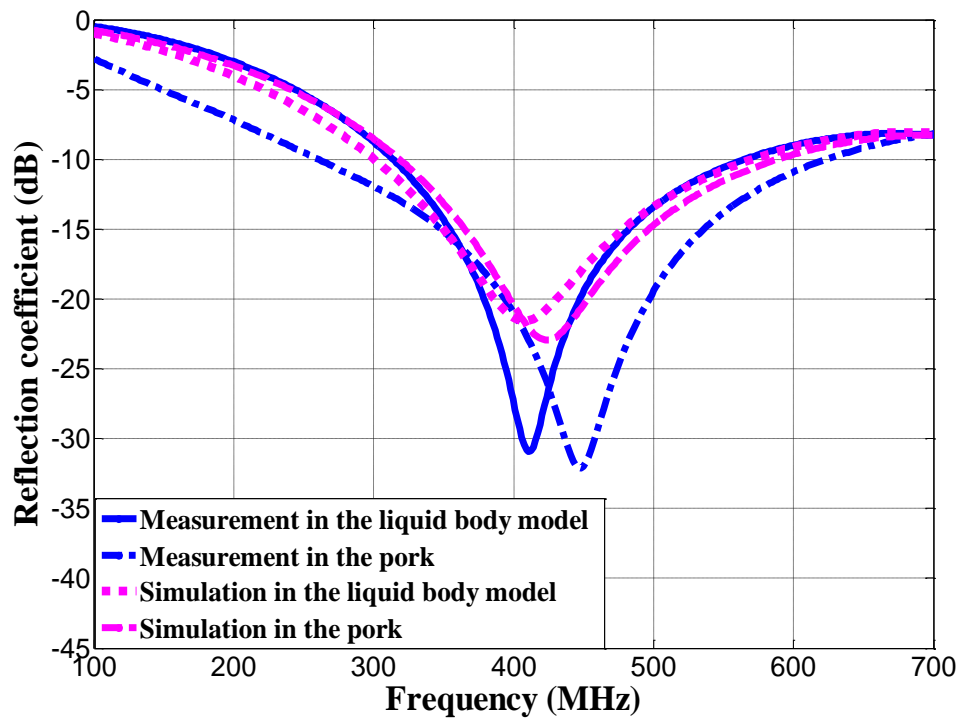


Fig. 3.21: The simulated and measure reflection coefficient of the 10 mm meandered loop antenna

Measurements are conducted at the centre of pork phantom. However, other measurements at different positions inside of it are attempted. Small variations are obtained from one position to another and both bands of interest were always covered for $S_{11} < -10$ dB. This is because the used pork phantoms have more muscle than fat. This means that the equivalent effective permittivity around the antenna is still close to its corresponding value in the liquid body phantom.

3.7.1.1 The Effect of the Insulation Layer on Measurements

It is well known that electrically small antennas (ESAs), when fed by a coaxial cable (unbalanced feed), can give rise to radiating currents on the outer part of the cable affecting the measurement results. Although, implantable antennas have the required electronics always integrated in the radiator itself, the problem may still apply when performing prototypes measurement. In this case the coaxial cable interferes with the radiation

characteristics due also to the presence of the body phantom [90]. In fact, the currents present on the external surface of outer conductor are dissipated in the high loss materials (constituting the simulating body tissues) as is well known in microwave hyperthermia applications [106, 107, 108, 109]. This effect is investigated for the 15 mm in length U-shaped loop antenna with and without an insulation layer. A comparison between measurement of both of these cases are shown in Fig. 3.22. The antenna is expected to resonate at 403 MHz. However, an initial measurement obtains resonance at 360 MHz.

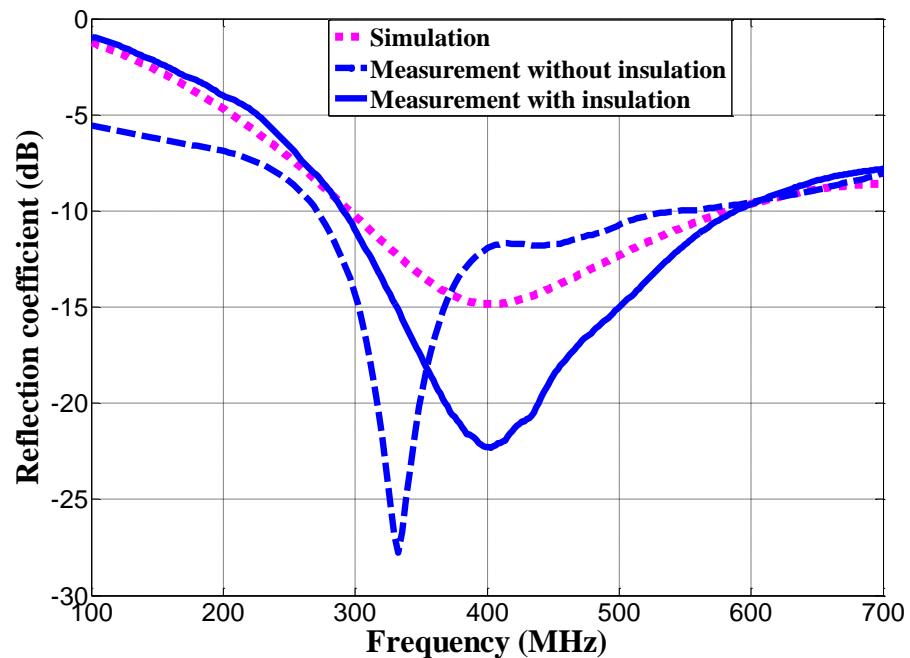


Fig. 3.22: The effect of insulation layer on measurements

This is mainly due to the cable effect as explained above. In particular, the conducting parts of the feeding cable cause the problem as they contribute in the radiation and shift the frequency down. It is pointing out that the effect of the other parts of the cable is mitigated by reducing the implant depth in the body phantom. Although the main bands of interest (MedRadio and 433 MHz ISM) are still covered, this could be a problem for the evaluation of narrowband antennas. To achieve more accurate measurements, the radiating parts which are in main contact with the body phantom are isolated using an insulation layer. This layer

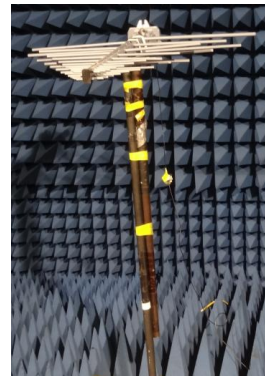
extends from the conducting soldering parts of the antenna to cover all parts of the antenna itself. The measurements after insulating the antenna and the conducting parts of the cable are shown in Fig. 3.22. The expected resonant frequency is exactly obtained.

3.7.2 Measurements of the Antenna Radiation Pattern and Gain

While measuring the radiation efficiency is a difficult task, the gain is measured in the anechoic chamber using the three antenna method. The gain reflects a very clear image about the radiation capability of the antenna which is small and of an expected directivity [42]. The measurement setup is shown in Fig. 3.23.



(a)



(b)



(c)

Fig. 3.23: Measurement setup for gain and radiation pattern measurements: (a) Log periodic receiving antenna, (b) Log periodic transmitting antenna, and (c) The implantable transmitting antenna.

Two log-periodic antennas are used as the transmitting and reference antennas. The third antenna is the implantable antenna (at the centre of a body model when is filled up with pork). The measured gains at 403 MHz are -25.5 and -31.4 dBi for the vertical and horizontal polarizations. The measured gain values at 433 MHz are -24.9 and -29.1 dBi for both polarizations, respectively which are about 0.5 dB larger than simulations. The larger gain at 433 MHz is due to the larger electrical size of the antenna. This measured gain value matches very well with the simulations results. The radiation pattern is measured as shown in Fig. 3.24.

The antenna has shown an omnidirectional pattern which is due to the almost symmetric structure of the used pork layers. When the antenna is surrounded by the same tissue layers, the same radiation is almost absorbed from the different antenna parts. Therefore, an omnidirectional radiation pattern is obtained.

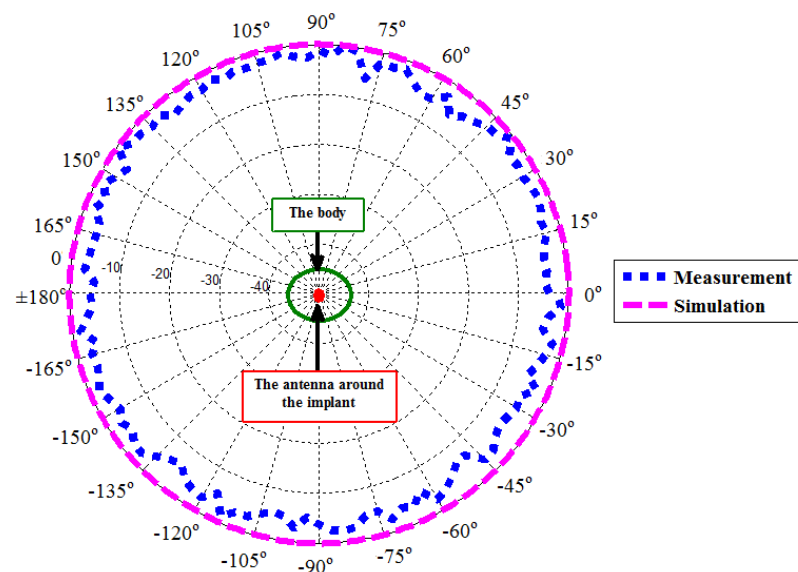


Fig. 3.24: The Xoy measured and simulated normalized far field patterns (vertical polarization) at 403 MHz. Maximum value corresponds to 0 dB. A top view of the body phantom and antenna around the implant are indicated at the center of the diagram.

3.7.3 Measurements of the Antenna Performance Robustness

The robustness of the antenna performance is measured against the following:

- Existence of the internal components.
- Insulation layer.
- Variations in the dielectric properties and structure of the body materials.

For the first case (robustness against the internal components), a copper cylinder of 8 mm in length is used to mimic the battery while different pieces of FR-4 is used to mimic the sensors and other non conducting components as shown in Fig. 3.25. The antenna is bent around the same cylinder/tube and measurement is conducted at the centre of the same body phantom. The result shows a very good matching with simulations. However, a smaller up-shift in the resonant frequency is obtained (from 403 to 443 MHz in comparison with from 403 to 460 MHz which was obtained by simulation). To measure the effect of the insulation layer thickness, an insulation layer of 0.4 mm in thickness of different dielectric materials (PTFE, PVC, tape [110-117]) is used. The results of the reflection coefficient for the case when an insulation layer of tape is used can be seen in Fig. 3.26. It can be seen from the figure that good matching with simulation is obtained. It is worth mentioning that almost the same results are obtained for all the other materials. To measure the robustness against different structure and tissues, measurements are conducted in the other piece of pork (piece 2) which has more fat layers as shown in Fig. 3.26. The reflection coefficient for the three cases is shown in Fig. 3.26. The figure shows that the resonant frequency is shifted up as expected because fat has a smaller relative permittivity than muscle which is only 5.6. This reduces the overall effective permittivity around the implantable antenna and device and thus shifts the resonant frequency up.



Fig. 3.25: Top view of the implant with the internal components.

No considerable effect is obtained on the radiation pattern for all of these cases as the pattern is mainly attributed to the surrounding human body tissues which is very similar for the two pieces of pork.

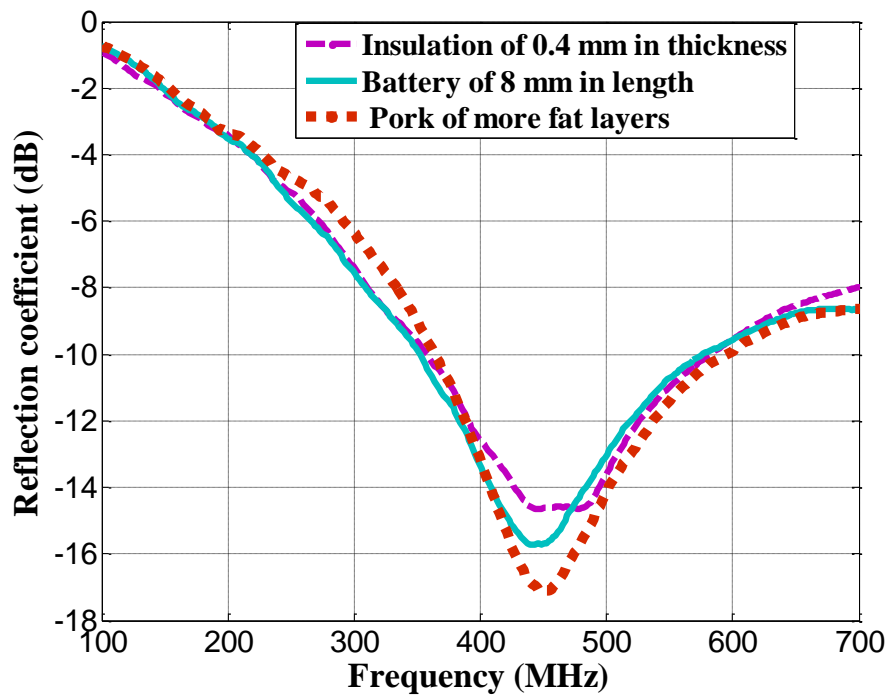


Fig. 3.26: The reflection coefficient of the proposed 15 mm U-shaped loop antenna with the internal components, insulation layer of 0.4 mm thickness and in pork with more fat layers.

After implantation in the actual human body, temperature and other parameters are expected to change the effective electromagnetic properties around the antenna and resonant frequency correspondingly. This could be evaluated by implanting the device with the

antenna and actual components over the targeted period of implantation and measuring its performance using the in vivo test. However, it is difficult to conduct the in vivo test which needs a license. Moreover, conducting the in vivo test with a direct implantation of the antenna in an animal over a short period of time is not very beneficial to evaluate the long-term antenna performance and could be obtained with other simpler methods. A simple tool of measuring the reflection coefficient over a large range of frequencies is developed. It is based on adding salt, water or sugar to pork to change the relative permittivity and conductivity (water increases the relative permittivity while sugar and salt decreases the real part of permittivity and increases the conductivity, respectively [16]). Then measurements of the new dielectric properties can be conducted with Agilent probe or other measuring procedures. Four new combinations of different electromagnetic properties are measured which are summarized in Table 3.6.

Table 3.6: New electromagnetic properties after adding salt, water or sugar

Sample	Relative permittivity	Conductivity (S/m)
1	51	1
2	61	3.5
3	63	4.1
4	53	1.8

The reflection coefficient of the new electromagnetic properties are shown in Fig. 3.27.

It is shown from the figure that different matching levels, bandwidth and resonant frequencies are obtained as expected for different dielectric properties. Nonetheless, both bands ((401-406) MHz MedRadio and 433 MHz ISM band are still covered for $S_{11} < -10$ dB for all these cases. This is due to the broad bandwidth of the proposed antenna. This

confirms the robust performance of the proposed antenna against material variations after long term implantation and in-body temperature effect.

It should be indicated that measurements for other antennas are also conducted and the following results are obtained:

- All of these antennas obtained the bands of interest for $S_{11} < -10$ dB.
- The measured gain values match simulated values very well.
- The radiation pattern of all of them is omnidirectional as expected for small antennas in homogeneous/almost homogeneous body model.
- Robustness against materials variation is obtained.

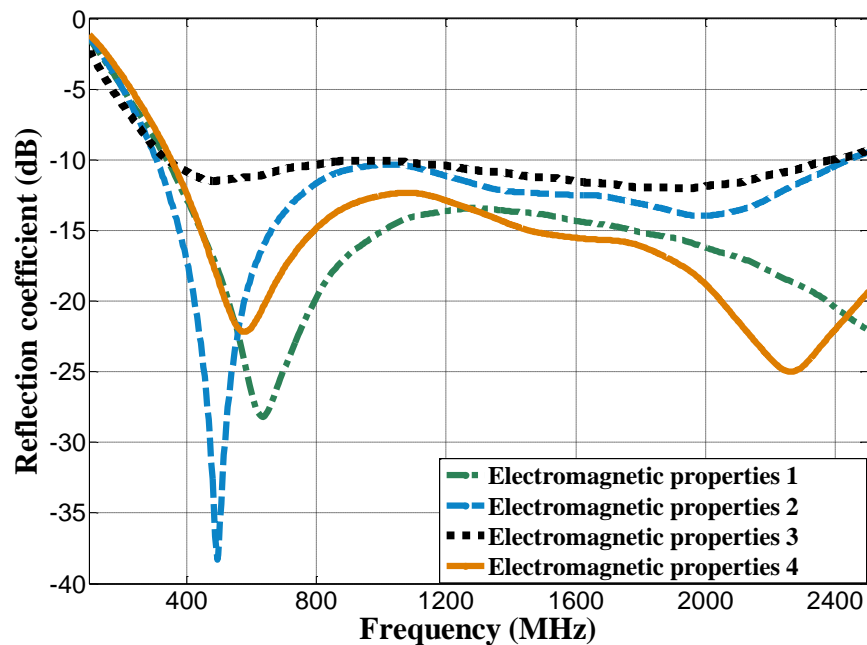


Fig. 3.27: The reflection coefficient of the proposed 15 mm U-shaped loop antenna with different electromagnetic properties.

3.8 Summary

A methodology to design implantable antennas design is formulated in this chapter. The methodology suits different design applications. It also deals with structure optimization to maximize power radiation. The methodology comprises the following two steps:

Step 1: Optimization of the antenna structure in the simplified body model. This is obtained by widening the loop antenna parts to reduce the loss resistance and thus increase the antenna radiation efficiency. However, this is accompanied with optimizing the spacing distance between the antenna vertical and horizontal parts which control the total effective capacitance and inductance to obtain resonance at the frequency of interest (at around 400 MHz) and a wide bandwidth (> 200 MHz). The optimization at this step is finished when the maximum possible radiation efficiency is obtained at around 400 MHz. This antenna design is optimized within a relatively short time in the simplified body model which have much smaller size and simpler structure than the anatomical body models.

Step 2: Evaluation of the antenna performance in an anatomical body model. The anatomical body model is either an adult or a child depending on the antenna application. The antenna gain at the intended position of actual implantation is compared to a threshold gain value that is specified based on the design requirement. If the antenna gain overcomes this threshold value while covering the bands of interest with good matching, the design is stopped and the final antenna is obtained. Otherwise, some techniques such as using metamaterials to increase the antenna gain are used and the design procedure is repeated through Steps 1 and 2.

Only Step 1 is discussed and applied in this chapter. The evaluation through Step 2 requires careful simulation and the consideration of different parameters which is to be investigated in depth in the next chapter. The proposed methodology is used to design U-shaped and meandered loop antennas for both of muscle and bone implants. The proposed antennas have the following desirable features:

- Wide bandwidth (> 200 MHz).
- A relatively large radiation efficiency for the design structure.
- Robust performance against internal components, insulation layers and material variations.
- Light weight
- Flexibility and conformity which could reduce the implant size or enable using more sensors for multi functions of the implant.

Small antennas such as the meandered 10 mm loop antenna are designed for small implants such as capsules for children. On the other hand, the larger antennas are designed for implants of adults.

The proposed antennas are realized by cutting a copper conducting sheet. In Vitro measurements are then conducted in a liquid body phantom and pork to evaluate and validate the proposed designs. The antenna performance is found to be robust against internal components, insulation layers and material variations. Measurements obtained the simulated bandwidth and realized gain values. The radiation pattern is found to be omnidirectional because the body phantoms are almost homogeneous. The cable effect during measurements is evaluated and mitigated to provide more accurate measurements.

A simple procedure to measure the antenna robustness against materials variation is used by adding salt, sugar or water to pork. Different electromagnetic properties are obtained and the proposed antennas are measured inside these materials. Despite of the different matching levels, resonant frequencies and bandwidths, the antennas have obtained a robust performance covering all the bands of interest for $S_{11} < -10$ dB.

Chapter Four

Evaluation in the Anatomical Body Model

4.1 Introduction

The anatomical body models are of much better resemblance to the real human body than the simplified body models. They also provide a reliable tool to evaluate the implantable antenna performance as variations happen from one simplified body model to another (this will be further explained in this chapter). Furthermore, they provide a unique tool to evaluate some parameters such as the implant orientation. Therefore, it is very important to evaluate the implantable antenna performance inside these models. However, such an evaluation should be accurate and many related parameters should be well understood. For example, simulations should include enough body area around the antenna; where considering only the specific organ of implantation could lead to inaccurate results especially about the radiation pattern, radiation efficiency and gain. This chapter of the thesis aims at the following objectives:

- Investigating the effect of simplified body models on the implantable antenna design and performance.
- Providing general guidelines for accurate and quick evaluations of implantable antennas inside the anatomical body models.

- Evaluating the performance of the 15 mm U-shaped loop antenna that was proposed in Chapter 3 at different positions and orientations in an adult human body (the CST Katja voxel) model.
- Evaluating the performance of the 10 mm meandered loop antenna that was proposed in Chapter 3 inside an anatomical body model of a child for the applications of wireless capsule endoscopy for children.
- Emphasizing the effect of the implantable antenna and device orientation on their performance.
- Comparing the orientation effect at different implantation positions. The orientation and position at which the antenna obtain the largest antenna radiation efficiency and gain are recommended for the applications of glucose monitoring.

To achieve these purposes, this chapter is arranged as follow:

Firstly, the main effect of simplified body models; shape, dimensions and aspect ratios are investigated and discussed. The 15 mm U-shaped loop antenna is then simulated in the arm of the CST Katja adult body model. Simulations comprise the following areas each time: the hand only, the trunk, the longitudinal half and the full body. The same analysis is also conducted for the case of hip implantation. The case that obtains the same performance of the full body over a shorter time is recommended for accurate and quick future simulations. After that, the performance of that antenna is simulated at three positions of implantation (the left arm, thigh and hip). Four orientations are also evaluated at each position. Finally, the antenna performance and orientation effect are evaluated for the small meandered loop antenna in a child anatomical body model for a potential application of ingestible capsule endoscopy for children.

The achievements of this chapter can be summarized as the following:

- The robustness of the performance of the proposed antennas in Chapter 3 is validated against different positions and orientations. The overall performance of implantable antennas is totally evaluated against these parameters for the first time.
- Investigations on the accurate evaluation of implantable antennas in the anatomical body models are conducted for the first time; the validity of the evaluation of some previous antennas is discussed. A specific part of the anatomical body model is recommended to be used for an accurate evaluation of implantable antennas which can save half of the simulation time and memory.
- A full analysis of the orientation effect on the performance of implantable antennas is performed. SAR dependence on the implant orientation is only and briefly indicated in [19]. However, the orientation effect on the reflection coefficient, radiation efficiency and gain is investigated in-depth in this work for the first time.
- A capsule antenna for children at 403 MHz and for different positions and orientations has been evaluated inside the digestive tract of an anatomical child body model.

4.2 The Effect of the Shape, Dimensions and Aspect Ratios of the Simplified Body Models on the Antenna Performance

It is very important to start the design of implantable antennas in a simplified body model. This is to save simulation time and memory [113]. In addition, this helps in selecting the antenna structure of the optimum characteristics (the largest radiation efficiency

and gain and wider bandwidth) within a relatively short time. However, different simplified body models lead to different antenna radiation characteristics. The validity and accuracy of simplified body models are discussed at this section. The effect of the simplified body shape, dimensions and aspect ratio (length to width, length to depth ratio, etc.) on the overall antenna performance is particularly investigated.

4.2.1 The Effect of the simplified Body Shape on the Antenna Performance.

In this section the effect of the simplified body model shape on the antenna resonant frequency, bandwidth and radiation pattern is investigated. Three different shapes (cylindrical, elliptic cylindrical and rectangular) are studied. In all of these body models the antenna is placed at the origin and a single orientation for the implantable antenna and device is selected. The body models of investigations are:

- Of a cylindrical shape, 90 mm in radius and 50 mm in height and muscle equivalent dielectric material.
- Of an elliptic cylindrical shape, the following dimensions ($180 \times 100 \times 50$ mm³) and muscle equivalent dielectric material.
- Of a rectangular shape, the following dimensions ($180 \times 100 \times 50$ mm³) and muscle equivalent dielectric material.

The top view of these body models are shown in Fig. 4.1. A negligible difference in the resonant frequency and bandwidth between the cylindrical and elliptic cylindrical body models is obtained while exactly the same reflection coefficient (S11) characteristics are obtained for the elliptic cylindrical and rectangular body models. This is because the elliptic cylindrical and rectangular body models have the same dimensions.

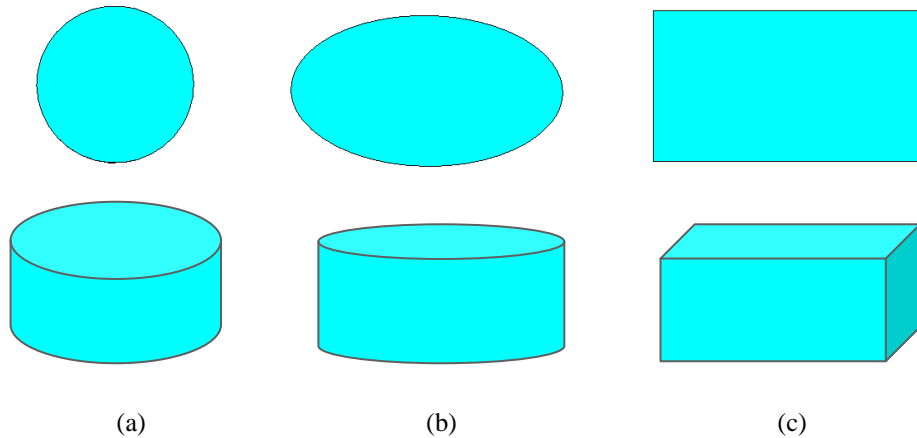


Fig. 4.1: Top and side views of the simplified body models of different shapes: (a) Cylindrical (b) Elliptic cylindrical (c) Rectangular.

The radiation patterns in these body models are obtained. To clarify the antenna radiation pattern around the body model, the pattern axes around the cylindrical body model is shown in Fig. 4.2. The azimuth radiation patterns are obtained at $\theta = 90^\circ$ as shown in Fig. 4.3. 14 dB difference in the main lobe magnitude is obtained between the largest value in the rectangular body model and the smallest value in the cylindrical body model.

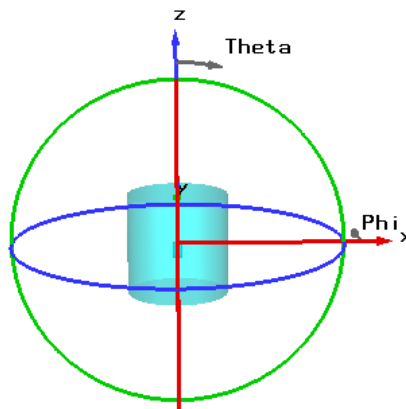


Fig. 4.2: the cartesian and polar coordinates around the simplified cylindrical body model

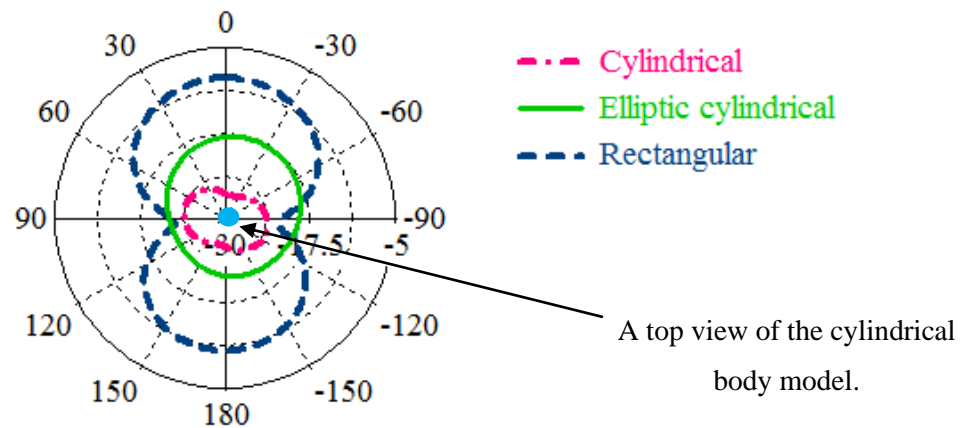


Fig. 4.3: The azimuth radiation pattern (at $\theta = 90^\circ$: perpendicular to the top view direction of the simplified body model) in simplified body models of different shapes.

The largest radiation efficiency is achieved in the rectangular body models. It is 1.55 times the radiation efficiency in the elliptic cylindrical body model although these body models have the same dimensions. It is 8.85 times the radiation efficiency in the cylindrical body model. The main lobe direction differs by 24 degrees between the elliptic cylindrical and rectangular body models. However, much larger degrees differences of 83 and 107 are obtained between the (cylindrical and the elliptic cylindrical) and (cylindrical and rectangular body models), respectively.

It can be concluded from this analysis that the shape of the simplified body model does not affect the reflection coefficient (S_{11}) characteristics (the resonant frequency and 10 dB bandwidth). However, the radiation efficiency, gain and radiation pattern are strongly affected by the shape of the simplified body model. This confirms the importance of evaluating the overall performance of implantable antennas in the anatomical body models.

4.2.2 The Effect of the Body Dimensions and Aspect Ratio on the Antenna Performance

It is expected that body models of a smaller size provide larger gain and radiation efficiency [3]. However, the gain and radiation efficiency may totally differ when the same body model of the same overall size has different aspect ratios (width to length, width to height and length to height). This effect is investigated at this section using the elliptical cylindrical body model that is used in this thesis. The initial $(180 \times 100 \times 50) \text{ mm}^3$ dimensions are interchanged to be $(180 \times 50 \times 100)$ and $(50 \times 100 \times 180) \text{ mm}^3$. The same U-shaped loop antenna is simulated at the centre of the each body model and always oriented parallel to the longitudinal axis of the body model as shown in Fig. 4.4.

A negligible change in the resonant frequency and bandwidth is also obtained this time.

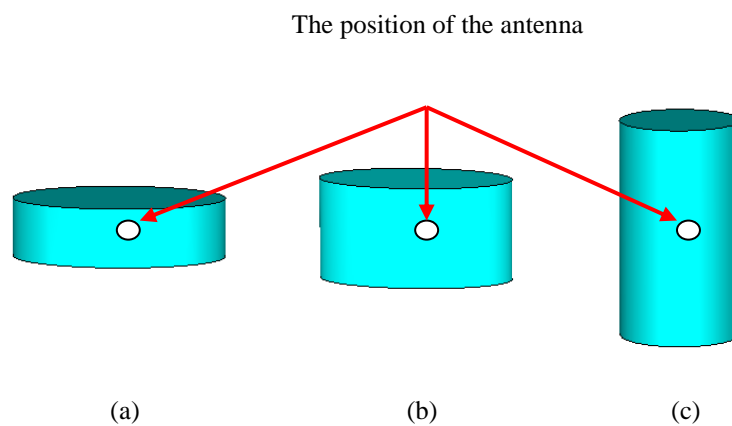


Fig. 4.4: An elliptical body model of different aspect ratios: (a) $(180 \times 100 \times 50) \text{ mm}^3$ (b) $(180 \times 50 \times 100) \text{ mm}^3$ (c) $(50 \times 100 \times 180) \text{ mm}^3$.

The radiation efficiency and realized gain in the body model of the second aspect ratio are 5 and 27.8% larger than in the body model of the first aspect ratio. The smallest radiation efficiency and realized gain are obtained for the body model of the maximum longitudinal length. They are 0.19 and 0.14 times the maximum obtained values in the body model of the second aspect ratio.

The polar radiation pattern of these cases are shown in Fig. 4.5.

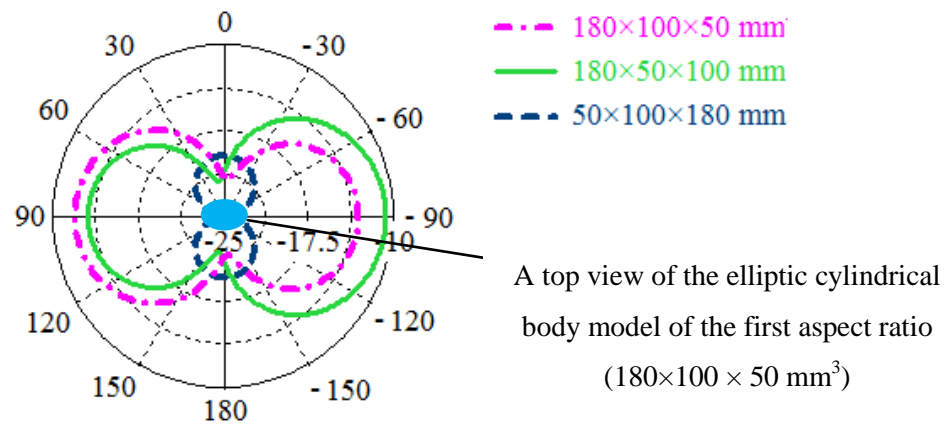


Fig. 4.5: The azimuth radiation pattern (perpendicular to the top view of the body model which is indicated in the figure) for different elliptic cylindrical body models of different aspect ratios.

The main lobe direction of the radiation pattern from the body of the first aspect ratio differs by 180 and 92 degrees from the case of the second and third aspects ratios, respectively. The main lobe magnitude differs by 8.9 dBV/m between the cases of the minimum and maximum field intensities. The maximum electric field intensity is obtained for the second case which differs by 1.2 dBV/m from the first case.

4.3 Performance of the Conformal U-shaped Loop Antenna in the Anatomical Body Model of an Adult

4.3.1 Performance for Different Body Parts of Simulation

The performance of the proposed 15 mm in length U-shaped loop antenna is evaluated in the arm of the CST Katja body model. The CST Katja voxel body model represents a 43-year old female with a height of 163 cm and weight of 62 kg [78]. It is understood that simulations with the full anatomical body model is time consuming. Therefore, simulations are firstly attempted while considering only some parts of the full Katja body model (hand only, trunk, longitudinal half of the body) and the performance is then compared with that in the full body. The same position of implantation in the hand is kept for all the cases of

investigations. The purpose of this analysis is to find if the performance in only some parts of the body model can provide accurate results while saving lots of time and memory. On the other hand, some designs rely on the use of only some parts of the anatomical body models such as in [20]. The validity of that consideration and use has to be investigated.

The parts which are included in each simulation are shown in Fig. 4.6.

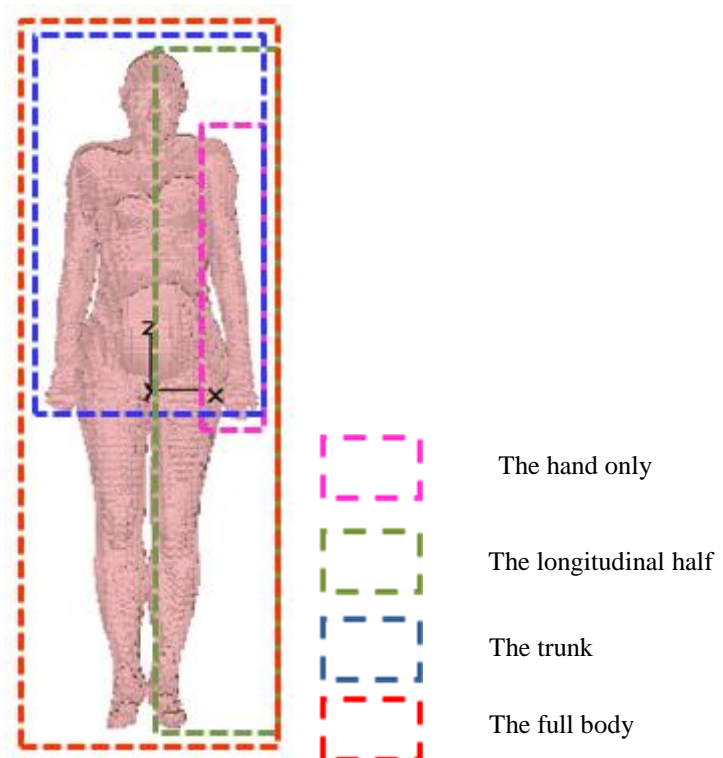


Fig. 4.6: The CST Katja voxel body parts of simulations.

The reflection coefficient for all these cases is shown in Fig. 4.7. It can be seen from the figure that the resonant frequency differs between some of these cases. Generally, the resonant frequency is shifted up from the case of hand only to the full body by 41 MHz. This is because the effective permittivity around the antenna for the case of the hand only is larger (the percent of muscle to the overall material of simulation is larger than for the case of the full body). However, the resonant frequencies for the cases of the upper and longitudinal halves of the human body are the same and equivalent to the case of the full body. The antenna bandwidth is over 200 MHz for all these cases. However, the smaller part of the

hand only tends to provide a slightly narrower bandwidth (30 MHz for this case of investigation).

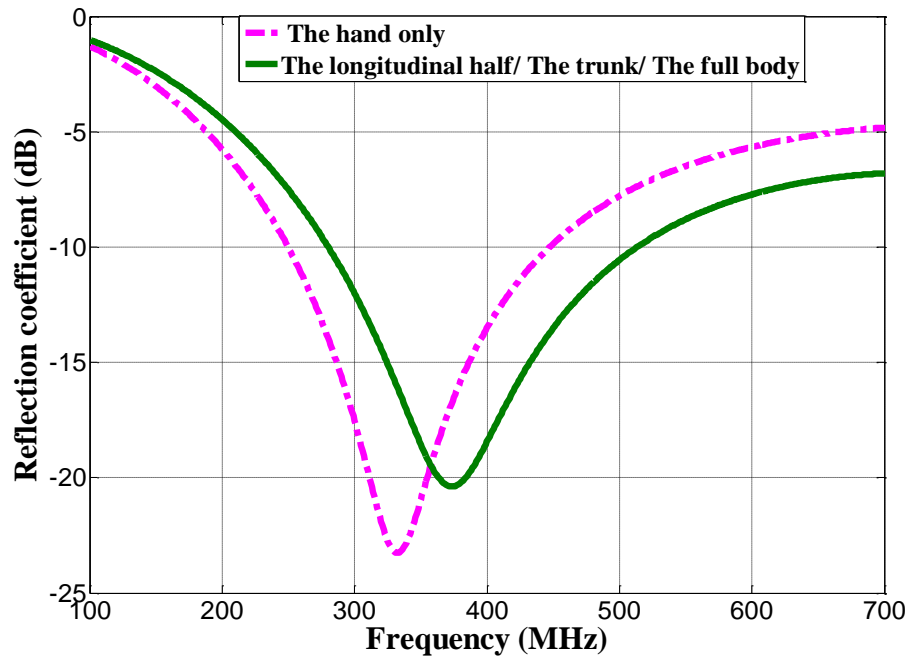


Fig. 4.7: The reflection coefficient for different parts of simulations for the 15 mm U-shaped implantable antenna at 10 mm beneath fat in the arm of the CST Katja voxel body model.

The antenna radiation characteristics at 403 MHz (radiation efficiency, gain and SAR) are also evaluated for these cases. The results are provided in Table 4.1.

It is indicated from the results in the table that the case of the hand only overestimates the gain by around 1.72 dB in comparison with the case of the full body. When the lossy area around the implantable antenna becomes larger (the case of the full body), the total effective conductivity increases and thus more losses are obtained. This decreases the antenna radiation efficiency and gain. However, a negligible difference in gain and radiation efficiency is obtained between the cases of the half parts (the longitudinal and upper (trunk)) and the full body model.

Table 4.1: The radiation characteristics for different parts of simulations for the U-shaped implantable antenna in the arm of Katja

	Radiation efficiency (%)	Maximum 3D-realized gain (dBi)	Maximum 1-g (RMS) SAR (W/kg) for an input power of 1W	Maximum 10-g (RMS) SAR (W/kg) for an input power of 1 W
The hand only	0.051	-28.12	317	48.8
The upper half (the trunk)	0.046	-29.8	226	44.8
The longitudinal half	0.048	-29.23	226	44.8
The full body	0.045	-29.84	226	44.8

The same 1g and 10g average SAR values are obtained for the three cases of the longitudinal, upper half (trunk) and full anatomical human body model. However, they are 40.3 and 9% smaller than the corresponding 1-g and 10-g SAR values, respectively for the hand only. This is because the percentage of bone to muscle and fat for the case of hand only is much smaller than for the case of the full anatomical body model. As long as bone has much larger mass density than muscle and fat, it reduces the overall SAR. Therefore, smaller SAR is obtained for the case of hand only (the equation to calculate SAR can be found in previous chapters).

It is known that the body aperture is very effective on the far-field radiation pattern. Therefore, the far field radiation pattern has been simulated for all these cases. The cartesian

and polar coordinates around the anatomical body model is shown in Fig. 4.8. The results are shown in Fig. 4.9.

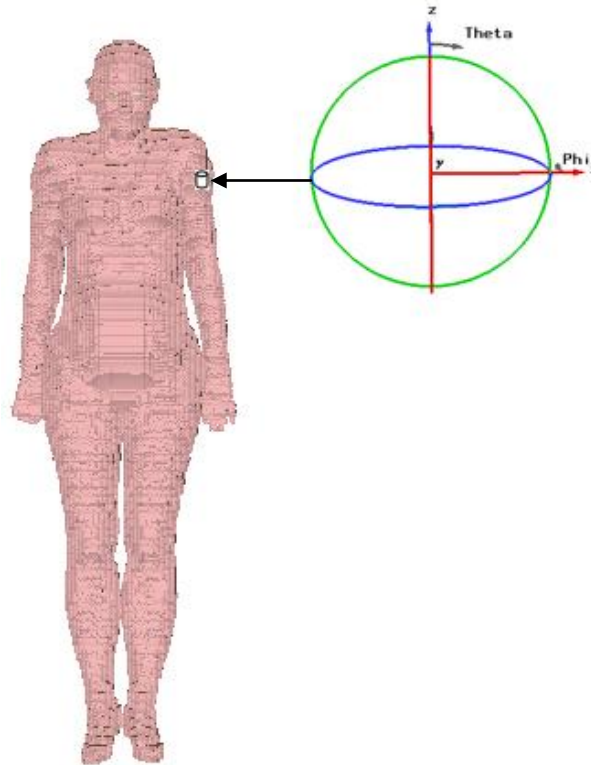


Fig. 4.8: The cartesian and polar coordinates around the CST Katja voxel body model.

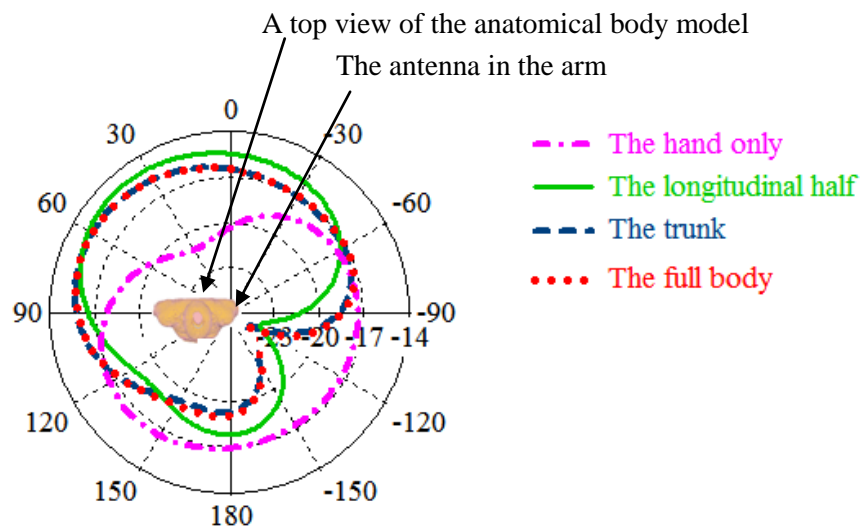


Fig. 4.9: The azimuth radiation pattern for different parts of simulation in the arm of the CST Katja voxel body model.

The same direction of the main lobe is obtained for the cases of the trunk and full body models while a difference of 20 degrees is obtained between the longitudinal half and the full body. It can be concluded that using the upper part (the trunk) of the Katja voxel body model provides a reliable source of data while saving a considerable time and memory.

The required simulation time, maximum memory and number of mesh cells for each case of simulation are summarized in Table 4.2. The table shows that the simulation time and physical memory inside the full body model are around 50 % higher than their corresponding values in the upper half of the body model. A high percentage of time and memory can be saved when the upper half of body model is only used while almost the same results about the antenna performance can be obtained. On the other hand, a considerable difference in the overall characteristics is obtained when only small parts of the body are used in the simulations in comparison with the full body model.

Table 4.2: Simulation time and memory for different parts of simulations for an antenna implanted in the left arm

	Total simulation time (s)	Peak memory used (kB)		Number of mesh cells
		Physical	Virtual	
The upper half (trunk) of the body model	2244	5255936	5470960	28571028
The full body model	4187	9410736	9631012	51672138

This shows that evaluation in only small part of simulation such as in [20] was not accurate enough to evaluate the overall antenna characteristics precisely. Larger gain values

are obtained when only a small part is included in comparison with the full body case and this underestimates the overall path losses.

The same analysis is performed in the area above the left hip in order to confirm and generalize the results. Simulations with the area above the hip only is firstly conducted, then with the trunk, longitudinal half and compared with the simulations in the full anatomical body model. The resultant reflection coefficient for the different parts of simulations when the antenna is implanted in the area above the left hip is shown in Fig. 4.8 and their radiation characteristics are summarized in Table 4.3.

Similar to the case when the antenna is placed in the arm, the largest difference of 13 MHz in the resonant frequency is obtained between the smallest part (the hip only) and the full body as shown in Fig. 4.10. The same resonant frequency is obtained for all the other cases. However, the gain value is also overestimated by 1 dB for the case of the hip only and longitudinal half in comparison with the trunk and full body.

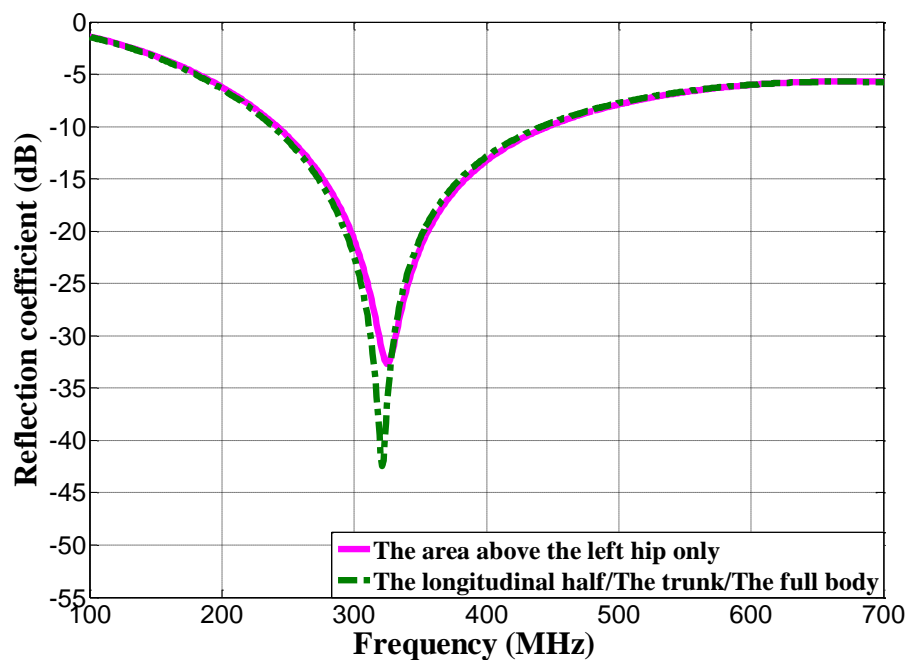


Fig. 4.10: The reflection coefficient for different parts of simulations for an implanted antenna in the area above the left hip.

The polar radiation pattern around the body model is shown in Fig. 4.11. The pattern is obtained in a normal direction to the top view of the area above the left hip. This direction is selected because the antenna is intended to transmit in this direction away from the human body towards the receiver in the free space. The main lobe direction is obtained in a preferred direction that is transversal and off the body for all of these cases. A phase difference of 86 degrees is obtained between the cases of the hip only and the full body model while almost the same direction of the main lobe is obtained for all the other cases. It can be concluded that using the upper part (trunk) of the Katja voxel body model can also provide a reliable source of data while saving around half the simulation time and memory. The required simulation time, maximum memory and number of mesh cells are summarized in Table 4.4.

Table 4.3: Radiation characteristics for different parts of simulations for the 15 mm U-shaped implantable antenna in the area above the left hip of Katja

	Radiation efficiency (%)	Maximum 3D-gain (dBi)	Maximum 1-g (RMS) SAR (W/kg) /$P_{in} = 1$ W	Maximum 10-g (RMS) SAR (W/kg) /$P_{in} = 1$ W
The hip only	0.03	-32.4	302	48.1
The upper half (the trunk)	0.012	-33	267	46
The longitudinal half	0.019	-32.4	266	45.7
The full body	0.018	-33.2	267	46, 0.046

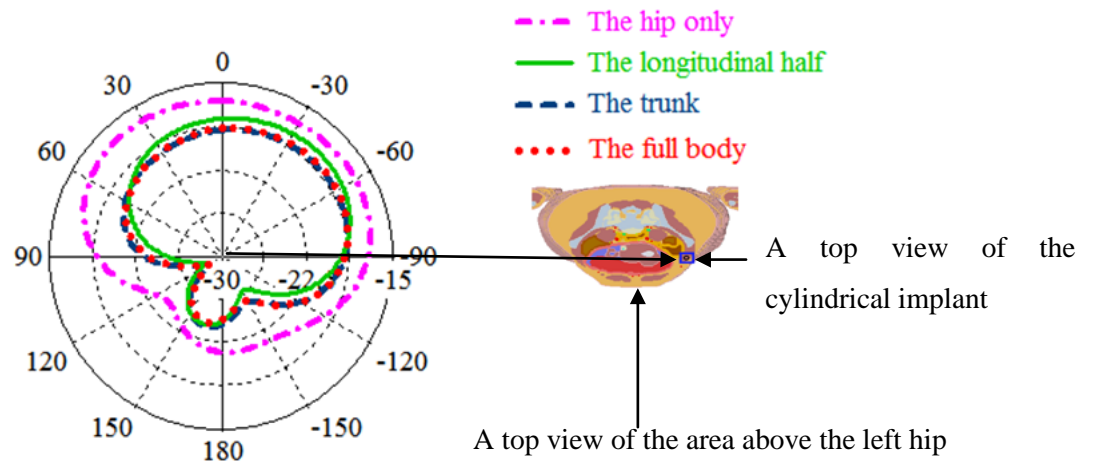


Fig. 4.11: The azimuth radiation pattern for different parts of simulation in the area above the left hip of the CST Katja voxel body model. The origin of the radiation pattern is at the centre of the cylindrical implant

Table 4.4: Simulation time and memory for different parts of simulations for an antenna implanted in the area above the left hip

	Total simulation time (s)	Peak memory used (kB)		Number of mesh cells
		Physical	Virtual	
The upper half (the trunk)	2122	5390892	5618828	29329776
The full body model	3900	9463672	9673536	313469677

Table 4.4 shows that the simulation time and physical memory inside the full body model are also around 50% larger than their corresponding values in the upper half of the body model. A large percent of time and memory can be saved when the upper half (trunk)

of the body model is only used in comparison with the full body while almost the same results about the antenna characteristics and performance can be obtained.

This confirms the importance of evaluating the antenna performance with enough body area around the antenna (not only the small part of implantation). Consideration of only small parts may lead to inaccurate data especially about the gain values.

4.3.2 Performance Evaluation at Different Positions and Orientations

For the purposes of general health monitoring such as glucose monitoring, the device is usually implanted beneath skin in the arm, leg and the area above the hips [115]. Therefore, the performance of the proposed implantable antenna is compared in these areas in order to recommend the optimum position of implantation for these purposes from antenna and propagation point of view. The optimum position is the position inside which the antenna obtains the largest radiation efficiency and gain and smallest SAR. The flexible 15 mm in length U-shaped loop and smaller meandered loop antenna inside an adult and a child body model, respectively are selected for these investigations. The radiation characteristics are compared for four orientations (around the same axis parallel to the longitudinal body axis) for the U-shaped loop antenna and around different axes for the case of the meandered antenna. Firstly, the orientation effect at each position is summarized and a comparison of the overall performance between the four positions is then conducted.

It should be pointed out here that the evaluations at this chapter represents the second step of the design methodology which was proposed in Chapter 3. Simulations are conducted to evaluate the resultant realized gain values and compare them with the targeted gain value (> -37 dBi) as explained in Chapter 3.

A cross section of the body at all the positions of implantation is shown in Fig. 4.12. The antenna is intended for muscle or beneath skin implants. Therefore, it has been placed in a muscle layer beneath fat [38]. Muscle or beneath-skin implants are normally placed beneath fat due to the following reasons:

- The fat layer is susceptible to great variations such as the body weight.
- Full encapsulation of the implantable device in the thin fat layer is impossible.
- Detuning normally happens when the antenna is implanted in fat because of the large difference between its electromagnetic properties from muscle [31].

A layout of the antenna for the four orientations is shown in Fig. 4.13. Each orientation is obtained by rotating the antenna 90 degrees counter clockwise. The reflection coefficient in the left arm at the four orientations around the z-axis is shown in Fig. 4.14.

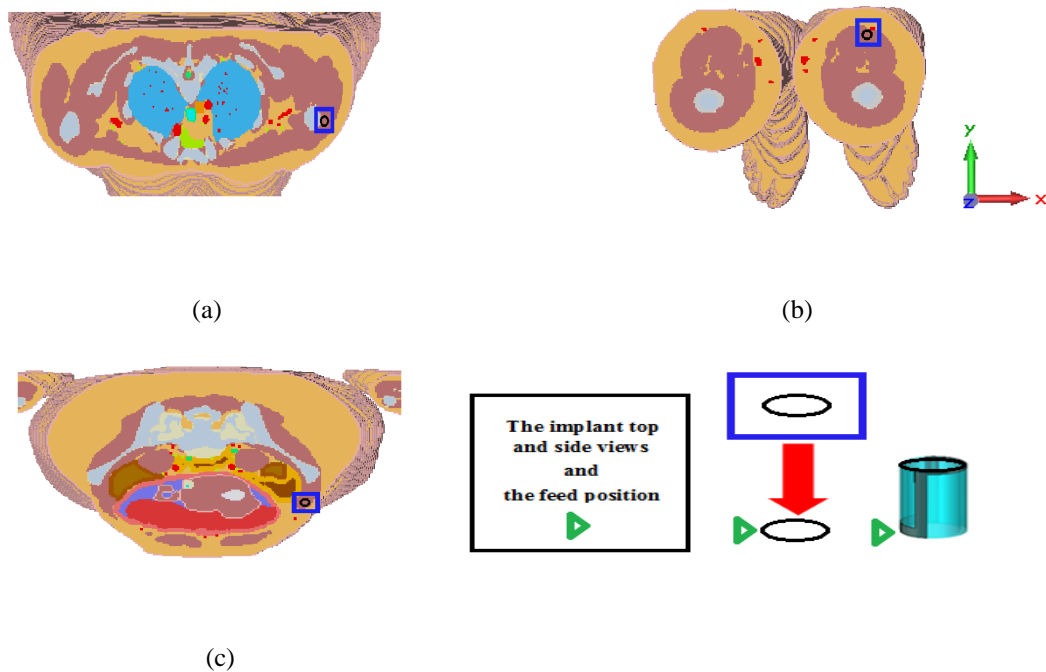


Fig. 4.12: The implantable antenna at: (a) the left arm (b) the left thigh (c) above the left hip inside the CST Katja voxel body model.

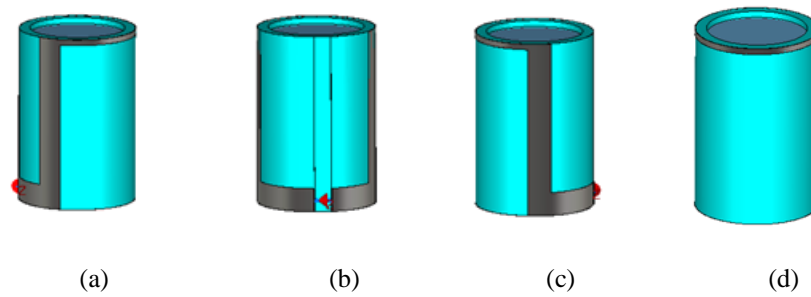


Fig. 4.13: The different four orientations of the 15 mm U-shaped loop antenna: (a) First orientation, (b) Second orientation, (c) Third orientation, and (d) Fourth orientation.

The resonant frequencies for the first, second, third and fourth orientations are 373, 331, 322 and 331MHz, respectively. Although almost the same 10 dB bandwidth of 200 MHz is obtained for all the orientations, 51 MHz difference in the resonant frequency is obtained between the first and the fourth orientations. Different matching levels are also obtained.

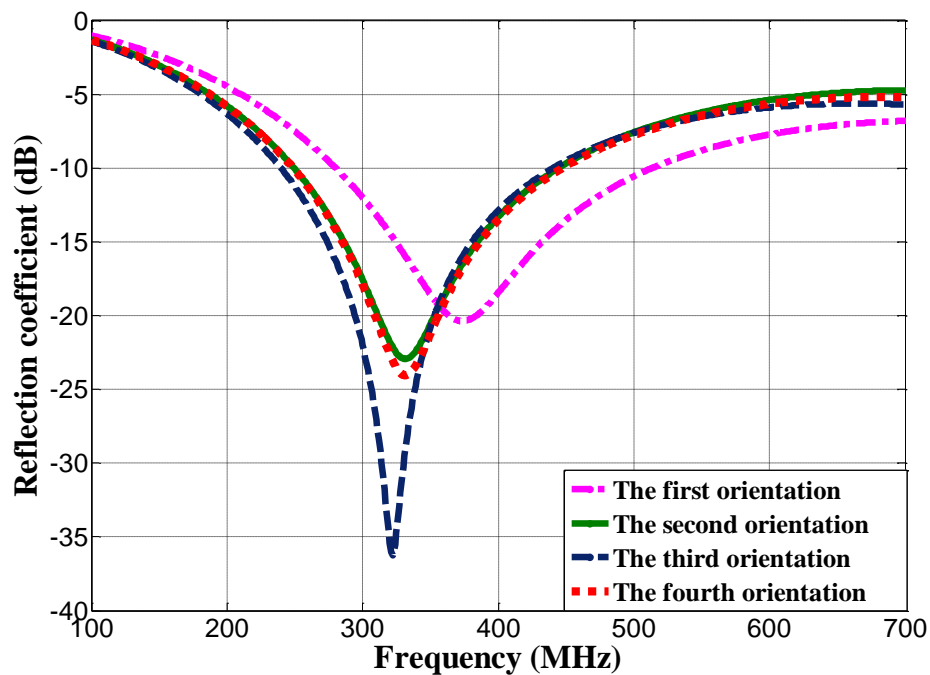


Fig. 4.14: The reflection coefficient at different orientations of the 15 mm in length U-shaped loop antenna inside the arm of the CST Katja voxel body model.

The overall radiation characteristics are summarized in Table 4.5.

The largest radiation efficiency and gain are obtained for the first orientation. The smallest maximum SAR is also obtained for this orientation. This can be linked to the equivalent relative permittivity around the different parts of the antenna. When the antenna longest parts are close to a thick muscle layer which are the layer of the largest conductivity for this case, losses and absorption around the antenna at this position increase. This reduces the overall radiation efficiency and gain and increases the SAR for this orientation.

The results show that the radiation efficiency and realized gain for the first orientation is 4.45 and 3.63 times the corresponding efficiency and realized gain values for the fourth orientation. The radiation efficiency and realized gain of the second orientation is relatively small. However, they are 16 and 21.34% larger than the radiation efficiency and realized gain of the fourth orientation. On the other hand, the radiation efficiency and realized gain of the third orientation are relatively large and are 14.65 and 24.65% smaller than the radiation efficiency and realized gain, respectively of the first orientation. The smallest computed maximum 1-g average SAR values are obtained for the first orientation which is 44.7, 23.5 and 39.4% smaller than the corresponding values of the second, third and fourth orientations, respectively.

The radiation patterns for all the four orientations are also computed and are shown in Fig. 4.15. The pattern is obtained in a normal direction to the top view of the area above the left hip in order to show the radiation pattern of interest around the body model. The main lobe direction is obtained at different angles of 62, 60, -74, and 92 degrees for the first, second, third and fourth orientations, respectively. Different field strength intensities are also obtained where a difference of up to 7.8 dBV/m between the best and worst cases is obtained.

Table 4.5: Radiation characteristics of the 15 mm U-shaped loop antenna at different orientations in the left arm of the CST Katja voxel body model.

Radiation characteristic Orientation	Radiation efficiency (%)	Maximum 3D-gain (dBi)	Maximum 1-g (RMS) SAR (W/kg)/$P_{in} = 1$ W	Maximum 10-g (RMS) SAR (W/kg)/$P_{in} = 1$ W
First	0.045	-29.84	226	44.8
Second	0.0116	-34.34	327	49
Third	0.04	-30.8	279	46.7
Fourth	0.01	-35.4	315	49

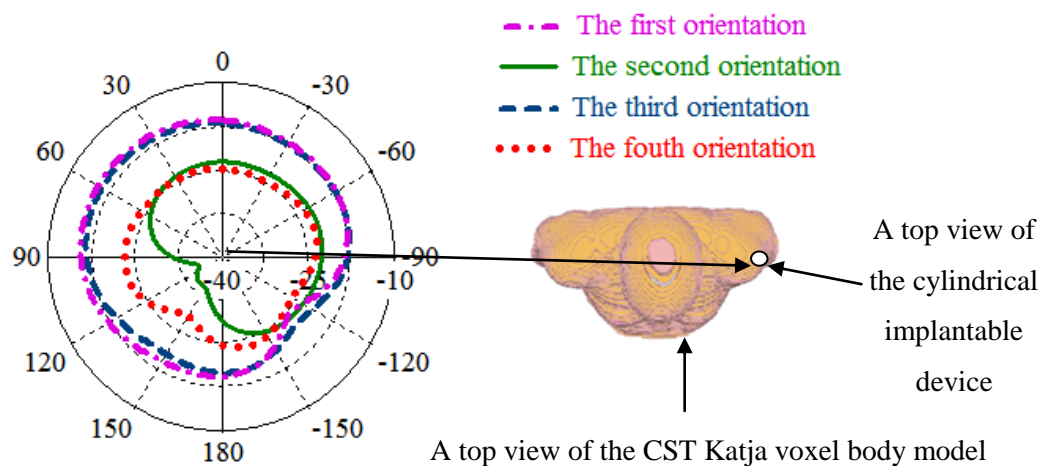


Fig. 4.15: The azimuth radiation pattern of the 15 mm U-shaped loop antenna at different orientations inside the arm of the CST Katja voxel body model. The centre of the radiation pattern is at the centre of the cylindrical implantable device.

The same analysis is repeated in the left thigh and the reflection coefficient for all the orientations are shown in Fig. 4.16. The resonant frequencies for the first, second, third and fourth orientations are 363, 327, 373 and 506 MHz, respectively. Larger difference of 179 MHz between the resonant frequencies for the different orientations is obtained for this case (in the thigh) than for the case in the arm. 100 MHz wider 10 dB bandwidth is obtained for the fourth orientation than for the other orientations. Different matching levels are also obtained. The deepest matching is obtained for the case of the second orientation.

The radiation characteristics are summarized in Table 4.6. The largest radiation efficiency is obtained for the third orientation which is 86.7, 115.4, 64.7% larger than the corresponding efficiency for the first, second and fourth orientations, respectively. The realized gain value for this orientation are 121, 204 and 161.8% larger than the corresponding gain values for the first, second and fourth orientations, respectively. The percentage of realized gain difference between the different orientations is different from the obtained percentages of radiation efficiency due to the difference in directivity for these orientations. The largest radiation efficiency and realized gain for the third orientation is due to the smallest effective conductivity for it in comparison with the other cases. This is also reflected on reducing the 1-g SAR for this orientation in comparison with other orientations which is 74, 76 and 17.8% smaller than the corresponding 1-g SAR values for the first, second and fourth orientations, respectively. It is obvious that all these characteristics differ from the case in the arm due to the difference in the overall structure and materials around the antenna.

The main lobe magnitudes are -17.9, -17.4, -14.9 and -18.3 dB, respectively which are obtained at the directions of 60, -146, 35 and 84 degrees, respectively. This shows a large difference between the magnitudes and main lobe direction of some orientations which requires a careful consideration of the optimum direction of the implantable device for the intended application during the evaluation and implantation processes.

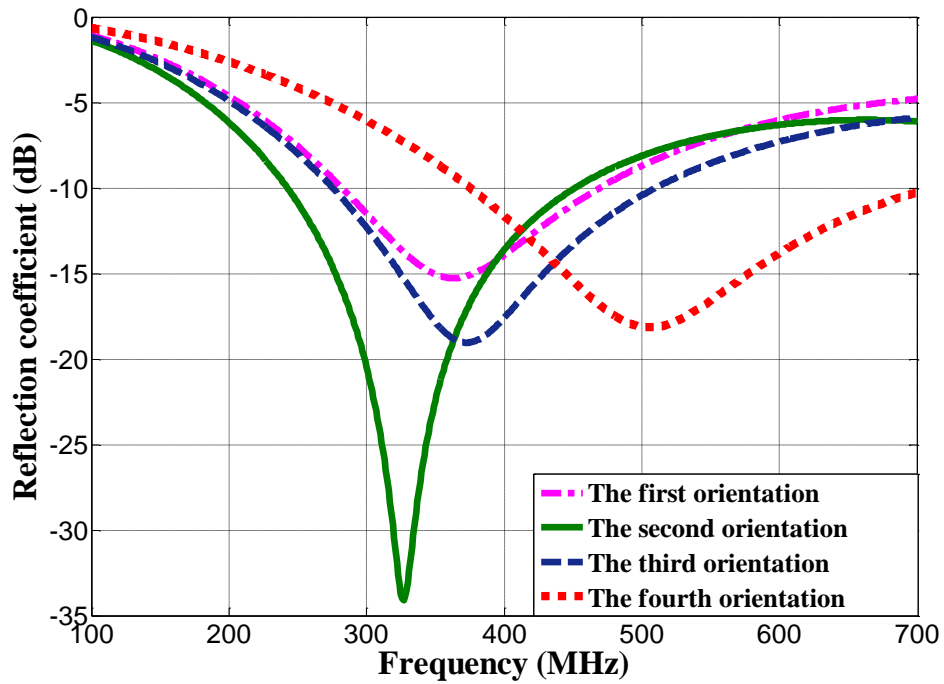


Fig. 4.16: The reflection coefficient at different orientations of the 15 mm U-shaped loop antenna inside the thigh of the CST Katja voxel body model

Table 4.6: Radiation characteristics of the 15 mm U-shaped loop antenna at different orientations in the left thigh of the CST Katja voxel body model

Radiation characteristic Orientation	Radiation efficiency (%)	Maximum 3D-gain (dBi)	Maximum 1-g (RMS) SAR (W/kg)/$P_{in} = 1$ W	Maximum 10-g (RMS) SAR (W/kg)/$P_{in} = 1$ W
First	0.03	-31	383	50.3
Second	0.026	-32.4	387	44.7
Third	0.056	-27.6	220	43.5
Fourth	0.034	-31.8	186.8	40.3

The radiation patterns at different orientations in the thigh is shown in Fig. 4.17.

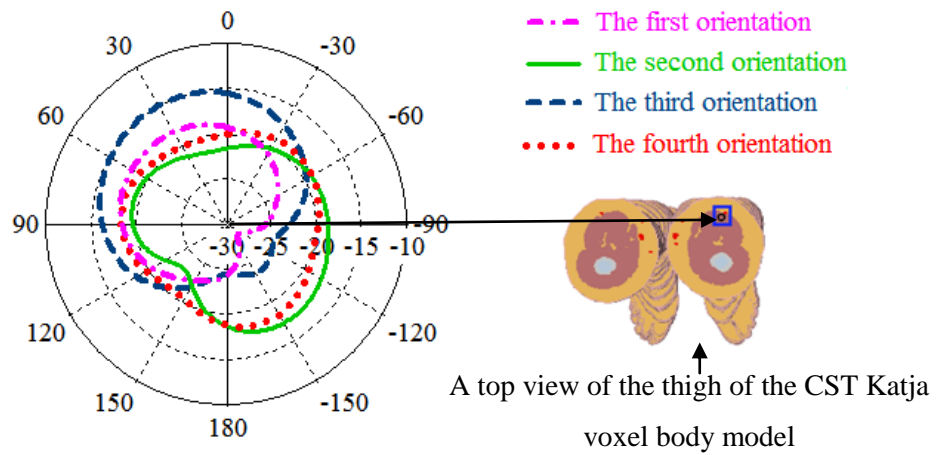


Fig. 4.17: The azimuth radiation pattern for different orientations inside the left thigh of the CST Katja voxel body model. The centre of the radiation pattern is at the centre of the cylindrical implantable device (encircled in the blue box).

The results for the area above the left hip are shown in Fig. 4.18.

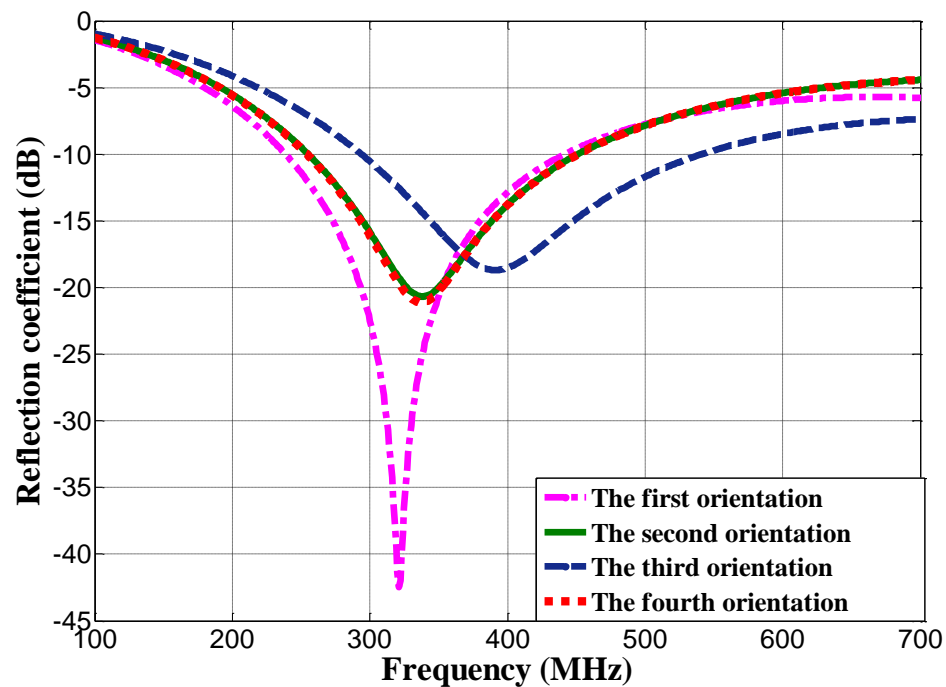


Fig. 4.18: The reflection coefficient at different orientations inside the area above the left hip of the CST Katja voxel body model

The resonant frequencies for the first, second, third and fourth orientations are 321, 338, 391 and 337 MHz, respectively. It can be seen from the figure that the resonant frequency is shifted down from the third to first orientation by 70 MHz. The frequency band margin above the MedRadio (401-406 MHz) band is only 50 MHz for the first three orientations. On the other hand, 150 MHz above this band is obtained for the third orientation. This is due to the same reason that is explained above; when the longest antenna parts are in close proximity to the tissue of the largest relative permittivity, the resonant frequency is shifted down. The radiation characteristics are computed for all orientations and summarized in Table 4.7.

The largest gain and radiation efficiency are obtained for the third orientation. The resonant frequency is also shifted up to around 400 MHz for this case. This is because most of the antenna parts are surrounded by a thinner muscle layer than that surrounds the antenna parts for the cases of other orientations. This reduces the overall loss and effective permittivity around the antenna for this orientation.

The radiation patterns of these orientations are shown in Fig. 4.19. The main lobe direction is obtained at -48, -66, -56 and -64 degrees for the first, second, third and fourth orientations, respectively.

It can be concluded from the previous results that the maximum realized gain and radiation efficiency are obtained for the third orientation in the thigh. Therefore, it is recommended for glucose monitoring. Although, maximum frequency deviations of 179 MHz between some orientations are obtained at this position in the thigh, the bandwidth is centred at around 400 MHz for the third orientation which is recommended for a long term implantation (guarantee the bands of interest coverage if frequency detuning occur). The

smallest 1-g and 10-g AVG SAR are also obtained at this orientation due to the smallest losses around the antenna at this position. The overall results show that the realized gain values at all the positions and orientations are > -37 dBi which is the targeted realized gain value as indicated by the design methodology in Chapter 3 except for the second and fourth orientations which obtain a communication over a shorter range. The gain values for the second and fourth orientations are enough to satisfy a link budget over 17 and 19 meters only for the second and fourth orientations, respectively. Referring to the proposed design methodology, further modifications or techniques have to be applied to increase the antenna radiation efficiency and gain to satisfy a link over 20 meters for the second and fourth orientations. This will be obtained using metamaterials based layers around the antenna as will be explained in Chapter 5.

Table 4.7: Radiation characteristics of the 15 mm U-shaped loop antenna at different orientations in the area above the left hip of the CST Katja voxel body model

Radiation characteristic Orientation	Radiation efficiency (%)	Maximum 3D-gain (dBi)	Maximum 1-g (RMS) SAR (W/kg) for an input power of 1W	Maximum 10-g (RMS) SAR (W/kg) for an input power of 1 W
First	0.0183	-33.16	267	46.5
Second	0.005	-39.33	333.5	50.35
Third	0.032	-31.1	255.76	46
Fourth	0.00812	-37.61	340	51

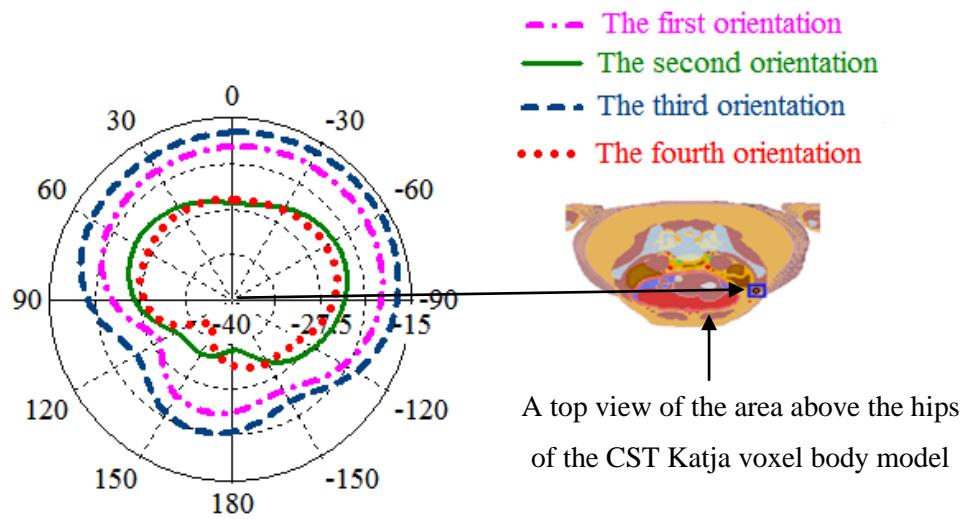


Fig. 4.19: The azimuth radiation pattern for different orientations inside the area above the left hip of the CST Katja voxel body model. The origin of the radiation pattern is at the centre of the cylindrical implantable device (encircled in the blue box).

4.4 Performance of the 10 mm Meandered Loop

Antenna in the Child Voxel Body Model

The small meandered antenna that we proposed in Chapter 3 is also evaluated in an anatomical body model. The small size of this antenna reduces its gain value in the adults anatomical body models such as Katja [118]. However, as long its size facilitates implantation in the small children bodies which are of much smaller losses than adults [81], this antenna is evaluated in a small child body model [3] for a potential application of capsule endoscopy for children. The antenna is simulated at three different organs inside the CST child anatomical model which are the stomach, colon and small intestine. The dielectric properties of these organs are summarized in Table 4.8. The resultant reflection coefficient when this antenna is simulated in these organs is shown in Fig. 4.20.

Table 4.8: Electromagnetic properties of the digestive tract organs [31]

The organ	The relative permittivity (ϵ_r)	The conductivity σ (S/m)
Colon	62.5	0.86
Stomach	67.5	1
Small intestine	66	1.9

It can be seen from the figure that a bandwidth of 200 MHz which covers all bands of interest is always maintained. The resonant frequencies are around 360 MHz for both of the stomach and the small intestine because they have almost the same relative permittivity as indicated in the table. The slight 15 MHz upshift of the resonant frequency inside the colon is due to its smaller relative permittivity which is around 62.5.

All the resonant frequencies are lower than the resonant frequency inside the simplified body model that is composed of muscle and this is mainly because of the larger relative permittivity of the stomach, small intestine and colon in comparison of muscle. However, muscle is still valid and preferable for the simplified body model equivalent material because the digestive tract could be empty sometimes (filled in air without contents). When the empty organs are filled up with air, their relative permittivity are expected to be smaller than when they are filled with contents. On the other hand, antennas that were evaluated in muscle equivalent simplified body model (including the antennas in this thesis) proved to provide a good performance in the anatomical body models [7, 99]. Therefore, it is selected for all the equivalent material of simplified body models in this thesis.

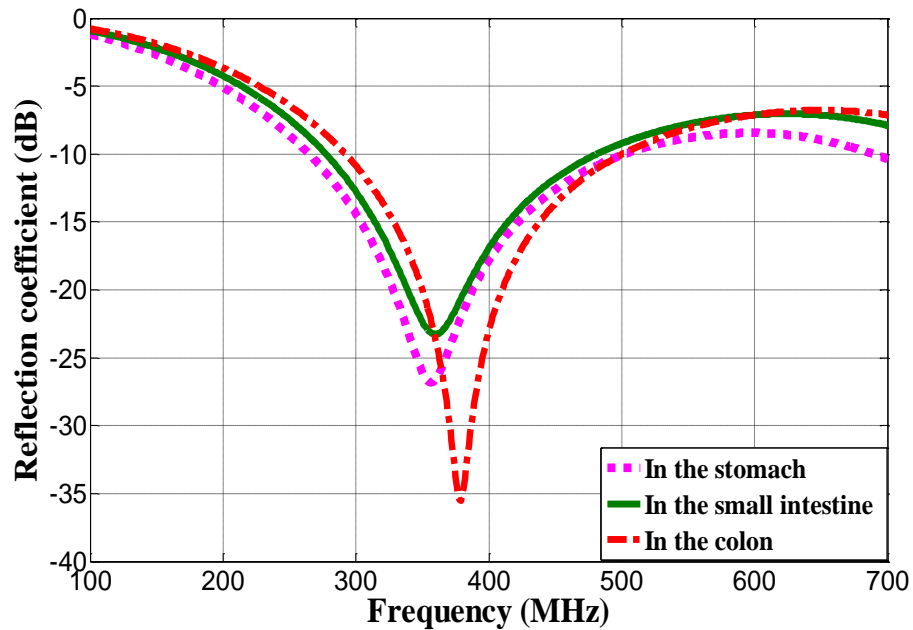


Fig. 4.20: The radiation pattern of the proposed 10 mm meandered loop antenna in different organs of the digestive tract of the CST child body model.

The 3D radiation pattern of the proposed antenna in these different organs of the accurate CST child voxel body models are shown in Fig. 4.21. Although the radiation pattern is symmetric and omnidirectional in the simplified body models, it becomes more directional and asymmetric in the accurate CST child body model because of its asymmetric structure. The radiation pattern in each of these organs is different from the others. However, the largest radiation is always obtained in a direction that is away from the body towards free space. This shows that more directive patterns is expected for most of implantable and ingestible antennas after their actual implantation in the real body models in correspondence with [80]. It also shows the importance of having an array of receiving on-body antennas for this case. Therefore, it is very important to evaluate the performance of capsule antennas in the anatomical body model. The gain and radiation efficiency in all these organs are summarized in Table 4.9. Different orientations of the capsule are attempted (the capsule is rotating while passing through the digestive tract) and the values in this table represent the smallest obtained values.

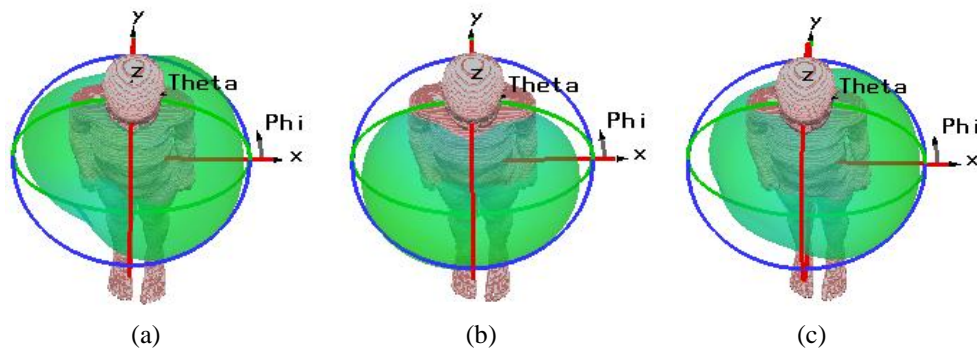


Fig. 4.21: Radiation pattern of the proposed 10 mm meandered loop antenna in the: (a) Colon, (b) Stomach, and (c) Small intestine of the CST child voxel body model.

Larger gain values and radiation efficiency are achieved in the organs of the smaller conductivity. Therefore, the largest gain value is obtained in the colon which is followed by the gain in the stomach and small intestine, respectively. 4.1 dB difference between the largest gain value in the colon and the smallest gain value inside the small intestine is obtained because of the 1.04 S/m difference between their conductivities.

Table 4.9: The realized gain of the proposed 10 mm meandered loop antenna inside the digestive tract of the CST child voxel body model at 403 and 433.

Organ	403 MHz		433 MHz	
	G_{\max} (dBi)	η_r (%)	G_{\max} (dBi)	η_r (%)
Colon	-33.2	0.0146	-32.1	0.0189
Stomach	-34.5	0.0132	-33.9	0.016
Small intestine	-37.3	0.0055	-35.8	0.0057

In order to save the simulation time, simulation of the SAR is only conducted in the small intestine as it has the largest conductivity and expected to obtain the largest RMS 1-g AVG SAR value. A computed value of 280 W/kg is obtained which means that the antenna can be provided by up to 2.86 mW (4.56 dBm) to satisfy the SAR limitations. This power is larger than 0 dBm which is normally provided to implantable devices and chips.

4.5 Summary

In this chapter an in-depth investigation has been conducted on the performance of implantable antennas in the anatomical body model. The investigation has shown the importance of evaluating the implantable antenna performance inside these body models. Unlike the case of simplified body models, the asymmetric structure of the anatomical body models change the overall antenna performance at different positions and orientations. While variations in the radiation efficiency and gain only are obtained at different positions of implantations in the simplified body model, the overall characteristics even the reflection coefficient vary from position to another inside the anatomical body model. The antenna resonant frequency is shifted down when the antenna longest parts are surrounded by tissues of large permittivity. A smaller radiation efficiency and gain and larger SAR are obtained when the antenna longest parts are surrounded by tissues of larger conductivity. The different positions and orientations also change the radiation pattern main lobe magnitude and direction. Up to 52.9, 340, 458.3 and 82% difference in the resonant frequency, radiation efficiency, gain and 1-g SAR are obtained from one position (arm, thigh and hip for this work) to another at the same antenna orientation. On the other hand, 15.7, 540, 347 and 30.4% difference in the resonant frequency, radiation efficiency, gain and 1-g SAR are obtained between the second and third orientations in the area above the left hip. This makes it very important to evaluate the antenna performance in these body models. On the other hand, this shows the importance of the wide bandwidth of implantable antennas to maintain 10 dB band coverage of the frequency ranges of interest. The investigations in this chapter also show the importance of the anatomical body model on the accurate evaluation of radiation pattern. The symmetric structure of the simplified body model makes the radiation pattern omni or almost omni-directional. This is due to the symmetrical absorption from the same material that surround the different antenna parts. On the other hand, the

different absorption from the different surrounding body tissues in the anatomical body model make the pattern more directive into some directions.

Because of the importance of the anatomical body models, different factors that lead to an accurate evaluation in these models are studied. The results show that simulations should include at least the trunk of the anatomical body model to obtain accurate results about the different antenna characteristics in the arm and above the hip. The same results are obtained when the full anatomical body model and trunk is taken in simulations. However, using the trunk only saves half the simulation time and memory.

The performance of the 10 mm meandered loop antenna that is proposed in Chaptr 3 is also validated in this chapter. Due to the antenna small size, evaluations are conducted at different orientations and organs of the digestive tract of an anatomical body model of a child for the applications of a wireless capsule endoscopy for children. The antenna good radiation characteristics make it a good candidate for these applications.

Chapter Five

Metamaterials Inspired-Structures for Implantable Applications

5.1 Introduction

It has already been shown that most of the input power that is fed to implantable antennas is absorbed by the surrounding human body tissues. It has also been shown that a magnetic type antenna such as a loop which has a smaller electric field than an electric type antenna in the near field region, is more efficient inside the human body. This is because the smaller electric near field reduces the absorbed power and increases the radiated power correspondingly. Metamaterials is an artificial material in which electromagnetic properties (μ , ϵ) can be controlled [122]. Metamaterials are of many attractive features in general. They can improve the overall matching and thus radiation from small antennas [123] and reduce the specific absorption rate (SAR) in the head [23]. They can also control the electromagnetic near fields around the antenna which can be exploited to reduce the absorbed power in the human body tissues. All of these characteristics could be very beneficial to improve the overall radiation from implantable antennas. Because of the attractive features of metamaterials and the potential radiation improvement of implantable

antennas by using them, their use for implantable applications is investigated in this chapter.

This chapter aims at the following aspects:

1. Investigating the use of complementary split ring resonators (CSRRs) to obtain the following functions:
 - Increase the overall radiation from the implantable antenna.
 - Decrease the specific absorption rate (SAR) in the human body tissues around the implantable antenna.
2. Investigating the use of multiple split ring resonators (MSRRs) based layer around the implantable antenna and device to obtain the following:
 - Improve the overall radiation from the implantable antenna.
 - Good matching which causes a robust performance in the anatomical and real bodies.
 - Decrease the specific absorption rate (SAR) in the human body tissues around the implantable antenna.

To achieve these purposes, this chapter is organized into two parts: CSRRs structures are first integrated to a loop antenna. The benefits of the CSRRs on the overall antenna performance are discussed. In the second part, a MSRRs based layer is designed and its performance around the 15 mm in length U-shaped loop and reported patch [12] antennas is studied. The principle of operation of the proposed layers and their effect on the overall antenna radiation and performance are then investigated and discussed.

The achievements of this chapter can be summarized as:

- New investigations about utilizing CSRR to improve the radiation and safety performance of implantable antennas are conducted. This is an interesting path of

investigations since normally the CSRR is introduced to reduce the antenna size, here it has been shown that it can reduce the electric near field hence the power loss. Such an investigation is very beneficial to boost more related research and open the doors to more efficient implantable antennas based on metamaterial structures.

- New investigations about utilizing a MSRRs based layer to improve the overall radiation and 10 dB matching of implantable antennas are conducted. The radiated power of the proposed 15 mm in length U-shaped loop antenna is increased by 52.14% at 403 MHz when a MSRRs based layer is bent around it.

5.2 A Broadband Implantable Loop Antenna Inspired by Complementary Split Ring Resonators

5.2.1 Design and Performance

Split Ring Resonators (SRR) are metamaterial structures that can produce negative relative permeability while complementary split ring resonators (CSRRs) are metamaterial structures that can produce negative relative permittivity [18, 124, 125, 126]. A loop antenna based on CSRRs is firstly designed and investigated at this section.

The antenna under investigations is shown in Fig. 5.1. It is a simple flexible loop antenna of an overall width and length of 30 and 15 mm, respectively which can be bent around an implant of 5 mm in radius and 15 mm in length. The antenna is designed following the design methodology proposed in Chapter 3. It is optimized initially in the same simplified elliptic cylindrical structure to obtain the largest radiation efficiency of 0.09, 0.15, 0.22, 0.26 and 0.46% and maximum realized gain of -27.9, -27.21, -25.21, -22.8 and -17.52 dBi in the off body direction at 403, 433, 868, 915 MHz and 2.45 GHz, respectively with a

good matching for $S_{11} < -10$. The antenna main parameters are the spacing between its vertical and horizontal parts which are affected by the width of the vertical and horizontal parts (w_x and w_y , respectively). The wider vertical and horizontal parts shift the resonant frequency up as shown in Fig. 5.2. This is because they decrease the effective feed capacitance and inductance, respectively [98]. The optimum widths of the vertical and horizontal parts are selected as: $w_x = 4$ mm and $w_y = 5.5$ mm.

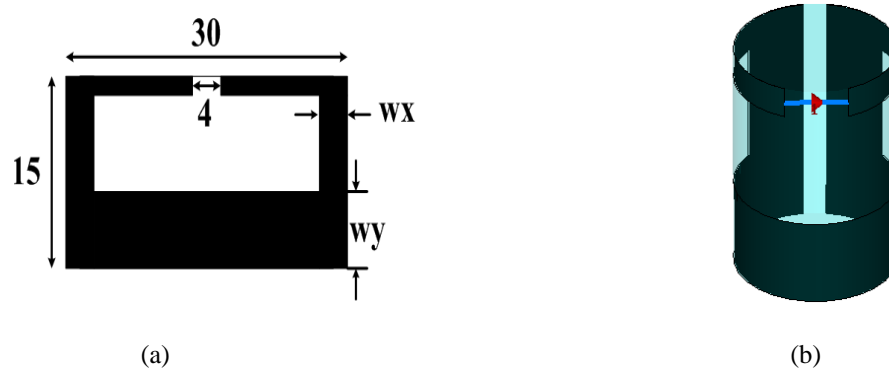


Fig. 5.1: The loop antenna of investigation (a) Flat structure (unit: mm), (b) Bent structure.

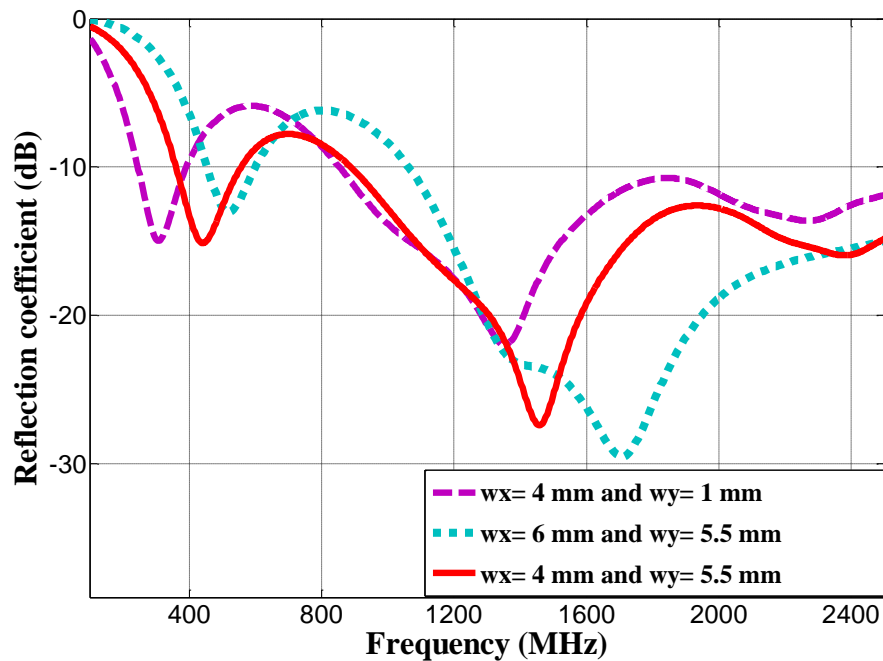


Fig. 5.2: The effect of the loop antenna parameters (w_x and w_y) on the reflection coefficient in a simplified body model.

CSRRs are added to the loop antenna as shown in Fig. 5.3 of the parameters in Table 5.1 to obtain the following two functions:

1) To improve the antenna impedance matching over the frequencies of interests (especially around 400-450 MHz band) as shown in Figs. 5.4 and 5.5. This is achieved because the CSRRs introduce negative permittivity (capacitance) [18, 124] and thus work to reduce the large inductive part of the loop antenna as shown in Fig. 5.5. This results in less reflection and thus a larger radiation. Fig. 5.4 shows that the loop antenna without CSRRs resonates at 456 MHz in the simplified body model. The antenna bandwidth is around 300 MHz which is obtained by controlling the antenna parameters based on the design methodology in Chapter 3. When this antenna is simulated in the arm of the CST katja voxel anatomical body model, the resonant frequency is shifted up as shown in the same figure. This is because the effective electromagnetic parameters (relative permittivity and conductivity) are different in the anatomical body model in comparison with the simplified body model. In addition to muscle, fat and bone which are of much smaller relative permittivity and conductivity than muscle [31] surround the antenna in the arm of the anatomical body model. This reduces the effective relative permittivity around the antenna which shifts the resonant frequency up as explained at Chapter 4. Nonetheless, the results the anatomical body model is close to the results in the simplified body model which confirms the validity of the simplified model.

Table 5.1: The final dimensions of the CSRRs unit cell (Units: mm)

G	X1	X2	X3	X4	Y1	Y2
2	1	1	3	8	0.5	1

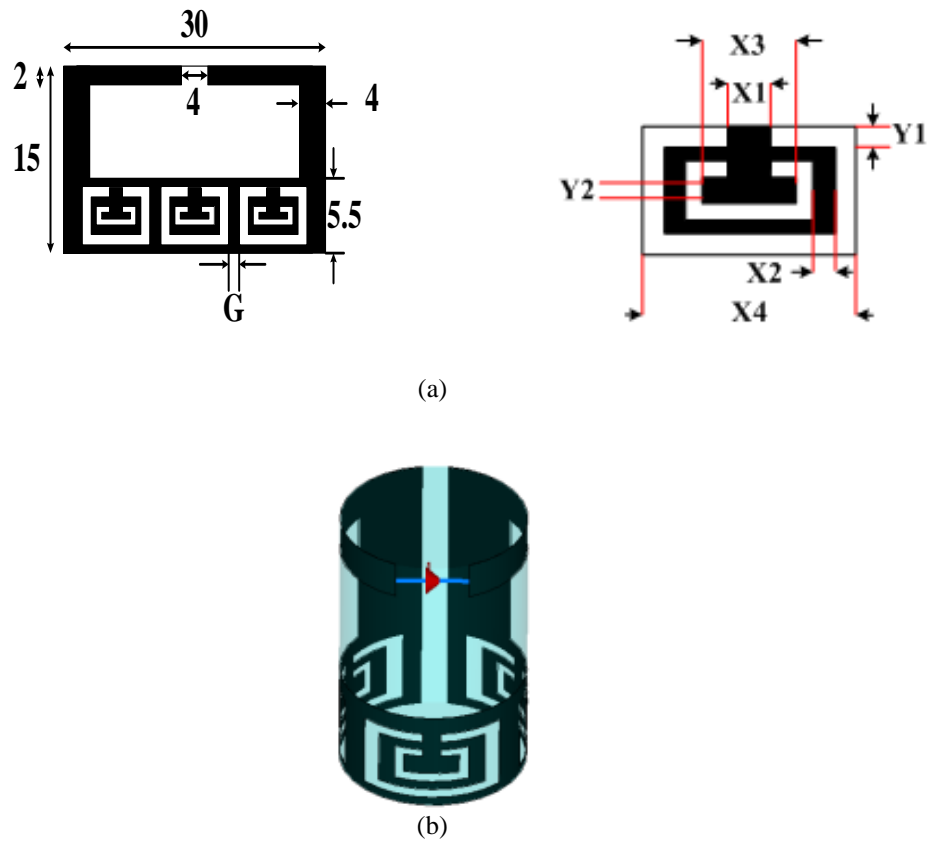


Fig. 5.3: The loop antenna with the CSRRs: (a) Flat structure (b) Bent structure

The loop antenna without the CSRRs has an overall inductive reactance as indicated in Fig. 5.5. When the CSRRs are used, a capacitive reactance is added. The overall structure forms an LC tank circuit of the following resonant frequency [22]:

$$f_r = \frac{1}{2\pi\sqrt{L_{eff}C_{eff}}} \quad (5.1)$$

Where L_{eff} (H) is the equivalent effective inductance and C_{eff} (F) is the equivalent effective capacitance of the circuit.

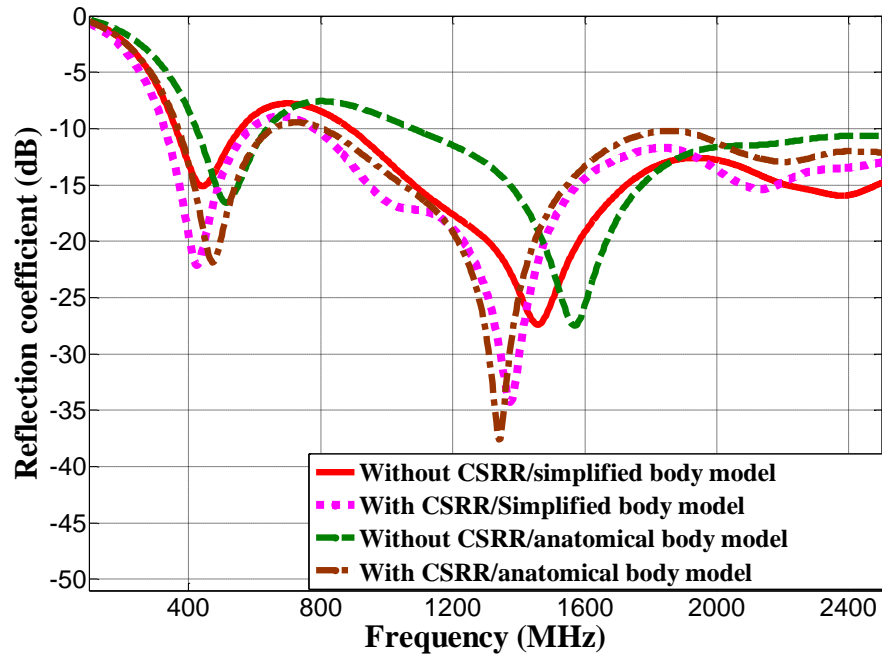


Fig. 5.4: The reflection coefficients of the proposed loop antenna with and without CSRRs inside a simplified and anatomical body models.

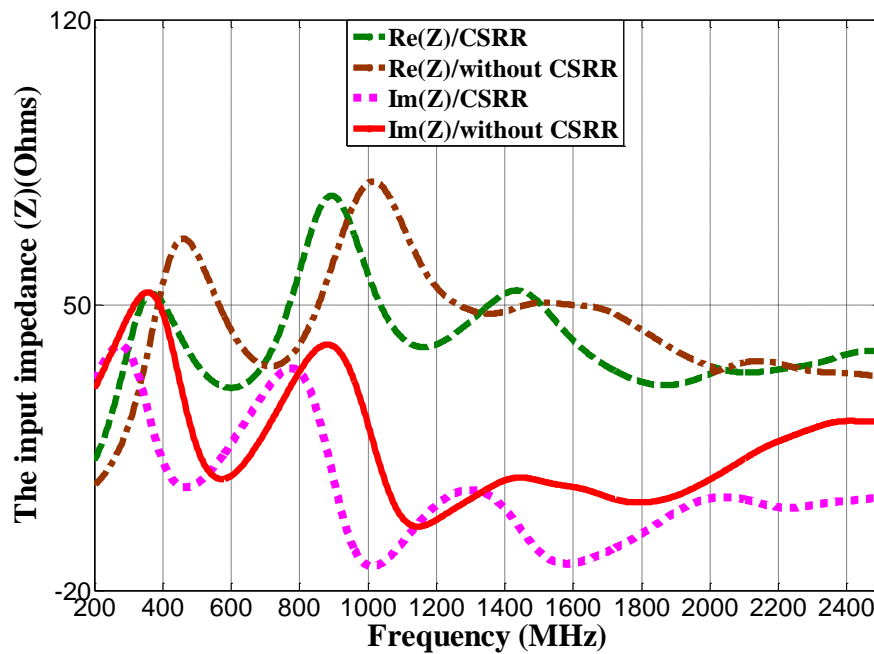


Fig. 5.5: The real (Re(Z)) and imaginary (Im(Z)) parts of the antenna input impedance with and without CSRRs.

The equivalent circuit structure of the proposed loop antenna with and without the CSRRs is shown in Fig. 5.6. The equivalent circuit parameters are summarized in Table 5.2. The parameters with and without CSRRs are the same except for $C2$ which increases from 30 to 50 pF when the CSRRs are added to the antenna structure. This is because CSRRs add capacitance to the circuit which shifts the resonant frequency down referring to Eq. (5.1) as shown in Fig. 5.4. The down-shift of the resonant frequency is limited due to the limitations of the physical dimensions of the antenna and CSRRs.

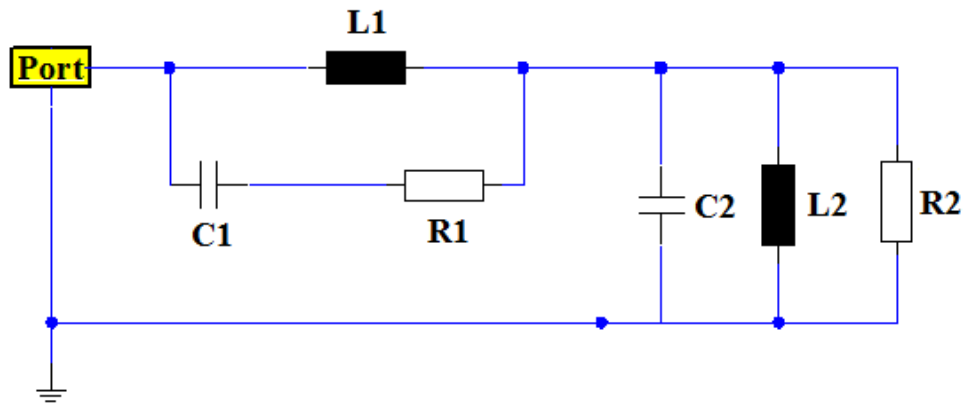


Fig. 5.6: The equivalent circuit for the proposed loop antenna with and without CSRRs

Table 5.2: The equivalent circuit parameters with and without CSRRs

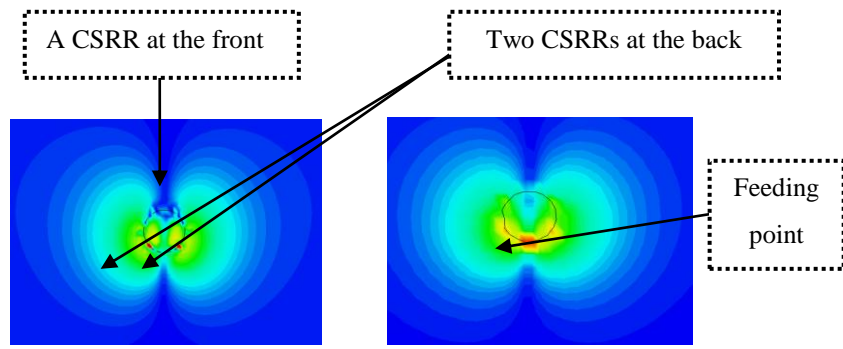
Component	Without CSRRs	With CSRRs
C2 (pF)	30	50
R2 (Ω)	30	30
L2(nH)	2	2
C1 (pF)	20	20
R1 (Ω)	25.44	25.44
L1 (nH)	13	13

2) To increase the antenna radiation efficiency and gain. In addition to the improvement on the impedance matching, the CSRRs reduce the electric near field of the antenna as shown in Fig. 5.7. When the electric near field is reduced, the absorbed power is also reduced as explained in Chapter 2. Thus the radiated power as defined in Eq. (5.2) [3] is increased accordingly. As a result, the antenna radiation efficiency and gain are increased. The SAR is also decreased as explained in Section 2.2.1.

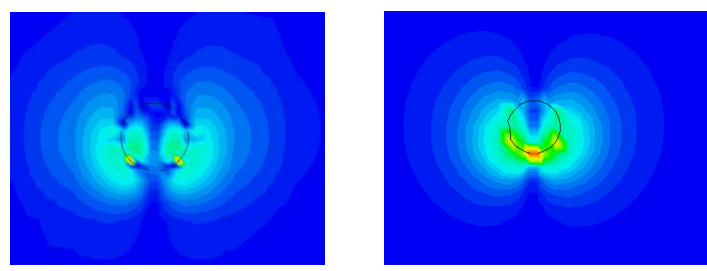
$$P_{in} = P_{rad} + P_{ref} + P_{abs} \quad (5.2)$$

where P_{in} (W) is the input power to the antenna, P_{ref} (W) is the reflected power and P_{rad} (W) is the radiated power.

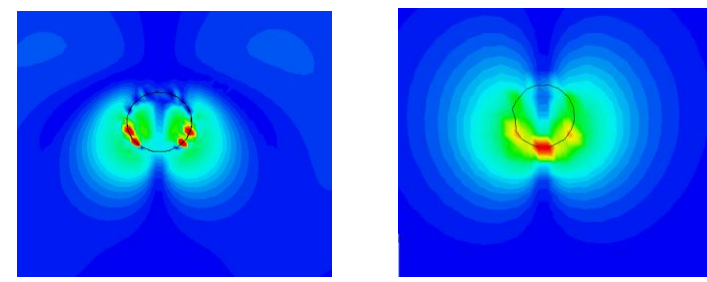
The CSRR unit cell dimensions are mainly restricted by the available physical dimensions of the structure. However, they are carefully selected to obtain the maximum possible improvement of the matching and radiation efficiency and gain with $S_{11} < -10$ dB for all the bands of interest. A parametric study was conducted and the final dimensions are selected as given in Table 5.1. When the spacing (G) shown in Fig. 5.3 is smaller than the selected value in the table, it confines a larger electric near field which is undesired as it increases power loss [3, 19]. This also shifts the resonant frequency above the MedRadio band as shown in Fig. 5.8. When (X1 and X2) are larger than the values in the table, they reduce the overall capacitance and thus shift the resonant frequency up. Y1 and Y2 are restricted by the available dimension of the lower part which is only 5.5 mm. The effect of some of the CSRR unit parameters are shown in Fig. 5.8.



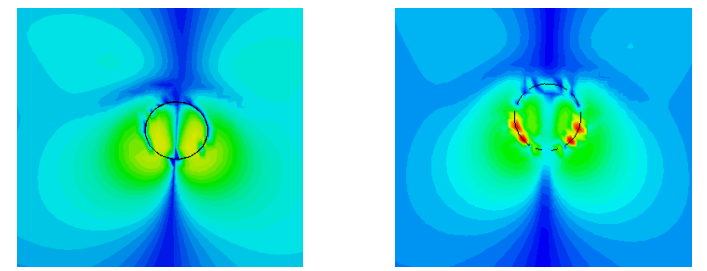
(a)



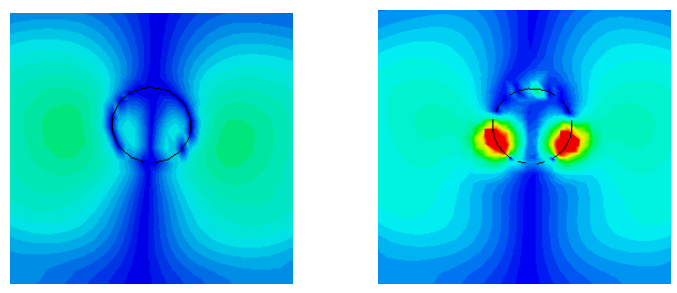
(b)



(c)



(d)



Without CSRRs

With CSRRs

(e)

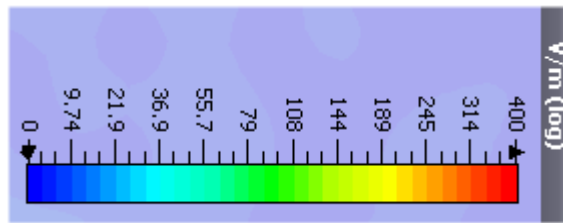


Fig. 5.7: The electric near field intensity with and without CSRRs in a simplified body model at: (a) 403 MHz, (b) 433 MHz, (c) 868 MHz, (d) 915 MHz, and (e) 2.45 GHz. The scale is the same for all above results in the figure.

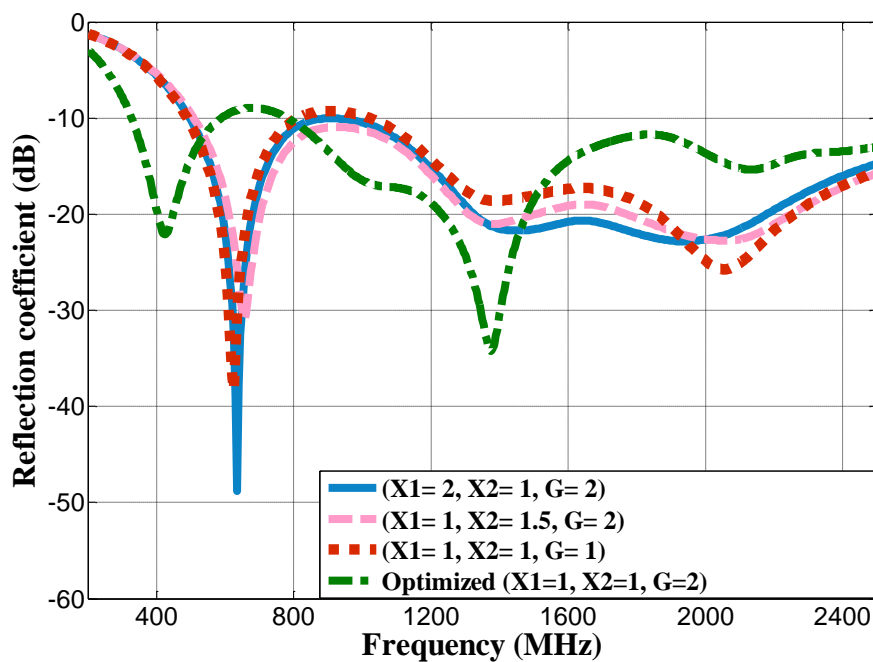


Fig. 5.8: The effect of the CSRRs unit parameters on the reflection coefficient S_{11} .

The computed total radiation efficiency and realized gain with and without CSRRs in the simplified body model are summarized in Table 5.3. The results in the table show that the antenna radiation efficiency and gain are increased by around 2 dB in average when the CSRRs are used.

Table 5.3: The total radiation efficiency and maximum realized gain of the proposed loop antenna with and without CSRRs in the simplified body model.

Frequency (MHz)	Radiation efficiency (%)		Max realized gain (dBi)	
	With CSRRs	Without CSRRs	With CSRRs	Without CSRRs
403	0.12	0.09	-26	-27.9
433	0.2	0.15	-25.1	-27.21
868	0.3	0.22	-24	-25.21
915	0.35	0.26	-21	-22.8
2450	0.53	0.46	-15	-17.52

Simulations are also conducted in the full anatomical body model which provides more accurate data than the simplified body model. The far-field pattern is shown in Fig. 5.9. The radiation becomes directional in the anatomical body model because of the different absorption levels from different tissues around the different parts of the antenna. However, the maximum radiation is obtained in the off-body direction toward free space. Larger field intensities are obtained at the higher frequencies because of the larger electrical size of the antenna at these frequencies [3]. The main lobe direction at 403 and 433 MHz is obtained at the same angle which is 0 deg. This differs by 90 degrees from the main lobe direction at 868 and 915 MHz. The main lobe direction at 2.45 GHz is obtained at around 23 degrees.

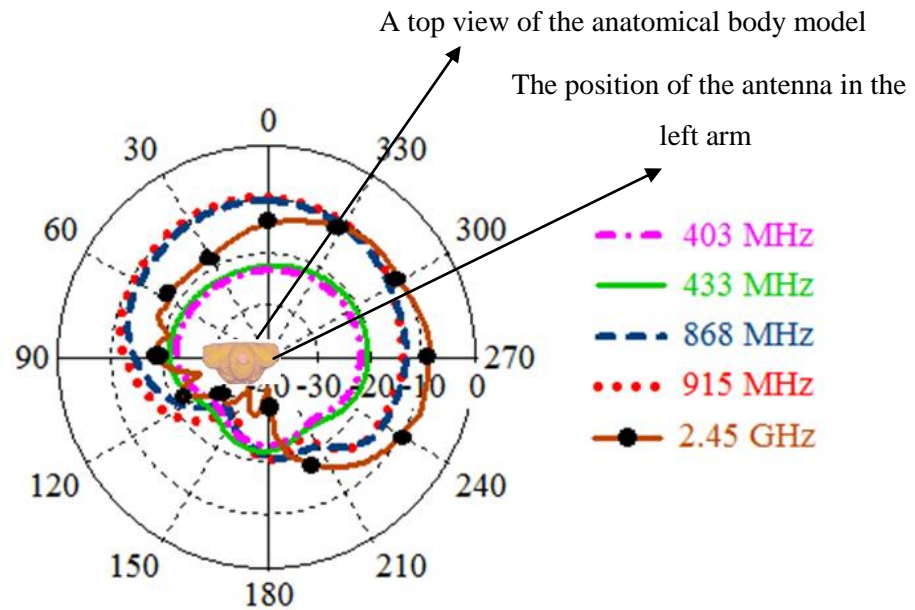


Fig. 5.9: The far-field polar radiation pattern of the proposed loop antenna with CSRR in the anatomical body model.

The radiation efficiency and gain are also computed in the anatomical body model. The results are summarized in Table 5.4. 2 dB improvement of the realized gain is obtained in the anatomical body model when the CSRRs are used. This confirms the beneficial effect of the CSRRs on improving the radiation from the human body.

The 3D far-field gain pattern around the anatomical body model for the antenna orientation and position which are shown in Fig. 5.10. The direction of the maximum gain is obtained at 281, 274, 15, 19 and 254 degrees for the above frequencies, respectively. The radiation becomes directional in the anatomical body model. This is because this body model is asymmetric. Different absorption levels are obtained from the different human body tissues that surround the antenna parts.

It should be pointed out that for an accurate and full evaluation, different orientations of the antenna are examined at this position in the arm. The largest radiation efficiency and gain and smallest 1-g average SAR at this position are obtained for the first orientation (when the antenna in Fig. 5.10 is rotated 90 degrees clockwise around the z-axis). The results are summarized in Table 5.5

Table 5.4: The smallest total radiation efficiency and 3D realized gain of the proposed loop antenna with and without CSRRs in the arm of the CST Katja voxel body model for the implant orientation that is shown in Fig. 5.10

Frequency (MHz)	Radiation efficiency (%)		Max 3D realized gain (dBi)	
	With CSRRs	Without CSRRs	With CSRRs	Without CSRRs
403	0.013	0.009	-36	-38.1
433	0.017	0.013	-35.3	-37.1
868	0.11	0.09	-34	-35
915	0.13	0.1	-29	-31
2450	0.17	0.14	-19.8	-22.24

It is indicated from the results in the table that the antenna radiation efficiency and gain are also increased when the CSRRs are used by around 2 dB in the anatomical body model at all the frequencies of interest. The smallest gain value at this orientation (shown in Fig. 5.10) is -36 dB. This value is larger than the targeted -37 dBi value for robust communication at a distance of 20 m (as explained in the section about the design methodology).

The average RMS 1-g SAR is computed in the anatomical body model. The simulation results are summarized in Table 5.6 and compared without CSRRs.

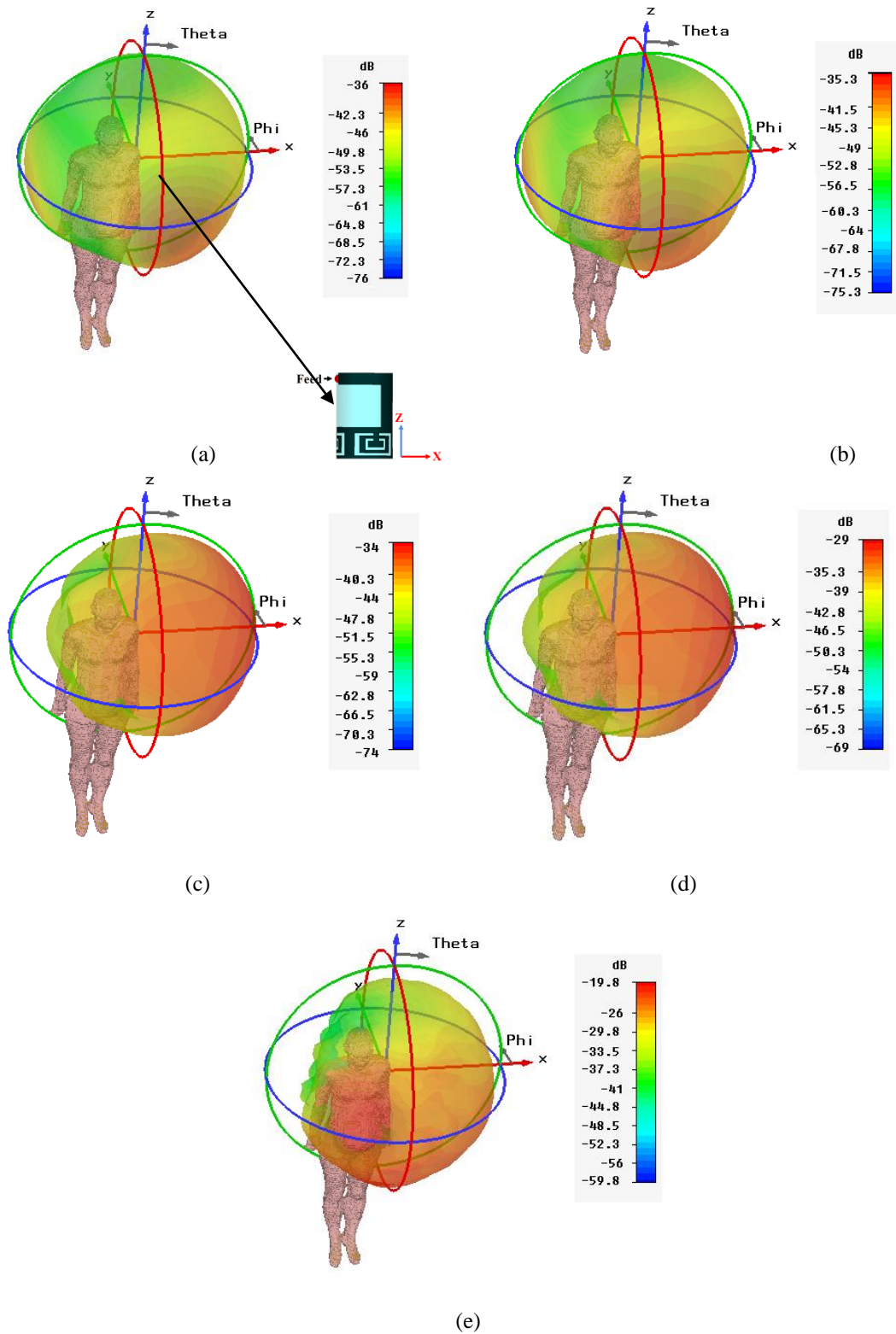


Fig. 5.10: The 3D far-field gain radiation patterns of the proposed antenna with CSRRs in the anatomical body model at (a) 403 MHz, (b) 433 MHz, (c) 868 MHz, (d) 915 MHz, and (e) 2.45 GHz.

Table 5.5: The largest total radiation efficiency and maximum 3D realized gain of the proposed loop antenna with CSRRs for the first implant orientation in the arm of the CST Katja voxel body.

Frequency (MHz)	Total radiation efficiency (%)	Realized gain (dBi)
403	0.04	-30.2
433	0.051	-29
868	0.33	-28
915	0.39	-25
2450	0.51	-17

Table 5.6: The maximum 1-g averaged SAR of the proposed loop antenna with and without CSRRs in the anatomical body model for an input power of 1 W.

Frequency (MHz)	SAR (W/kg)	
	With CSRRs	Without CSRRs
	1-G AVG	1-G AVG
403	115	180
433	112.5	178
868	108	175
915	101	170
2450	99	166

The results show that the maximum 1-g SAR can be decreased significantly when the CSRRs are used. The maximum input power to the antenna to satisfy the SAR limits of 1.6 W/kg with CSRRs at the frequency (403 MHz) in which the implantable device acts as a transmitter can be up to 13.9 mW (11.43 dBm).

5.2.2 Realization and Measurements

The structure is realized by cutting a piece of copper sheet and measurements are conducted in pork while the antenna is bent around the implant as shown in Fig. 5.11. Pork is selected because it provides a good heterogeneous medium to measure the implantable antenna performance over a broad range of frequencies. A small cylindrical tube of Propylene is used as the implant [3]. However, simulations are conducted to evaluate the effect of the dielectric properties of the implant material on the antenna performance and a negligible effect on both of the reflection coefficient and radiation efficiency is obtained. The dielectric properties of the used pork is measured using Agilent 85070E dielectric probe and dielectric properties of ($\epsilon_r = 59.2, 59, 56.7, 56$ and 51.9) and ($\sigma = 0.77, 0.84, 0.96, 1$ and 1.74 S/m)) for muscle and ($\epsilon_r = 6.4, 6.1, 5.8, 5.75$ and 5) and ($\sigma = 0.061, 0.062, 0.055, 0.058$ and 0.12 S/m)) for fat are recorded at 403, 433, 868, 915 MHz and 2.45 GHz, respectively. The antenna inside the pork phantom is shown in fig. 5.12.



Fig. 5.11: Antenna prototypes.

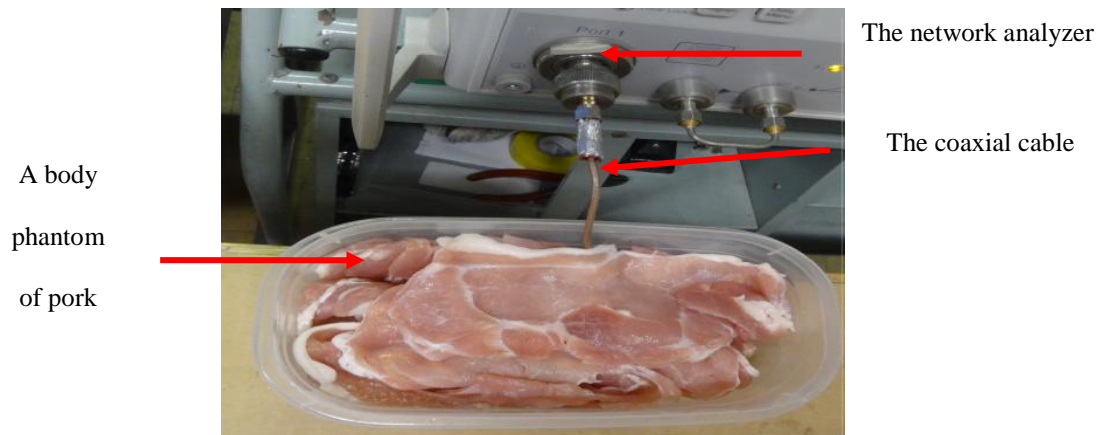


Fig. 5.12: The antenna inside a pork phantom.

Measurements of the reflection coefficient are conducted while the antenna is surrounded by non-uniform layers of both fat and muscle and the results are shown in Fig. 5.13. For comparison purposes, simulation in a non-uniform piece of the anatomical body model that mimics the pork phantom is conducted. Both the simulated and measured results are well below -10 dB and in good agreement at the frequencies of interest, but there are discrepancies which are mainly due to the fabrication errors and the connector which was not taken into account in the simulation.

To emphasize the benefits of using the CSRRs, the transmission coefficient between the proposed antenna and an external meandered loop antenna is compared for the cases with and without CSRRs at the same conditions (spacing of 2.5 meters to meet the far field condition, same input power, antenna position and orientation). The results are shown in Fig. 5.14. Over 2 dB larger transmission coefficient is obtained when the CSRRs are etched on the antenna. This is because of the larger radiation efficiency and gain are obtained when CSRRs are used.

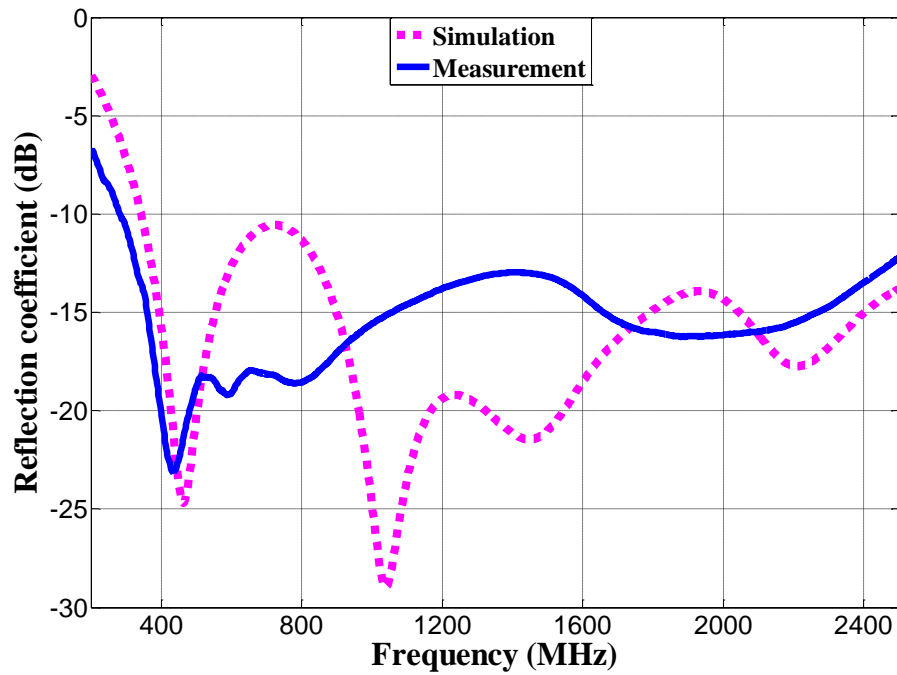


Fig. 5.13. The measured and simulated reflection coefficient S11 for the proposed antenna in pork

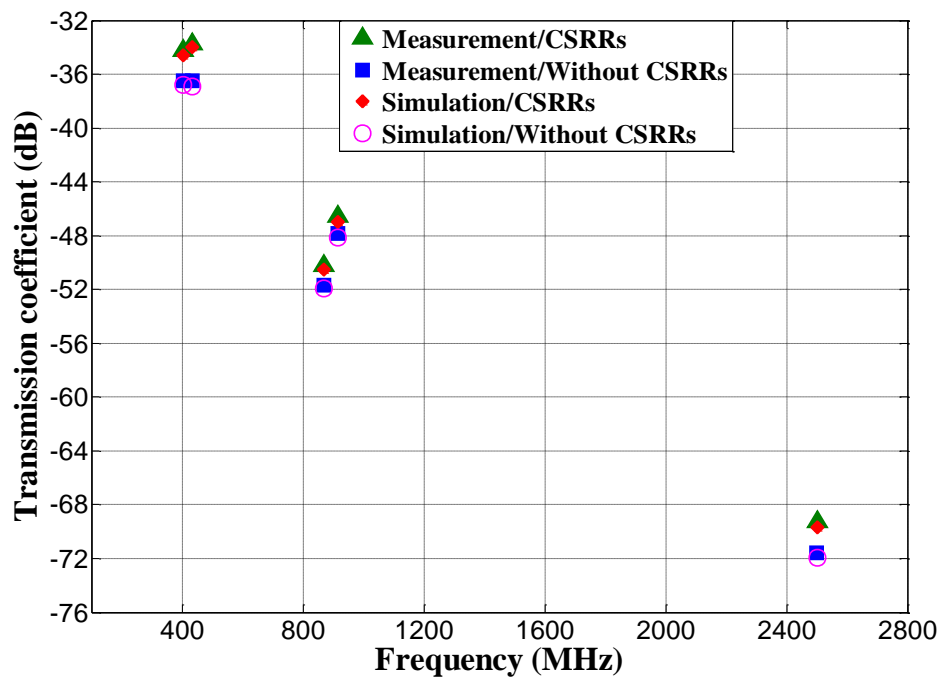


Fig. 5.14: The measured and simulated transmission coefficient for the proposed antenna in pork with and without CSRR.

5.3 Layers Based on Multiple Split Ring Resonators (MSRRs) around the Implantable Antenna

This section investigates the use of layers based on MSRRs around the implantable antenna to improve its performance and radiation. Similar to CSRRs, the proposed layer works to improve the antenna matching and overall radiation. However, this layer is used around the antenna and not integrated to the antenna structure itself.

The proposed layer is mainly influenced by the designs in [82, 127, 128]. The layer is constructed by printing MSRRs on the top of a dielectric layer of a relative permittivity of 3 ($\epsilon_r = 3$). Each unit cell of the MSRRs unit is composed of two rings which are printed at broad directions on the top and bottom of a dielectric layer as shown in Fig. 5.15. The number of the unit cells on each layer is mainly influenced by the antenna size around which the proposed layer is placed.

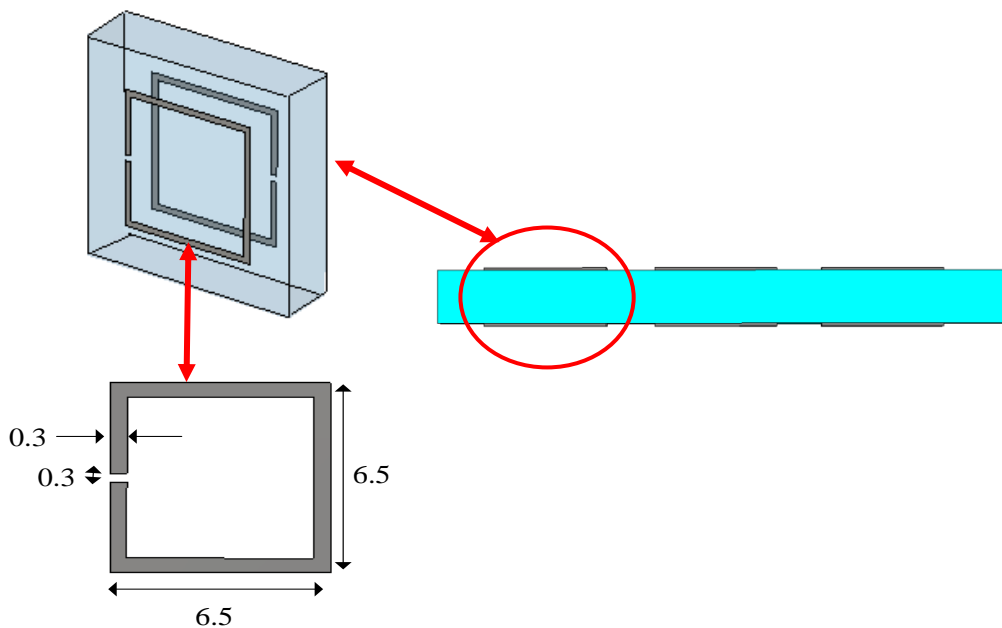


Fig. 5.15: The unit cell of the proposed MSRR based layer

The main objective of using this layer is to decrease the antenna electric near field and increase its magnetic field. This will decrease the absorbed power accordingly as explained before. As long as the rings are printed on the dielectric layer, MSRRs are used instead of CSRRs.

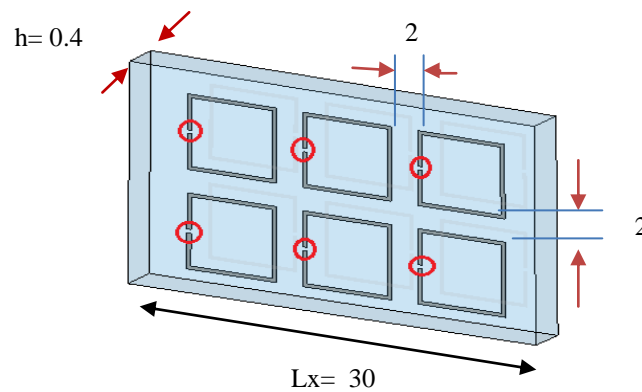
5.3.1 Performance around the 15 mm U-shaped Loop Antenna

The performance of the proposed layer around the 15 mm flexible U-shaped implantable loop antenna which was proposed in Chapter 3 is evaluated at this section. The proposed layer has an overall width of 30 mm and length of 15 mm to fit around an implant of 5 mm in radius and 15 mm in length. An array of (2×3) SRRs are printed on each side of the layer as shown in Fig. 5.16. The proposed layer is bent around the implantable antenna and wrapped around a cylinder of 5 mm in radius and 15 mm in length as shown in Fig. 5.16. Simulations are then conducted in the elliptic cylindrical body model of relative permittivity of 57.1 and conductivity of 0.79 S/m which resemble the dielectric properties of a human muscle in the MedRadio band. Simulations are repeated with a normal dielectric layer (without MSRRs) of the same relative permittivity and dimensions for the purposes of comparison. The reflection coefficients for both cases are shown in Fig. 5.17. The antenna resonates at 414 MHz and have a bandwidth of 230 MHz.

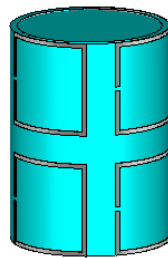
Dimensions of each cell, number of cells and spacing between them are carefully selected to obtain the following targets:

- A good matching. This is desired to overcome the frequency detuning which may happen after implantation in the real human body [1, 81, 129]. The good matching will also reduce the overall reflections and thus increase overall radiation.

- A broad 10 dB bandwidth of wider than 200 MHz to guarantee coverage of the bands of interest regardless of any frequency shift that may happen in the real human body.
- The largest possible increase of radiation efficiency, gain and overall radiated power in comparison with the case without the MSRRs based layer.
- Keep a light weight and small overall size of the implantable device.



(a)



(b)

Fig. 5.16: The MSRRs based layer to bend around the 15 mm U-shaped loop antenna: (a) Flat structure (b) Bent around a cylindrical implant; (units: mm).

Both bands (MedRadio and 433 MHz ISM) of interest are still obtained for $S_{11} < -10$ dB when the MSRRs based layer is used. However, a better matching is obtained when the MSRRs based layer is used.

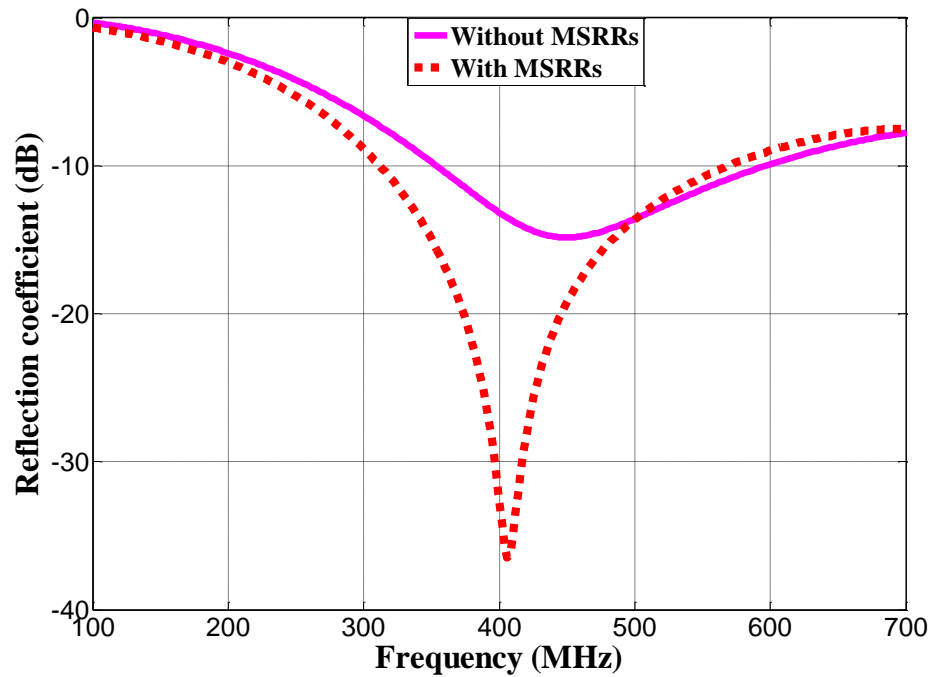


Fig. 5.17: The reflection coefficient S_{11} with and without MSRRs based layer in the simplified body model

The overall structure with the MSRRs can be modelled as an LC circuit as shown in Fig. 5.18.

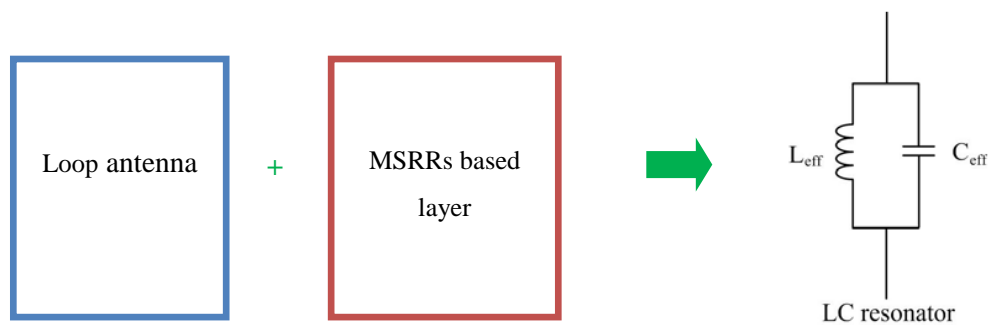


Fig. 5.18: The concept of matching the U-shaped loop antenna using MSRRs based layer

While the reactance of the U-shaped loop antenna of investigation in free space is zero, it becomes negative in the human body model. This is due to the capacitive loading of the surrounding human body tissues that have large effective permittivity. This contributes to increase the total effective capacitance in the circuit. To compensate for this capacitive

reactance, an inductive reactance is added by the MSRRs based layer. The resultant overall structure has a real part of 50 Ohms and a zero reactive component as shown in Fig. 5.19.

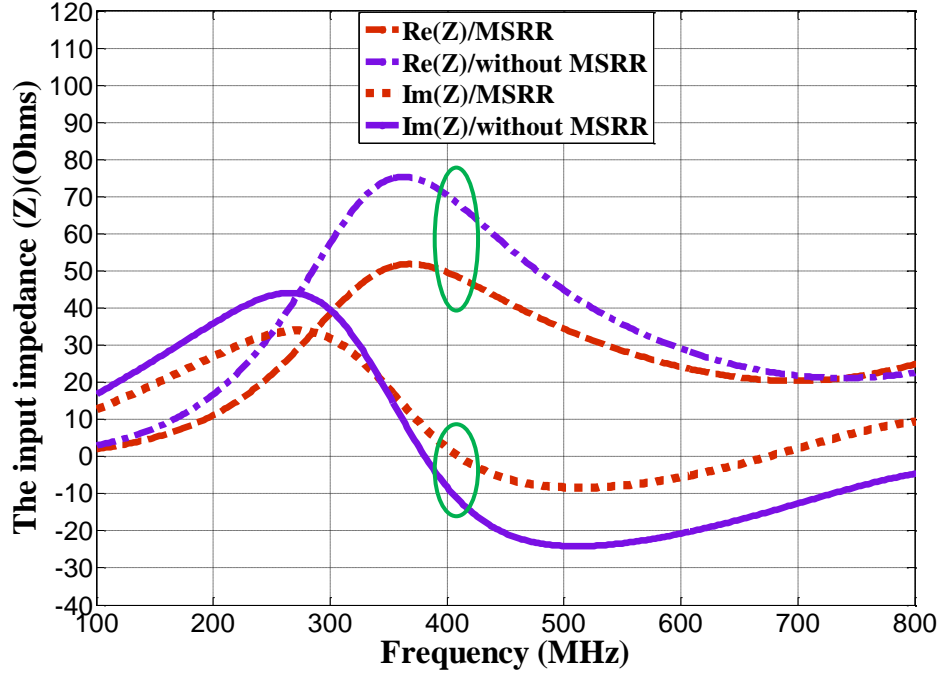


Fig. 5.19: The real (Re(Z)) and imaginary (Im(Z)) parts of the antenna input impedance with and without MSRRs in the simplified body model.

The simulations show that the radiated power is increased when this MSRRs based layer is used. The percentage of power improvement of the radiated power $P_{improvement}$ (%) is defined in Eq. (5.3).

$$P_{improvement} (\%) = \frac{P_{t,MSRRs} - P_{t,NoMSRRs}}{P_{t,NoMSRRs}} \quad (5.3)$$

where $P_{t,MSRRs}$ is the radiated power when the MSRRs based layer is used and $P_{t,NoMSRRs}$ is the radiated power when no MSRRs based layer is used.

Using the simulated results by CST in to Eq. (5.3), an improvement percentage of 52.14% is obtained. This is actually obtained because the MSRRs based layer decreases the

electric near field and increases the magnetic field as shown in Figs. 5.20 and 5.21, respectively which is reflected on a smaller absorbed power as explained above.

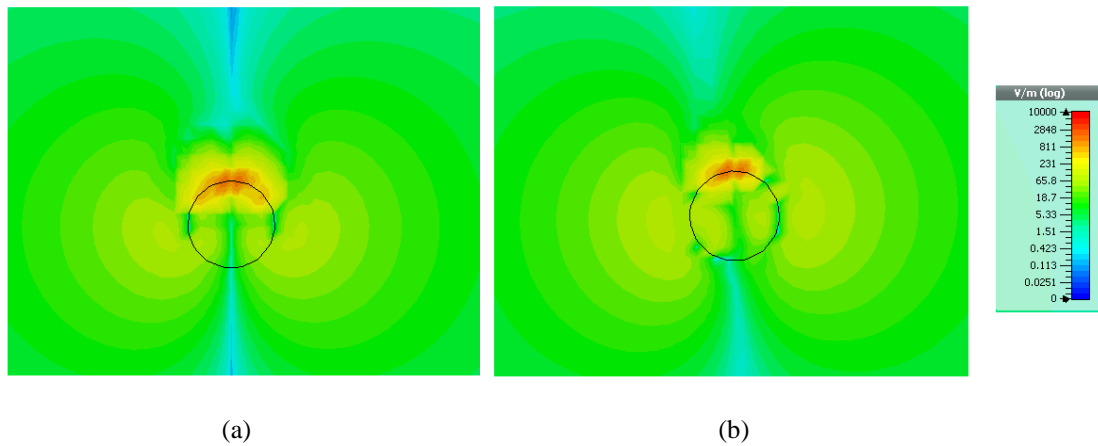


Fig. 5.20: The electric field around the antenna in the simplified human body at 403 MHz: (a) Without MSRRs, (b) With MSRRs

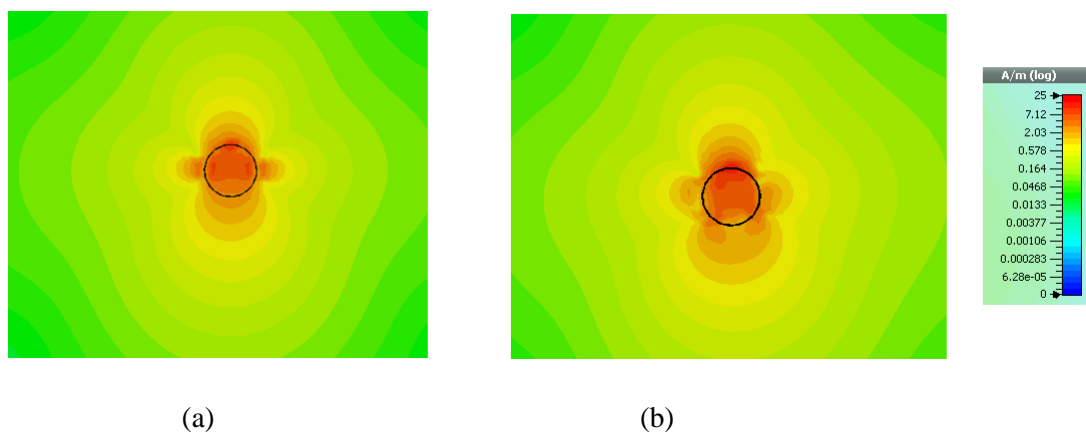


Fig. 5.21: The magnetic field around the antenna (shown in a top view) at the centre of the simplified human body at 403 MHz: (a) Without MSRRs, (b) With MSRRs

The radiated power is increased in the lossy human body due to the reduction of the absorbed power when the MSRRs based layer is used. To verify this special behaviour of the MSRRs based layer and verify its special behaviour in the lossy human body, both structures (with and without MSRRs) are simulated in a lossless simplified body model of the same shape and dimensions of the lossy body model that is used above. The MSRRs based layer

improves the antenna matching as shown in Fig. 5.22 even in a lossless body model. The resonant frequency in the lossless body model is higher than the resonant frequency in the lossy body model in correspondence with the results in [7]. The radiation efficiency at a frequency of comparison is found to be the same for both structures in the lossless body model. This agrees very well with the proposed concept about the special behaviour of the proposed layer around the loop antenna inside the lossy human body in correspondence with magnetic sources.

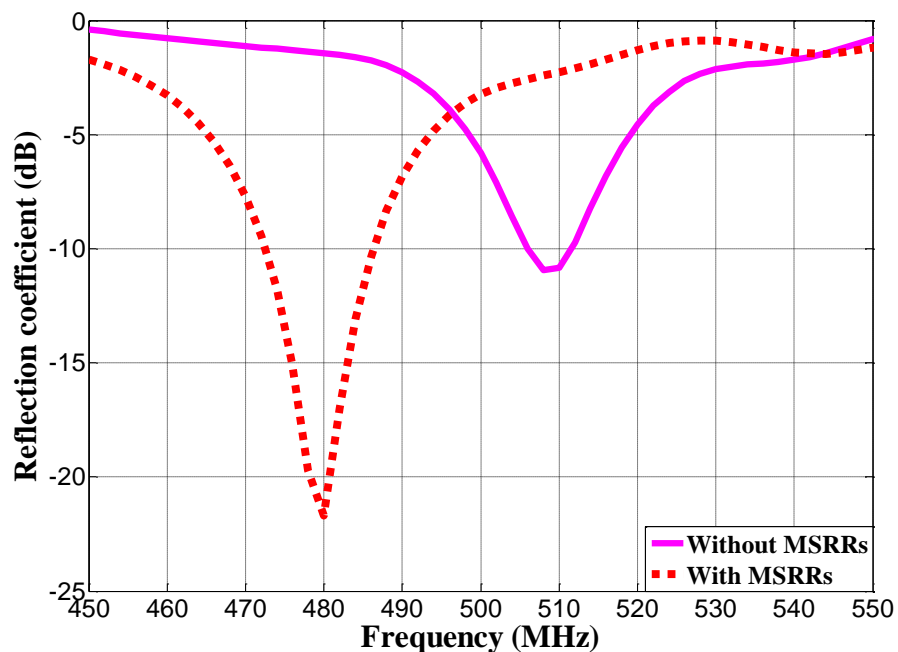


Fig. 5. 22: The reflection coefficient of the proposed antenna with and without the MSRRs based layer in a lossless simplified body model.

The following points should be indicated:

1. The control of the permittivity and permeability is indicated by the change of the electric and magnetic fields, respectively which is found to be obtained when the suggested structures in this chapter are used.

2. The beneficial effect of the proposed structures is mainly obtained due to the reduction of the electric field in close proximity to the antenna which is reflected on a smaller absorbed power and larger radiated power as indicated above. This is confirmed by the reduction of SAR which will not be obtained if these structures contribute by other means of improvement such as improving the radiation pattern in a specific direction.
3. The radiation pattern with and without the proposed structures is almost the same. This confirms that the proposed structures have no effect on the radiation pattern for the cases of investigation.
4. The magnetic field increases when the proposed structures are used as shown in Fig. 5.21. This is reflected on increasing the antenna gain referring to Eqs. (2.13-2.15) and as indicated in the results of Table 5.4.

5.3.1.1 Performance with Different Layer Thicknesses

Different layer thicknesses are simulated to study the effect of the layer thickness on the overall radiation improvement and band coverage. The layers of smaller thicknesses (thinner than 0.4 mm) have almost the same effect of the same radiated power, matching and bandwidth. However, a desirable effect of an extra band coverage for important implantable applications is obtained with an insulation thickness of 0.5 mm. The performance with a layer of 0.5 mm in thickness is shown in Fig. 5.23. When the thickness of the insulation layer becomes 0.5 mm, the resonant frequency of the antenna is shifted up. This is due to the smaller effective permittivity around the antenna as the thicker insulation layer replaces more body tissues. This frequency up-shift has the advantage of covering the 2.45 GHz. However, this is accompanied with mismatching ($S_{11} > -10$ dB) over the MedRadio (401-406 MHz) band when a normal dielectric layer is used. As the MSRR based layer improves the antenna matching over the MedRadio band, it manages to maintain coverage of the entire

MedRadio and 433 MHz bands and at same time to cover the 2.45 GHz ISM band for $S_{11} < -10$ dB which support the functionality of power saving by using a wakeup receiver.

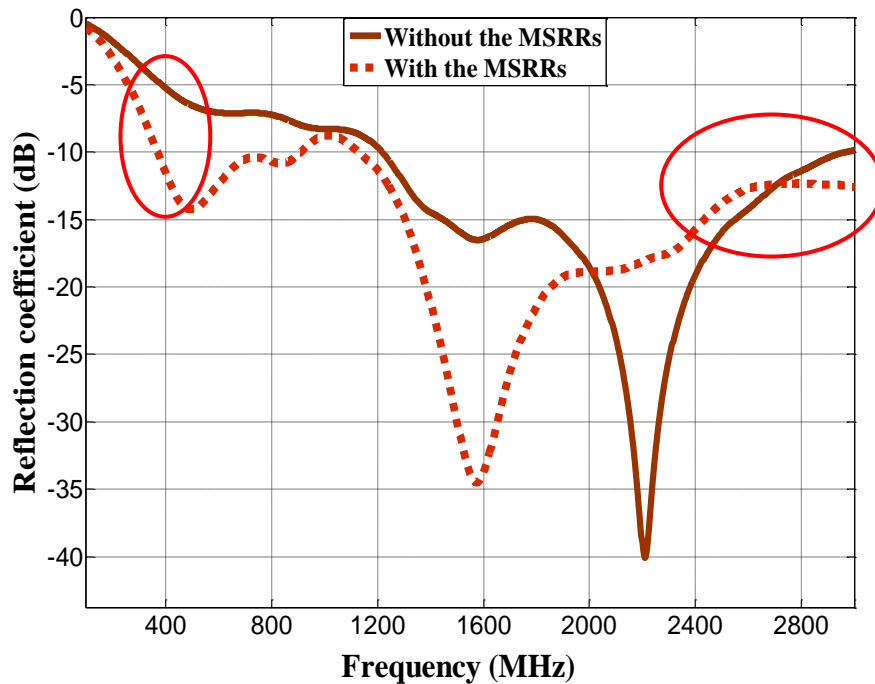


Fig. 5.23: The reflection coefficient of the proposed antenna with and without the MSRRs based layer of 0.5 mm in thickness.

5.3.1.2 Performance in the Anatomical Body Model

To verify the results in the anatomical body model which has a multilayer and heterogeneous structure of much better resemblance of the real human body, simulations are conducted in the arm of the CST Katja body model as shown in Fig. 5.24.

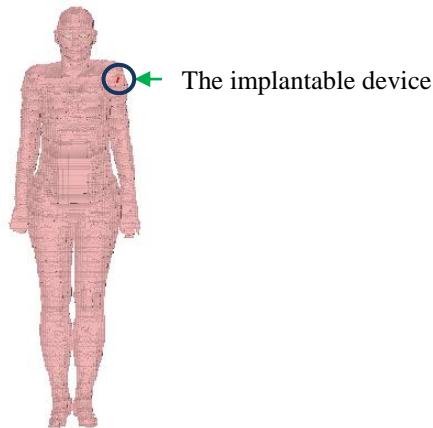


Fig. 5.24: The antenna in the arm of an anatomical body model of an adult.

It is worth mentioning that for an accurate evaluation in these body models which are asymmetric, different orientations should be examined even at the same position. However, the objective of the investigation at this section is to verify the improvement on the overall antenna characteristics when the MSRRs based layer is used. Therefore, the results are only compared for one orientation at the same position. The resultant reflection coefficient with and without MSRRs for an insulation thickness of 0.4 mm is shown in Fig. 5.25. In agreement with the results in the simplified body model, a better matching is obtained when the MSRR based layer is used. 1.8 dB of power improvement is obtained for this case at 403 MHz. This matches with the results in the simplified body model. The resonant frequency is slightly shifted up for this orientation where most of the antenna and layer parts are surrounded by more fat than muscle. It is also worth mentioning that simulation with an insulation thickness of 0.5 mm is also examined. The entire matching is disturbed when MSRR based layer is not used over this thickness in agreement with the results in the simplified body model.

The 3D far-field gain radiation patterns with and without the anatomical body model are shown in Fig. 5.26. The maximum radiation is obtained at the same direction for both

cases. However, 52.4% larger 3D maximum gain is obtained when the MSRRs based layer is used.

As the 1-g AVG SAR is more restricted than the 10-g SAR, it is computed inside this model and is shown in Fig. 5.27. The figure shows that 23.81% smaller 1-g AVG SAR is obtained when the MSRRs based layer is used. Stronger SAR distributions are also seen in close proximity to the antenna when the MSRRs based layer is not used.

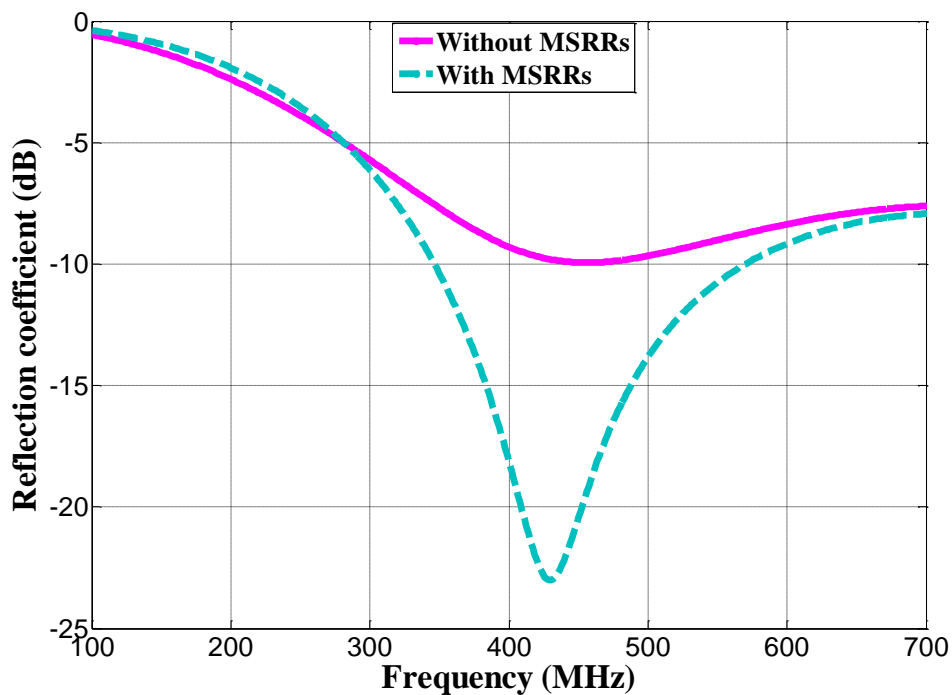


Fig. 5.25: The reflection coefficient with and without MSRRs in the arm of an anatomical body model of an adult.

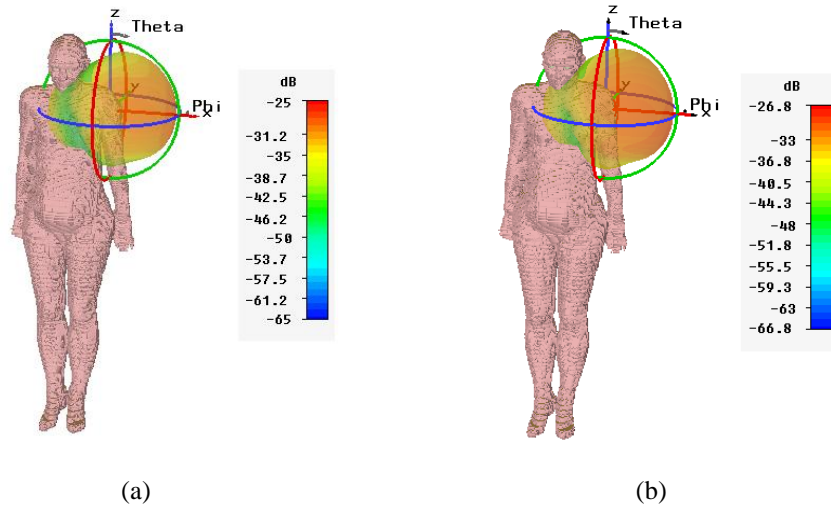


Fig. 5.26: The 3D far-field gain radiation patterns of the antenna at 403 MHz: (a) With MSRRs, (b) Without MSRRs.

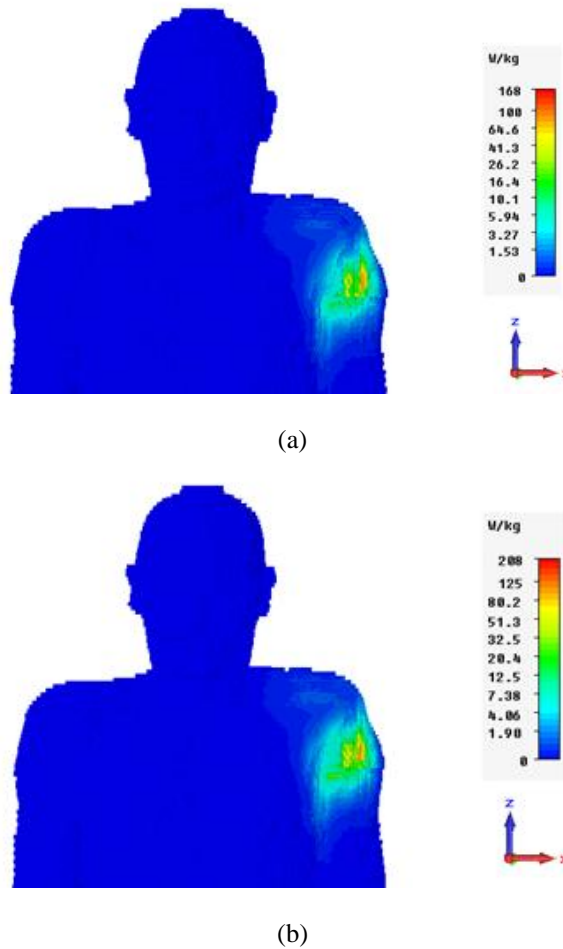


Fig. 5.27: The max 1-g AVG SAR at 403 MHz in the arm of an anatomical body model of an adult: (a) With MSRRs, (b) Without MSRRs.

5.3.1.3 Investigations about Biocompatibility

The existence of the conducting MSRRs on the top of the insulation layer in direct contact with the human body requires further actions to satisfy biocompatibility in comparison with the case without them. Therefore, it should be used under the following two conditions:

- The layer is obtained using biocompatible conductors such as Titanium and gold [130-133].
- The layer top is surrounded by a thin biocompatible insulating layer. For example, a layer of 0.4 mm in thickness is surrounded by an extra layer of 0.1 mm in thickness (the performance should be compared with an insulating layer of 0.5 mm in thickness for this case to verify the advantage of its use).

Both of these cases are investigated at this section. Firstly, simulations with Titanium instead of copper is conducted. The reflection coefficient and radiation improvement is found to be almost the same. This is also verified for gold.

For a cheaper option, the second condition is also attempted. The improvement on the reflection coefficient and radiation characteristics is also obtained for this time when the MSRR based layer is used due to the following two reasons:

- A smaller lossy area of the human body is obtained around the antenna when a thicker MSRR based layer is used.
- The same improvement that is obtained over the same thickness as discussed in this work.

5.3.1.4 Realization and Measurements

5.3.1.4.1 The Reflection Coefficient

A measurement of the MSRR based layer effect is conducted. The layer is realized by cutting a copper sheet of MSRR shapes and printing them on the top of a layer of 0.4 mm in thickness. It is worth pointing out that two layers are attempted, Polyvinyl chloride (PVC) and a normal tape layer. The overall results are found to be almost the same. This agrees with the findings in [3] (the dielectric properties of the real layers around loop antenna in the lossy human body has no effect on the overall loop performance). This is also verified by simulations. A prototype of the proposed layer when bent around the implant is shown in Fig. 5.28.

Two sets of measurements are conducted; with and without the MSRR based layer. Measurements are conducted in pork that is shown in Fig. 5.12.

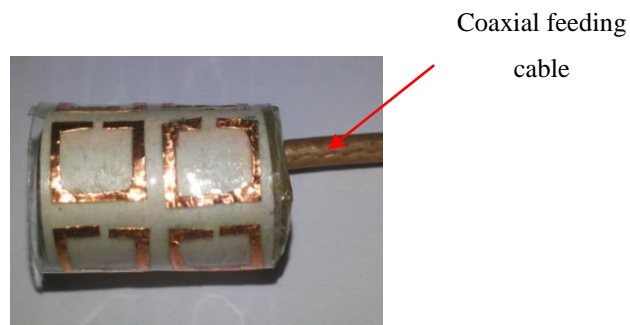


Fig. 5.28: The realized MSRR based layer around the 15 mm in length U-shaped loop antenna.

The antenna reflection coefficient for the 15 mm U-shaped loop antenna with the proposed MSRR based layer is measured at the centre of the body phantom. Measurements are then conducted without MSRR based layer over the same layer thickness. The results are shown in Fig. 5.29. A good matching with the simulation results is observed. A better 10 dB matching is always obtained when the MSRR based layer is used as desired.

It is worth pointing out that the effect of the antenna position inside the pork on the measured reflection coefficient is found to be negligible. To verify this, simulations are conducted at different positions inside a symmetrical simplified body model. In agreement with measurements, a negligible difference in the overall reflection coefficient characteristics is obtained. This is because the body model of simulations is symmetric and pork which is used in measurements is almost symmetric (mostly composed of muscle).

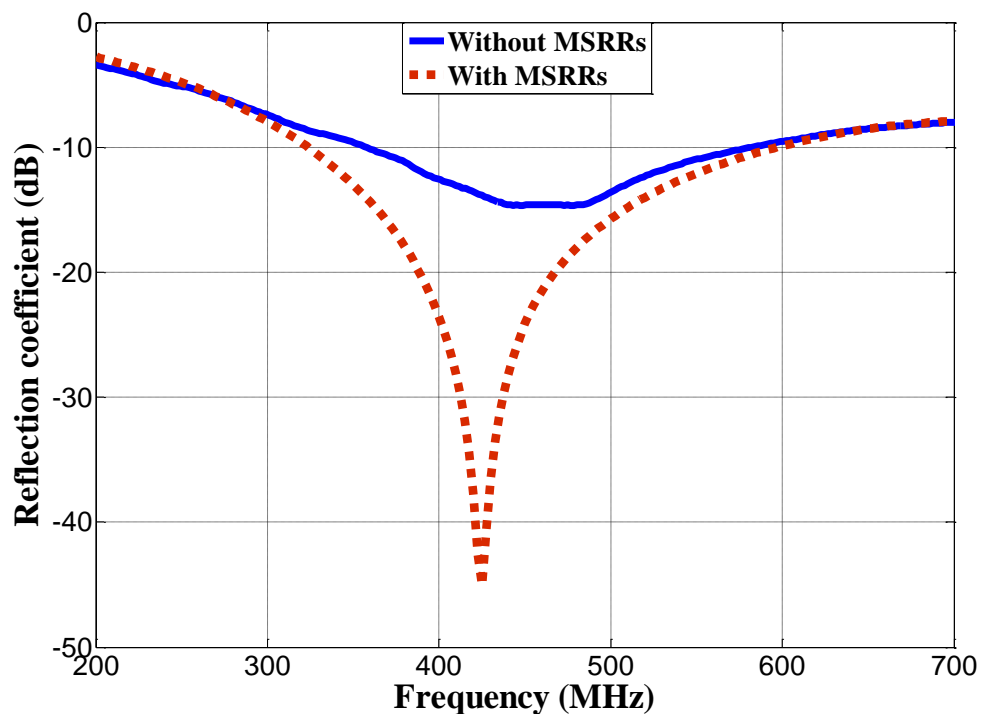


Fig. 5.29: The measured reflection coefficient S11 with and without MSRRs.

5.3.1.4.2 The Percent of Power Improvement

The power received from the proposed antenna by an external antenna was measured with and without the MSRR based layer. The antenna was placed at the centre of the phantom inside the anechoic chamber. Chokes were clamped to the cable near the antenna to reduce the cables effect. The distance between the implantable and the external antenna was around 2.5 meters in order to guarantee reception in the far field. 53% of power

improvement was measured. This matches with the simulations very well with an error of only 1.65%.

5.3.1.4.3 Gain Measurements

The gain of the proposed antenna with and without the MSRRs based layer is measured using the three antenna method. The measurement setup is the same as the gain measurement setup in Chapter 3.

The measured maximum gain values at 403 and 433 MHz with and without the proposed layer are summarized in Table 5.7.

Table 5.7: The measured gain (dBi) with and without MSRRs based layer in a simplified body model of pork.

Frequency (MHz)	With MSRRs		Without MSRRs	
	Simulated	Measured	Simulated	Measured
403	-24.5	-23.7	-26	-25.5
433	-23.35	-22.92	-25.5	-25

The simulation and measurement results are matched very well. 1.5 and 1.8 dB larger gain values are obtained at 403 MHz in simulations and measurements, respectively when the MSRR based layer is used. A larger improvement on the antenna gain is obtained at 433 MHz when this layer is used where 2.15 and 2.05 dB larger gain values are obtained in simulations and measurements, respectively.

The benefit of using MSRRs based layers is also verified for a patch antenna that is already existing in literature. The effect of using a MSRR based layer on the antenna reflection coefficient and radiation efficiency and gain is investigated at the following section.

5.3.2 Performance around an Implantable Patch Antenna

3×4 unit cells of the MSRRs are printed on both sides of the dielectric layer as shown in Fig. 5.30. The layer is placed on the top of a patch antenna in [12] and its performance is compared with a normal superstrate layer around it. The antenna structure is shown in Fig. 5.31.

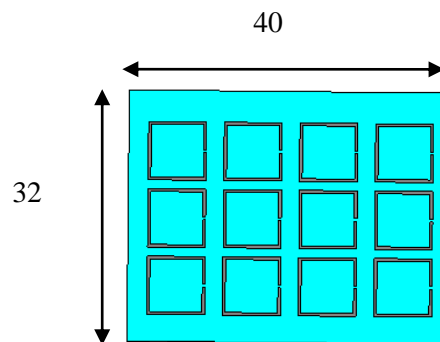


Fig. 5.30: The proposed MSRRs based layer which is to bend around the patch antenna in [6]

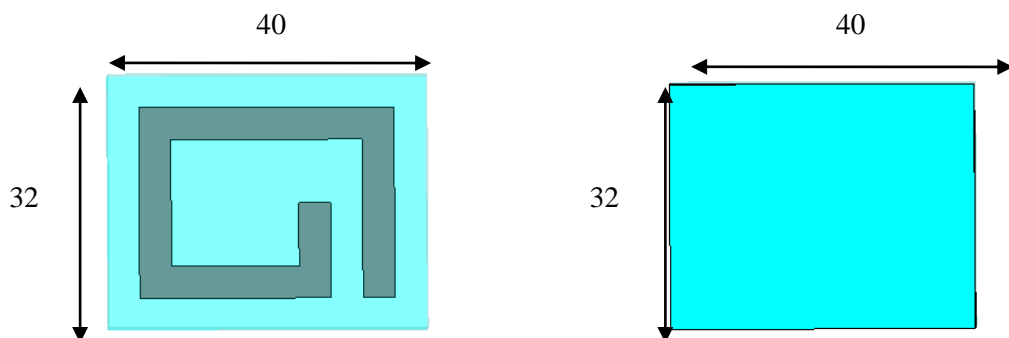


Fig. 5.31: The antenna based on the design in [6]: (a) The radiating layer, (b) The superstrate layer; units in mm.

The reflection coefficients with and without the proposed layer are shown in Fig. 5.32. The figure shows clearly that the MSRRs based layer improves the antenna matching ($S_{11} < -10$ dB) and shifts the resonant frequency down to 340 MHz. Although there are many ways to shift the antenna resonant frequency down, this method improves the antenna radiation efficiency. Because the antenna is of a narrow bandwidth, the resonance at the MedRadio band completely disappears. Therefore, the antenna is redesigned over smaller physical

dimensions (20×16 mm). The same number of (3×4) unit cells is used. However, the dimensions of each ring is minimized to the half. This has the advantage of minimizing the antenna size as desired for implantable applications and at the same time tune the antenna to work at the MedRadio band. The antenna length and width are decreased by 100% and the antenna covers the overall MedRadio band with a very good matching ($S_{11} < -20$ dB). When the antenna size and area become smaller, More losses are introduced because of the larger lossy body area around the antenna and thus its radiation efficiency are expected to decrease. Despite of this, the antenna maintains 10% larger radiation efficiency although its size is decreased (and thus the surrounding lossy area is increased) by 100%.

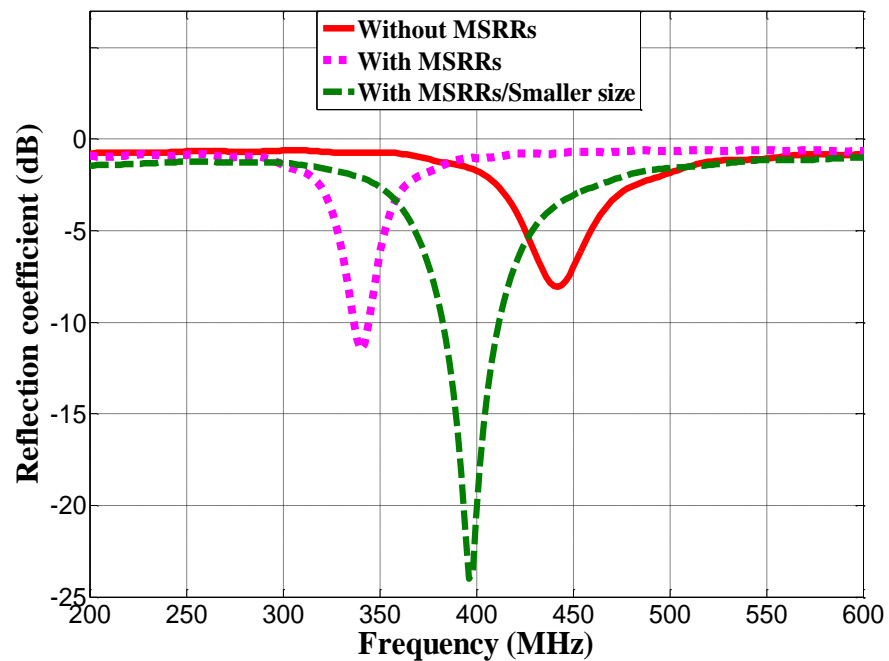


Fig. 5.32: The reflection coefficient S_{11} of the antenna in reference [12] with and without the proposed MSRR based layer.

5. 4 Summary

Due to the attractive features of metamaterials, this chapter has investigated the use of them for implantable applications. CSRRs have been integrated to a loop antenna while MSRRs are proposed as a top layer around the 15 mm U-shaped loop antenna. For both cases, metamaterials have been found to improve the antenna performance as the following:

- Improved the antenna matching (S_{11} much less than -10 dB). The overall structure with the metamaterial works as an LC tank circuit. The CSRRs introduce additional capacitance while MSRRs introduce inductance which compensates for the antenna inductive or capacitive reactance, respectively. This has the effect of reducing the reflected power to the source and increasing the radiated power.
- Reduced the near field intensity. This reduces the absorbed power and thus increases the radiation efficiency (up to 44.4% when CSRRs are added to the loop antenna of investigation and 52.14% when MSRRs are added around the 15 mm U-shaped loop antenna).
- Reduced the specific absorption rate (SAR).

Overall, the investigations in this chapter have provided a beneficial insight into the use of metamaterials to improve the overall radiation, matching and safety levels of implantable antennas. This is very beneficial to boost new implantable antennas of a larger radiation efficiency and robust performance.

Chapter Six

Path Loss Estimation for Implantable Applications

6.1 Introduction

The communication link from the implantable device to an external receiver in free space comprises two paths; inside the human body and from the human body to the external receiver in free space. This is reduced to almost one path for the case of a wearable receiver where communication occurs from the human body to the wearable or on body receiver that is attached directly to the skin or clothes [134]. In correspondence with the free space, the overall path losses for telemetric links are distance and frequency dependent. However, the case is much more complicated in the human body; more parameters such as the orientation, position and tissue of implantation affect the overall path losses. This is mainly due to the different effective relative permittivity and conductivity of the different tissues which result in different attenuation and absorption levels. Different reflection levels also occur at the boundary between the tissues. Overall, the in body path loss contributes to the overall losses of in-in, in-on and in- off body communications. Therefore, an accurate estimation of the path loss will enable accurate design considerations and boost more applications for the Implantable Body Sensor Network (IBSN), wireless power transfer and bio-telemetric health monitoring. This estimation should be conducted in the anatomical body models which are

of much better resemblance of the actual human bodies or small simplified body models that mimic small animals.

As indicated in Chapter 2, although some path losses were estimated for body communication channels, they have the following shortcomings:

- Underestimation of the overall in-in path loss because of using antennas of large physical sizes [134].
- Lack of an accurate in-in body path loss estimation at 403 MHz in the anatomical body models. Moreover, the effect of the orientation and position of the implantable antenna and device on the overall path loss was not quantified at that frequency [134].
- Lack of investigating the overall body orientation effect on the in-off body path losses [20].
- Lack of in-off body path loss estimation at 433 MHz for the applications of wireless power transfer (most of the existing estimations are at much lower frequencies for near field coupling).
- Lack of deep investigations of the optimum antenna type for in-on or on-in body communication.

To overcome the existing shortcomings, this chapter aims at the following objectives:

- Evaluating the communication between two U-shaped loop antennas which were presented in Chapter 3 for the applications of IBSN.
- Estimating the in-off path losses at 433 MHz for the applications of wireless power transfer.

- Quantifying the overall human body orientation effect around the external receiver on the overall path loss.
- Investigating the optimum on-body antenna type for reception from or transmission to the human body.

To obtain these objectives, this chapter is organized as the following: Firstly, the communication path loss between some implantable U-shaped loop antennas at 403 MHz is characterized inside an anatomical body model of an adult. The antennas are placed at a common position of implanting pacemakers and glucose monitoring devices. The orientation effect of the implantable device and antenna on the overall path loss is estimated and quantified. Then, the effect of the overall body orientation around the external receiver is quantified at 403 MHz. This is followed by estimating the path loss between an implantable and external antenna at a distance of up to 50 cm and a frequency of 433 MHz. Finally, a study about the optimum wearable/on body antenna type to communicate with implantable antennas is conducted.

The main contributions in this chapter can be summarized as the following:

- A new set of data about the overall path loss and link budgets between some implantable antennas of a small size at 403 MHz in the anatomical body model for communications between a pacemaker and glucose health monitoring implant is provided. This provides a valuable source of data about the overall path loss between such areas of implantation and for doctors about the optimum position of implantation.
- The variations of in-body path losses for different orientations of implantable antennas are investigated. This helps in selecting the orientation of the optimum performance for in-in body communications and provides the link margins for the case of rotating capsule antennas.

- The loss of a wireless power transfer path link over a distance of up to 50 cm and a frequency of 433 MHz is estimated. This provides an important data for power transfer system designers and evaluates its actual possibility for adults and small animals.
- The optimum antenna type for on-in body communication or in close proximity to the human body is investigated. The results show that loop antennas are of a better performance than patch antennas and improve the overall communication with implantable antennas in the near field. This study is very important to select the antenna type that improves such type of communication.

6.2 Communication between Implantable Antennas

In IBSN, implantable sensors coexist with each other (e.g. pacemaker with organ monitoring sensor or glucose sensor) [134]. To investigate the possibility of using our proposed antennas to communicate with an implantable pacemaker, a communication link is established between the proposed 15 mm U-shaped loop antenna at the position of a pacemaker [135] and a glucose monitoring device in the arm, hip and thigh which are possible positions of implantation for glucose monitoring devices [136]. The position of implantations of both devices are shown in Fig. 6.1. The pacemaker implant is placed directly beneath shoulder and its orientation is fixed at the first orientation for all the investigations. The orientation of the glucose monitoring implant is changed by rotating the implantable device 90 degrees counter clock wise each time at the same position. Each orientation is shown in Fig. 6.2.

The link budget is estimated based on the link parameters in Table 6.1 [134]. The path loss is an important link parameter. It is computed at three different positions (the arm, hip and thigh) and four orientations at each position as shown in Figs. 6.3-6.5.

The distance which determines the position is measured from beneath the fat layer directly. For example, a distance of 0 mm means that the implant longitudinal edge (E) shown in Fig. 6.2 is directly beneath fat and a distance of 5 mm means that this edge is 5 mm beneath fat.

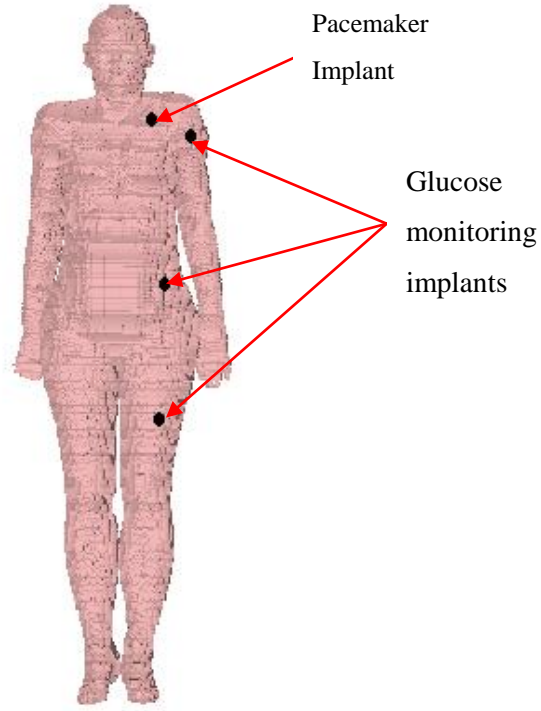


Fig.6.1: The positions of pacemaker and glucose monitoring devices in the human body

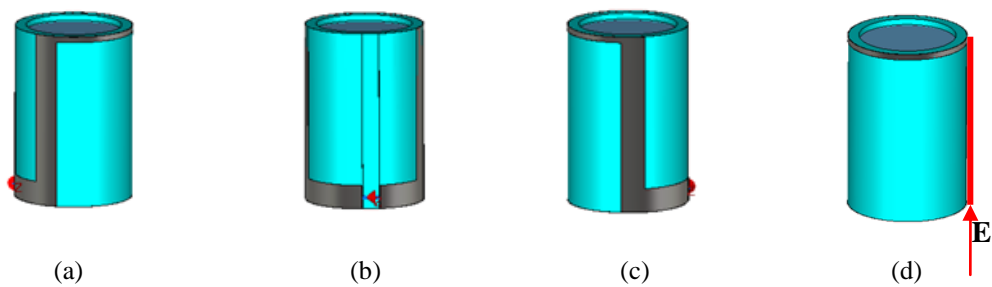


Fig. 6.2: The orientation of the pacemaker and glucose monitoring implantable antennas: (a) First (b) Second (c) Third (d) Fourth.

Table 6.1 : Parameters of a communication link between pacemaker and glucose monitoring devices

Link parameter	Value
Transmitted power, P_{TX} (μW)	25
Ambient temperature, AT (K)	310
Bit rate, B_r (Kb/s)	7
Boltzmann's constant, K_B (J/K)	1.38×10^{-23}
Coding gain, G_c (dB)	0
Fixing or deterioration gain, G_d (dB)	2.5
Energy per bit to noise power spectral density ratio, E_b/N_0 (dB) (ideal PSK)	9.6
Noise spectral density, N_0 (dBm/Hz)	-173
Bit error rate	1×10^{-5}

The Path loss (P_L) is defined as the ratio of input power at port 1 (P_{in}) to the power received at port 2 (P_{RX}) in a two-port setup. P_L is defined as $1/|S_{21}|^2$ with respect to 50Ω when the generator at the transmitter has an output impedance of 50Ω and the receiver is terminated with 50Ω [134] The setup is regarded as two-port circuit for which the $|S_{21}|$ dB with reference impedances of 50Ω at both ports.

$$P_L (dB) = \left(\frac{P_{in}}{P_{Rx}} \right) = -10 \log_{10} |S_{21}|^2 = -|S_{21}| (dB) \quad (6.1)$$

It should be pointed out that this path loss takes the gain of both antennas into considerations. This is due to the difficulty of estimating the implantable antenna gain values separately from the human body losses. However, the overall antenna gain values with the human body model is very reliable for such antennas with this small size (over-estimation

is impossible). The path loss is computed for a distance of up to 25 cm for the considerations of beneath-skin and deep implantations.

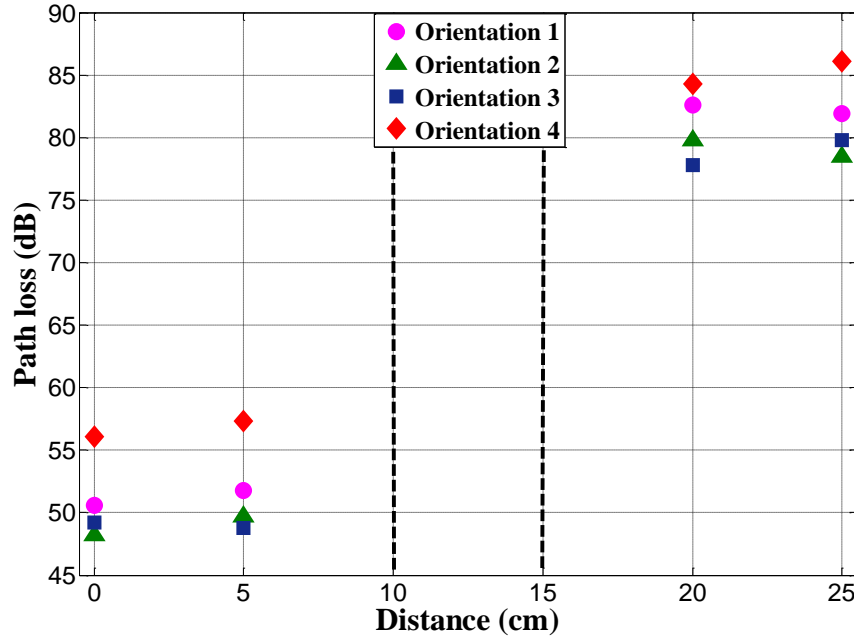


Fig. 6.3: The path loss between a pacemaker and glucose monitoring device in the left arm at 403 MHz

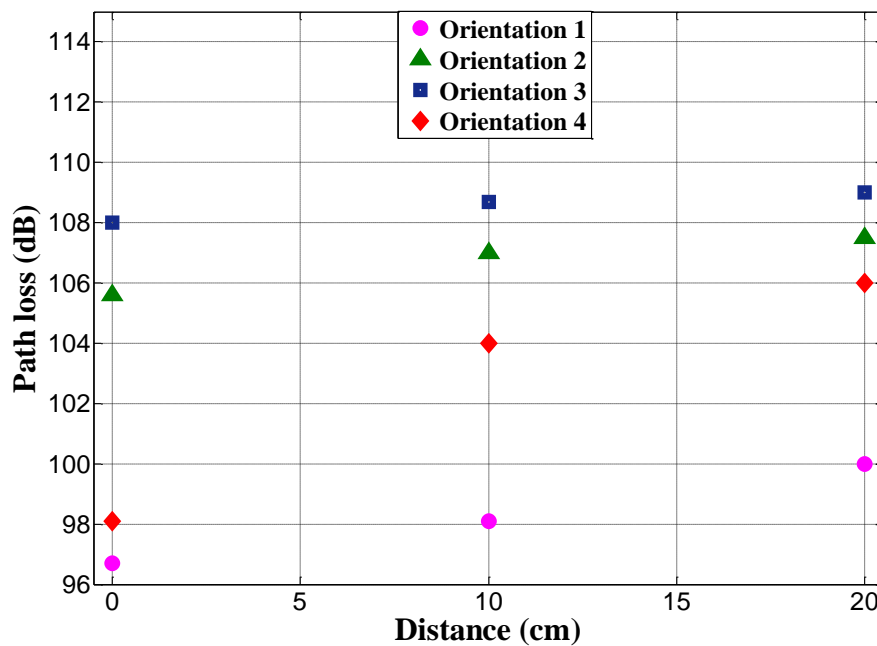


Fig. 6.4: The path loss between a pacemaker and glucose monitoring device in the area above the left hip at 403 MHz.

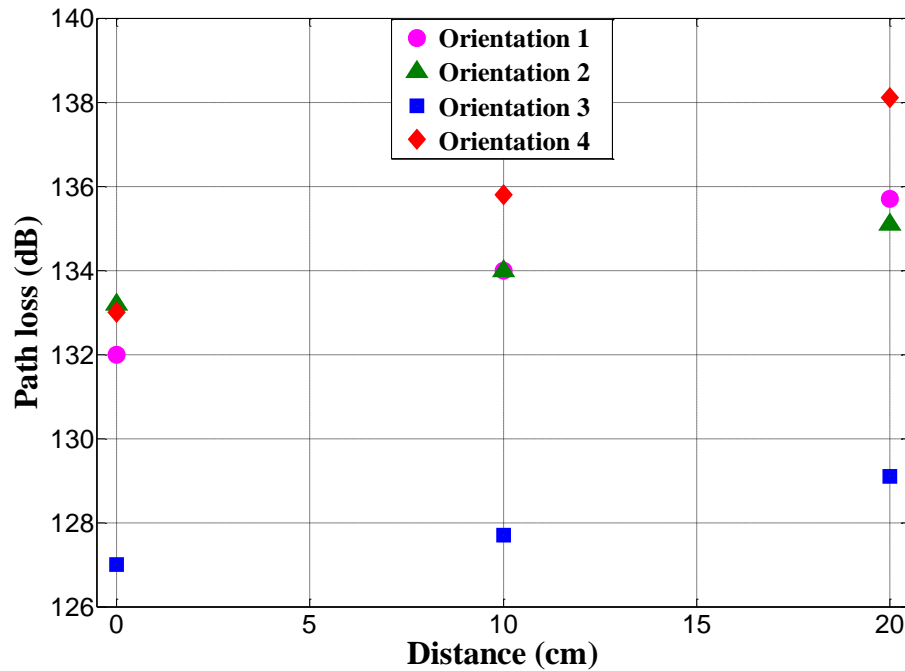


Fig. 6.5: The path loss between a pacemaker and glucose monitoring device in the left thigh at 403 MHz.

The dashed lines in Fig. 6.3 represent the bone area in the arm. Results are not provided for this region because the implantable device is usually placed in muscle or beneath skin for the intended applications. Although the distance between the implantable devices is decreased for the case of the deep implantation (longer distances beneath the skin), the overall path loss increases. This is mainly due to misalignment between the antennas. The smallest path loss is obtained for the case of implantation in the left arm because of the close proximity between the organs of implantation (the left arm and beneath the left shoulder). When the organs of implantation are close to each other, smaller path losses are obtained because of the smaller number of tissue layers. This causes smaller reflection and attenuation losses. This also explains that the largest path loss is obtained for the case between the left thigh and beneath the left shoulder.

The communication happens when the link carrier to noise density (C/N_0) exceeds the required (C/N_0) referring to Eqs. (6.2-6.3) [70, 134].

$$\text{Link}(C/N_0)(dB) = P_{TX} - P_{L,organ} - N_0 \quad (6.2)$$

$$\text{Required}(C/N_0)(dB) = (E_b/N_0) + 10\log_{10}(B_r) - G_c + G_d \quad (6.3)$$

Considering the link parameters in Table 6.1, the (C/N_0) is calculated as 50.55 dB. The link (C/N_0) should be larger than 50.55 dB for this communication to build up. To satisfy this, the path loss should be smaller than 106.45 dB.

This shows that communication between the pacemaker and glucose monitoring devices cannot be built up for the following cases which have losses that are larger than 106.45 dB:

- For all the cases of investigations in the left thigh.
- At the third orientation in the area above the left hip at distances of 0, 10 and 20 cm.
- At the second orientation in the area above the left hip at distances of 10 and 20 cm.

This is because of the long distance and misalignment between the antenna at these positions and orientations and the antenna below the left shoulder. The largest link margin is obtained for the second orientation in the arm at a distance of 5 mm beneath fat. It should be pointed out that a communication is always built up between the antenna in the left arm and below the left shoulder.

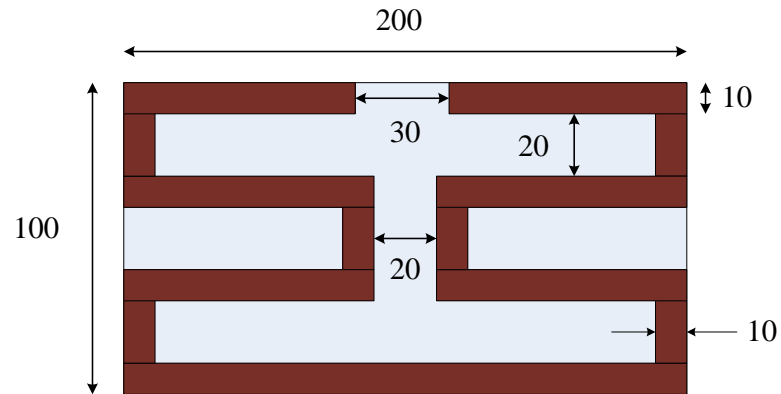
Figs. 6.3-6.5 show that a path loss of 32 dB can be obtained for only 20 mm difference in the distance at the same organ such as the case for the first orientation at the arm. The alignment between the maximum radiation of both antennas changes at these positions. The

largest path loss is obtained when the two antennas are misaligned. The results in the figures can be used as a source of data for other designers about the path loss for such a channel. The smallest path loss is obtained between the glucose monitoring implant in the arm beneath fat directly and the pacemaker. This is because the antennas are very close to each other and their main beams are pointed to each other.

6.3 The Effect of the Body Model Orientation on the Overall Path Loss

One of the most important requirements of the wireless health monitoring devices is the friendly use and free motion ability of users. Therefore, implantable antennas should be of a robust performance to guarantee communication for different body rotations around the receiver. The effect of different body orientations around the receiver on the overall path loss and link budget should also be quantified and estimated. Some physical parameters should be monitored during sleeping time [137]. This means that a minimum signal level should be received for that case which differs from the case of standing or sitting up. To estimate the variations of the body orientation on the overall path loss, the communications between the conformal 15 mm U-shaped loop antenna in a simplified body model that represents a small animal (such as a rabbit or cat) and an external meandered loop antenna at a distance of 2.5 m is built up in simulations. The simplified body model is used for this investigation because of the difficulty of conducting measurements in the full real body model. Moreover, this body model provides a good resemblance of the body shape. In addition, average gain values are obtained inside this body model (for example, the maximum gain value of the proposed antenna inside of it differs by only 1.8 dB from the maximum gain value in the left thigh as shown in Chapters 3 and 4. The structure of the receiving meandered antenna and its reflection coefficient are shown in Figs. 6.6 and 6.7,

respectively. Its design parameters are optimized to resonate at 403 MHz in free space with a realized gain value of 2.15 dBi.



(a)



(b)

Fig. 6.6: The receiving meandered loop antenna: (a) Structure (unit: mm) (b) Fabricated prototype

The variation of the path loss is evaluated for different body orientations which represent both cases of sleeping and standing. The antenna is placed at the centre of the body model as shown in Fig. 6.8. The receiving antenna is always kept at the same orientation which is shown in Fig 6.9.

The simulated and measured values for different body orientations are summarized in Table 6.2.

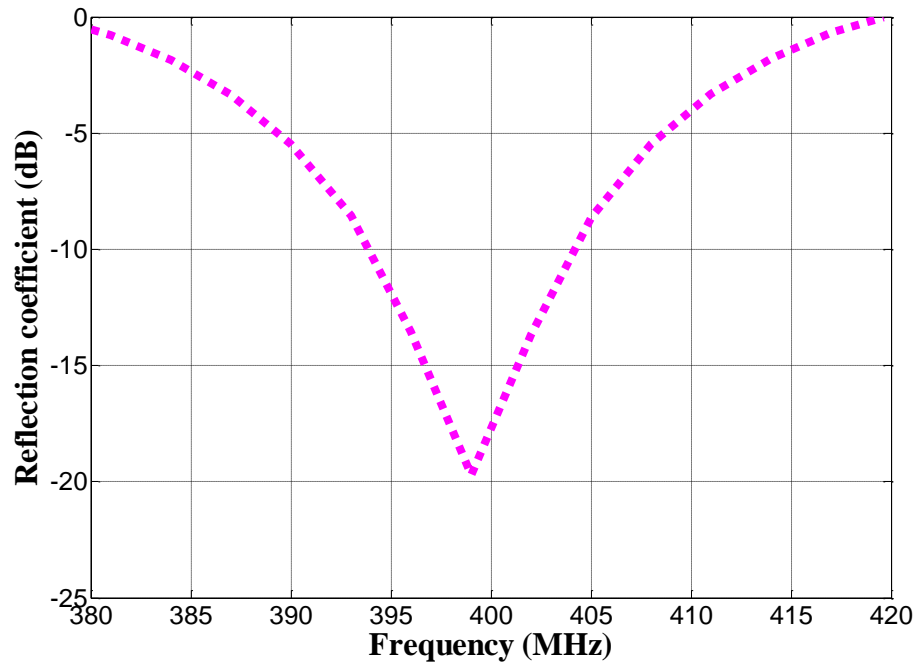
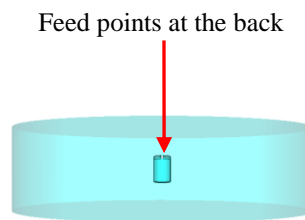


Fig. 6.7: The reflection coefficient of the external meandered receiving antenna.



6.8: The implantable antenna inside the simplified human body

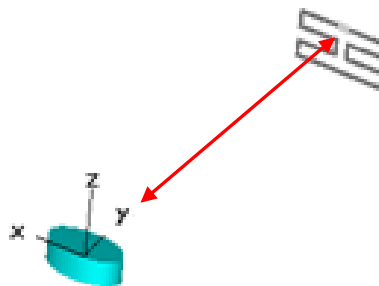
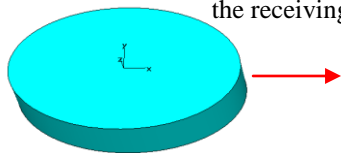
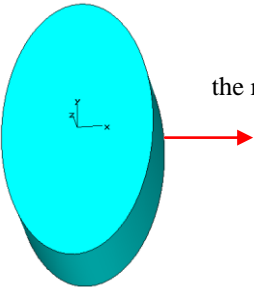
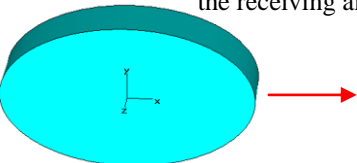
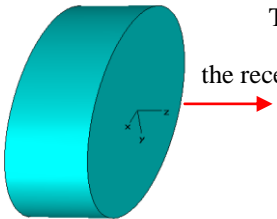
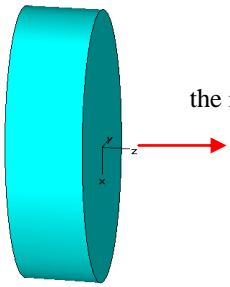


Fig. 6.9: The setup of the communication link between the implantable antenna inside the simplified human body and external loop antenna.

Table 6.2: The path loss of different body orientations

	Body orientation	The simulated path loss value (dB)	The measured path loss value (dB)
1	<p>Towards the receiving antenna</p> 	78.3	78
2	<p>Towards the receiving antenna</p> 	61.7	63
3	<p>Towards the receiving antenna</p> 	71.9	71.7
4	<p>Towards the receiving antenna</p> 	61.8	60.88
5	<p>Towards the receiving antenna</p> 	69.9	70.7

A good matching between simulations and measurements is always obtained. The variations for different body orientations are due to the misalignment and polarization variations for different orientations. The smallest path loss is obtained when the main lobes of both antennas are aligned to each other. 16.6 dB path loss difference is obtained between the worst and optimum cases of some body orientations. The received power for most of implantable devices should be larger than -99 dBm.

As long as the largest path loss value is 78.3 dB, communication will be always guaranteed over 2.5 m for an input power of 0 dBm. A significant difference is obtained for different orientations. This shows the importance of estimating and quantifying this effect for the intended in-off body path of investigation in order to estimate the required margin for the communication path loss.

6.4 Path Loss Estimation of a Wireless Power Transfer Channel

One of the important requirements for implantable antennas is to consume small power and to be of a rechargeable battery or passive. This enables a longer life time of the implantable device and avoid surgeries to replace the battery [138]. To enable these functionalities, many antennas that cover the 433 MHz which is mainly allocated for the purposes of wireless power transfer are proposed in this thesis. The wireless power is normally transmitted by an external antenna which is placed outside the body at a distance of up to 50 cm [42]. This distance represents a good choice as the free space loss is increased at longer distances which reduces the received power by the implantable device. This section is aiming at estimating these path losses from an anatomical body model and a simplified body model of an animal for distances up to 50 cm at 433 MHz. The simulation results from inside a simplified and anatomical body are shown in Fig. 6.10. Measurements in the

anechoic chamber are also conducted between the implantable antenna in a simplified body model of pork and external receiving antenna. Measurements are compared with simulations.

The figure shows that the path loss increases at longer distances which is because the free space loss is larger at these distances. On the other hand, the larger path loss for the case of the antenna in the anatomical body model in comparison with that in the simplified body model (5 dB in average) is because the anatomical model has larger dimensions than the simplified body model. It is also non-uniform and hence additional losses due to attenuations and reflections between body tissues are obtained inside of it. 15 dB larger path losses are obtained at 50 cm in comparison with it at 5 cm for the case of the antenna in the anatomical body model. This shows that power transfer is preferred at closer distances to the human body especially for short term power transfer.

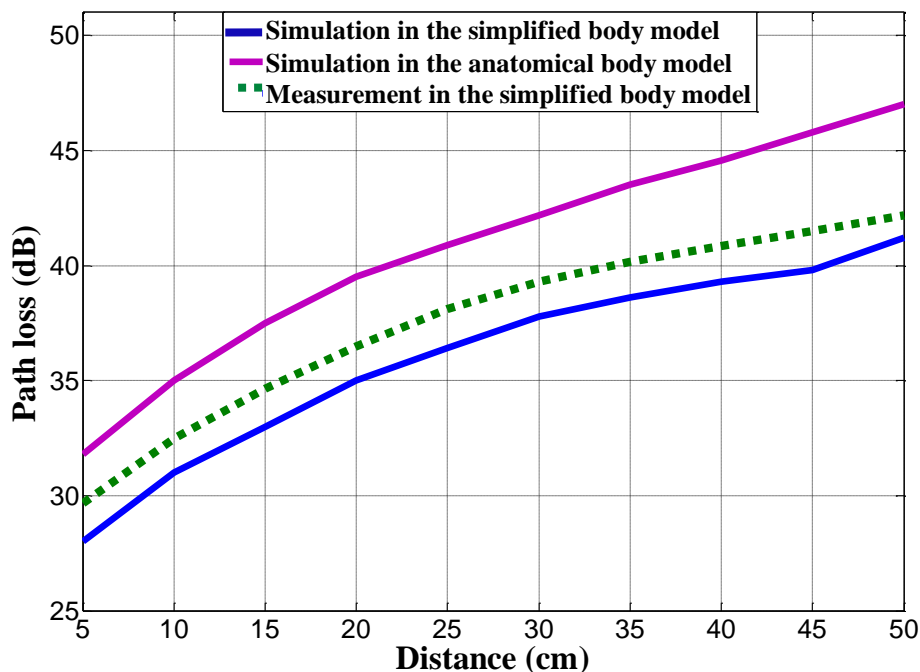


Fig. 6.10: The path loss between U-shaped implantable and meandered loop antennas at 433 MHz.

Measurements in pork are in good agreement with the simulation results in the simplified body model in general with an average difference of 1-1.5 dB at each position. This difference is due to the following reasons:

- Measurements are conducted in pork which is of multilayer (muscle and fat). The measured relative permittivity of its muscle and fat are 59 and 5.2, respectively while the measured conductivity of its muscle and fat are 0.84 and 0.062 S/m, respectively at 433 MHz. These values are larger than the corresponding values for liquid body models. This causes larger attenuations losses.
- Pork is asymmetric of different tissues and thus larger reflection losses at the boundary between them are obtained than in the simplified symmetric body model of simulation.

However, it is always better to consider the worst case which is the case of measurements in pork. Moreover, pork provides more realistic structure of the body of humans and small animals.

6.5 Investigations about the Optimum Antenna Type for Near Field Communications with Implantable Antennas

One important branch of communications is the on-in body communications where an antenna on the human body communicates with the implantable antenna. Such communications comprise transmitting to the implantable antenna for stimulation functionality [139] or reception from the implantable antenna such as the case for ingestible capsule receiver. In both cases, communication occurs in the near field region of the

antennas. Therefore, both antennas (transmitting and receiving) are affected by the losses of the human body tissues. It is very important to study the optimum antenna type that improves the overall communications. In this section the performance of loop and patch antennas is compared. These antennas are specifically selected because of the following:

- Loop antennas have shown a preferred performance in the lossy human body because they have a smaller electric near field than electrical type antennas.
- Patch antennas have shown a good performance for on-body communications because of their ground which reflects the body effect [140, 141]. The ground also serves to increase the gain in comparison with the corresponding antennas without ground.

Two flexible, loop and patch antennas are designed as shown in Fig. 6.11. Both antennas are assumed to bend around a simplified body model of a cylindrical shape, muscle equivalent material and following dimensions (radius 80 and length 140 mm). A clothing layer ($\epsilon_r=3$) of 10 mm in thickness is placed between the body model and antenna.

To provide an accurate comparison, both antennas are simulated firstly around a lossless human body of a relative permittivity of 57.1 and a conductivity of zero. Then around the same body model of the same dimensions but when the conductivity is 0.79 S/m. The 15 mm in length U-shaped loop implantable antenna is placed at the centre inside the model. This allows an accurate evaluation of the effect of losses on the on-body antenna gain and thus the overall path loss. The reflection coefficient of both antennas around the lossless and lossy human body is shown in Fig. 6.12.

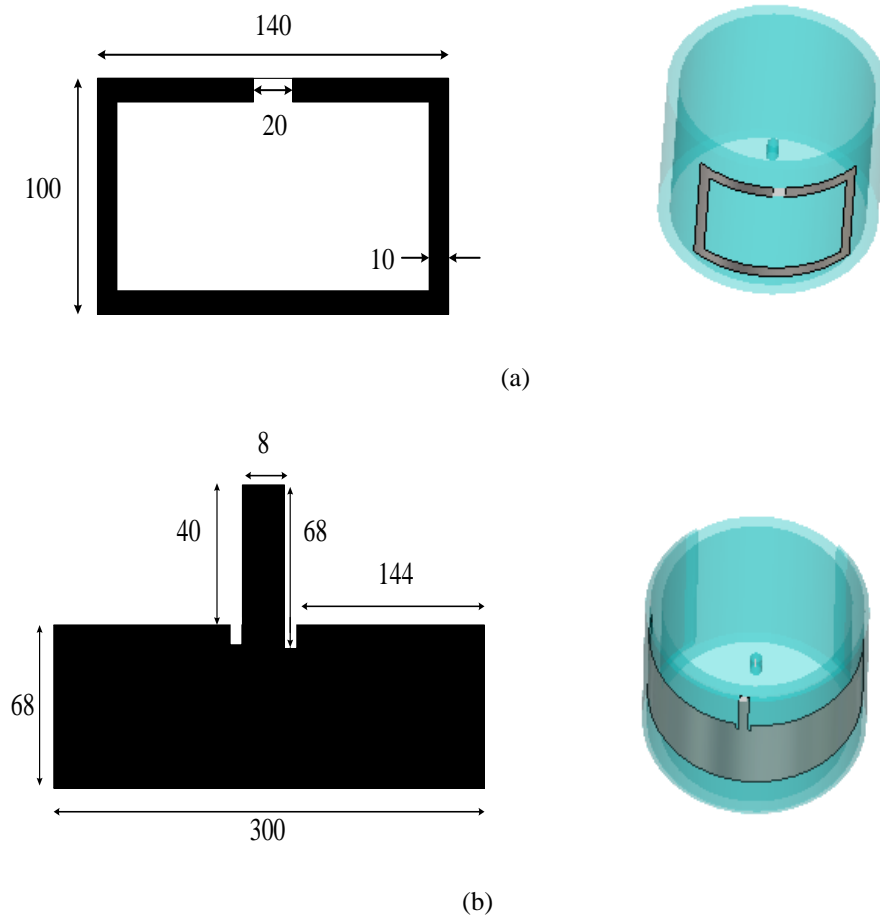


Fig. 6.11: Antennas on a simplified human body model: (a) Loop antenna, (b) Patch antenna; units in mm.

The realized gain, efficiency and transmission coefficient between both of these antennas and an implantable U-shaped loop antenna at the centre of the human body are provided in Table 6.3. 436 MHz is selected for the comparison because S_{11} is less than -10 dB for both antennas at it. It is also very close to both of 403 and 433 MHz which are the frequencies of interest in this thesis.

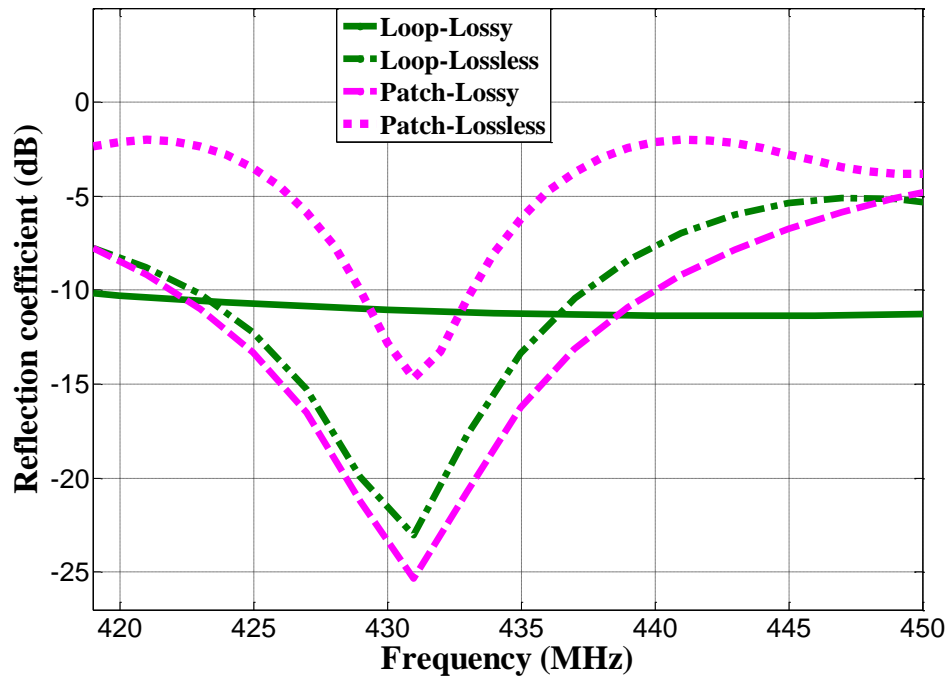


Fig. 6.12: The reflection coefficient (S11) of the wearable loop and patch antennas of comparison.

Table 6.3: Gain, Radiation efficiency and transmission coefficient of loop and patch antennas in close proximity to the human body

	Realized gain (dB)	Total radiation efficiency (%)	Transmission coefficient (dB)
Loop Lossless body	-2.4	0.27	-14
Patch Lossless body	-7	0.071	-42
Loop Lossy body	-8.83	0.045	-24
Patch Lossy body	-19.8	0.0038	-62

The purpose of this section is to compare the change in the gain and transmission coefficient for each antenna between the lossless and lossy human body. It can be noticed from the results in the table that the reduction in the gain and transmission coefficient for the case of patch antenna is larger than that for the case of loop antenna on the human body (10 dB for loop whereas 20 dB for patch). This is mainly due to the stronger electric near field of electrical type antennas such as patch in close proximity to the human body. When the electric near field is larger, larger power is absorbed and this reduces the overall radiated power as explained in Chapters 2 and 5. Unlike the case of the on-body patch antenna that communicate with an off-body receiver, the radiator of the on-body antenna that communicates with an implantable antenna is placed on the human body. Therefore, most of its radiation is absorbed by the human body. The ground of the patch is placed at some distance away from the human body and therefore, it has no effect in reflecting the human body losses. Although the ground works generally to direct the patch antenna radiation and improve its gain, its effect is small at relatively low frequencies such as around 400 MHz which is not enough to overcome the near field coupling loss with the radiator.

6.6 Summary

Due to the importance of in-in body and some related communications, the path loss of some in-in and in-off body channels has been estimated in this chapter. In particular, the loss of the path between the 15 mm U-shaped loop antenna for pacemaker and glucose monitoring devices at the hip, arm and thigh are estimated. The results in this chapter show that the communication between the pacemaker and glucose monitoring implantable antennas for the cases of investigations in this chapter is always built when the glucose monitoring implant is in the left arm. However, it cannot be built up for the following cases:

- For all the orientations of the glucose monitoring implant in the left thigh at distances up to 20 cm from beneath the fat layer.

- At the third orientation of the glucose monitoring implant in the area above the left hip at distances of 0, 10 and 20 cm.
- At the second orientation of the glucose monitoring implant in the area above the left hip at a distance of 10 and 20 cm.

The path loss is found to be dependent on the implantable device orientation even around the same axis. It also depends on the following factors:

- The distance between antennas.
- The structure and number of layers between antennas. When more tissues lie between the antennas, more attenuations and reflections are obtained.
- The tissue of implantation, larger losses are obtained when the antenna radiates from tissues of larger conductivity.
- Polarization and alignment between both antennas.

The variation in the path loss for different body orientations should be quantified for in-off body communication for link margin considerations. More than 16.6 dB larger path losses are obtained when the simplified body model rotates around the antenna receiver at 2.5 meters.

Another important link which is related to implantable applications is the wireless power transfer link. Therefore, the path loss of a wireless power transfer channel from an external meandered loop antenna to an implantable antenna in a simplified and an anatomical body models over 50 cm is estimated. 2.5 to 5 dB difference of the path loss is obtained between the simplified and anatomical body models at distances of 5 to 50 cm, respectively. On the other hand, 1-1.5 dB larger path loss is obtained at each position of measurements in pork in comparison with simulations in the simplified body model. This is due to the larger

reflection between muscle and fat tissues in pork and the larger size of the anatomical body model.

The optimum antenna type for more efficient on-in body communications is also investigated. Loop antennas are found to be more efficient for such type of communication. When the transmission coefficient from on-body loop and patch antennas to an implantable antenna is compared between lossless and lossy body models, 10 dB smaller transmission coefficient is obtained when an on-body patch is used. Therefore, loop or magnetic type antennas are preferred for such type of communications.

Chapter 7

Conclusions and Future Work

7.1 Conclusions

The interest in biomedical telemetry for medical applications has significantly increased which is mainly due to its beneficial applications. The applications involve capsule endoscopy, cardiac care and health parameters (i.e. heart rate, glucose, temperature and pressure) monitoring, etc. which are facilitated by different wearable and implantable devices. In comparison with wearable devices, the implantable device provides a unique tool to access some vital signals from inside the human body at critical times. However, the design of implantable devices is very challenging and comprises the integration of many small components. Although that most of the implant's sub-components can be efficient for small sizes, this is not the case for the implantable antenna. Normally, the size reduction causes a degradation of the electromagnetic antenna performance. Therefore, new techniques and structures are presented at this work to tackle these contradictory conditions. The main contributions and achievements in this regard are discussed in each chapter of this thesis which can be summarized as:

1. New flexible implantable antennas of the following characteristics are developed:

- Light weight.
- Wide bandwidth
- Relatively large radiation efficiency
- Can be used for small implants
- Work for multiple bandwidths which enable the functionalities of power saving and wireless power transfer.

Although some of these conditions are contradictory, they are satisfied because of the antenna flexibility which enables the exploitation of larger sizes for the same implant dimensions. The larger physical dimension leads to a wide bandwidth and gain. To enable flexibility, light conducting and dielectric materials are used. This reduces the overall antenna weight. While some flexible antennas were presented before, the proposed antennas in this thesis outperform them. This is because the proposed antennas are optimized through a two step design methodology for a larger radiation efficiency, wide bandwidth and robustness in the anatomical body model.

2. New investigations about the effect of the simplified body shape, structure and aspect ratios on the performance of implantable antennas are investigated for the first time. The results show that the simplified body model can only be relied upon to give an initial indication about the reflection coefficient characteristics and antenna radiation capability.
3. The validity of the evaluating parameters of the implantable antenna performance in the anatomical body model is investigated in this thesis. New effective parameters such as the implantable antenna and device orientation and the body part that is taken in simulations on the overall antenna performance are thoroughly investigated

and quantified. Such investigations are very important and contribute to the following:

- Give a beneficial insight into the accurate evaluation and validation of implantable antennas in the anatomical body model.
 - Confirm the necessity of selecting the optimum antenna and device orientation during the surgery process.
3. For the experimental work, a new simple method in the lab is developed to measure the performance robustness of the implantable antenna performance against material variations and in-body temperature variations after the actual implantation in the human body. The method is based on adding salt, sugar and water to pork to change its electromagnetic properties. This enables measuring the antenna performance in different media of different effective electromagnetic properties in the lab.
 4. New investigations about using metamaterials to improve the overall radiation from implantable devices are conducted for the first time. A significant improvement in the radiated power and SAR reduction is obtained when CSRRs and MSRRs based layer are integrated to and bent around loop antennas. A new function of the CSRRs and MSRRs in the lossy human body is illustrated for the first time. The CSRRs are found to reduce the near field intensity and thus power absorption in the human body. This is reflected on a larger overall radiated power and a smaller SAR. Such investigations provide a beneficial insight into the use of Metamaterials to improve the overall radiation, matching and safety levels of implantable antennas.
 5. Due to the importance of implantable antennas in different body communications (in-in, in-on, and in-off body), different related path losses are estimated and quantified. The following contributions in this regard are obtained:

-
- The effect of the implantable antenna and device orientation on the overall path loss between a pacemaker and glucose monitoring implantable antennas is estimated and quantified between implantable antennas in the full anatomical body model at 403 MHz for the first time. The results show the importance of quantifying this effect for an accurate estimation of link budget and margin.
 - The orientation effect of the overall body on the communication path loss between an implantable and external receiving loop antenna is estimated at a frequency of 403 MHz and a distance of 2.5 m. The results show that a significance difference in the overall path loss is obtained for some orientations. Therefore, it is very important to quantify this effect for an accurate estimation of the link budget.
 - The overall path loss between an implantable loop and external meandered loop antennas at 433 MHz are evaluated at a distance of up to 50 cm. The results obtain a path loss of around 28 dB in a simplified body model that mimics a small animal at a distance of 5 cm between the implantable and external antenna. 4 dB larger loss is obtained at the same distance when the antenna is implanted in the anatomical body model. An overall path loss of around 46.5 dB is obtained at 50 cm when the antenna is implanted in the anatomical body model. Therefore, it is recommended to work at short distances for an efficient wireless power transfer to the implantable antenna.
 - The optimum wearable/on body antenna type to communicate with implantable antennas is investigated. The results show that a loop antenna outperforms patch antenna in the near field region of an implantable loop antenna.

6. A planar meandered loop antenna is designed in free space for the applications of off-body communications (transmission or reception from the implantable antenna). The antenna works for the MedRadio (401-406 MHz) and 433 MHz ISM bands.

7.2 Future Work

Many issues related to implantable antennas have been addressed in this thesis. However, other issues under the following categories may be considered for further investigations:

- **The antenna design:** More antennas based on new materials such as biodegradable materials should be designed. The main attraction of a biodegradable device and antenna, to both surgeons and patients, is that it harmlessly degrades over time. This means that there is no need for an additional removal operation. Although, some implantable antennas based on biodegradable silk have been recently proposed, much more designs are still required. Organic based materials would also be more biocompatible over long term of implantation. Another issue with the implantable antenna design is that most of the proposed designs were of linear polarization. This is because most of the implantable devices are fixed at a single position. However, circularly polarized implantable antennas which receive power while rotating inside the human body are also required.
- **Metamaterials for implantable applications:** While valuable results about using metamaterials for implantable antennas are obtained at this work, more related structures could be developed. The recommended structures should be optimized to reduce the electric field intensity around the most effective radiating parts and increase the magnetic field. This can be another future path for implantable antennas

- of further larger radiation. It could also be beneficial to investigate the effect of metamaterials on the radiation pattern of implantable antennas in the human body.
- **Body path losses:** Although the losses of the communication path between an implantable pacemaker and a glucose monitoring device are quantified in this thesis, the path losses of other important links such as between pacemaker and bone implants should be estimated and quantified. Communication between the implantable antenna and mobile phone is another important path that should be estimated and characterized. The challenge of the latter path is that different sub-paths (the mobile in the hand, close to head, in free space or multipath) should be estimated.
- **Wireless power transfer:** This is a hot research area which is very beneficial to develop passive implants. Such implants save the pain and cost of replacing or charging the implant battery. Therefore, a very beneficial future path is to develop an overall rectenna system to power the implantable device and antenna.
- **Development of an entire implantable device:** The realization of an entire implantable device to transfer data from inside the human body to an external receiver is an important future research line. This requires working on different sub areas which combine medicine and engineering. It would be also very beneficial for such a device to support the functionality of wireless power transfer and wake up receiver.

References

- [1] J. C. Lin and Y. J. Wang, "An implantable microwave antenna for intracranial hyperthermia," *Proceedings of IEEE*, vol. 75, no. 8, pp. 1132-1133, Aug. 1987.
- [2] S. M. N. Rao, A. Mharte, D.O. Popa, J.-C. Chiao, Th. Ativanichayaphong, J. Sin, H. E. Stephanou, "MEMS based implantable drug delivery system," *VII International Conference on Micro Electro Mechanical Systems*, El Paso, TX, USA and Ciudad Juarez, Mexico, Sep. 21-22, 2005, pp. 1-4.
- [3] F. Merli, "Implantable antennas for biomedical applications," Ph.D .dissertation, Dept. Elect. Eng., EPFL Univ., Lausanne, Switzerland, 2011.
- [4] D. Sagan, "RF integrated circuits for medical applications: Meeting the challenge of ultra low power communication, ". [online]: <http://stf.ucsd.edu/presentations/2007/2007-08%20STF%20-%20Zarlink%20ULP%20transceivers.pdf>
- [5] Medical Device Radio Communications Service (MedRadio), Federal Communication Commission (FCC) Std. CFR, Part 95.601-673 Subpart E, Part 95.1201-1221 Subpart I, 2009, formerly Medical Implanted Communication System (MICS). [Online] :[http://wireless.fcc.gov/services/index.htm?job=service home&id=medicalimplant](http://wireless.fcc.gov/services/index.htm?job=service%20home&id=medicalimplant).
- [6] Peter D. Bradley, "Ultra Low-Power RF Communications for Implanted Medical Applications and Low Duty-Cycle Systems", white paper, EETimes-Asian, Nov. 2006.
- [7] F. Merli, L. Bolomey, J. F. Zürcher, G. Corradini, E. Meurville, and A. Skrivervik, "Design, realization and measurements of a miniature antenna for implantable wireless communication systems," *IEEE Trans. Antennas Propagat.*, vol. 59, no. 10, pp. 3544-3555, Oct. 2011.
- [8] IEEE Standard for Safety Levels with Respect to Human Exposure to Radio Frequency Electromagnetic Fields, 3 kHz to 300 GHz, IEEE Standard C95.1-1999, 1999.
- [9] IEEE Standard for Safety Levels with Respect to Human Exposure to Radio Frequency Electromagnetic Fields, 3 kHz to 300 GHz, IEEE Standard C95.1-2005, 2005.

- [10] Sharing between the Meteorological Aids Service and Medical Implant Communications Systems (MICS) operating in the Mobile Service in the Frequency Band 401-406 MHz, International Telecommunications Union Recommendation (ITU-R) Std. ITU-R Recommendation SA 1346, 2001, available (for registered users) at : www.itu.int
- [11] T. Karacolak, A. Z. Hood, and E. Topsakal, "Design of a dual-band implantable antenna and development of skin mimicking gels for continuous glucose monitoring," *IEEE Trans. Microw. Theory Tech.*, vol. 56, no. 4, pp. 1001 – 1008, Apr. 2008.
- [12] J. Kim and Y. Rahmat-Samii, "Implanted antennas inside a human body: simulations designs, and characterizations," *IEEE Trans. Microw. Theory Tech.*, vol. 52, no. 8, pp. 1934–1943, Aug. 2004.
- [13] J. Kim and Y. Rahmat-Samii, "Planar inverted-F antennas on implantable medical devices: Meandered type versus spiral type," *Microwave and optical technology letters.*, vol. 48, no. 3, pp. 567–572, Mar. 2006.
- [14] A. Kiourti and K. Nikita, "Miniature scalp-implantable antennas for telemetry in the MICS and ISM bands: Design, safety considerations and link budget Analysis," *IEEE Trans. Antennas Propagat.*, vol. 60, no. 8, pp. 3568-3575, Aug. 2012.
- [15] M. Asili, R. Green, S. Seran, and E. Topsakal, "A small implantable antenna for MedRadio and ISM Bands", *IEEE Antennas and Wireless Propagat. Lett.*, vol. 11, pp. 1683 – 1685, Jan. 2013.
- [16] M. Scarpello, D. Kurup, H. Rogier, D. Ginste, F. Axisa, J. Vanfleteren, W. Joseph, L. Martens, and G. Vermeeren, "Design of an implantable slot dipole conformal flexible antenna for biomedical applications," *IEEE Trans. Antennas Propagat.*, vol. 59, no. 10, pp. 3556-3564, Oct. 2011.
- [17] C. Schmidt, F. Casado, A. Arriola, I. Ortego, P. Bradely, and D. Valderas, "Broadband UHF implanted 3-D conformal antenna design and characterization for in-off body wireless links," *IEEE Trans. Antennas Propagat.*, vol. 62, no. 3, pp. 1433-1444, Mar. 2014.

- [18] X. Cheng, D. Senior, C. Kim, W.K. Yoon, "A compact omnidirectional self packaged patch antenna with complementary split-ring resonator loading for wireless endoscope applications," *IEEE Antennas and Wireless Propagat. Lett.*, vol. 10, pp. 1532-1535, Dec. 2011.
- [19] L. Xu, M. Q.-H. Meng, H. Ren and Y. Chan, "Radiation characteristics of ingestible wireless devices in human intestine following radio frequency exposure at 430, 800, 1200 and 2400 MHz," *IEEE Trans. Antennas Propagat.*, vol. 57, no. 8, pp. 2418-2428, Aug. 2009.
- [20] M. R. Basar, F. Malek, K. M. Juni, M. I. M. Saleh, M. S. Idris, L. Mohamed, N. Sauden, N. A. Mohd Affendi and A. Ali, "The use of a human body model to determine the variation of path losses in the human body channel in wireless capsule endoscopy". *Progress In Electromagnetics Research*, vol. 133, no. 3, pp. 495-513, 2013.
- [21] F. J. Huang, C. M. Lee, C. L. Chang, L. K. Chen, T.C. Yo and C. H. Luo, "Rectenna application of miniaturized implantable antenna design for triple-band biotelemetry communication," *IEEE Trans. Antennas Propag.*, vol. 59, no. 7, pp. 2646-2652, July 2011.
- [22] R. W. Ziolkowski and A. Erentok, "Metamaterial - based efficient electrically small antennas." *IEEE Trans. Antennas Propagat.*, vol. 54, no. 7, pp. 2113-2130, Jul. 2006.
- [23] N. Hwang, and f. C. Chen "Reduction of the Peak SAR in the human head with Metamaterials," *IEEE Trans. Antennas Propagat.*, vol. 54, no. 12, pp. 2113-2130, Dec. 2006.
- [24] S. Pasakawee, "Left-handed metamaterials realized by complementary split-ring resonators for RF and microwave circuit applications," Ph.D dissertation, Faculty of Engineering and Physical Sciences, Univ of Manchester, Manchester, UK, 2012.
- [25] Q. Shen, B. Hou, Z. Chen, and Z. L. Wang, "Effect of gap width on enhanced magnetic fields in mrtallic split ring resonators," *AIP Advances* 2, 042175 (2012); DOI: 10.1063/1.4770319
- [26] F. Merli, B. Fuchs, J.R. Mosig and A.K. Shrivervik, "The effect of insulating layers on

- the performance of implanted antennas” *IEEE Trans. Antennas Propagat*, vol. 59, no. 1, pp. 21-31, Jan. 2011.
- [27] C. J. Sa´nchez-Ferna´ndez, O´scar Quevedo-Teruel, J. Requena-Carri´on, L. Incl´an-S´anchez, Eva Rajo-Iglesias, Malcolm Ng Mou Kehn , “Dual- band implantable antenna based on short-curcuted SRR” in *Proc. EuCAP*, Barcelona, Spain, 2010, pp.1-4.
- [28] D. Kurup, W. Joseph, G. Vermeeren and L. Martens , “Specific absorption rate and path loss in specific body location in heterogeneous human model,” *IET Microwaves, Antennas and propagation*, vol. 7, no. 1, pp. 35-43, 2013.
- [29] A. Almomainy and Y. Hao, “Modeling and characterization of biotelemetric radio channel from ingested implants considering organ contents” *IEEE transactions on Antennas and propagation*, vol. 57, no. 4, pp. 999-1005, Apr. 2009.
- [30] K. Roman, G. vermeeren, A. Thielens, W. Joseph and L. Martens , “Characterization of path loss and absorption for a wireless radio frequency link between an in-body endoscopy capsule and a receiver outside the body” *UERASIP Journal on Wireless Communications and networking*, a springer open journal.
- [31] “Calculation of the dielectric properties of body tissues,” Institute for Applied Physics, Italian National Research Council, <http://niremf.ifac.cnr.it/tissprop/>
- [32] P. Zakavi, N. C. Karmakar, and I. Griggs, “Wireless orthopedic pin for bone healing and growth: Antenna development”,” *IEEE Trans. Antennas and Propagations*, vol. 58, no. 12, pp. 4069 - 4074, Dec. 2010.
- [33] R. W. P. King and G. S. Smith, "Antennas in matter: Fundamentals, theory and applications, 1st ed. Cambridge, Massachusettes, and London, England: The MIT Press, 1981.
- [34] http://en.wikipedia.org/wiki/ISM_band
- [35] http://en.wikipedia.org/wiki/Link_budget
- [36] http://en.wikipedia.org/wiki/Free-space_path_loss
- [37] Y. Huang and K. Boyle, *Antennas from theory to practice*, 1st ed. Uk, Chichester. John

Wiley & Sons Ltd, 2008.

- [38] R. Moore, "Effects of a surrounding conducting medium on antenna analysis," *IEEE Trans. Antennas Propag.*, vol. 11, no. 3, pp. 216–225, May 1963.
- [39] T. Wittig, "SAR overview". <https://www.cst.com/Content/Events/UGM2007/05-Witting.pdf>
- [40] C. Tsao, Co. Raytheon, and Ma. Norwood, "Radiation resistance of antennas in lossy media", *IEEE Trans. Antennas and Propagations*, vol. 19, no. 3, pp. 443 - 444, May. 1971.
- [41] R. E. Collin and F. J. Zucker, "Antenna theory part II, ser. Inter-University Electronics series" McGraw-Hill book, 1969, vol.7
- [42] S. Yun, K. Kim, and S. Nam, "Outer-wall loop antenna for ultrawideband capsule endoscope system", *IEEE Antennas and Wireless Propagat. Lett.*, vol. 9, 1135- 1138, 2010.
- [43] J. Kim and Y. Rahmatt-Samii, "Planar inverted-F antennas on implantable medical devices: Meandered type versus spiral type," *Microwave and Optical Technology .Lett.*, vol. 48, no. 3, pp. 567-672, Mar. 2006.
- [44] A. Sani, M. Rajab, R. Foster, and Y. Hao, "Antennas and propagation of implanted RFID for pervasive healthcare applications," in *Proc. IEEE*, vol. 98, no. 9, pp. 1648–1655, 2010.
- [45] S. M. Islam, K. P. Esselle, D. Bull, and P. M. Pilowsky, "A miniaturized implantable PIFA antenna for indoor wireless telemetry," in *Proc. International Conference Electromagnetics in Advanced Applications (ICEAA)*, Cape Town, South Africa, 2012, pp. 526 - 530.
- [46] L. J. Xu, Y. X. Guo, and W. Wu, "Dual-band implantable antenna with open-end slots on ground," *IEEE Antennas and Wireless Propagat. Lett.*, vol. 11, 1564-1567, 2012.
- [47] F. Gozasht, and A. S. Mohan, "Miniaturized slot PIFA antenna for tripleband implantable biomedical applications," in *Proc. IEEE MTT-S International Microwave*

- Workshop Series on RF and Wireless Technologies for Biomedical and Healthcare Applications (IMWS-BIO)*, Singapore, 2013, pp. 1 - 3.
- [48] W. Xia, K. Saito, M. Takahashi and K. Ito, "Performances of an implanted cavity slot antenna embedded in the human arm," *IEEE Trans. Antennas Propag.*, vol. 57, no. 4, pp. 894-899, April 2009.
- [49] L. Xuyang, M. Jalilvand, W. You, W. Wiesbeck, and T. Zwick, "An implantable stripline-fed antenna for biomedical applications," in *Proc. IET International Radar Radar Conference*, Xi'an, China, 2013, pp. 1-4.
- [50] Li-Jie Xu, Yong-Xin Guo, Wen Wu, "Miniaturised slot antenna for biomedical applications", *Electronics Letters*, vol. 49, no. 17, pp. 1060 – 1061, 2013.
- [51] W. Lei, and W.X. Guo, "A miniaturized implantable loop antenna at MICS and ISM bands for biomedical applications," in *Proc. IEEE MTT-S International Microwave Workshop Series on RF and Wireless Technologies for Biomedical and Healthcare Applications (IMWS-BIO)*, Singapore, 2013, pp. 1 - 3.
- [52] Z. N. Chen, G. C. Liu, and T. See, "Transmission of RF signals between MICS loop antennas in free space and implanted in the human head," *IEEE Trans. Antennas Propag.* vol. 57, no. 6, pp. 1850–1854, 2009.
- [53] N. H. Ramli, E. N. Ahyat, M. R. Kamarudin, N. A. Samsuri, M. K.A, Rahim, and N.H. Khamis, "Design & optimization of a compact ring monopole antenna for wireless implantable body area network (WiBAN) applications," in *Proc. Asia-Pacific Microwave Conference Proceedings (APMC)*, Melbourne, VIC, 2013, pp. 1 - 3.
- [54] S. A. Kumar, and T. Hanmuganatham, "Implantable CPW fed slot monopole antenna for biomedical applications," in *Proc. IEEE International Conference on Computational Intelligence & Computing Research (ICCIC)*, Singapore, 2011, pp. 1602 - 1609.
- [55] C.-M. Lee, T.-C. Yo, C.-H. Luo, C.-H. Tu and Y.-Z. Juang, "Compact broadband stacked implantable antenna for biotelemetry with medical devices," *IET Journals and Magazines*, vol. 43, no. 12, pp. 660-662, 7 Jun. 2007.

- [56] W.-C. Liu, F.-M. Yeh, and M. Ghavami, "Miniaturized implantable broadband antenna for biotelemetry communication," *Microwave and Optical Technology Letters*, vol. 50, no. 9, pp. 2407–2409, 2008.
- [57] A. Kiourti, K. A. Psathas, J. R. Costa, C. A. Fernandes, and K. S. Nikita, "Dual-Band implantable antennas for medical telemetry: A fast design methodology and validation for intra-cranial pressure monitoring," *Progress in Electromagnetics Research (PIER)*, vol. 141, pp. 161-183, 2013.
- [58] C. K. Wu, T. F. Chien, C. L. Yang, and C. H. Luo, "Design of novel S-shaped quad-band antenna for MedRadio/WMTS/ISM implantable biotelemetry applications," *International Journal of Antennas and Propagation*, pp. 1-12, 2012.
- [59] S. Soora, K. Gosalia, M. S. Humayun, and G. Lazzi, "A comparison of two and three dimensional dipole antennas for an implantable retinal prosthesis," *IEEE Trans. Antennas Propag.*, vol. 56, no. 3, pp. 622–629, Mar. 2008.
- [60] M. Z. Azad and M. Ali, "A miniature implanted inverted-F antenna for GPS application," *IEEE Trans. Antennas Propag.*, vol. 57, no. 6, pp. 1854–1858, June 2009.
- [61] E. Y. Chow, A. Kahn, and P. P. Irazoqui, "High data-rate 6.7 GHz wireless transmitter for neural prostheses," in *Proc. 29th Annual International Conference of the IEEE Engineering in Medicine and Biology Society EMBS*, 2007, 22–26, 2007, pp. 6580–6583.
- [62] Y. Yasir Ahmed, Y. Hao, and C. Parini, "A 31.5 GHz patch antenna design for medical implants," *International Journal of Antennas and Propagation*, DOI:10.1155/2008/167980, p. 6, Article ID 167980, 2008.
- [63] T. Houzen, M. Takahashi, K. Saito, and K. Ito, "Implanted planar inverted-F antenna for cardiac pacemaker system," in *Proc. International Workshop on Antenna Technology: Small Antennas and Novel Metamaterials iWAT 2008*, 4–6, 2008, pp. 346–349.
- [64] A. J. Johansson, "Wireless Communication with Medical Implants: Antennas and Propagation," Ph.D. dissertation, Lund University, Lund, June 2004.

- [65] Q. Wang, K. Wolf, and D. Plettemeier, "An UWB capsule endoscope antenna design for biomedical communications," in *Proc. 3rd International Symposium on Applied Sciences in Biomedical and Communication Technologies (ISABEL)*, Rome, Italy, 2010, pp.1-6.
- [66] S. Lei, K. Chang, and Y. J. Yoon "A dual spiral antenna for wideband capsule endoscope system," in *Proc. Asia-Pacific Microwave Conference*, Bangkok, 2007, pp.1-4.
- [67] S. H. Lee, K. Chang, K. J. Kim, and Y. J. Yoon, "A conical spiral antenna for wideband capsule endoscope system," in *Proc. Asia-Pacific Microwave Conference*, San Diego, CA, 2008, pp.1-4.
- [68] E. A. Johannessen, L. Wang, L. Cui, T. B. Tang, M. Ahmadian, A. Astaras, S. W. J. Reid, P. S. Yam, A. F. Murray, B. W. Flynn, S. P. Beaumont, D. R. S. Cumming, and J. M. Cooper, "Implementation of multichannel sensors for remote biomedical measurements in a microsystems format," *IEEE Trans. Biomed. Eng.*, vol. 51, no. 3, pp. 525–535, Mar. 2004.
- [69] T. Dissanayake, K. P. Esselle, and M. R. Yuce, "Dielectric loaded impedance matching for wideband implanted antennas," *IEEE Trans. Microw. Theory Tech.*, vol. 57, no. 10, pp. 2480–2487, Oct. 2009.
- [70] H.Y. Lin, M. Takahashi, K. Saito, and K. Ito "Performance of implantable folded dipole antenna for in-body wireless communication," *IEEE Trans. Antennas Propagat.*, vol. 61, no.3, pp. 1361-1370, Apr. 2009.
- [71] C. L. Yang, C. L. Tsay, K. T. Cheng and C. H. Chen, "Low-invasive implantable devices of low-power consumption using high-efficiency antennas for cloud health care," *IEEE Journal on Emerging and Selected Topics in Circuits and System*, vol. 2, no.1, pp. 14-23, Mar. 2012.
- [72] P. Izdebski, H. Rajagopalan, and Y. Rahmat-Samii, "Conformal ingestible capsule antenna: A novel chandelier meandered design," *IEEE Trans. Antennas Propagat.*, vol. 57, no.4, pp. 900-909, Apr. 2009.

- [73] H. Yu, "Electronic pills for medication compliance monitoring," PhD thesis, University of Florida, USA, 2010.
- [74] J. C. Wang, E. G. Lim, Z. Wang, Y. Huang, T. Tillo, Z. Meng and R. Alrawashdeh, "UWB planar antennas for wireless capsule endoscopy," in *Proc. iWAT*, Karlsruhe, Germany, 2013, pp.340-343.
- [75] A. Kiourti and K. S. Nikita, "Design of implantable antennas for medical telemetry: Dependence upon operation frequency, tissue anatomy, and implantation Site," *International Journal of Monitoring and Surveillance Technologies Research.*, vol. 10, pp. 16-33, Jan-Mar. 2013.
- [76] <http://www.CST.com>
- [77] <http://www.ansys.com>
- [78] https://www.cst.com/Content/Events/downloads/euc2013/5-4-2_CST_EUC.pdf
- [79] <https://www.scribd.com/doc/210057783/Cst-Microwave-Studio>
- [80] A. Kiourti and K. S. Nikita, "A review of implantable patch antennas for biomedical telemetry: Challenges and solutions," *IEEE Antennas and Propagation Magazine*, vol. 54, no.3, pp. 210-228, 2012.
- [81] N.Vidal, S. Courto, J. M.Lopez Villegas, J. Siero and F.M. Ramos, "Detuning study of implantable antennas inside the human body," *Progress in Electromagnetics Research (PIER)*, vol. 124, pp. 265-283, 2012.
- [82] H. Attia, O. Siddiqui, and O. M. Ramahi, "Artificial magneto superstrates for gain and efficiency improvement of microstrip antenna arrays", in *Proc. PIERS.*, Cambridge, USA, 2010, pp. 878-881.
- [83] Wang, G., J. Fang, and X. Dong, "Resolution of near-field microwave target detection and imaging by using flat LHM lens," *IEEE Trans. Antennas Propag.*, vol. 55, No. 12, 3534–3541, 2007.
- [84] Gong, Y. and G. Wang, "Superficial tumor hyperthermia with flat left-handed metamaterial lens," *Progress In Electromagnetics Research (PIER)*, Vol. 98, 389–405, 2009.

- [85] H. Tao, S. Hwang, M. Liu, B. Panilaitis, M. A. Brenckle, D. L. Kaplan¹, R. D. Averitt, A. Rogers and F. G. Omenetto, "Fully Implantable and Resorbable Metamaterials," in *Proc. Lasers and Electro-Optics (CLEO)*, San Jose, CA, 2012, pp.1-2.
- [86] D.A. Tonn, and R. Bansal, "Insulated antenna with metamaterial coating operating in lossy medium", *Electronics Letters*, vol. 42, no. 9, pp. 505-506, Apr. 2006.
- [87] Y. Yang, G. Fang, Dutkiewicz, Sh. Dongya, "Statistical characterization of the 400 MHz in-body propagation channel in-door environments," in *Proc. International Symposium on Communications and Information Technologies (ISCIT)*, Gold Coast, QLD, 2012, pp. 48-53.
- [88] D. Kurup, W. Joseph, G. Vermeeren, and L. Martens, "In-body path loss model for homogeneous human tissues," *IEEE Trans. Electromagnetic Compatibility.*, vol. 54, no. 3, pp. 556-564, Jun. 2012.
- [89] D. Kurup, W. Joseph, G. Vermeeren and L. Martens, "Path loss model for in-body communication in homogeneous human muscle tissue," *Electronics Letters.*, vol. 45, no.7, pp. 556-564, Apr. 2009.
- [90] D. Kurup, W. Joseph, E. Tanghe, G. Vermeeren and L. Martens, "Antenna independent path loss model for in-body communication in homogeneous tissue," *Electronics Letters.*, vol. 45, no.7, pp. 556-564, Apr. 2009.
- [91] S. Park, W. Kim, J. Lee, Y. S. Chung, and C. Cheon, "A new receiver antenna with buffer layer for wireless capsule endoscopy in human body", in *Proc. AP-S 2008.*, San Diego, CA, 2008, pp. 1-4.
- [92] A. Gordillo and I. Balasingham, "On directive antennas application to implant - on -body UWB communications," in *Proc. 19th Annual Wireless and Optical Communications Conference (WOCC).*, Shanghai, China, 2010, pp. 1-5.

- [93] M. Mark, T. Björninen, Y. D. Chen, S. Venkatraman, L. Ukkonen, L. Sydänheimo, J. M. Carmena, and J. M. Rabaey, "Wireless Channel Characterization for mm-Size Neural Implants", in *Proc. Annual Conference of the Engineering in Medicine and Biology Society (EMBC)*, Buenos Aires, Argentina, 2008, pp. 1565-1568.
- [94] C. Lue, Y. X. Guo, H. Sun, and S. Xiao, "Design and safety considerations of an implantable rectenna for far field wireless power transfer," *IEEE Trans. Antennas Propagat.*, vol. PP, no.99, DOI: 10.1109/TAP.2014.2352363.
- [95] "Agilent 85070E Dielectric Probe Kit 200 MHz to 50 GHz". [online]: <http://literature.cdn.keysight.com/litweb/pdf/5989-0222EN.pdf>
- [96] F. Merli, A. K. Skrivervik. Parini, Y. Zhinong, , " Design and measurement considerations for implantable antennas for telemetry applications," in *Proc. EuCAP 2010*, Barceolona, Spain,2010, pp. 1-5.
- [97] A. Kiourti, K. A. Psathas, P. Lelovas, N. Kostomitsopoulos, and K. S. Nikita, "In Vivo tests of implantable antennas in rats: Antenna size and intersubject considerations", *IEEE Antennas and Wireless Propagation Letters*, vol. 12, 1396-1399, 2013.
- [98] S. Best and J. Morrow, "On the significance of current vector alignment in establishing the resonant frequency of small space-filling wire antennas", *IEEE Antennas and Wireless Propagat. Lett.*, vol. 2, no.1, pp.201- 204, 2003.
- [99] R. Alrawashdeh, Y. Huang, and P. Cao, "Flexible meandered loop antenna for implants in the MedRadio and ISM bands," *Electronics Letters.*, vol. 49, no.24, pp. 1515-1517, Nov. 2013.
- [100] T. Houzen, M. Takahashi and K. Ito, "Implanted antenna for an artificial cardiac pacemaker system," in *Proc. Progress In Electromagnetics Research Symposium (PIERS)*, Prague, Czech Republic, 2007, pp. 51-54.
- [101] S. Yanasi, M. Takahashi, K. Saito, and K. Ito, "Study of implantable antenna for artificial knee joints," in *Proc. International Symposium on Antennas and Propagation (ISAP)*, Nagoyo , Japan, 2012, pp. 1244-1247.

- [102] R. Alrawashdeh, Y. Huang, and A. Abu Bakar sajak, "A flexible loop antenna for biomedical bone implants," in *Proc. EuCAP*, The Hague, Netherlands, 2014, pp. 861-864.
- [103] D. Bland and C. Skurla, "Stability of implants in total knee replacement surgery", Pdf file, <http://www.baylor.edu/content/services/document.php/41144.pdf>
- [104] <http://bonesmart.org/knee/knee-replacement-implant-materials/>
- [105] R. Alrawashdeh, Y. Huang, and P. Cao, "A flexible loop antenna for total knee replacement implants in the MedRadio band," in *Proc. LAPC*, Loughborough, UK, 2013, pp. 225-228.
- [106] W. Hurter, F. Reinbold, and W. J. Lorenz, "A dipole antenna for interstitial microwave hyperthermia," *IEEE Trans. Microwave Theory Tech.*, vol. 39, no. 6, pp. 1048–1054, Jun. 1991.
- [107] J. C. Lin and Y.-J. Wang, "The cap-choke catheter antenna for microwave ablation treatment," *IEEE Trans. Biomed. Eng.*, vol. 43, no. 6, pp. 657–660, Jun. 1996.
- [108] M. E. Ladd and H. H. Quick, "Reduction of resonant RF heating in intravascular catheters using coaxial chokes." *Magn Reson Med*, vol. 43, no. 4, pp. 615–619, Apr. 2000.
- [109] I. Longo, G. B. Gentili, M. Cerretelli, and N. Tosoratti, "A coaxial antenna with miniaturized choke for minimally invasive interstitial heating," *IEEE Trans. Biomed. Eng.*, vol. 50, no. 1, pp. 82–88, Jan. 2003.
- [110] <http://en.wikipedia.org/wiki/Polytetrafluoroethylene>
- [111] <http://www.mddionline.com/article/fluoropolymers-fitting-bill-medical-applications>
- [112] <http://www.modernplastics.com/pdf/mp-tecapeekmt2.pdf>
- [113] http://en.wikipedia.org/wiki/Polyvinyl_chloride
- [114] <http://www.namsa.com/portals/0/documents/biocomp-whatsasuppliertodo-w6-95.pdf>
- [115] <http://www.mddionline.com/article/selecting-materials-medical-products-pvc-metallocene-polyolefins>
- [116] <http://www.pvc.org/en/p/benefits-of-pvc>

- [117] <http://www.pvcmed.org/learning-centre/pvc-medical-applications/>
- [118] R. Alrawashdeh, Y. Huang and Q. Xu, "Evaluation of implantable antennas in Anatomical body models," CST white paper, Apr. 2014. Available: <https://www.cst.com/Applications/Article/Evaluation-Of-Implantable-Antennas-In-Anatomical-Body-Models>.
- [119] M. Rütshlin, "Body wearable antennas simulation challenges: Antenna examples: RFID, ISM, UWB,":https://www.cst.com/Content/Events/downloads/euc2013/3-1-4_CST_EUC.pdf
- [120] <http://www.diabetes.co.uk/news/2013/Mar/implantable-device-may-lead-to-better-blood-glucose-monitoring-99327465.html>
- [121] J. Gemio, J. Parrón, and J. Soler, "Human body effects on implantable antennas for ISM bands applications: Models comparison and propagation losses," *Progress In Electromagnetic Research (PIER)*, vol. 110, pp. 437–452, 2010.
- [122] Y. Aoyagi and K. Kajikawa, *Optical properties of advanced materials*. Springer, 2013.
- [123] A. Erentok, and R. W. Ziolkowski, Chen "Metmaterial-Inspired efficient electrically small antennas," *IEEE Trans. Antennas Propagat.*, vol. 56, no. 3, pp. 691-707, Mar. 2008.
- [124] D. Baena, J. Bonache, F. Martin, R. M. Sillero, F. Falcone, T. Lopetegui, M. A. G. Laso, J. Gemio, J. Garcia-Garcia, I. Gill, M. F. Poggio, and M. Sorolla, "Equivalent-circuit models for split-ring resonators and complementary split-ring resonators coupled to planar transmission lines," *IEEE Trans. Microw. Theory Tech.*, vol. 53, no. 4, pp. 1451–1461, Apr. 2005.
- [125] R. Marques's, F. Martin, and M. Sorolla, *Metamaterials with negative parameters: Theory, design and microwave applications*, Hoboken, New Jersey USA and Canada Wiley & Sons Ltd, 2008.
- [126] C. Calos, and T. Itoh, *Electromagnetic metamaterials: Transmission line theory and microwave applications*, Hoboken, New Jersey USA and Canada Wiley & Sons Ltd,

2006.

- [127] S. Maslovski, P. Ikonen, I. Kolmakov, and S. Tretyakov, "Artificial magnetic materials based on the new magnetic particle: Metasolenoid," *Progress In Electromagnetics Research (PIER)*, vol. 54, pp. 61-81, 2005.
- [128] H. Attia, L. Yousefi, M. M. Bait-Suwailam, M. M. S. Boybay, and O. M. Ramahi, "Enhanced-Gain microstrip antenna using engineered magnetic superstrates," *IEEE Antennas and Wireless Propagat. Lett.*, vol. 8, no. 1, pp. 1198- 1201, 2009.
- [129] N. Vidal, S. Curto, J. M. Lopez-Villegas, J. Sierio, and F. M. Ramos, "Detuning effects on implantable antenna at various human positions," in *Proc. EuCAP*, Prague, 2011, pp. 1231-1234.
- [130] <http://www.engadget.com/2010/08/19/implantable-antenna-designed-using-silk-and-gold/>
- [131] C. Oldani and A. Dominguez, Titanium as a biomaterial for implants, Available: <http://cdn.intechopen.com/pdfs-wm/26862.pdf>
- [132] http://en.wikipedia.org/wiki/Titanium_biocompatibility
- [133] <http://en.wikipedia.org/wiki/Gold>
- [134] D. Kurup, W. Joseph, G. Vermeeren, and L. Martens, "Specific absorption rate and pathloss in specific body location in heterogeneous human model," *IET Microw. Antennas Propag.*, vol. 7, no. 1, pp. 35-43, 2013.
- [135] http://www.hopkinsmedicine.org/healthlibrary/test_procedures/cardiovascular/pacemaker_insertion_92,P07980/
- [136] <http://www.diabetes.co.uk/news/2013/Mar/implantable-device-may-lead-to-better-blood-glucose-monitoring-99327465.html>
- [137] <http://www.technologyreview.com/news/420020/glucose-monitors-get-under-the-skin/>

- [138] C. W. Chang, and J. C. Chiou, "A wireless and batteryless microsystem with implantable grid electrode/3-dimensional probe array for ECoG and extracellular neural recording in rats," in *Sensors (Basel)*, vol. 13 (4); Apr. 2013; <http://www.ncbi.nlm.nih.gov/pmc/articles/PMC3673103/>
- [139] K. Kato, H. Matsuki, F. Sato, T. Satoh, and N. Handa, "Duplex communicable implanted antenna for magnetic direct feeding method: Functional electrical stimulation," in *J. Appl. Phys.* 105, 07B316 (2009); <http://dx.doi.org/10.1063/1.3068642>
- [140] J. A. Conway, W. G. Scanlon, and D. Linton, "Low-profile microstrip patch antenna for over-body surface communication at 2.45 GHz," in *Proc. 65th J IEEE Vehicular Technology conferece*, VTC2007-Spring, Dublin, 2007, pp. 392-396.
- [141] http://en.wikipedia.org/wiki/Patch_antenna

Appendix A

Electromagnetic Fields and Power Considerations for Electric and Magnetic Dipoles in a Dissipative Medium

It should be pointed out the content of this appendix is taken from [37].

A.1 Electromagnetic Fields of Infinitesimal Radiating Sources in a Lossy Medium

Infinitesimal electric and magnetic dipoles are evaluated when the dipoles are embedded in an infinite homogeneous medium of electric constants: σ is the conductivity, μ is the permeability, and ϵ is the dielectric permittivity. The cases will be considered when the dipole sources vary as $e^{j\omega t}$ and also for various transient sources.

Considering the case of a small current element of length dl which represents an electric dipole is oriented in the z direction and is situated at the origin of a spherical coordinate system (r, θ, ϕ) as indicated in Fig. A.1. The current in the element is I .

The electric and magnetic field components for this source are:

$$E_{\theta} = \frac{Idl}{4\pi(\sigma + j\omega\varepsilon)r^3} (1 + \gamma r + \gamma^2 r^2) e^{-\gamma r} \sin \theta \quad (\text{A.1})$$

$$E_r = \frac{Idl}{2\pi(\sigma + j\omega\varepsilon)r^3} (1 + \gamma r) e^{-\gamma r} \cos \theta \quad (\text{A.2})$$

$$H_{\phi} = \frac{Idl}{4\pi r^2} (1 + \gamma r) e^{-\gamma r} \sin \theta \quad (\text{A.3})$$

where γ is the propagation constant.

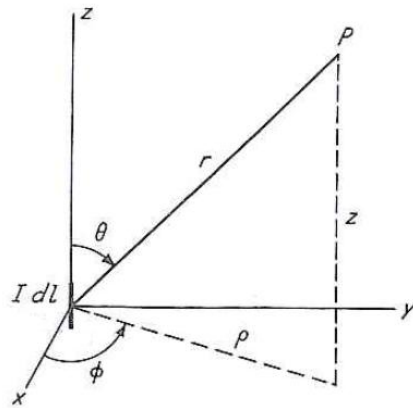


Fig. A.1: Electric dipole and coordinate systems [37].

When the current element is embedded in a lossy medium, the displacement currents are then very much smaller than the conduction currents, i.e. the total current density is:

$$J = (\sigma + j\omega\varepsilon)E \approx \sigma E \quad (\text{A.4})$$

The propagation constant then becomes:

$$\gamma^2 = j\sigma\mu\omega - \varepsilon\mu\omega^2 \approx j\sigma\mu\omega \quad (\text{A.5})$$

This approximation is valid for frequencies such that $\sigma \gg \varepsilon\omega$. For this case, the fields of the current element can be written as:

$$E_{\theta} = \frac{Idl}{4\pi\sigma r^3} (1 + \gamma r + \gamma^2 r^2) e^{-\gamma r} \sin \theta \quad (\text{A.6})$$

$$E_r = \frac{Idl}{2\pi\sigma r^3}(1 + \gamma r)e^{-\gamma r} \cos \theta \quad (\text{A.7})$$

$$H_\phi = \frac{Idl}{4\pi r^2}(1 + \gamma r)e^{-\gamma r} \sin \theta \quad (\text{A.8})$$

where $\gamma = (j\omega\mu\omega)^{1/2}$.

A small loop of current of area dA and circulating current I is equivalent to a linear element of magnetic current $J_m dl$ oriented in the direction of the loop axis. The two are related in magnitude by the following:

$$J_m dl = j\omega IdA \quad (\text{A.9})$$

where the dipole axis (loop axis) is oriented in the z direction and is situated at the origin.

The magnetic dipole field components are:

$$E_\phi = -\frac{j\omega IdA}{4\pi r^2}(1 + \gamma r)e^{-\gamma r} \sin \theta \quad (\text{A.10})$$

$$H_r = \frac{IdA}{2\pi r^3}(1 + \gamma r)e^{-\gamma r} \cos \theta \quad (\text{A.11})$$

$$H_\theta = \frac{IdA}{4\pi r^3}(1 + \gamma r + \gamma^2 r^2)e^{-\gamma r} \sin \theta \quad (\text{A.12})$$

The energy crossing an enclosing spherical surface around the source is calculated in the following section. The displacement currents are considered to be negligible.

A.2 The Radiated Power around Sources in a Lossy Medium

The mean Poynting vector in the radial direction is:

$$S_r = \frac{1}{2}(E \times H^*)_r = \frac{1}{2}E_\theta H_\phi^* \quad (\text{A.13})$$

The values of E_θ and H_ϕ :

$$E_\theta = \frac{Idl}{4\pi\sigma r^3} \sin\theta \left\{ \begin{aligned} &[(1+m)\cos m + (m+2m^2)\sin m]e^{-m} + \\ &j[(m+2m^2)\cos m - (1+m)\sin m]e^{-m} \end{aligned} \right\} \quad (\text{A.14})$$

and

$$H_\phi = \frac{Idl}{4\pi r^2} \sin\theta \left\{ \begin{aligned} &[(2+2m)\cos m + 2m\sin m]e^{-m} - \\ &j[(2+2m)\sin m - 2m\cos m]e^{-m} \end{aligned} \right\} \quad (\text{A.15})$$

$$\text{where } m = \left(\frac{\sigma\mu\omega}{2} \right)^{1/2} r$$

Now, the average real power propagated in the radial direction is given by:

$$\begin{aligned} P_r &= \frac{1}{2} \text{Re}(E \times H^*)_r \quad (\text{A.16}) \\ &= \frac{1}{2} \text{Re} E_\theta H_\phi^* \end{aligned}$$

The asterisk denotes the complex conjugate. Using Eqs. (A.14-A.15), it is found that:

$$P_r = \left(\frac{Idl}{4\pi\sigma} \right)^2 \frac{\sin^2\theta}{\mu\omega} \left[\frac{\alpha^2}{r^5} + \frac{2\alpha^3}{r^4} + \frac{2\alpha^4}{r^3} + \frac{2\alpha^5}{r^2} \right] e^{-2\alpha r} \quad (\text{A.17})$$

$$\text{where } \alpha = \left(\frac{\sigma\mu\omega}{2} \right)^{1/2}.$$

The total power P_{rad} crossing an enclosing sphere of radius $r = R$ can be calculated by integrating P_r over the surface of the sphere; thus,

$$P_{rad} = \int_0^{2\pi} \int_0^\pi P_r R^2 \sin\theta d\phi d\theta \quad (\text{A.18})$$

$$P_{rad} = \frac{1}{6\pi\mu\omega} \left(\frac{Idl}{\sigma} \right)^2 \left(\frac{\alpha^2}{R^3} + \frac{2\alpha^3}{R^2} + \frac{2\alpha^4}{R} + 2\alpha^5 \right) e^{-2\alpha R} \quad (\text{A.19})$$

Near the dipole, the first term in $1/R^3$ predominates and the total power is:

$$P_{rad} \approx \frac{1}{6\pi\mu\omega} \left(\frac{Idl}{\sigma} \right)^2 \frac{\alpha^2}{R^3} \quad (\text{A.20})$$

An expression similar to (A.17) is obtained for the magnetic dipole:

$$P'_r = \left(\frac{IdA}{4\pi} \right)^2 \left(\frac{\mu\omega}{r^5} \right) (1 + \alpha r) \alpha^2 r^2 e^{-2\alpha R} \sin^2 \theta \quad (\text{A.21})$$

For small values of r :

$$P'_r \approx \frac{\sigma\mu^2\omega^2}{2r^3} \left(\frac{IdA}{4\pi} \right)^2 \sin^2 \theta \quad (\text{A.22})$$

The total power crossing a spherical surface of radius R near the dipole is then:

$$P_{rad} \approx \frac{\sigma\mu^2\omega^2 (IdA)^2}{12\pi R} \quad (\text{A.23})$$

Appendix B

Comparison between Homogeneous and Heterogeneous Human-Shaped Body Models

A homogeneous human-shaped body model is shown in Fig. B.1. The homogeneous body model is defined to be composed of muscle at 403 MHz. Laura body model is used as the heterogeneous body model. The multilayer structure of the Laura voxel body model was shown in Chapter 4. The antenna is placed in the chest.

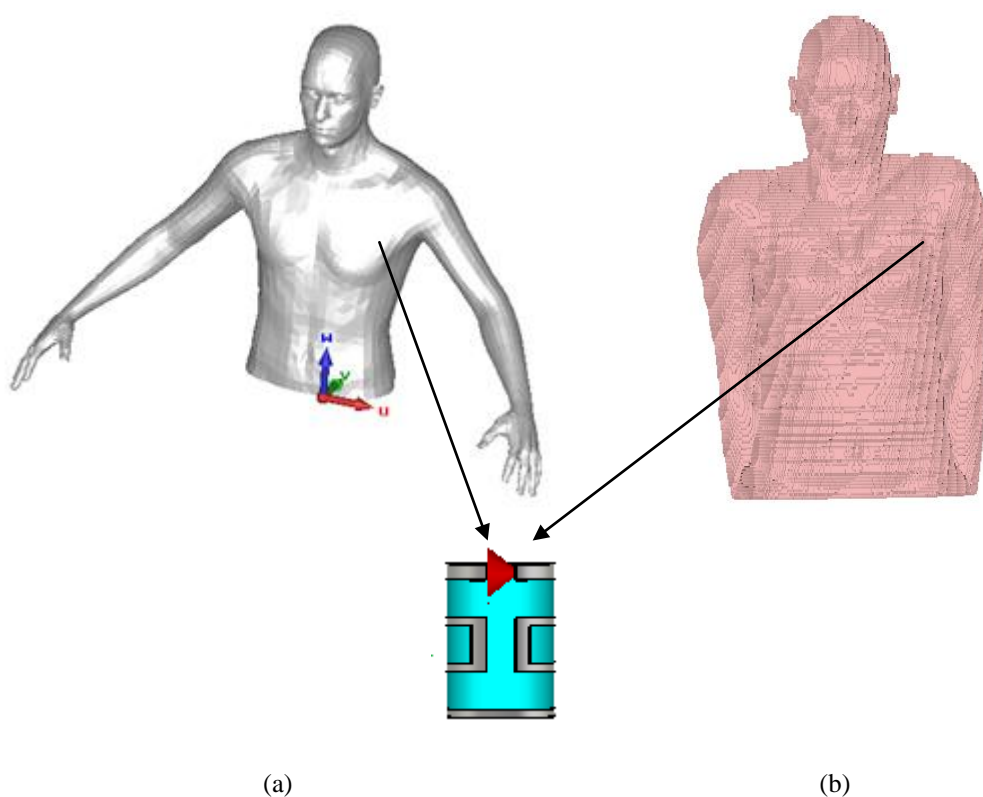


Fig. B. 1: A human-shaped body model: (a) Homogeneous, (b) Heterogeneous.

Four parameters for the small meandered loop antenna which was proposed in Chapter 3 are compared:

- The resonant frequency
- The antenna radiation efficiency
- The antenna gain
- The specific absorption rate (1-g SAR)

The results are summarized in Table B.1.

Table B. 1: The radiation characteristics of the meandered loop antenna in homogeneous and heterogeneous human-shaped body models

	Homogeneous human-shaped body models	Heterogeneous human-shaped body model
Resonant frequency (MHz)	338	413
Radiation efficiency (%)	0.0028	0.005
Max 3D gain (dBi)	-48.8	-45
Max 1-g SAR (W/kg) / $P_{in}=1$ W	740	580

The resonant frequency is shifted from 413 MHz in the heterogeneous human-shaped body model to 338 MHz in the homogeneous human-shaped body model. This is because of the larger effective permittivity in the homogeneous body model which is composed of muscle only. The antenna obtained a small radiation efficiency and gain of 0.005% and -45 dBi, respectively in the adult Laura body model because of its small size. These radiation

efficiency and gain values are decreased to 0.00283% and -48.8 dBi in the homogeneous human-shaped body model. The 1-g SAR for an input power of 1 W in Laura and the homogeneous body-shaped model is computed as 580 and 740 W/kg, respectively.

From the results, it can be concluded that the homogeneous human-shaped model exaggerates the overall body losses in comparison with anatomical body models. This is because it is composed of muscle only which have larger conductivity than fat as explained in Chapter 4. This is reflected on smaller radiation efficiency and gain and larger SAR.